

AISC E&R Library



B432

NR2

Structural Stability
Research Council

**ANNUAL
TECHNICAL SESSION
Proceedings**

1987

STRUCTURAL STABILITY RESEARCH COUNCIL

PROCEEDINGS

1987 ANNUAL
TECHNICAL SESSION

"STABILITY OF CIRCULAR STIFFENED SHELLS"

ORGANIZED BY:

STRUCTURAL STABILITY RESEARCH COUNCIL

CONFERENCE SPONSORED BY:

CHEVRON USA, INC.

SHELL OIL COMPANY

AMERICAN IRON AND STEEL INSTITUTE

CENTER FOR ADVANCED TECHNOLOGY
FOR LARGE STRUCTURAL SYSTEMS (ATLSS)

COOPERATING SPONSOR:

AMERICAN PETROLEUM INSTITUTE

March 24-25, 1987
Houston, Texas

THE OPINIONS, FINDINGS, CONCLUSIONS AND
RECOMMENDATIONS EXPRESSED HEREIN ARE THOSE OF
THE AUTHORS AND DO NOT NECESSARILY REFLECT THE
VIEWS OF THE STRUCTURAL STABILITY RESEARCH COUNCIL
OR THE CONFERENCE SPONSORS.

STRUCTURAL STABILITY RESEARCH COUNCIL

Fritz Engineering Laboratory
Lehigh University
Bethlehem, Pennsylvania 18015 U.S.A.

(215) 758-3522/TELEX 710-670-1086UD

FOREWORD

This is the first time I have had the responsibility of preparing the Foreword for the Annual Technical Session Proceedings. Perhaps it is appropriate that I take this opportunity to thank the membership for the honor accorded me as the elected Chairman of SSRC. On behalf of the membership I must express our appreciation to Past Chairman John Springfield for his four years of effective, conscientious and diligent leadership; we look forward to his continued counsel on the Executive Committee.

"Stability of Circular Stiffened Shells" was the title of the Theme Session of the SSRC 1987 Annual Technical Session held at the Adam's Mark Hotel in Houston on March 24-25, 1987. In addition to the Theme Session, the 24 papers that were presented also covered topics germane to the SSRC task groups and reporters, and are the substance of these Proceedings. A highlight of the conference was the excellent Tuesday luncheon presentation by Cor Langewis on "Conoco's Green Canyon Tension Leg Well Platform Project", the first tension leg platform designed for North American waters. Approximately 100 people from 6 countries attended the meetings, despite the current depressed condition of the oil industry. We trust that a far larger number of engineers will find these printed Proceedings to be of value.

My thanks to C. D. Miller, D. R. Sherman, C. C. Capanoglu, R. M. Meith and R. K. Kinra who served as the Theme Session Program Committee, and G. F. Fox, L. S. Beedle, J. L. Durkee and G. S. Stewart who served as the Sessions Program Committee.

We also appreciate the assistance of those who helped with the local arrangements, including S. X. Gunzelman, J. W. Cox, and W. J. Austin and a contingent of Rice University student helpers. The facilities and service provided by the Adam's Mark Hotel were outstanding.

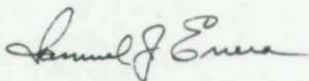
We are also most grateful to our sponsors. We thank the American Iron and Steel Institute, Chevron USA, Inc., Shell Oil Company and the Engineering Research Center for Advanced Technology for Large Structural Systems (ATLSS) at Lehigh University for their contributions toward the funding of the conference.

The Annual Technical Session would not be the success it is without the collective talents of the Council's Headquarters staff led by the Director, Lynn S. Beedle. Our thanks to Lynn, the Technical Secretary, Graham Stewart, the Administrative Secretary, Lesleigh Federinic and Diana Walsh, Headquarters secretary. A special thanks to Sue Stewart for her help at the registration area this year. The arranging of all the many, many details and the smoothness with which the sessions run is all due to these folks.

We invite you to look ahead with us to future scheduled meetings:

- | | | |
|------|---|--|
| 1988 | - | Minneapolis, Minnesota
"Computer Technology Applied to
Structural Stability" |
| 1989 | - | New York City
4th International Colloquium -
"Stability of Metal Structures" |
| 1990 | - | St. Louis, Missouri
"Bridges" |

I look forward to seeing you at these sessions.



Samuel J. Errera
Chairman

Bethlehem, Pennsylvania
August 1987

CONTENTS

	<i>Page</i>
FOREWORD	i
<u>BEAM-COLUMNS - (TG-9)</u>	
BEHAVIOR AND STRENGTH OF NONPROPORTIONALLY LOADED IMPERFECT BEAM-COLUMNS RESTRAINED PARTIALLY Z. Razzaq and S. P. Darbhamaulla	1
<u>THIN-WALLED METAL CONSTRUCTION - (TG-15)</u>	
DYNAMIC INSTABILITY OF FRAMES HAVING THINWALLED COLUMNS S. Sridharan and M. Ashraf Ali	13
POST-BUCKLING BEHAVIOUR AND EFFECTIVE WIDTH OF EDGE-STIFFENED PLATE ELEMENTS UNDER COMBINED COMPRESSION AND BENDING X. Zhou and S. Wang	27
<u>DOUBLY CURVED SHELLS AND SHELL-LIKE STRUCTURES - (TG-17)</u>	
GENERAL BUCKLING OF SHELL-LIKE STRUCTURES - SUMMARY OF CLOSED FORM SOLUTIONS K. P. Buchert	39
THE BUCKLING BEHAVIOUR OF SINGLE LAYER, SHALLOW BRACED DOMES R. E. McConnel	49
THE EFFECT OF STRUCTURAL STIFFNESS ON THE PROGRESSIVE COLLAPSE OF SPACE TRUSSES N. F. Morris	55

UNSTIFFENED TUBULAR MEMBERS - (TG-18)

BEAM-COLUMN BEHAVIOR OF UNSTIFFENED FABRICATED STEEL TUBES H. G. L. Prion and P. C. Birkemoe.....	65
ULTIMATE BEHAVIOUR OF CIRCULAR TUBULAR MEMBERS WITH LARGE INITIAL IMPERFECTIONS J. Taby and T. Moan	79
ULTIMATE CAPACITY OF DAMAGED TUBULAR BEAM COLUMNS: AN EXPERIMENTAL STUDY I. Lotsberg and P. C. Birkemoe.....	105
STUDY OF CARRYING CAPACITY OF FABRICATED TUBULAR COLUMNS UNDER AXIAL COMPRESSION X. M. Yang, G. Z. Wang and S. F. Li	113

STIFFENED CYLINDRICAL MEMBERS - (TG-22)

APPLICATION OF THE NUMERICAL INTEGRATION METHOD TO STABILITY OF RING-STIFFENED CYLINDERS J. E. Goldberg and D. V. Pathak	125
RETROFITTING OF A LOCALLY BUCKLED TUBULAR COLUMN A. Ostapenko and S. C. Apte.....	135

STABILITY UNDER SEISMIC LOADING - (TG-24)

THE EFFECT OF ELASTIC SUPPORT AND SHEAR DEFORMATION ON STATIC AND DYNAMIC CHARACTERISTICS F. Y. Cheng and C. P. Pantelides.....	149
STUDY ON A STRUCTURAL STEEL FRAMEWORK DAMAGED BY THE 1985 MEXICO EARTHQUAKE T. Yamada, K. Tagawa and Y. Nakamura	163
BRACE FAILURES AND COLUMN BUCKLING IN STEEL STRUCTURES S. C. Goel and X. Tang.....	175

CONNECTION RESTRAINT CHARACTERISTICS - (TG-25)

COMPRESSIVE TESTS OF GUSSET PLATE CONNECTIONS	
J. J. Cheng and S. Z. Hu	191

STABILITY OF ANGLE STRUTS - (TG-26)

CONCENTRIC AXIALLY COMPRESSED ANGLE COLUMNS -- COMPARISON OF EXPERIMENTAL AND CALCULATED FAILURE STRESSES	
M. K. S. Madugula and S. Mohan	205
THE INTERCONNECTION OF WIDELY SPACED ANGLES	
M. C. Temple and J. C. Tan	221

PLATE & BOX GIRDERS - (TG-27)

STABILITY OF STEEL BOX GIRDERS RESULTING FROM MODEL STUDIES	
Z. Manko	233
APPLICATION OF THE FINITE STRIPS METHOD TO STEEL BOX GIRDERS STABILITY ANALYSIS	
Z. Manko	245

"STABILITY OF CIRCULAR STIFFENED SHELLS"AFTERNOON THEME SESSION

SSRC 4TH EDITION OF GUIDE - CHAPTER ON STIFFENED CYLINDERS	
D. R. Sherman	259
ON THE BEHAVIOR OF DAMAGED AND INTACT STIFFENED CYLINDRICAL SHELLS	
P. J. Dowling and B. F. Ronalds	265

AFTERNOON THEME SESSION (Continued)

STRENGTH OF DAMAGED RING STIFFENED CYLINDERS SUBJECTED TO SIMULTANEOUS EXTERNAL PRESSURE AND AXIAL COMPRESSIVE LOADING A. C. Walker, S. McCall and M. K. Kwok	275
API BULLETIN 2U INTERACTION EQUATION FOR STIFFENED CYLINDERS SUBJECTED TO AXIAL COMPRESSION AND EXTERNAL PRESSURE C. D. Miller and J. F. Vojta.....	287
GENERAL BUCKLING OF RING AND STRINGER STIFFENED CYLINDERS T. H. Soreide, S. Valsgard and B. Brodtkorb.....	299

EVENING PANEL DISCUSSION

STABILITY OF CIRCULAR STIFFENED SHELLS FROM RESEARCH TO PRACTICE - INCORPORATING RESEARCH INTO CERTIFICATION STANDARDS J. E. Herz	325
DEVELOPMENT OF API BULLETIN 2U FOR STABILITY DESIGN OF CYLINDRICAL SHELLS R. K. Kinra.....	329
<i>List of Attendees</i>	343
<i>Contributor Index</i>	351
<i>Name Index</i>	353
<i>Subject Index</i>	357

BEHAVIOR AND STRENGTH OF NONPROPORTIONALLY LOADED IMPERFECT
BEAM-COLUMNS RESTRAINED PARTIALLY

Zia Razzaq and Siva Prasad Darbhamalla
Old Dominion University
Norfolk, Virginia 23508

INTRODUCTION

Beam-column research in the past has been heavily oriented toward studies based on proportional loadings (Refs. 2,3, and 5). Thus, the axial force and bending moments are all increased simultaneously in a proportional manner until the load-carrying capacity of the member is reached. The results of a preliminary study of four different nonproportional load paths for uniaxially loaded beam-columns have been presented previously by the authors (Ref. 4). In the present paper, a detailed theoretical study is summarized for both uniaxially and biaxially loaded I-section beam-columns subjected to various load paths. For the biaxially loaded beam-columns, the torsional effects are neglected in this study. The torsional effects may be negligible when width-to-depth ratio of a wide-flange section is nearly 1.0 as shown by Sharma and Gaylord (Ref. 6) in a study of biaxially loaded beam-columns subjected to proportional loading. The behavior of beam-columns is explained in the presence of residual stresses, initial out-of-straightness, rotational end restraints, and material unloading. Also, strength interaction curves are obtained and compared to those based on the tangent modulus theory.

PROBLEM DEFINITION

Figure 1 shows an imperfect beam-column with biaxial partial rotational end restraints subjected to an axial load P and external equal end moments M_x and M_y . The rotational end restraints have linear characteristics with stiffnesses k_x and k_y about the x and y axes. The initial out-of-straightness in the xz and yz planes is represented by u_1 and v_1 , respectively, and assumed as half-sine waves each having an amplitude of $L/1,000$. The material of the beam-column is elastic-perfectly-plastic with $E=29,000$ ksi and a yield stress of 36 ksi. Lehigh-type initial residual stresses are adopted (Ref. 5) with a maximum compressive residual stress of 0.3 times the material yield stress.

UNIAXIALLY LOADED BEAM-COLUMNS

The study presented in Ref. 4 by the authors showed that major axis response of beam-columns is not load path dependant for all practical purposes. Also, it was found that the minor axis response is load path dependant when elastic rotational restraints are used. Therefore, in the detailed study presented herein, beam-columns are loaded about the minor axis in the presence of elastic partial rotational equal end restraints.

Table 1 summarizes the maximum external loads for uniaxially loaded

imperfect W8x31 beam-columns with partial rotational equal end restraints subjected to two different load paths. A total of six beam-columns numbered 1 through 6 are investigated to encompass three lengths ($L=8, 12,$ and 16 ft.), and two end restraint stiffnesses, k_2 and k_3 , given by:

$$k_2 = 13,333 \text{ in-kip/rad}$$

$$k_3 = 24,000 \text{ in-kip/rad}$$

These k values were used previously by the authors (Ref. 5) in a restraint modelling effect study on the strength of beam-columns. The pinned-end members do not exhibit significant elastic unloading and are not included here. The behavior of fixed-end members is qualitatively similar to those with $k=k_3$. In this and subsequent tables and figures, p and m are the dimensionless axial load, and moment values, respectively. The axial load is nondimensionalized by the cross-sectional squash load, P_y . The major axis moment is nondimensionalized relative to the major axis yield moment, M_{YX} , while the minor axis moment is nondimensionalized relative to the minor axis yield moment, M_{Yy} , of the cross section.

The two different load paths adopted are designated as LP m-p and LP p-m and are defined as follows:

LP m-p : Load path in which the external equal end moment M_y is applied first incrementally and held constant, followed by a gradually increasing axial load P until the member load-carrying capacity is reached.

LP p-m : The axial load corresponding to the load carrying capacity obtained in LP m-p is applied first incrementally and held constant, followed by gradually increasing equal end moments until the member load-carrying capacity is reached.

The maximum external loads p and m for the various beam-columns analyzed are given in Table 1 and plotted in Figures 2 through 4 in the form of interaction curves between p and m . The corresponding tangent modulus curves were also obtained for LP m-p and included in these figures for comparison.

Figure 2 for $L=8$ ft. shows that for the intermediate p and m values, LP m-p results in peak loads higher than those obtained by LP p-m. This is because significant material unloading takes place when LP m-p is used. The tangent modulus curve is, surprisingly, unconservative for a substantial range of p and m values. These conclusions may not necessarily be valid for other values of L as seen from the interaction curves in Figures 3 and 4 for $L=12$ and 16 ft., respectively. In Figure 3, LP m-p curve results in peak loads lower than those obtained by LP p-m when p is relatively large, whereas the converse is true for smaller p values. The tangent modulus curve is conservative as compared to the curve for LP m-p. However, it is unconservative compared to the LP p-m curve when m is relatively large. The interaction curves in Figure 4 with $L=16$ ft. exhibit similar character as those in Figure 3, except that the tangent modulus curve is unconservative for relatively large values of m compared to the curves for both the load paths.

BIAXIALLY LOADED BEAM-COLUMNS

Table 2 shows a comparison of predicted p values and those published in References 1 and 6 for pinned-end beam-columns subjected to a biaxially eccentric load. The cross section, length, and the equal end eccentricities e_x and e_y of the load for the beam-columns are also given in this table. The results from Reference 1 are based on an experimental investigation, whereas those from Reference 6 are theoretical. The ratio of predicted to the reference maximum p values is given in the last column. Clearly, the results are in good agreement.

Table 3 gives the maximum external loads for biaxially loaded imperfect W8x31 beam-columns ($L=12$ ft.) with partial rotational equal end restraints subjected to various load paths. The biaxial end moments m_x and m_y are applied simultaneously while holding their ratio proportional to the ratio of the sectional radii of gyration about the respective axes, that is,

$$m_x/m_y = r_x/r_y.$$

The results given in this table are plotted in Figure 5 in the form of interaction curves between p and m_x . The moment m_x can be found using the equation given above. The LP m - p curve is above the LP p - m curve for the entire range of p and m values. However, the tangent modulus interaction curve with LP m - p is found to be quite unconservative for a considerable range of the peak loads. A plausible explanation for this phenomenon could be as follows. The tangent modulus approach results in a more "ductile" behavior than that obtained with the analysis which includes material unloading. Although it may appear that such ductile response would lead to a conservative set of peak loads, it may also result in a fictitious distribution of strains in the member particularly in the presence of rotational end restraints. The approach based on material unloading is free of such fictitious strains, thus the ensuing deflections are correct, which following the principle of least work must therefore result in lower peak loads. However, this type of behavior is not observed when relatively large axial load or large end moments are applied since in these cases the P - Δ effects are less predominant in comparison to those encountered in the "intermediate" range of p and m values.

CONCLUSIONS

The effect of various load paths on the behavior and strength of beam-columns loaded uniaxially about the minor axis is more pronounced than that on the biaxially loaded ones. Neglecting significant material unloading due to nonproportional loads may lead to unconservative estimation of the load-carrying capacities of beam-columns. Thus, the tangent modulus approach is found to be unconservative for a number of uniaxially loaded beam-columns. Even a greater degree of unconservativeness is noticed for the biaxially loaded beam-columns studied herein.

REFERENCES

1. Birnstiel, C., " Experiments on H-Columns Under Biaxial Bending," Journal of the Structural Division, ASCE, Vol. 94, No. ST10, October, 1968.
2. Chen, W. F., and Atsuta, T., Theory of Beam-Columns, Volume 2, McGraw-Hill Inc., New York, 1977.
3. Johnston, B. G., (ed.), Guide to Stability Design Criteria for Metal Structures, Wiley, New York, 1976.
4. Razzaq, Z., and Darbhamaulla, S. P., " Nonproportionally Loaded Elasto-Plastic Steel Beam-Columns Restrained Partially," Presented in the International Conference on Steel Structures, Budva, Yugoslavia, September 28- October 1, 1986 (submitted for publication).
5. Razzaq, Z., and Darbhamaulla, S. P., " Restraint Modelling Effect on Beam-Column Strength," Annual Technical Session, SSRC, Washington D.C., Proceedings, SSRC, April 15-16, 1986.
6. Sharma, S. S., and Gaylord, E. H., " Strength of Steel Beam-Columns with Biaxially Eccentric Load," Journal of the Structural Division, ASCE, Vol. 95, No. ST12, December, 1969.

Table 1 Maximum external loads for uniaxially loaded imperfect beam-columns with partial rotational equal end restraints and various load paths (W 8x31).

Beam-column	L (ft.)	k	Load path (LP)		Maximum External Loads				
1	8	k_2	m-p	p	0.000	0.075	0.737	0.961	--
				m	3.211	3.000	1.500	0.000	--
			p-m	p	0.000	0.075	0.737	0.961	--
				m	3.211	2.990	1.733	0.000	--
2	8	k_3	m-p	p	0.000	0.169	0.669	0.865	0.958
				m	4.689	4.000	2.500	1.000	0.000
			p-m	p	0.000	0.169	0.669	0.865	0.958
				m	4.689	4.190	2.155	1.114	0.084
3	12	k_2	m-p	p	0.000	0.238	0.749	0.867	--
				m	3.736	3.000	1.500	0.001	--
			p-m	p	0.000	0.238	0.749	0.867	--
				m	3.736	3.344	0.845	0.144	--
4	12	k_3	m-p	p	0.000	0.360	0.550	0.744	0.893
				m	5.014	4.500	3.000	1.500	0.000
			p-m	p	0.000	0.360	0.550	0.744	0.893
				m	5.014	3.842	3.476	1.825	0.258
5	16	k_2	m-p	p	0.000	0.182	0.273	0.496	0.751
				m	5.561	4.500	3.000	1.500	0.000
			p-m	p	0.000	0.182	0.273	0.496	0.751
				m	5.561	3.032	3.590	1.593	0.007
6	16	k_3	m-p	p	0.000	0.100	0.352	0.649	0.795
				m	6.983	6.000	4.500	1.500	0.000
			p-m	p	0.000	0.100	0.352	0.649	0.795
				m	6.983	5.483	3.923	2.087	0.386

Table 2 Comparison of predicted and previously published maximum loads for pinned-end beam-columns with biaxially eccentric load*.

Reference number	Cross section	L (in.)	e_x (in.)	e_y (in.)	p		$\frac{p \text{ predicted}}{p \text{ reference}}$
					Predicted	Reference	
1	H 6x6	96	1.61	2.78	0.426	0.421	1.01
1	H 5x5	120	2.38	2.51	0.284	0.297	0.96
6	W 12x65	180	18.40	3.76	0.186	0.199	0.93
6	W 12x65	270	18.40	3.76	0.167	0.169	0.99
6	W 12x65	360	18.40	3.76	0.149	0.144	0.97

$$* m_x = Pe_x / M_{yx} ; m_y = Pe_y / M_{yy}$$

Table 3 Maximum external loads for biaxially loaded imperfect beam-columns with partial rotational equal end restraints and various load paths (L=12 ft. ; W 8x31).

Beam-column	k	Load path (LP)	Maximum External Loads					
			p	m_x	m_y	m_x	m_y	m_x
7	k_2	m-p	p	0.000	0.251	0.525	0.876	0.869
			m_x	1.078	0.864	0.405	0.070	0.000
			m_y	0.631	0.506	0.237	0.041	0.000
		p-m	p	0.000	0.250	0.500	0.750	0.869
		m_x	1.078	0.864	0.405	0.070	0.000	
		m_y	0.631	0.506	0.237	0.041	0.000	
8	k_3	m-p	p	0.000	0.276	0.503	0.919	0.904
			m_x	1.255	0.952	0.471	0.039	0.000
			m_y	0.735	0.558	0.276	0.023	0.000
		p-m	p	0.000	0.250	0.500	0.750	0.904
		m_x	1.255	0.952	0.471	0.039	0.000	
		m_y	0.735	0.558	0.276	0.023	0.000	

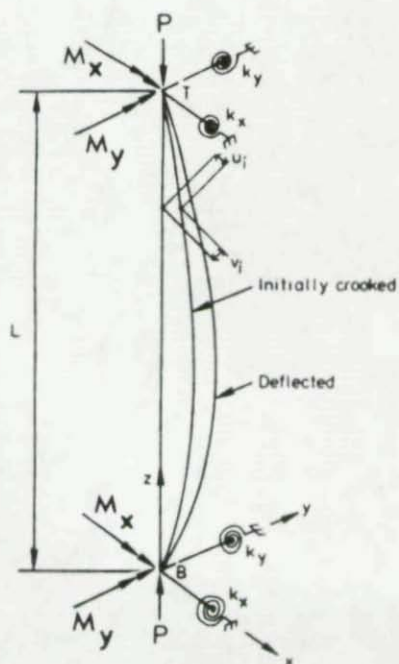


Figure 1 Imperfect Beam-Column with Biaxial Restraints

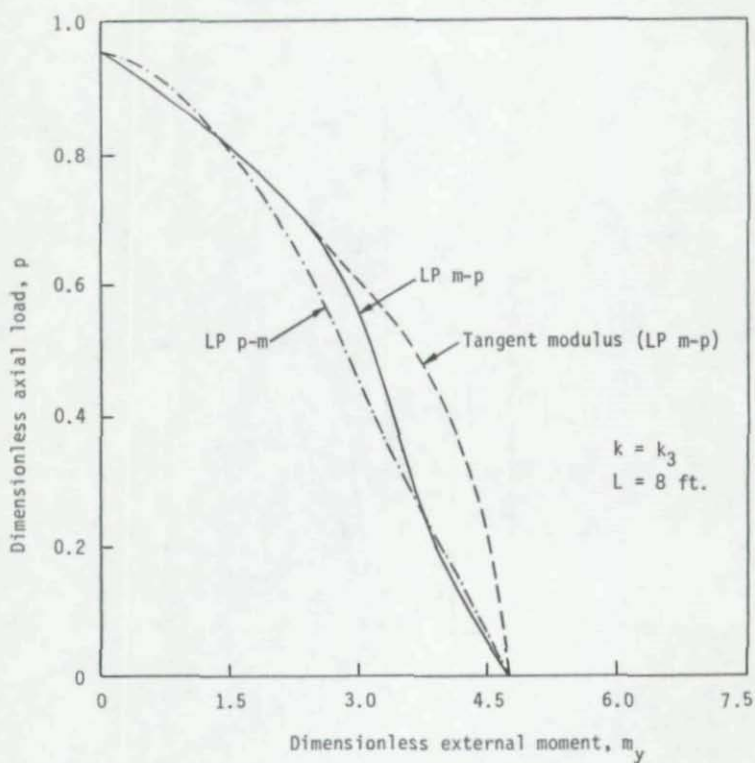


Figure 2 Interaction Curves for Uniaxially Loaded Partially Restrained Beam-Column 2

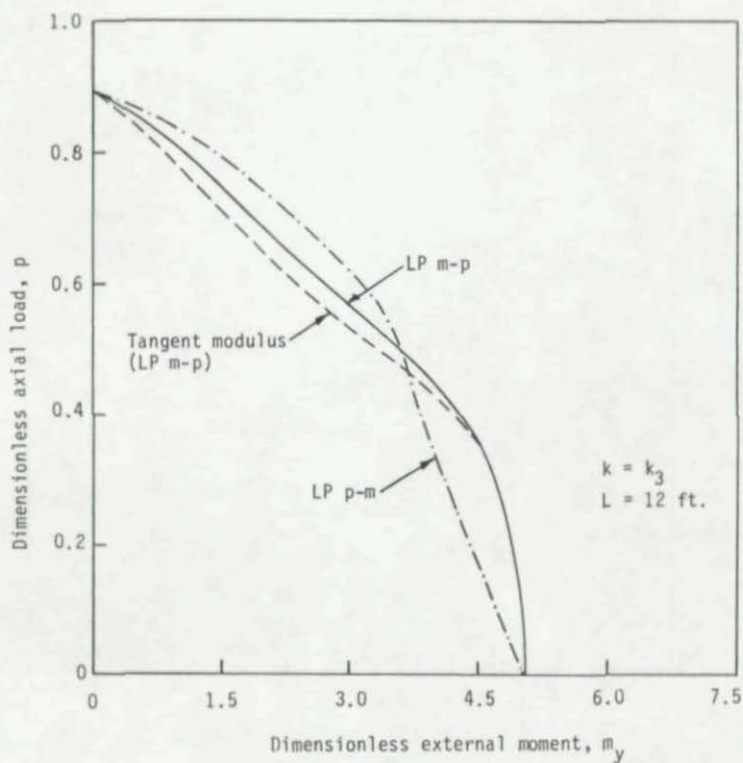


Figure 3 Interaction Curves for Uniaxially Loaded Partially Restrained Beam-Column 4

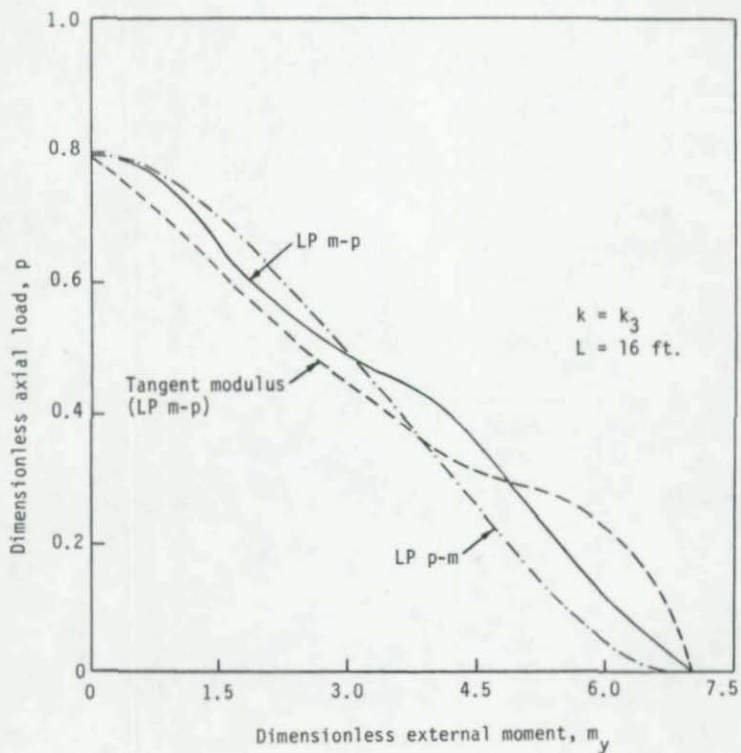


Figure 4 Interaction Curves for Uniaxially Loaded Partially Restrained Beam-Column 6

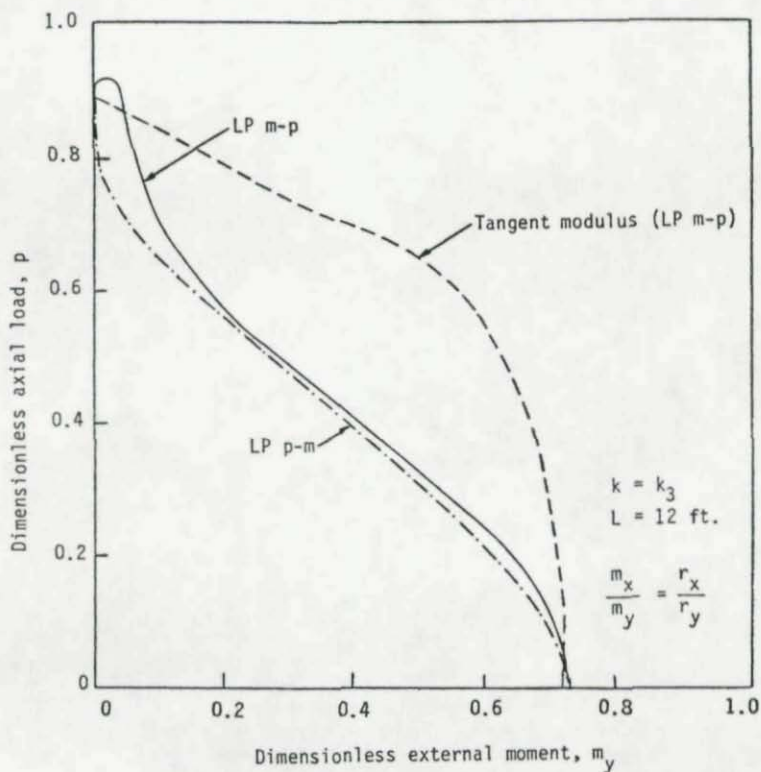
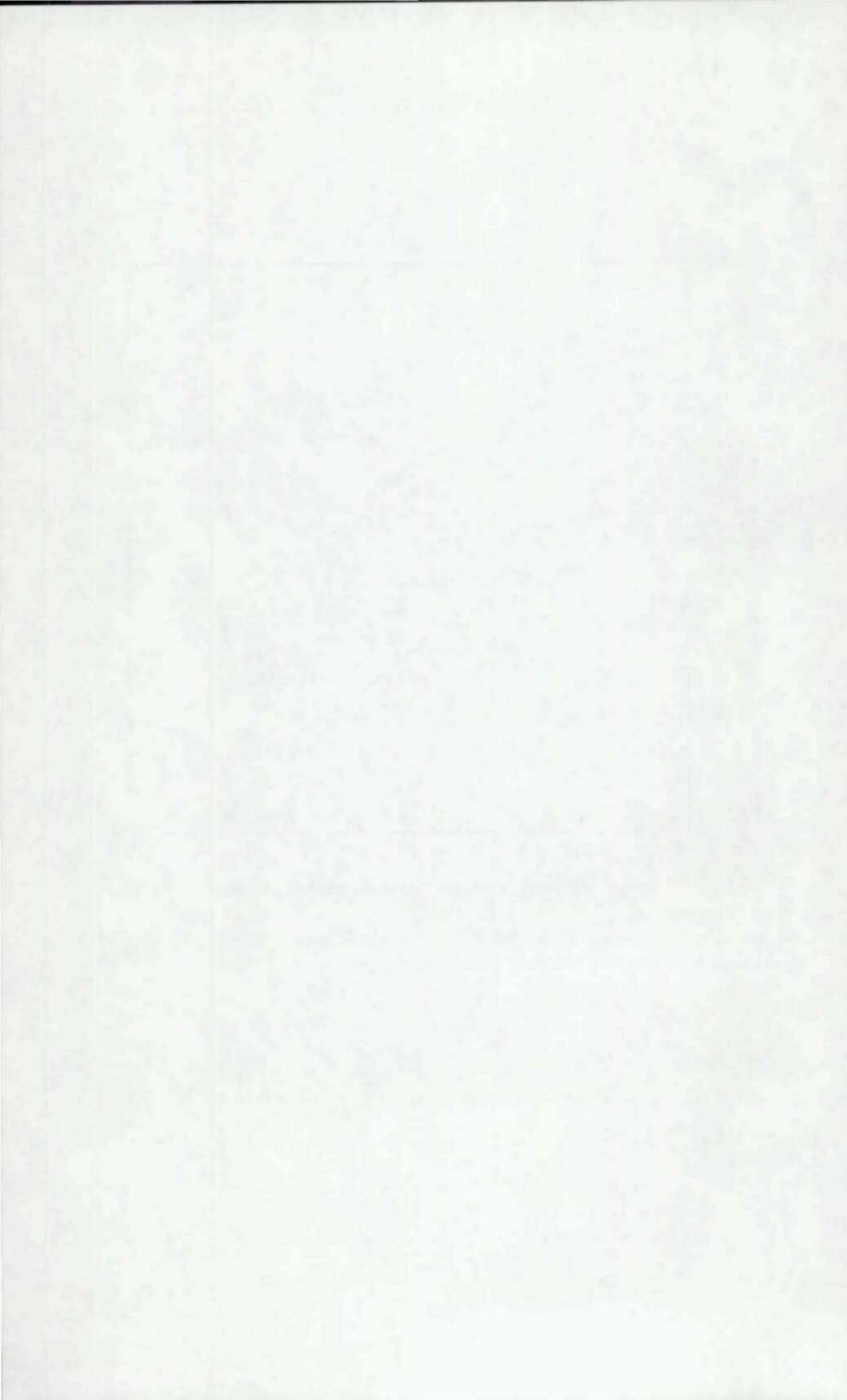


Figure 5 Interaction Curves for Biaxially Loaded Partially Restrained Beam-Column 8



DYNAMIC INSTABILITY OF
FRAMES HAVING THINWALLED COLUMNS

By Srinivasan Sridharan and M. Ashraf Ali
Department of Civil Engineering
Washington University in St. Louis, MO

SUMMARY

Dynamic instability of single story frames having thin-walled columns has been investigated. The lateral loads sustained by the frame are step loads, while the axial loads are deemed to be quasi-statically applied. The analytical model employed by the authors has the capability of modelling the combined action of two "companion" local modes whose amplitudes are variable along the length of the column and any type of end conditions of the members.

For given levels of axial loads sustained by the columns, the magnitudes of lateral loads causing instability can be significantly smaller than those corresponding to static buckling, provided the dynamic load is of sufficient duration. There exists, however, a threshold value of axial force carried by the columns, below which there is no elastic instability - static or dynamic.

For columns with overall critical loads several times greater than the local critical load, there is no danger of elastic instability, but the deflections under dynamic lateral loads of less than 1% of the axial load may reach such huge values that there is a serious danger of localized plastic collapse. It is also shown that moment frames having thin-walled columns such as fabricated out of cold formed steel are extremely vulnerable to moderate seismic excitations.

INTRODUCTION

Local buckling and the interaction of local with overall buckling are primary considerations in the design of thinwalled columns. A serious consequence of local buckling is the reduction of stiffness of the column-section in its resistance to bending. Thus overall buckling occurs at a load much smaller than the Euler critical load of the column. The phenomenon is known to be imperfection-sensitive when the ratio (α) of the overall critical stress (σ_0) to the local critical stress (σ_1) is close to unity.¹⁻³

The utilization of the postbuckling strength of plate elements in the design of the thin-walled columns such as made of coldformed steel is not therefore possible without mastering the associated problem of interactive buckling. In a recent paper⁴ the authors have discussed a state of the art analytical model for the interactive buckling problem. The model is primarily intended for doubly symmetric column sections. Extension to more general cross-sectional shapes has been accomplished recently⁵, but in the present paper attention is restricted to the doubly symmetric case. Features of this model will be briefly recapitulated in this paper.

In the present paper the dynamic behavior of thinwalled columns is investigated using the interactive buckling model developed by the authors. Axial compression is considered to be the primary source of instability and the dynamic response is triggered by suddenly applied lateral loads. The analytical model employed has the capability of modelling the action of two "companion" local modes whose amplitudes are variable along the length of the column and can depict any type of end conditions. Thus the interactive buckling in members of frameworks can be studied. For simplicity, attention is confined in the present study to a single story frame consisting of two flexible thin walled columns connected by a rigid member. Buckling under

step loading and base excitation is studied. Comparisons are made with the static case wherever applicable.

THEORY

Features of the new analytical model

The essential features of the new analytical model are summarized in the sequel. For a detailed treatment, the interested reader is referred to ref. 4 and 5:

1. The interaction of overall bending/buckling of the column with the local buckling mode associated with the lowest critical stress (σ_1) - henceforth called the "primary local mode" - triggers a secondary local buckling mode having the same wavelength as the primary one. In a realistic interactive buckling analysis of a doubly symmetric compression member, these "companion" modes must be considered together. If the primary mode is symmetric (antisymmetric) with respect to the axis of bending, then the secondary mode is antisymmetric (symmetric) with respect to the same axis. This feature was demonstrated in ref. (4) and (6). Thus, the new analytical model incorporates the two companion local modes.
2. The amplitudes of the two local modes do not remain constant, but must be given freedom to vary along the length of the member. This phenomenon of "amplitude modulation" is demonstrated in ref. (4) and is accounted for in the model in an elegant manner using the concept of a "slowly varying" function first introduced by Koiter (7).
3. The model employs a new beam element which has cubic polynomial shape functions for the description of overall axial and lateral displacements and linear variations for the functions modulating the local amplitudes. The cross-sectional deformations as given by the

local modes together with the associated second order fields are duly embedded into the element. The description of overall displacements in terms of a F.E. model makes it possible to deal with arbitrarily prescribed end-conditions and to account for changes in the overall displacement profile which occur due to interaction with the local modes under continued loading.

EXAMPLES

Simplified model of a single story frame (Fig. 1) consisting of two columns connected by a rigid beam at their top levels is the example studied in this paper. The frame is deemed to carry axial loads of P applied to each column and a lateral load Q applied at the level of the beam. While P is deemed to be always applied statically and prior to Q , the latter may be applied statically or dynamically. This situation is typical of frames in thin-walled metal buildings. The relationship between P and $Q(Q_s)$ in the context of static instability was touched upon in ref. 4. A similar relationship between P and a suddenly applied (step load) $Q(Q_d)$ is investigated in the present paper. The instability in this case is one in which the frame would lose its ability to oscillate and exhibit divergence - the characteristic mode of dynamic instability of conservative systems. In the example, the frame is deemed to carry masses at the level of the beam each equal to P/g (Fig. 1) where P is the axial load carried by the columns and given in gravitational units and g is the acceleration due to gravity. These masses are due to the dead weight of the super structure supported by the columns. The material is assumed to be structural steel with $E = 30,000$ ksi, $\nu = 0.3$, specific gravity of 7.32. In all the calculations reported herein, the column was divided into 5 elements. For the extraction of the eigen modes and the second order fields, advantage is

taken of the symmetry and 24 strip elements were used over half the column. These have been shown to be adequate to obtain results of engineering accuracy.⁵

I-section column

Fig. 2(a) shows the cross-sectional details of the column and 2(b-c) the local modes of buckling. The lateral loading is applied so as to cause bending about the weaker axis. An initial imperfection in the shape of the primary local buckling mode with a maximum amplitude of $0.1t$ is assumed for the column. In all the calculations 't' was set to be 0.1 in. and this value is typical for cold formed sheet steel. For a column length of $2000t$ ($\alpha = 1.06$) the natural period of overall oscillations of the frame including the superimposed masses works out to be 4.7 sec and 6.4 sec respectively for P/P_{c1} equal 0.60 and 0.76. (P_{c1} is the critical load corresponding to the primary local buckling mode). A time step of 0.5 sec was found to yield sufficiently accurate results for the deflections and produced convergence in 2-4 iterations in all the cases investigated.

The dynamic response for $Q < Q_d$ is illustrated in Fig. 3. The axial load on the columns is $0.6 P_{c1}$ and $Q/Q_d = 0.44$ ($Q_d = 0.101$ kips). It is found that the structure has an oscillatory response. Unlike in the linear problem, the maximum amplitudes are more than twice the corresponding static deflections. This is because of the increasing loss of stiffness due to local buckling of the structure with increasing deflections. Note that the local modes are driven by the overall bending and their frequencies coincide with that of the overall oscillation of the frame. Note also that the deflections in the form of secondary local mode vanish as the structure returns to its straight configuration. To lateral loads equal or greater

than the critical local Q_d , the structure responds by deflections which increase indefinitely with time (not illustrated).

Fig. 4(a-b) shows the relationship between P/P_{c_1} and Q_d/P_{c_1} for two cases, with lengths of 2000t ($\alpha = 1.06$, case (a)) and 1760t ($\alpha = 1.37$, case (b)) respectively. For each case the corresponding relationship between P/P_{c_1} and Q_s/P_{c_1} is also shown in the Fig. 4(a-b). Note that Q_s and Q_d are the lateral loads corresponding to elastic instability (static and dynamic respectively) with no limit set on the yield stress σ_y of the material.

From Fig. 4(a-b) it is seen that there is a threshold value of axial load below which no elastic buckling - static or dynamic - occurs. In this range column responds to the lateral load by developing deflections (static case) and oscillations (dynamic case). The deflections and the amplitudes of oscillations increase indefinitely with Q . Column thus behaves like a solid Euler column with a reduced critical load.

For values of axial loads above the threshold value, Q_s is always found to be greater than Q_d . Fig. 4(a-b) also plots ψ , the reduction due to the suddenness of application of the lateral load expressed as a percentage of Q_s , (i.e. $\psi = (1 - Q_d/Q_s) \times 100$) against P/P_{c_1} . As the axial load increases both Q_s and Q_d approach zero but at differing rates. For a value of axial load about 70% of P_{c_1} , the percentage reduction ψ , in the case of column (a) is seen to be about 28% - a significant reduction which should be important in design.

Though qualitatively similar, the behavior of columns (a) and (b) differ from each other noticeably. The range of P/P_{c_1} over which elastic buckling is a problem in the presence of the lateral load reduces to 0.19,

($0.91 > P/P_{c_1} > 0.72$) for the shorter column (b) from 0.26 ($0.81 > P/P_{c_1} > 0.55$) of column (a). As the length decreases further, there is a continued reduction of this range (not illustrated). There occurs too a reduction in the values of ψ for column (b) over the entire range over which dynamic instability is a problem.

Seismic Response:

The same frame (with I-section columns, case (a)) is now investigated for seismic response. An idealized ground acceleration with a peak value of 20 in/sec^2 ($\approx 0.05g$) is considered (Fig. 5a). The total duration of the earthquake is assumed to be 3 sec. The column carries an axial load of $P = 0.6P_{c_1}$. In Fig. 5b the lateral displacement at the top of the column (W_{\max}) is plotted against time, \bar{t} . Note that the irregularity in the response at $\bar{t} = 3$ sec is due to the transition from forced vibration to the free vibration phase. The structure oscillates freely reaching deflections of more than $L/50$. The peaks of local buckling amplitude once again, synchronize with those of the lateral displacement. Note that the period of vibration is more than twice the period of vibration of the frame which is obtained neglecting the local buckling deformation.

Even though the frame vibrates without apparently losing its stability, the stresses at critical sections as given by the elastic analysis reach such magnitudes as may very well cause yielding in practice. At time $\bar{t} = 4.5$ sec, the frame reaches its first peak of displacement. It is found that with $\sigma_y = 50 \text{ ksi}$, most of the flange would have yielded in compression or tension. Thus there exists a potential danger of collapse due to frequent excursions of the material into the plastic range. The analysis is repeated twice, in one case increasing the peak ground

acceleration to 30 in/sec^2 ($\approx 0.078 \text{ g}$) (case (ii)) and in the other keeping the ground acceleration as 0.05g but increasing the axial load P to $0.644 P_{c1}$ (case (iii)). In either case, the structure becomes dynamically unstable developing displacements which increase indefinitely with time.

CONCLUSIONS

Dynamic instability of single story frames having thin-walled columns has been investigated. The lateral loads sustained by the frame are dynamic in character, while the axial loads are deemed to be quasi-statically applied.

Under lateral step loads (of infinite duration) the frames develop divergence type of instability at loads which can be significantly smaller than the corresponding static load causing instability. However there exists a threshold value of the axial force carried by the columns, below which there is no elastic instability, static or dynamic. The elastic behavior of the columns is controlled by the two parameters α and γ .

For columns with $\alpha \gg 1$, there is no danger of elastic instability, but the deflections under dynamic lateral loads of less than 1% of axial load may reach such huge values as may very well precipitate localized plastic collapse.

Moment frames having thin walled columns such as made up of cold formed steel are seen to be extremely vulnerable to moderate seismic excitations. The full seriousness of the problem can, however, be clearly quantified only by studying the collapse behavior with plasticity duly accounted for.

ACKNOWLEDGMENT

The work reported in this paper was funded by a grant from the National Science Foundation (Grant No. CEE-8318423). Any opinions expressed herein are solely the responsibility of the authors and do not necessarily reflect those of the NSF.

REFERENCES

1. W. T. Koiter and M. Skaloud, "Interventions", *compartiment Post-critique des Plaques Utilisees en construction Memoires de la Societe Royale des Sciences de Liege; 5^{me} Serie*, vol. VII, fasc. 5, pp. 64-68, 103-104, (1963).
2. V. Tvergaard "Imperfection-Sensitivity of a wide Integrally Stiffened Panel under Compression" *Int-J. Solids and Structures*, vol. 9, pp. 177-192 (1973).
3. Benito, R. and Sridharan, S. "Interactive Buckling Analysis with Finite strips", *International Journal for Numerical Methods in Engineering*, vol. 21, pp. 145-161 (1985).
4. S. Sridharan and M. Ashraf Ali "Interactive Buckling in Thin-walled Beam-Columns", *Journal of Engineering Mechanics, ASCE*, Vol. III, No. 12, pp. 1670-1486, (1985).
5. M. Ashraf Ali, "A New Analytic Model for Elastic Interactive Buckling", Thesis Submitted to Washington University in partial fulfillment of the requirements for the D.Sc. Degree, Dec. 1986.
6. S. Sridharan and M. Ashraf Ali "An Improved Interactive Buckling Analysis of Thin-walled Columns Having Coubly Symmetric Sections" *International Journal of Solids and Structures*, Vol. 22, No. 4, pp. 429-443 (1986).

7. W. T. Koiter and M. Pignataro "An Alternate Approach to the Interaction Between Local and Overall Buckling in Stiffened Panels", IUTAM Symposium, Cambridge, MA (1974), ("Buckling of Structures", B. Budiansky, Ed., Springer Verlag, 1976, pp. 133-148).

APPENDIX I: NOTATION

E	:	Young's modulus
L	:	Length of column
P	:	Axial load carried by column
P_{c_1}	:	Critical value of P corresponding to local buckling in the primary mode
Q	:	Lateral load carried by frame
Q_s	:	Static lateral load causing elastic instability
Q_d	:	Dynamic lateral load causing elastic instability
W_{max}	:	Maximum value of W, the lateral displacement of the column
g	:	Acceleration due to gravity
α	:	σ_0/σ_1
ξ_1, ξ_2	:	Amplitudes of the primary and secondary local modes respectively
σ_0	:	The critical stress corresponding to overall buckling
σ_1, σ_2	:	The critical stress corresponding to the primary and secondary local buckling modes respectively

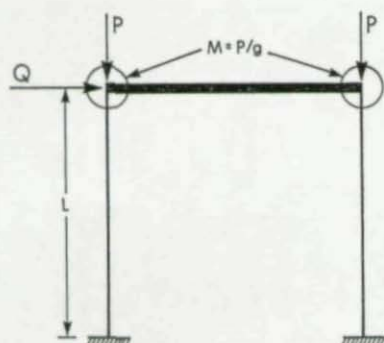


Fig. 1. The model of a single story frame: A pair of columns connected by a rigid beam.

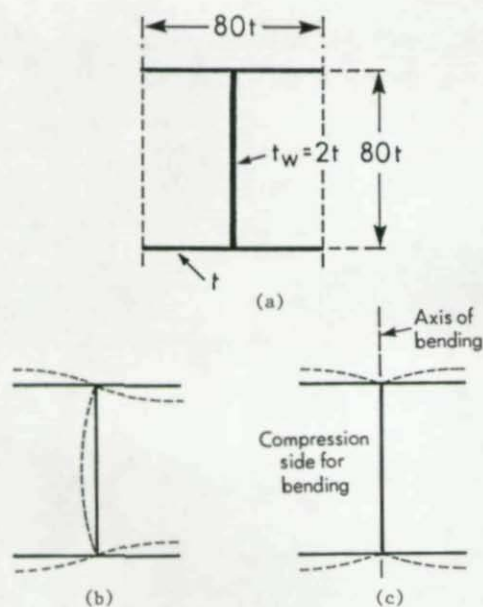


Fig. 2. (a) Cross-sectional dimensions of the column.
 (b) The primary local mode. ($\sigma_1/E = 0.621 \times 10^{-3}$; half-wave length = $80t$)
 (c) The secondary local mode. ($\sigma_2/E = 0.754 \times 10^{-3}$)

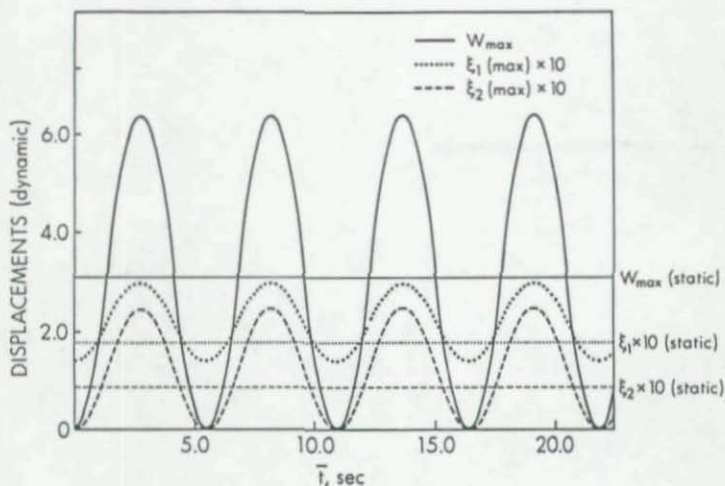


Fig. 3. Variation of the Displacements of the Frame with Time for $Q < Q_d$.

(Note that W_{max} , ξ_1 and ξ_2 are nondimensionalized by division of the corresponding displacement by 't')

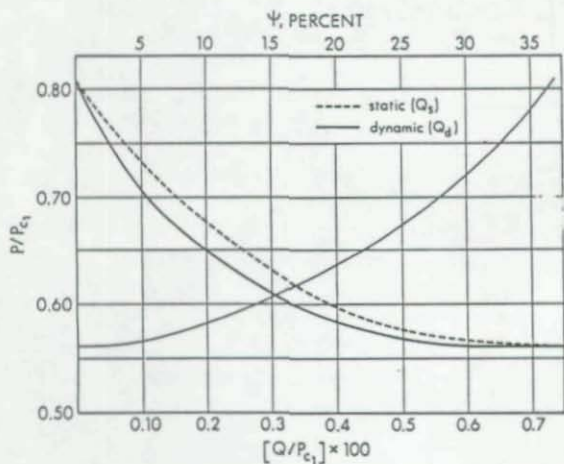


Fig. 4(a). Variation of the Lateral Load Q Causing Instability with the Axial Load P .
Case(a): $I = 2000 t$

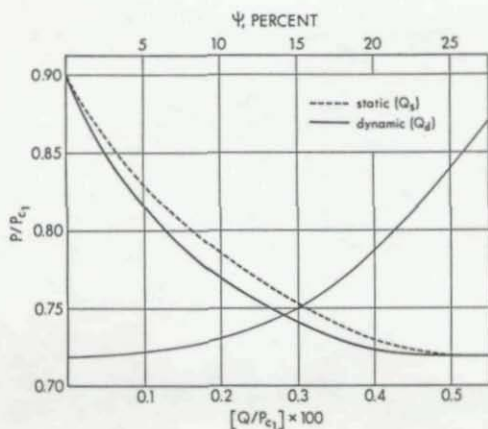


Fig. 4(b). Variation of Q (corresponding to instability) with P .
for case (ii) $L = 1760t$

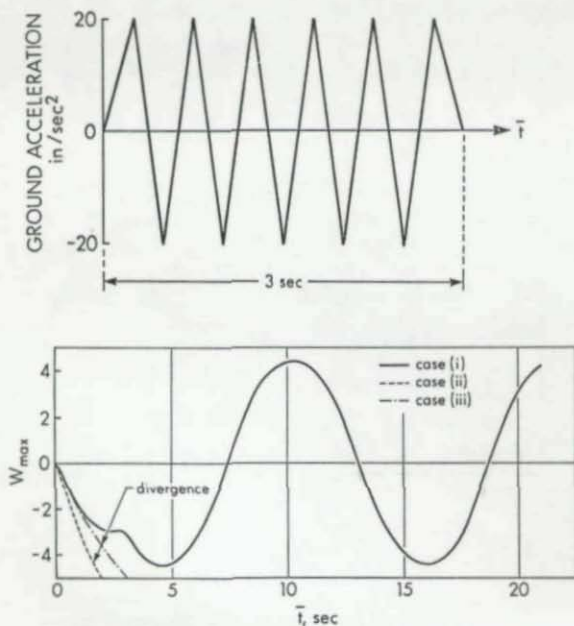
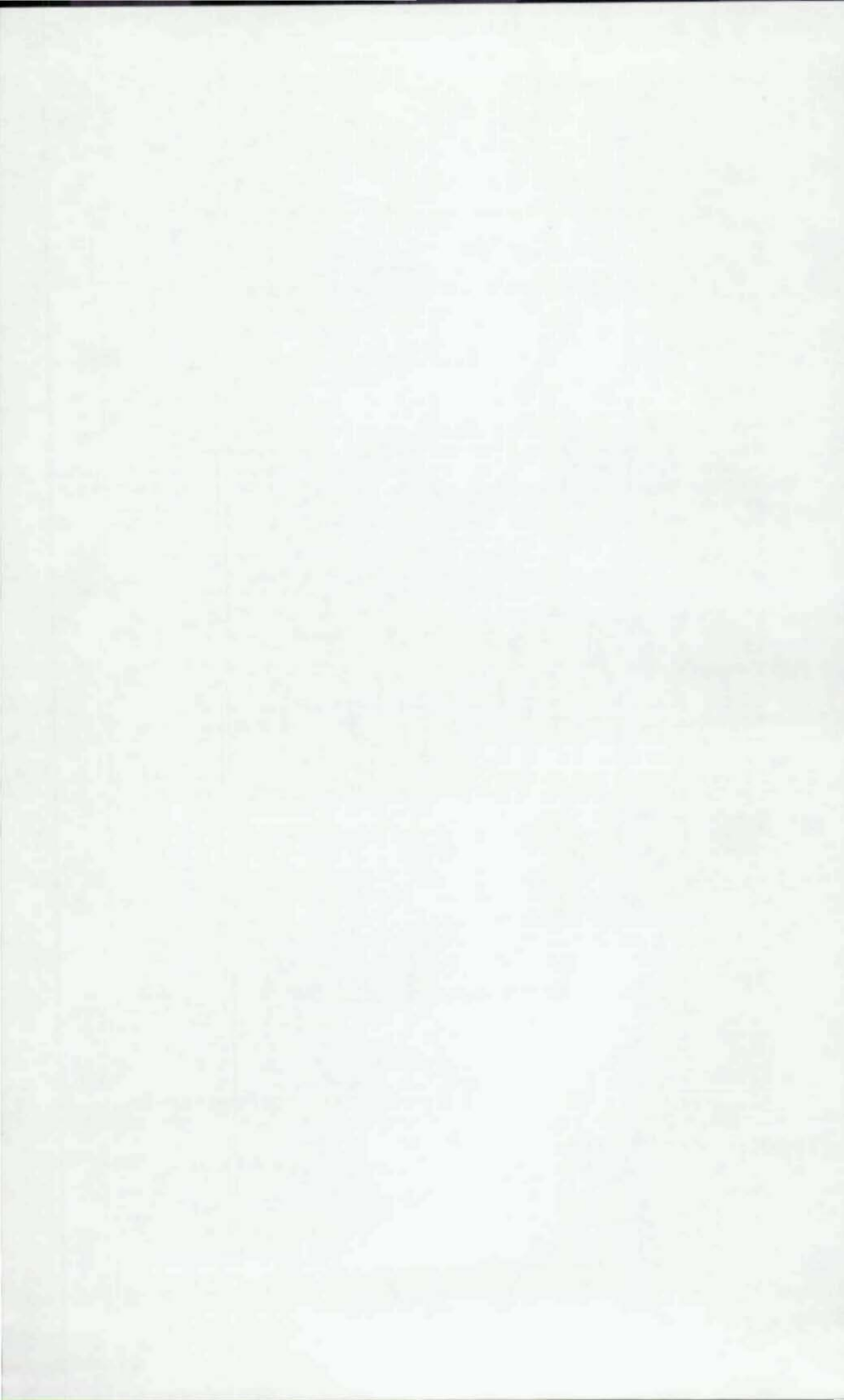


Fig. 5(a). Ground acceleration vs time. (b) The variation of W_{\max} with time.



Post-Buckling Behaviour and Effective Width
of Edge-Stiffened Plate Elements
Under Combined Compression and Bending

by

Xuhong Zhou* and Siji Wang**

SUMMARY

The post-buckling behaviour and effective width of edge-stiffened plate elements under combined compression and bending are investigated theoretically and experimentally in this paper. A semi-energy method is used. Because of the complexity in both boundary conditions and loading conditions the deflection along the transverse section is assumed to be a transcendental function similar to the vibration function of beams, whose eigenvalues are determined by the boundary conditions of the unloaded edges. The stress function can thus be solved by substituting the deflection function into von Kármán's compatibility equation. Using the principle of stationary potential energy a set of simultaneous non-linear algebraic equations for determining the parameters of the deflection function can be derived. Based on the Stowell-Ilyushin theorem, a criterion for post-buckling strength is established. Therefore, the ultimate load for such plate elements can be determined. For design purpose a simplified effective width formula is presented. Theoretical results are verified by a total of 28 cold-formed lipped channel and lipped angle column tests. The specimens are designed in various width-to-thickness ratios, aspect ratios and eccentricities. A comparison of theoretical ultimate loads with experimental results is presented and agreement is seen to be good.

INTRODUCTION

Cold-formed open sections having lips, such as lipped channels, lipped angles, hat sections etc., are widely used as structural members. The flanges or legs in such sections are commonly treated as edge-stiffened plate elements, whose ultimate strength is considerably larger than that of a unstiffened plate element of similar dimensions and material properties.

The behaviour of edge-stiffened plate elements under uniform compression were studied theoretically and experimentally by

*Research and Teaching Assistant, Dept. of Civil Engineering, Hunan Univ., Changsha, Hunan, China.

**Professor, Dept. of Civil Engineering, Hunan Univ.

Desmond, et al (1). Rhodes and Harvey examined the post-buckling behaviour of eccentrically loaded plate with the unloaded edges elastically restrained against rotation using Ritz method (2,3). However, their theoretical boundary conditions seem to be less practical than conditions of stiffened edges.

This paper is concerned with an elastic large deflection analysis of edge-stiffened plate elements under combined compression and bending. The method developed by Rhodes and Harvey (2,3) is extended in this paper.

THEORETICAL ANALYSIS

1. Basic Assumptions and Boundary Conditions

The basic assumptions made in the analysis are the following: (1) Only the elastic behaviour is considered; (2) edge stiffener is an elastically supported beam, whose effect of rotational restraints on the flange is ignored. (3) at the web-flange junction the moment applied to the flange is proportional to the rotations of the edges. (4) the unloaded edges of flange are free from normal and shear stresses. (5) the loaded edges are compressed in such a way that their in-plane movements vary linearly along the width of the plate and free from shear stresses.

The edge-stiffened plate elements in this study are shown in Fig.1. The deflected form of W is taken as

$$W = \cos \frac{\pi x}{eb} \sum_{n=1}^{\infty} A_n Y_n(y) \quad (1)$$

where $e=L/mb$, m is the number of buckle half-waves.

Applying Eq.(1), it is seen that the following boundary conditions can be obtained

$$Y_n|_{y=0} = 0 \quad (2)$$

$$Y_n'|_{y=0} = \frac{R}{b} Y_n'|_{y=b} \quad (3)$$

$$\tau_{xy}|_{y=0} = -\frac{\partial^2 F}{\partial x \partial y}|_{y=0} = 0 \quad \sigma_x|_{y=0} = \frac{\partial^2 F}{\partial x^2}|_{y=0} = 0 \quad (4)$$

$$\left[Y_n'' - \nu \left(\frac{\pi}{eb} \right)^2 Y_n \right]_{y=b} = 0 \quad (5)$$

$$\left[Y_n'' - (2-\nu) \left(\frac{\pi}{eb} \right)^2 Y_n' - \frac{EI}{D} \left(\frac{\pi}{eb} \right)^4 Y_n \right]_{y=b} = 0 \quad (6)$$

$$\tau_{xy}|_{y=b} = -\frac{\partial^2 F}{\partial x \partial y}|_{y=b} = 0 \quad \sigma_x|_{y=b} = \frac{\partial^2 F}{\partial x^2}|_{y=b} = 0 \quad (7)$$

$$\tau_{xy}|_{x=0, x/2} = -\frac{\partial^2 F}{\partial x \partial y}|_{x=0, x/2} = 0 \quad (8)$$

$$u(0) = u_1, \quad u(b) = u_2 = u_1(1-\xi) \quad \text{for case 1;} \quad (9a)$$

$$u(0) = u_2 = u_1(1-\xi), \quad u(b) = u_1 \quad \text{for case 2.} \quad (9b)$$

where R/b is defined as the rotational restraint coefficient and varies between 0 for a simply supported edge and ∞ for a clamped edge; F is airy stress function; I =moment of inertia of the cross section of stiffener about its own centroid axis parallel to the flange; τ_{xy}, σ_y = shear stress in the x-y plane

and direct stress in the y direction; $\xi = \frac{u_1 - u_2}{u_1}$.

2. Deflection Function and Stress Function

The functions of $Y_n(y)$ are chosen as vibration functions of beam of the form

$$Y_n(y) = d_{1n} \sin \frac{\lambda_n y}{b} + d_{2n} \cos \frac{\lambda_n y}{b} + d_{3n} \operatorname{sh} \frac{\lambda_n y}{b} + d_{4n} \operatorname{ch} \frac{\lambda_n y}{b} \quad (10)$$

where $d_{1n} \sim d_{4n}$ are constants to be determined.

Substituting $Y_n(y)$ into Eqs. (2), (3), (5) and (6), a series of homogeneous linear algebraic equations can thus be obtained as follows

$$d_{4n} = -d_{2n} \quad (11)$$

$$d_{1n} R + 2d_{2n} \lambda_n + d_{3n} R = 0 \quad (12)$$

$$d_{1n} \left\{ \lambda_n^2 + v \left(\frac{\pi}{e} \right)^2 \right\} \sin \lambda_n + d_{2n} \left\{ \left[\lambda_n^2 + v \left(\frac{\pi}{e} \right)^2 \right] \cos \lambda_n + \right. \\ \left. + \left[\lambda_n^2 - v \left(\frac{\pi}{e} \right)^2 \right] \operatorname{ch} \lambda_n \right\} + d_{3n} \left\{ v \left(\frac{\pi}{e} \right)^2 - \lambda_n^2 \right\} \operatorname{sh} \lambda_n = 0 \quad (13)$$

$$d_{1n} \left\{ \lambda_n^2 \cos \lambda_n + (2-v) \left(\frac{\pi}{e} \right)^2 \lambda_n \cos \lambda_n + \frac{EI \pi^4}{De^4 b} \sin \lambda_n \right\} + \\ + d_{2n} \left\{ \lambda_n^2 (\operatorname{sh} \lambda_n - \sin \lambda_n) - (2-v) \left[\left(\frac{\pi}{e} \right)^2 \lambda_n (\operatorname{sh} \lambda_n + \sin \lambda_n) \right. \right. \\ \left. \left. + \frac{EI \pi^4}{De^4 b} (\cos \lambda_n - \operatorname{ch} \lambda_n) \right] \right\} + d_{3n} \left\{ (2-v) \left(\frac{\pi}{e} \right)^2 \cdot \lambda_n \operatorname{ch} \lambda_n - \right. \\ \left. - \lambda_n^2 \operatorname{ch} \lambda_n + \frac{EI \pi^4}{De^4 b} \operatorname{sh} \lambda_n \right\} = 0 \quad (14)$$

The nontrivial solutions of these equations can be found by equating to zero the following determinant

R	$2\lambda_n$	R	
$\left(\lambda_n^2 + v \left(\frac{\pi}{e} \right)^2 \right) \sin \lambda_n$	$\left[\lambda_n^2 + v \left(\frac{\pi}{e} \right)^2 \right] \cos \lambda_n +$ $+ \left[\lambda_n^2 - v \left(\frac{\pi}{e} \right)^2 \right] \operatorname{ch} \lambda_n$	$\left[v \left(\frac{\pi}{e} \right)^2 - \lambda_n^2 \right] \operatorname{sh} \lambda_n$	= 0 (15)
$\left[\lambda_n^2 + (2-v) \left(\frac{\pi}{e} \right)^2 \lambda_n \right] \times$ $\times \cos \lambda_n + \frac{EI \pi^4}{De^4 b} \sin \lambda_n$	$\lambda_n^2 (\operatorname{sh} \lambda_n - \sin \lambda_n) -$ $-(2-v) \left(\frac{\pi}{e} \right)^2 \lambda_n (\operatorname{sh} \lambda_n +$ $+ \sin \lambda_n) + \frac{EI \pi^4}{De^4 b} (\cos \lambda_n$ $- \operatorname{ch} \lambda_n)$	$\left[(2-v) \left(\frac{\pi}{e} \right)^2 \lambda_n - \lambda_n^2 \right] \times$ $\times \operatorname{ch} \lambda_n + \frac{EI \pi^4}{De^4 b} \operatorname{sh} \lambda_n$	

It is possible to solve transcendental equations (15) for λ_n . Substituting the values of λ_n into Eq. (11)~(14) and setting $d_{1n} = 1$, the constants $d_{2n} \sim d_{4n}$ are determined.

For simplicity, introduce symbol of operation as follows

$$L(\zeta, \eta) = \frac{\partial^2 \zeta}{\partial x^2} \cdot \frac{\partial^2 \eta}{\partial y^2} + \frac{\partial^2 \zeta}{\partial y^2} \cdot \frac{\partial^2 \eta}{\partial x^2} - 2 \frac{\partial^2 \zeta}{\partial x \partial y} \cdot \frac{\partial^2 \eta}{\partial x \partial y} \quad (16)$$

The stress distribution in plate must now obey von Kármán's

compatibility equation

$$\nabla^4 F = -\frac{1}{2} E L (W, W) \quad (17)$$

Substituting from Eq.(1) for W gives

$$\nabla^4 F = \frac{E \pi^2}{2e^2 b^2} \sum_{m=1}^{\infty} \sum_{n=1}^{\infty} A_n A_m \left[(Y'_m Y'_n - Y_m Y_n'') + (Y_m Y_n'' - Y'_m Y'_n) \cos \frac{2\pi x}{eb} \right] \quad (18)$$

Thus a solution for stress function can be obtained in the form

$$F = F_1(y) + F_2(y) \cos \frac{2\pi x}{eb} \quad (19)$$

From Eq.(18) it can be seen that

$$F_1''''(y) = \frac{E \pi^2}{2e^2 b^2} \sum_{m=1}^{\infty} \sum_{n=1}^{\infty} A_n A_m (Y'_m Y'_n + Y_m Y_n'') \quad (20)$$

$$\begin{aligned} F_2''''(y) - 2 \left(\frac{2\pi}{eb} \right)^2 F_2''(y) + \left(\frac{2\pi}{eb} \right)^4 F_2(y) = \\ = \frac{E \pi^2}{2e^2 b^2} \sum_{m=1}^{\infty} \sum_{n=1}^{\infty} A_n A_m (Y_m Y_n'' - Y'_m Y'_n) \end{aligned} \quad (21)$$

Integrating Eq.(20) twice gives

$$F_1''(y) = \frac{E \pi^2}{4e^2 b^2} \sum_{m=1}^{\infty} \sum_{n=1}^{\infty} A_n A_m Y_m Y_n + B_1 y - B_2 \quad (20)'$$

The integration constants B_1 and B_2 are used to satisfy the conditions on the loaded edge as will be seen later. To obtain a solution F_2 Eq.(10) is used. The solution to Eq.(21) takes the form

$$F_2(y) = \frac{E \pi^2}{2e^2 b^4} \sum_{m=1}^{\infty} \sum_{n=1}^{\infty} A_n A_m \phi_{mn}(y) \quad (22)$$

Particular solution is

$$\bar{F}_2(y) = \frac{E \pi^2}{2e^2 b^4} \sum_{m=1}^{\infty} \sum_{n=1}^{\infty} A_n A_m \bar{\phi}_{mn}(y)$$

where

$$\begin{aligned} \bar{\phi}_{mn}(y) = & A_{1mn} \sin \frac{\lambda_m y}{b} \sin \frac{\lambda_n y}{b} + A_{2mn} \sin \frac{\lambda_m y}{b} \cos \frac{\lambda_n y}{b} \\ & + A_{3mn} \sin \frac{\lambda_m y}{b} \operatorname{sh} \frac{\lambda_n y}{b} + A_{4mn} \sin \frac{\lambda_m y}{b} \operatorname{ch} \frac{\lambda_n y}{b} \\ & + A_{5mn} \cos \frac{\lambda_m y}{b} \cos \frac{\lambda_n y}{b} + A_{6mn} \cos \frac{\lambda_m y}{b} \operatorname{sh} \frac{\lambda_n y}{b} \\ & + A_{7mn} \cos \frac{\lambda_m y}{b} \operatorname{ch} \frac{\lambda_n y}{b} + A_{8mn} \operatorname{sh} \frac{\lambda_m y}{b} \operatorname{sh} \frac{\lambda_n y}{b} \\ & + A_{9mn} \operatorname{sh} \frac{\lambda_m y}{b} \operatorname{ch} \frac{\lambda_n y}{b} + A_{10mn} \operatorname{ch} \frac{\lambda_m y}{b} \operatorname{ch} \frac{\lambda_n y}{b} \end{aligned} \quad (23)$$

Substituting Y_n and $\bar{F}_2(y)$ into Eq.(21), we obtain a series of simultaneous linear algebraic equations to determine constants

$$\begin{aligned} A_{1mn} \left[\lambda_m^4 + \lambda_n^4 + 6\lambda_m^2 \lambda_n^2 + 2 \left(\frac{2\pi}{e} \right)^2 (\lambda_m^2 + \lambda_n^2) + \left(\frac{2\pi}{e} \right)^4 \right] \\ - 4A_{2mn} \left[\lambda_m^2 + \lambda_n^2 + \left(\frac{2\pi}{e} \right)^2 \right] \lambda_m \lambda_n = -b^4 (d_{1m} d_{1n} \lambda_m + d_{1m} d_{2n} \lambda_n) \lambda_m \end{aligned} \quad (24)$$

$$A_{2m} \left[\lambda_m^2 + \lambda_m^2 + 6\lambda_m^2 \lambda_m^2 + 2 \left(\frac{2\pi}{e} \right)^2 (\lambda_m^2 + \lambda_m^2) + \left(\frac{2\pi}{e} \right)^4 \right] \\ + 4A_{2m} \left[\lambda_m^2 + \lambda_m^2 + \left(\frac{2\pi}{e} \right)^2 \right] \lambda_m \lambda_m = b^4 (2d_{1m} d_{2m} \lambda_m \lambda_m - d_{1m} d_{2m} (\lambda_m^2 + \lambda_m^2)) \quad (25)$$

$$A_{3m} \left[\lambda_m^2 + \lambda_m^2 - 6\lambda_m^2 \lambda_m^2 + 2 \left(\frac{2\pi}{e} \right)^2 (\lambda_m^2 - \lambda_m^2) + \left(\frac{2\pi}{e} \right)^4 \right] \\ + 4A_{3m} \left[\lambda_m^2 - \lambda_m^2 + \left(\frac{2\pi}{e} \right)^2 \right] \lambda_m \lambda_m = b^4 (d_{1m} d_{3m} (\lambda_m^2 - \lambda_m^2) + 2d_{4m} d_{2m} \lambda_m \lambda_m) \quad (26)$$

$$A_{4m} \left[\lambda_m^2 + \lambda_m^2 - 6\lambda_m^2 \lambda_m^2 + 2 \left(\frac{2\pi}{e} \right)^2 (\lambda_m^2 - \lambda_m^2) + \left(\frac{2\pi}{e} \right)^4 \right] \\ + 4A_{4m} \left[\lambda_m^2 - \lambda_m^2 + \left(\frac{2\pi}{e} \right)^2 \right] \lambda_m \lambda_m = b^4 (d_{1m} d_{4m} (\lambda_m^2 - \lambda_m^2) + 2d_{3m} d_{2m} \lambda_m \lambda_m) \quad (27)$$

$$-4A_{1m} \left[\lambda_m^2 + \lambda_m^2 + \left(\frac{2\pi}{e} \right)^2 \right] \lambda_m \lambda_m + A_{2m} \left[\lambda_m^2 + \lambda_m^2 + 6\lambda_m^2 \lambda_m^2 \right. \\ \left. + 2 \left(\frac{2\pi}{e} \right)^2 (\lambda_m^2 + \lambda_m^2) + \left(\frac{2\pi}{e} \right)^4 \right] = -b^4 (d_{2m} d_{2m} \lambda_m + d_{1m} d_{1m} \lambda_m) \lambda_m \quad (28)$$

$$4A_{4m} \left[\lambda_m^2 - \lambda_m^2 + \left(\frac{2\pi}{e} \right)^2 \right] \lambda_m \lambda_m + A_{6m} \left[\lambda_m^2 - 6\lambda_m^2 \lambda_m^2 + \lambda_m^2 \right. \\ \left. - 2 \left(\frac{2\pi}{e} \right)^2 (\lambda_m^2 - \lambda_m^2) + \left(\frac{2\pi}{e} \right)^4 \right] = -b^4 (d_{2m} d_{3m} (\lambda_m^2 - \lambda_m^2) + 2d_{1m} d_{4m} \lambda_m \lambda_m) \quad (29)$$

$$4A_{3m} \left[\lambda_m^2 - \lambda_m^2 - \left(\frac{2\pi}{e} \right)^2 \right] \lambda_m \lambda_m + A_{7m} \left[\lambda_m^2 + \lambda_m^2 - 6\lambda_m^2 \lambda_m^2 \right. \\ \left. - 2 \left(\frac{2\pi}{e} \right)^2 (\lambda_m^2 - \lambda_m^2) + \left(\frac{2\pi}{e} \right)^4 \right] = b^4 (d_{2m} d_{4m} (\lambda_m^2 - \lambda_m^2) - 2d_{1m} d_{3m} \lambda_m \lambda_m) \quad (30)$$

$$A_{8m} \left[\lambda_m^2 + \lambda_m^2 + 6\lambda_m^2 \lambda_m^2 - 2 \left(\frac{2\pi}{e} \right)^2 (\lambda_m^2 + \lambda_m^2) + \left(\frac{2\pi}{e} \right)^4 \right] \\ + 4A_{10m} \left[\lambda_m^2 + \lambda_m^2 - \left(\frac{2\pi}{e} \right)^2 \right] \lambda_m \lambda_m = b^4 (d_{3m} d_{3m} \lambda_m - d_{4m} d_{4m} \lambda_m) \lambda_m \quad (31)$$

$$A_{9m} \left[\lambda_m^2 + \lambda_m^2 + 6\lambda_m^2 \lambda_m^2 - 2 \left(\frac{2\pi}{e} \right)^2 (\lambda_m^2 + \lambda_m^2) + \left(\frac{2\pi}{e} \right)^4 \right] \\ + 4A_{9m} \left[\lambda_m^2 + \lambda_m^2 - \left(\frac{2\pi}{e} \right)^2 \right] \lambda_m \lambda_m = b^4 (d_{3m} d_{4m} (\lambda_m^2 + \lambda_m^2) - 2d_{4m} d_{3m} \lambda_m \lambda_m) \quad (32)$$

$$4A_{8m} \left[\lambda_m^2 + \lambda_m^2 - \left(\frac{2\pi}{e} \right)^2 \right] \lambda_m \lambda_m + A_{10m} \left[\lambda_m^2 + \lambda_m^2 + 6\lambda_m^2 \lambda_m^2 \right. \\ \left. - 2 \left(\frac{2\pi}{e} \right)^2 (\lambda_m^2 + \lambda_m^2) + \left(\frac{2\pi}{e} \right)^4 \right] = b^4 (d_{4m} d_{4m} \lambda_m - d_{3m} d_{3m} \lambda_m) \lambda_m \quad (33)$$

The solution to Eq. (21) is compounded from the particular integral and complementary function solutions. Thus

$$\phi_{m\alpha}(y) = \bar{\phi}_{m\alpha}(y) + A_{11m} c h \frac{2\pi}{eb} y + A_{12m} s h \frac{2\pi}{eb} y + \\ + A_{13m} \frac{y}{b} c h \frac{2\pi}{eb} y + A_{14m} \frac{y}{b} s h \frac{2\pi}{eb} y \quad (34)$$

Substituting Eq. (19) into Eqs. (4) and (7) obtain four conditions as follows

$$\phi_{m\alpha}(0) = 0, \quad \phi'_{m\alpha}(0) = 0, \quad \phi_{m\alpha}(b) = 0, \quad \phi'_{m\alpha}(b) = 0 \quad (35)$$

These conditions are satisfied if

$$A_{11m} = -(A_{3m} + A_{7m} + A_{10m}) \quad | \quad (36)$$

$$A_{12m} \left(\frac{2\pi}{e} \right) + A_{13m} = -(A_{2m} + A_{4m} + A_{9m}) \lambda_m - A_{6m} \lambda_m \quad (37)$$

$$\begin{aligned} A_{11m} C h \frac{2\pi}{e} + A_{11m} s h \frac{2\pi}{e} + A_{13m} C h \frac{2\pi}{e} + A_{14m} s h \frac{2\pi}{e} \\ = -A_{1m} \sin \lambda_m \sin \lambda_m - A_{2m} \sin \lambda_m \cos \lambda_m - A_{3m} \sin \lambda_m s h \lambda_m \\ - A_{4m} \sin \lambda_m C h \lambda_m - A_{5m} \cos \lambda_m \cos \lambda_m - A_{6m} \cos \lambda_m s h \lambda_m \\ - A_{7m} \cos \lambda_m C h \lambda_m - A_{8m} s h \lambda_m s h \lambda_m \\ - A_{9m} s h \lambda_m C h \lambda_m - A_{10m} C h \lambda_m C h \lambda_m \end{aligned} \quad (38)$$

$$\begin{aligned} A_{11m} \left(\frac{2\pi}{e} \right) s h \frac{2\pi}{e} + A_{12m} \left(\frac{2\pi}{e} \right) C h \frac{2\pi}{e} + A_{13m} \left(C h \frac{2\pi}{e} + \right. \\ \left. + \left(\frac{2\pi}{e} \right) s h \frac{2\pi}{e} \right) + A_{14m} \left(s h \frac{2\pi}{e} + \frac{2\pi}{e} C h \frac{2\pi}{e} \right) \\ = A_{2m} \lambda_m \sin \lambda_m \sin \lambda_m + [(A_{3m} + A_{9m}) \lambda_m - \\ - (A_{1m} + A_{10m}) \lambda_m] \sin \lambda_m \cos \lambda_m + (A_{4m} \lambda_m \\ - A_{5m} \lambda_m) \sin \lambda_m s h \lambda_m + (A_{7m} \lambda_m - A_{8m} \lambda_m) \sin \lambda_m C h \lambda_m \\ - A_{12m} \lambda_m \cos \lambda_m \cos \lambda_m - (A_{17m} \lambda_m + A_{18m} \lambda_m) \cos \lambda_m s h \lambda_m \\ - (A_{4m} \lambda_m + A_{6m} \lambda_m) \cos \lambda_m C h \lambda_m - A_{9m} \lambda_m s h \lambda_m s h \lambda_m \\ - [(A_{3m} + A_{9m}) \lambda_m + (A_{10m} + A_{11m}) \lambda_m] s h \lambda_m C h \lambda_m \\ - A_{9m} \lambda_m C h \lambda_m C h \lambda_m \end{aligned} \quad (39)$$

Solving the linear algebraic Eqs. (36), (37), (38) and (39), the constants $A_{11m} \sim A_{14m}$ are determined.

Eq. (8) is satisfied irrespective of the forms of F_1 and F_2 . According to the theory of large deflection and derivation above, the in-plane displacement of the plate middle surface in the direction y is

$$\begin{aligned} u(y) = \int_0^{L/2} \frac{\partial u}{\partial x} dx = \int_0^{L/2} \left(\frac{1}{E} \left(\frac{\partial^2 F}{\partial y^2} - \nu \frac{\partial^2 F}{\partial x^2} \right) - \frac{1}{2} \left(\frac{\partial w}{\partial x} \right)^2 \right) dx \\ = \frac{L}{2E} F_1'' - \frac{\pi^2 L}{8e^2 b^2} \sum_{m=1}^{\infty} \sum_{n=1}^{\infty} A_m A_n V_m V_n = \frac{L}{2E} (B_1 y - B_2) \end{aligned} \quad (40)$$

Eq. (9) is satisfied if

$$B_1 = -\frac{2E}{Lb} u_1 \xi, \quad B_2 = -\frac{2E}{L} u_1 \quad \text{for case 1;} \quad (41a)$$

$$B_1 = \frac{2E}{Lb} u_1 \xi, \quad B_2 = -\frac{2E}{L} u_1 (1 - \xi) \quad \text{for case 2.} \quad (41b)$$

3. Analysis of Energy Method

The total strain energy stored in the buckle plate system is given by

$$V = V_1 + V_2 + V_3 + V_4 + V_5$$

in which V_1 , V_2 = strain energies of bending and mid-plane deformations of the flange; V_3 = strain energy of the elastically restraining medium of the unloaded edge restrained from rotation; V_4 = strain energy of the edge stiffener; V_5 = potential

energy of the external forces. These energies are given by the following expressions

$$V_1 = \frac{1}{2} D \int_{-c/2}^{c/2} \{ (\nabla^2 w)^2 - (1-\nu) L(w, w) \} dx dy$$

$$= \frac{DL}{4} \sum_{n=1}^N A_n^2 \int_0^1 \left[Y_n'^2 + \left(\frac{\pi}{eb} \right)^4 Y_n^2 \right] dy - \frac{DL}{2} \left(\frac{\pi}{eb} \right)^2 \int_0^1 \left(\sum_{n=1}^N A_n Y_n' \right)^2 dy - \frac{DL}{2} \nu \left(\frac{\pi}{eb} \right)^2 \sum_{n=1}^N \sum_{m=1}^N A_n A_m \int_0^1 Y_n' Y_m' dy$$

$$V_2 = \frac{t}{2E} \int_{-c/2}^{c/2} \{ (\nabla^2 F)^2 - (1+\nu) L(F, F) \} dx dy = \frac{t}{2E} \int_{-c/2}^{c/2} (\nabla^2 F)^2 dx dy$$

$$= \frac{LtE\pi^4}{32e^4b^3} \sum_{n=1}^N \sum_{m=1}^N \sum_{p=1}^N \sum_{q=1}^N A_n A_m A_p A_q \int_0^1 \left\{ 2 \left[\phi_{nm}'^2 - \left(\frac{2\pi}{eb} \right)^2 \phi_{nm} \right] \left[\phi_{pq}'^2 - \left(\frac{2\pi}{eb} \right)^2 \phi_{pq} \right] + b^4 Y_n Y_m Y_p Y_q \right\} dy + \frac{Lt\pi^2}{4e^2b^2} \sum_{n=1}^N \sum_{m=1}^N A_n A_m \int_0^1 B_1 Y_n Y_m dy - \frac{Lt\pi^2}{4e^2b^2} \sum_{n=1}^N B_2 A_n^2 \int_0^1 Y_n^2 dy + \frac{Lt}{2E} \int_0^1 (B_1 y - B_2)^2 dy$$

$$V_3 = \frac{D}{2} \int_{-c/2}^{c/2} \left(\frac{\partial^2 w}{\partial y^2} + \nu \frac{\partial^2 w}{\partial x^2} \right)_{y=0} \left(\frac{\partial w}{\partial y} \right)_{y=0} dx = \frac{D}{2} \int_{-c/2}^{c/2} \frac{\partial^2 w}{\partial y^2} \Big|_{y=0} \cdot \frac{\partial w}{\partial y} \Big|_{y=0} dx$$

$$= \frac{DL}{4} \sum_{n=1}^N \sum_{m=1}^N A_n A_m Y_n''(0) Y_m'(0)$$

$$V_4 = \frac{EI}{2} \int_{-c/2}^{c/2} \left(\frac{\partial^2 w}{\partial x^2} \right)_{y=b} dx = \frac{LEI}{eb} \left(\frac{\pi}{eb} \right)^4 \sum_{n=1}^N \sum_{m=1}^N A_n A_m Y_n(b) Y_m(b)$$

Note that the expressions for V_1 and V_2 have been simplified by using the orthogonality of $Y_n(y)$ and the stress boundary conditions, respectively, i.e.

$$\int_{\Gamma} L(F, F) dx dy = \oint_{\Gamma} \left(\frac{\partial F}{\partial \nu} \cdot \frac{\partial^2 F}{\partial x^2} dx + \frac{\partial F}{\partial \nu} \cdot \frac{\partial^2 F}{\partial y \partial x} dy \right) = 0$$

where \oint_{Γ} — integration along the edges of flange.

It is unnecessary to find an expression for V_5 since V_5 is not related to the coefficients A_n .

Now applying the condition of stationary potential energy obtains

$$\frac{\partial V}{\partial A_i} = \frac{LtE\pi^4}{8e^4b^3} \sum_{n=1}^N \sum_{m=1}^N \sum_{p=1}^N \sum_{q=1}^N A_n A_m A_p A_q \int_0^1 \left\{ b^4 Y_n Y_m Y_p Y_q + \left[\phi_{nm}'^2 - \left(\frac{2\pi}{eb} \right)^2 \phi_{nm} \right] \left[\phi_{pq}'^2 + \phi_{pq}^2 - \left(\frac{2\pi}{eb} \right)^2 (\phi_{pq}' + \phi_{pq}) \right] \right\} dy$$

$$- \sum_{n=1}^N A_n \left\{ \frac{Lt\pi^2}{2e^2b^2} B_1 \int_0^1 Y_n Y_n dy + \frac{LD\pi^2}{e^2b^2} \int_0^1 Y_n Y_n' dy - \frac{LD\pi^2}{2e^2b^2} \nu Y_n' Y_n - Y_n^2 Y_n \right\} + \frac{LD}{4} Y_n''(0) Y_n'(0) - Y_n''(0) Y_n'(0) + \frac{LEI\pi^4}{2e^4b^4} Y_n(b) Y_n(b) \Big\}$$

$$+ A_i \left\{ \frac{LD}{2} \int_0^1 \left[Y_i'^2 + \left(\frac{\pi}{eb} \right)^4 Y_i^2 \right] dy - \frac{Lt\pi^2}{2e^2b^2} B_2 \int_0^1 Y_i^2 dy \right\} = 0 \quad (i=1, 2, \dots, N) \quad (42)$$

Eqs.(42) are a set of simultaneous non-linear algebraic equations in the coefficients. Cancelling the non-linear terms, a set of linear homogeneous equations can be obtained. The critical mid-plane displacement u_{ic} , describing bifurcation can thus be found by equating to zero the determinant of coefficients.

Using equilibrium condition and Eq.(35) the load on the flange is found from

$$P = -t \int_0^b \sigma_x dy = -t \int_0^b F_1''(y) dy$$

$$= btB_2 - \frac{1}{2} b^2 t B_1 - \frac{\pi^2 E t}{4e^2 b^2} \sum_{n=1}^N \sum_{s=1}^N A_n A_s \int_0^b Y_n Y_s dy \quad (43)$$

$$M = -t \int_0^b \sigma_x y dy = -t \int_0^b F_1''(y) y dy$$

$$= -\frac{1}{2} b^2 t B_2 - \frac{1}{3} b^3 t B_1 - \frac{\pi^2 E t}{4e^2 b^2} \sum_{n=1}^N \sum_{s=1}^N A_n A_s \int_0^b Y_n Y_s y dy \quad (44)$$

Setting $M = Pd$ obtains

$$b^2 t \left(\frac{1}{2} d - \frac{1}{3} b \right) B_2 - bt \left(d - \frac{1}{2} b \right) B_1 - \frac{\pi^2 E t}{4e^2 b^2} \sum_{n=1}^N \sum_{s=1}^N A_n A_s \int_0^b Y_n Y_s (y-d) dy = 0 \quad (45)$$

where d is expressed in terms of $\alpha = \frac{\sigma_1 - \sigma_2}{\sigma_1}$, i.e.

$$d = \frac{1 - \frac{2}{3} \alpha}{1 - \frac{1}{2} \alpha} \cdot \frac{b}{2} \quad \text{for case 1;} \quad (46a)$$

$$d = \frac{1 - \frac{1}{3} \alpha}{1 - \frac{1}{2} \alpha} \cdot \frac{b}{2} \quad \text{for case 2.} \quad (46b)$$

In post-buckling analysis, the values of ξ and coefficients $A_1 \sim A_N$ corresponding to a given u_1 ($u_1 > u_{ic}$) can be found by solving $N+1$ non-linear Eqs.(42) and (45). As this investigation is not really concerned with loads greater than about three times the buckling load, the use of only one or two terms in deflection series will give sufficient accuracy for engineering practice. Finally the plate displacements, stresses, etc., are all found from the theory of large deflection.

4. Criterion of Post-Buckling Strength

According to Stowell-Ilyushin's theorem, the condition of plastic yield of plate can be approximately expressed as follows (4)

$$\sigma_{xx} = f_y \quad (47)$$

where σ_{xx} = maximum stress in the plate in x direction after buckling, including non-linear membrane and bending stresses; f_y = yield strength of plate.

If the condition of Eq.(47) is satisfied, the load on the plate reaches the ultimate capacity. The nominal stress σ_1 corresponding to the ultimate load is considered as post-buckling strength σ_c of the plate elements.

5. Effective Width Method

For design purpose, actual buckled plate is replaced by a equivalent unbuckled plate as shown in Fig.2. The width of equivalent plate is so called effective width. The principle of equivalence is (a) the load-carrying capacities of both plate are equal; and (b) when the nominal maximum stress of the actual plate reaches post-buckling strength σ_c , the nominal maximum stress of the equivalent plate reaches yield strength f_y . It follows that the effective width is

$$b_e = \frac{b}{4} \frac{\sigma_c}{f_y} \left(2 - \alpha + \sqrt{(2 - \alpha)^2 + 8\alpha \frac{f_y}{\sigma_c}} \right) \quad (48)$$

EXPERIMENTS

Experimental investigation of 28 cold-formed lipped channel and lipped angle columns under load with various eccentricities has been carried out at Hunan University. The cross-sectional shapes of the specimens are shown in Fig.3. Their dimensions and sectional properties are given in Table 1. It can be seen that they are designed in five sorts of width-to-thickness ratios ($b/t=30, 40, 50, 60$ and 90). A thick plate was welded to each end of the specimens, and both ends were seated on cruciform knife supports. The theoretical ultimate loads are compared with experimental results in Table 1.

CONCLUSION

Edge-stiffened plate elements under combined compression and bending really have load-carrying capacity after buckling. It can be used in design. Based on the theoretical analysis in this paper, the values of effective width of edge-stiffened plate elements can be tabulated for design purpose. In order to consider the effects of imperfections, strain hardening, nonlinearity of material and interaction buckling of columns, further study is underway.

APPENDIX 1. REFERENCES

1. Desmond, T. P., Pekoz, T. and Winter, G., "Edge stiffeners for Thin-Walled Members," *J. of Struct. Div. ASCE*, Vol.107, No.ST2, Feb., 1981.
2. Rhodes, J. and Harvey, J. M., "The Post-Buckling Behavior of Thin Flat Plates in Compression with the Unloaded Edges Elastically Restrained against Rotation," *J. Mech. Eng. Sci.*, Vol.13, No.2, 1971.
3. Rhodes, J. and Harvey, J. M., "Effects of Eccentricity of Load or Compression on The Buckling and Post-Buckling Behaviour of Flat Plates," *Int. J. Mech. Sci.* Vol.13, 1971.
4. Bleich, F., "Buckling Strength of Metal Structures," McGraw-Hill, New York 1952.

TABLE 1. COMPARISON OF THEORETICAL AND EXPERIMENTAL RESULTS

Spec.	Measured dimensions (mm)					$\frac{b}{t}$	α	λ	P_{cr}^T	P_u^T	P_u	$\frac{P_u}{P_{cr}^T}$
	n	b	a	t	L							
SC42-30	108.8	71.9	19.8	2.43	500	29.54	0.193	22.0	-	21530	22076	1.025
SC56-40	138.2	111.5	22.2	2.47	700	45.72	0.706	19.3	-	18850	22388	1.188
SC84-60	128.8	89.7	16.5	1.49	600	60.76	0.416	21.2	-	6250	6756	1.082
SC90-90	137.7	134.5	20.6	1.48	700	90.88	-0.493	16.4	2800	5790	5981	1.033
SA30	-	72.5	20.9	2.48	350	29.75	0.558	33.7	-	9910	10692	1.079
SA40	-	97.7	22.4	2.46	450	39.74	-1.057	39.1	-	10500	11384	1.085
SA60	-	91.5	16.5	1.47	400	62.37	-1.029	50.6	-	3200	3362	1.051
SA90	-	135.4	21.4	1.49	500	90.63	-0.329	57.1	-	5010	4555	0.909
LC42-30a	110.8	73.3	19.4	2.47	990	29.67	-0.799	38.8	-	10050	12512	1.245
LC42-30b	110.4	73.2	18.5	2.48	990	29.50	-0.195	39.0	-	19200	20415	1.064
LC42-30c	102.3	75.2	18.5	2.47	2100	30.50	1.181	75.1	-	8580	9666	1.127
LC70-50a	108.3	74.8	16.0	1.49	980	50.10	0.606	38.4	2550	5410	5060	0.935
LC70-50b	105.5	75.2	16.0	1.50	980	50.33	-0.609	38.2	1600	4400	4663	1.060
LC84-60	121.3	93.1	16.7	1.47	2520	62.20	0.563	75.2	-	5000*	4970	0.994
LC90-90	134.9	135.5	18.7	1.45	2830	93.10	0.354	59.0	2500	5570	5471	0.982
LA30a	-	74.4	20.0	2.48	620	30.00	0.856	38.4	-	7770	7637	0.983
LA30b	-	74.0	20.7	2.45	620	30.20	-1.504	38.3	-	5290*	6149	1.163
LA30c	-	74.3	19.8	2.47	1000	30.77	-1.635	78.5	-	3800*	4300	1.132
LA30d	-	74.1	20.5	2.48	1000	29.97	0.919	58.0	-	5750*	5499	1.128
LA40a	-	98.2	23.2	2.48	850	39.60	0.949	39.1	-	9170	8859	0.966
LA40b	-	99.8	22.1	2.47	1820	41.50	0.895	78.0	-	5960*	7907	1.135
LA50a	-	74.3	15.9	1.50	590	50.12	-1.875	75.2	-	1200*	1020	0.850
LA50b	-	75.5	15.9	1.50	590	50.60	-1.638	69.5	-	1550*	1521	0.922
LA50c	-	75.3	15.7	1.49	950	50.40	-1.397	103.5	-	1200*	1135	0.946
LA50d	-	75.7	14.3	1.49	950	50.80	0.905	58.2	1500	2400	2323	0.968
LA60	-	90.0	17.8	1.49	720	60.50	0.381	38.6	-	4800	4135	0.862
LA90a	-	135.5	20.3	1.47	1130	92.60	-0.371	107.3	-	3200*	2274	0.711
LA90b	-	135.3	22.2	1.47	1750	92.20	-0.567	142.2	-	2400*	1739	0.725

P_{cr}^T = Experimental critical load at buckling (Kg);

P_u^T, P_u = Experimental and theoretical ultimate loads of specimens (Kg);

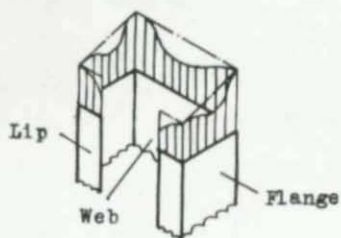
L = Column length;

λ = Slenderness ratio;

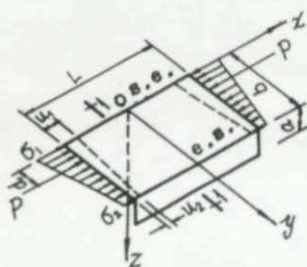
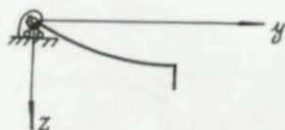
$\alpha = \frac{\sigma_1 - \sigma_2}{\sigma_1}$ (The minus before α implies that the maximum stress applies to edge stiffener, as shown in Fig.1c.)

* Flexural buckling of columns;

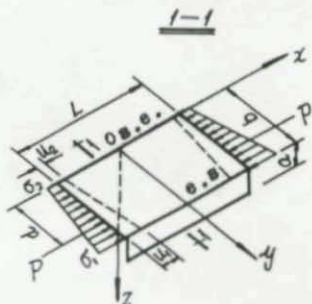
* Torsional-flexural buckling of columns.



a) Cold-formed member

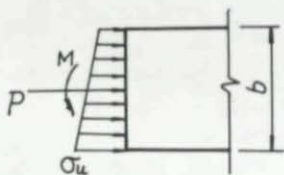


b) Case 1. Maximum stress applies to stiffened edge

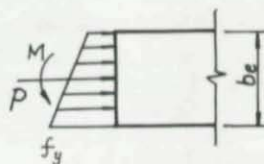


c) Case 2. Maximum stress applies to edge stiffener

Fig.1. Edge-stiffened plate elements

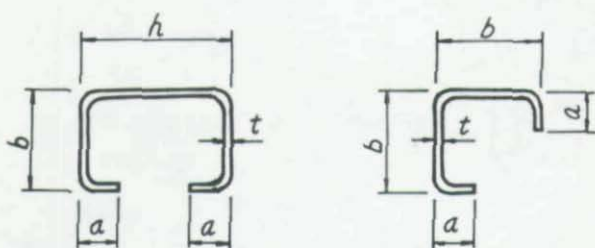


a) Actual plate



b) Equivalent plate

Fig.2. Effective width of edge-stiffened plate



a) Lipped channel

b) Lipped angle

Fig.3. Cross sections of specimen

GENERAL BUCKLING OF SHELL-LIKE STRUCTURES
SUMMARY OF CLOSED FORM SOLUTIONS
by Kenneth P. Buchert, Professor of Engineering,
Southern Illinois University of Edwardsville

I. INTRODUCTION

A shell-like structure is one that resists loads in a manner similar to that of a thin shell. That is, the major mode of resistance is by membrane action by which forces are carried from point to point by biaxial tension or compression and by shear in the plane of the shell. In addition to the membrane resistance, the shell-like structure has bending resistance to help resist loads. It also has in-plane shear resistance. Examples of shell-like structures are latticed shells, reticulated shells, stiffened shells, orthotropic shells, sandwich shells, framed shells, concrete shells, wooden shells and composite shells. Figure 1 illustrates several kinds of shell-like structures.

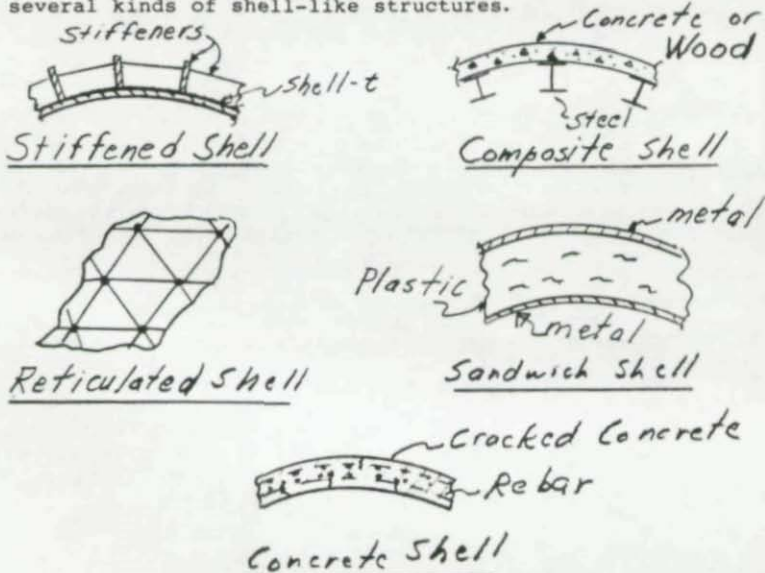


Figure 1. Types of Shell-Like Structures.

The closed form equations of shell-like structures involve what is called an equivalent membrane thickness t_m and an equivalent bending thickness t_b . The equivalent membrane thickness is found by equating the tensile or compressive effective area per unit length to the membrane thickness. The equivalent bending thickness is found by equating the bending moment of inertia per unit length to the bending moment of inertia of an equivalent unstiffened shell. (See References 1, 2, and 3). For example the equivalent membrane and bending thickness of a stiffened shell are given by:

$$t_m = A/d + t \quad t_b/12 = I/d$$

where A is the area of a stiffener, d is the stiffener spacing and I is the combined moment of inertia of the shell and stiffener over a length d . If the stiffeners vary in size and spacing in different directions equivalent membrane and bending thickness are found for the principal directions and are then substituted in the proper equations. For example, a stiffened cylinder will usually have different membrane and bending properties in the axial and circumferential directions.

II. CLOSED FORM GENERAL BUCKLING EQUATIONS (See References 1&2)

1. Spherical shell-like structures with t_m and t_b are the same in the principal directions

$$\sigma_{cr} R / \eta E t_m = 0.35 \left(t_b / t_m \right)^{3/2}$$

where σ_{cr} is the critical buckling stress (in the case of external pressure $\sigma_{cr} = \rho R / 2 t_m$), R is the radius of curvature, η is the plasticity reduction factor, E is the modulus of elasticity, t_m is the equivalent membrane thickness and t_b is the equivalent bending thickness. The plasticity reduction factor is given by

$$\eta = \frac{3}{4E} (E_T + E_S/3)$$

where E_T is the tangent modulus at σ_{cr} and E_S is the secant modulus. The original wave length of buckle is

$$w.l. = 2(t_m R)^{1/2} (t_b / t_m)^{3/4}$$

In order for the equations to be applicable, there must be two or three stiffeners within the wave length of buckle. The effects of deviations from a perfect surface are covered in Section III.

2. Spherical shell-like structures with different t_m and t_θ in the principal directions.

$$\frac{\sigma_{cr} R}{\eta E t_m} = 0.09 \frac{G^{\frac{1}{2}} I^{\frac{1}{2}}}{H} \left(\frac{t_{\theta 1}}{t_{m 1}} \right)^{3/2}$$

$$D = \frac{w.l.1}{w.l.2}, \quad E = \frac{t_{m2}}{t_{m1}}, \quad F = \frac{t_{\theta 2}}{t_{\theta 1}}$$

$$\begin{aligned} G = & \frac{1}{2} D^4 + D^3(1-D) + D^2(1-D)^2 \\ & + \frac{1}{2} D(1-D)^3 + \frac{1}{6} (1-D)^4 + \frac{1}{4} D^4(E,-1) \\ & + \frac{2}{3} (E,-1) D^3(1-D) + \frac{3}{4} (E,-1) D^2(1-D)^2 \\ & + \frac{2}{5} (E,-1) D(1-D)^3 + \frac{1}{2} (E,-1)(1-D)^4 \end{aligned}$$

$$H = \frac{1}{2} D^2 + \frac{1}{2} D(1-D) + \frac{1}{6} (1-D)^2$$

$$\begin{aligned} I = & \frac{3}{2} + \frac{9}{4} (F-1) + \frac{3}{2} (F-1)^2 + \frac{3}{8} (F-1)^3 \\ & + \frac{1}{2} F^3 + \frac{3}{4} F^2(1-F) + \frac{1}{2} F(1-F)^2 \\ & + \frac{1}{8} (1-F)^3 \end{aligned}$$

D is the ratio of the wave lengths in the 1 and 2 directions. σ_{cr} will occur when D is selected such that σ_{cr} will be a minimum. The effects of deviations from a perfect surface are covered in Section III.

3. Spherical Segment when wave length is restricted (for example buckling between stiffeners of a stiffened shell when the spacing between stiffeners is less than the wave length of buckle of an unstiffened shell.)

$$\frac{\sigma_{cr} t}{\eta E R} = 0.00226 \frac{d^2 t}{R^3} + \frac{3.7 t^3}{d^2 R}$$

where t is the shell thickness. The effects of deviations from a perfect surface are covered in Section III.

4. Shell-like structures with positive Gaussian curvature (such as ellipsoids and paraboloids)

$$\frac{\sigma_{cr} R}{\eta E t} = 0.13 \frac{A^{1/2}}{B} \frac{R^2}{R_1^2}$$

where $R = R_1 + (R_2 - R_1) \frac{2x}{\pi}$, $R_1 > R_2$

see Fig. 2.

$$C = \frac{R_1}{R_2}, \quad C_2 = \frac{\beta_2}{\beta_1} = \text{Minimum}$$

$$\begin{aligned} A = & \frac{1}{2} + (C_2 - 1) + (C_2 - 1)^2 + \frac{1}{2}(C_2 - 1)^3 + \frac{1}{10}(C_2 - 1)^4 \\ & + \frac{1}{2}(C_2 - 1) + \frac{4}{3}(C_2 - 1)(C_2 - 1) + \frac{3}{2}(C_2 - 1)(C_2 - 1)^2 \\ & + \frac{4}{5}(C_2 - 1)(C_2 - 1)^3 + \frac{1}{6}(C_2 - 1)(C_2 - 1)^4 + \frac{1}{6}(C_2 - 1)^2 \\ & + \frac{1}{2}(C_2 - 1)^2(C_2 - 1) + \frac{3}{5}(C_2 - 1)^2(C_2 - 1)^2 \\ & + \frac{1}{3}(C_2 - 1)^2(C_2 - 1)^3 + \frac{1}{14}(C_2 - 1)^2(C_2 - 1)^4 \end{aligned}$$

$$\begin{aligned} B = & \frac{1}{2} + \frac{1}{2}(C_2 - 1) + \frac{1}{6}(C_2 - 1)^2 + \frac{3}{4}(C_2 - 1) \\ & + (C_2 - 1)(C_2 - 1) + \frac{3}{8}(C_2 - 1)(C_2 - 1)^2 + \frac{1}{2}(C_2 - 1)^2 \\ & + \frac{3}{7}(C_2 - 1)^2(C_2 - 1) + \frac{3}{10}(C_2 - 1)^2(C_2 - 1)^2 \\ & + \frac{1}{8}(C_2 - 1)^3 + \frac{1}{5}(C_2 - 1)^3(C_2 - 1) \\ & + \frac{1}{12}(C_2 - 1)^3(C_2 - 1)^2 \end{aligned}$$

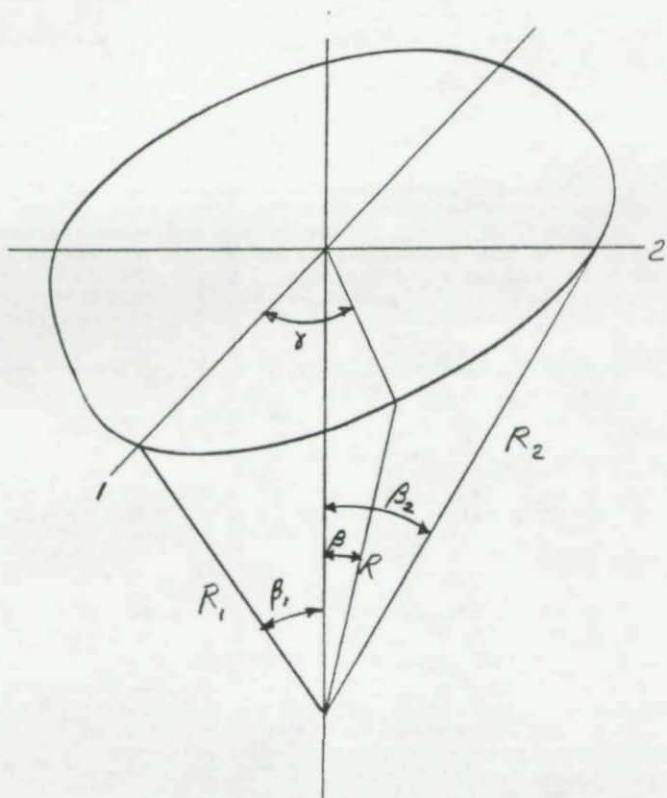


Figure 2 - Notation

5. Cylindrical shell-like structures or shell-like structures with zero Gaussian curvature
 - a. Cylindrical shell-like structures under external pressure:

$$\frac{\sigma_{2cr} R}{\eta E t_{m2}} = 0.98 \frac{t_{m1}^{1/8}}{t_{m2}^{15/8}} \frac{t_{B2}^{9/4}}{L} R^{1/2}$$

where σ_{2cr} is the critical buckling stress in the circumferential direction, R is the radius of the cylinder, t_{m1} is the equivalent membrane thickness in the axial direction, t_{m2} is the equivalent membrane thickness in the circumferential direction, t_{B1} and t_{B2} are the equivalent bending thicknesses and L is the length of the cylinder.

$$\eta = \frac{(E_s E_T)^{1/2}}{E} \left(\frac{1}{4} + \frac{3}{4} \frac{E_T}{E_s} \right)$$

$$w.l. = 1.33 R^{1/2} L^{1/2} t_{B2}^{3/8} / t_{m1}^{1/8}$$

- b. Cylindrical shell-like structure under axial compression. In this case one must check for both symmetric and asymmetric buckling. For symmetric buckling:

$$\frac{\sigma_{1cr} R}{\eta E t_{m1}} = \frac{0.5 t_{m2}^{1/2} t_{B1}^{3/2}}{t_{m1}^2}$$

$$\eta = \frac{E_T^{1/2} E_s^{1/2}}{E}, \quad w.l. = \frac{R t_{B1}^{3/2}}{0.55 t_{m2}^{1/2} L}$$

For asymmetric buckling:

$$\sigma_{1cr \text{ asymmetric}} = (\sigma_{1cr \text{ symmetric}}) (U)$$

$$U = \frac{\frac{t_{B2}^3}{t_{B1}^3} \beta^2 + \frac{1}{4} \left[1 + \frac{t_{B2}^3}{t_{B1}^3} \right]^{1/2}}{\frac{t_{m2}}{t_{m1}} \beta^2 + 1}$$

$$\beta^2 = P \pm (P^2 + Q)^{1/2}$$

$$P = \frac{1}{2} \left(\frac{1-\alpha}{\alpha-\delta} \right), \quad Q = \frac{t_{m1}}{t_{m2}} \frac{(1-\alpha)}{(\alpha-\delta)}$$

$$\alpha = \frac{t_{m1}}{t_{m2}} \frac{t_{B2}^3}{t_{B1}}$$

$$\gamma = \frac{1 + \frac{t_{B2}^3}{t_{B1}}}{5 - \frac{t_{m2}}{t_{m1}}}$$

- c. Cylindrical shell-like structure under radial compression:

$$\frac{\sigma_{2cr} R}{\eta E t_{m2}} = 0.86 \frac{t_{m1}^{1/4} t_{B2}^{9/4} R^{1/2}}{t_{m2}^2 L}$$

The wave length of buckle is approximately one fourth of the circumference. The plasticity reduction factor is

$$\eta = \frac{(E_s E_T)^{1/2}}{E}$$

- d. Cylindrical shell-like structure under shear

$$\frac{N_{12cr} R}{\eta E} = 0.63 \frac{t_{m1}^{3/16} t_{B2}^2 R^{1/4}}{t_{m2}^{3/16} t_{B1}^{11/8} L^{1/2}}$$

where N_{12cr} is the critical shear load per unit length.

$$\eta = \frac{E_s}{E}$$

6. Shell-like structures with negative Gaussian curvature. For a hyperbolic paraboloid:

$$p_{cr} = \frac{2}{\sqrt{3}} E t_m^2 \left(\frac{t_B}{t_m} \right)^{3/2} \frac{C^2}{a^2 b^2}$$

where p_{cr} is the critical vertical pressure, C is the corner elevation, a is the length along the X axis and b is the length along the Y axis. The equation for the HP is

$$Z = \frac{C}{ab} x y$$

The wave length of buckle is $w.l. = \left[\frac{1}{48} \frac{t_B^3}{t_m} \left(\frac{ab}{C} \right)^2 \right]^{1/4}$

III. EFFECT OF DEVIATIONS FROM A PERFECT SURFACE ON THE BUCKLING LOAD.

Deviations from a perfect surface may be due to a combination of many causes. Some of these causes are the deviations of the "as-built" structure, deviations or deflections caused by the external loads acting upon the "as-built" structure, deviations caused by the deflections of the boundary, deviations due to concentrated loads, deviations due to non-linear effects such as concrete cracking, deviations due to connection effects such as yielding of attachment welds, deviations due to the combination of applied loads and residual stresses and many other effects. In applications, the sum of all the deviations are added together and their effects are determined over the wave length of buckle. See Figure 3.

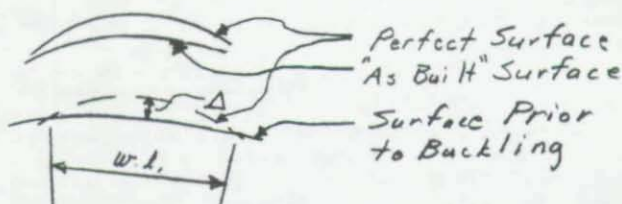


Figure 3 - Δ as a function of Wave Length.

If the sum of the deviations is Δ the quantity Δ/t_m is determined. The reduction factor can then be determined by using Figure 4.

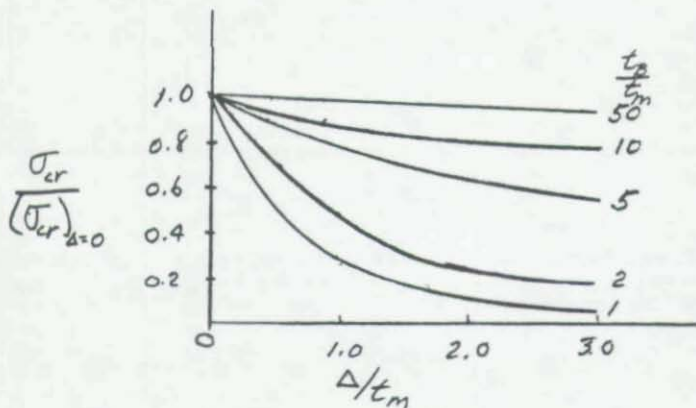


Figure 4 - Effects of Deviations from a Perfect Surface on the Buckling Load.

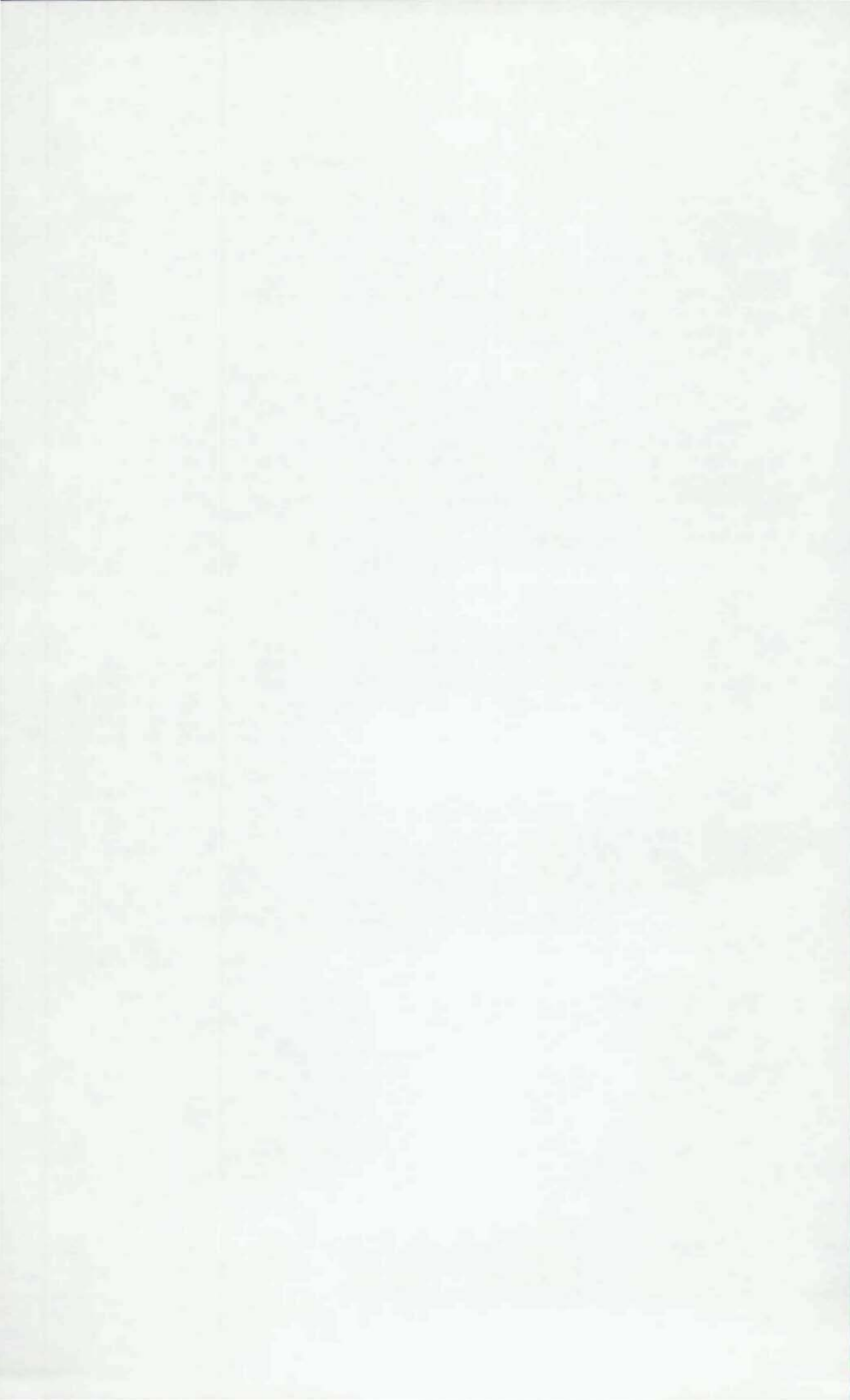
The curves apply to the reductions for spherical shell-like structures, shell-like structures with positive Gaussian curvature, cylindrical shell-like structures under external pressure, axial compression, shear and shell-like structures with negative Gaussian curvature. In general deviations do not have a significant effect on cylinders under radial pressure.

IV. SUMMARY

The previous sections give some of the details for determining the initial general buckling load of a number of shell-like structures. After initial general buckling, the structural will continue to deflect and in most cases ultimate failure will result. Stiffened shell-like structures can buckle locally between stiffeners in some cases and the overall structure can remain stable against general buckling. References 1 and 2 give more complete details and give examples on the basic results for buckling of shell and shell-like structures. Hundreds of tests have been conducted on shell-like structures. Deviations from perfect surfaces have been measured on many of these tests and the results generally agree with the equations presented herein. It should be noted that the deviations can be large enough to give essentially zero buckling loads. In addition, numerous tests have shown that the zero deviation buckling load can be reached with accurately built structures. Models used to determine buckling loads must simulate actual conditions. For example, plastic models cannot be used to simulate composite construction for concrete-steel structures because, in general, concrete cracking and steel yielding and effects of residual stresses cannot be simulated with plastic. Non-linear computer and closed form equations are often used to find the deviations from a perfect surface that are then used in the closed form equations. Since, in general, the wave length of buckle is relatively small, the buckling of shell-like structures with non-uniform loads can be determined using the formulas given herein by calculating the local compressive stress and comparing it to the buckling load calculated by the equations presented herein.

V. REFERENCES

1. Buchert, K. P., "Buckling of Shell & Shell-Like Structures," book published by K. P. Buchert & Associates, 1973.
2. Buchert, K. P., "Split Rigidity Theory of Plates, Shells & Stability," book published by K. P. Buchert, 2nd Edition, 1985.
3. Johnston, B. "Guide to Stability Design of Metal Structures," Third Edition, John Wiley, New York, 1976.



THE BUCKLING BEHAVIOUR OF SINGLE LAYER, SHALLOW BRACED DOMES

R.E. McConnel

Department of Engineering, University of Cambridge

The author presented a paper to the same general title at the 1984 SSRC meeting in San Francisco (Ref. 1). This present paper will review the current state of the continuing numerical and experimental work being carried out at Cambridge on the behaviour of shallow single layer braced domes, and will conclude that there is still much work to be done.

1. NONLINEAR COMPUTER PROGRAM DEVELOPMENT

The stability theory employed in the programs developed in conjunction with the work reported in this paper, was briefly outlined in the 1984 SSRC paper (Ref. 1), and has been covered in detail elsewhere by See and McConnel (Ref. 2), and by Kani and McConnel (Ref. 3). Briefly stated, buckling is indicated if any eigenvector of the full current tangent stiffness matrix becomes negative during the load history. This theory is based on the form of the spectral resolution of the tangent stiffness matrix, i.e. its form when transformed into its own eigenvector space, and not on the more usual energy arguments. This means that in principle at least the development should hold for elasto-plastic materials. However, this is impractical, as it would require a consideration of all possible tangent stiffness matrices at the current displacement, given that any yielded material in the structure might unload in the next displacement increment in a bifurcation mode. In spite of these problems, successful nonlinear material calculations have been performed (see Ref. 4, and below) on imperfect structures which show a clear limit point response with no bifurcation. This is because the problems outlined above can be avoided in such situations, as the strain history is largely uni-directional.

Returning to the basic elastic theory, the examination of even one eigenvalue at every iteration step in a large nonlinear iteration analysis would be quite impractical. Fortunately, in elastic problems, it can be shown that there is a one to one relationship between negative eigenvectors and negative main diagonal terms in the decomposed stiffness matrix (Refs. 4, 5), so that it is only necessary to observe these main diagonal terms during each matrix decomposition to detect instability.

With the earliest program developed in the current programme (See, Ref. 2), it was necessary to repeat any analysis that detected bifurcation via negative diagonal terms. This repeated analysis needed to be 'deflected' onto its bifurcation path by either initial geometric or load imperfection in the form of the eigenvector associated with the negative eigenvalue. The current program avoids

the necessity of stopping the analysis and beginning again, by introducing a suitable local imperfection into the analysis just prior to the load level at which the negative diagonal was detected. If this imperfection is very small (and it need not be large to set off the bifurcation mode), and if it is removed shortly after the solution procedure is established on the bifurcation path, the program will generate the structures theoretical (perfect) primary and bifurcation paths. This form of analysis is illustrated in Fig. 1 (reproduced here from Ref. 3) as the 'perturbed perfect analysis' path.

Such bifurcation (or secondary) equilibrium paths can also be obtained from energy based formulations. However, while such methods can adequately deal with 3 degree-of-freedom problems of the type shown in Fig. 1, they cannot be applied to multi-degree-of-freedom systems such as those shown in Fig. 2. Such limitations do not apply to tangent stiffness based numerical calculations.

2. IMPERFECTIONS

It is well known that random imperfections in real structures mean that any elastic critical bifurcation predicted by the theoretical analysis of a perfect (symmetric) model of the structure never occurs in practice. A simple numerical explanation of this observed real behaviour can be easily deduced from the spectral resolution of the tangent stiffness matrix. If therefore, random imperfections of either shape and/or load are introduced to any perfect numerical model, then all bifurcation points should be avoided and only realistic limit point behaviour should result. It would, however, still be advisable to retain checks for negative diagonals during decomposition. Such an approach also has other advantages in relation to the analysis of materially nonlinear structures, as discussed above in section 1.

Unfortunately, the inclusion of imperfections normally requires the introduction of at least one extra node per member, which leads to a two, three, or more fold increase in the size of the tangent stiffness matrix. Because of this problem, a study was directed at developing a numerical method for the introduction of imperfections which avoided extra mid-member nodes by considering them directly in the formulation of the element analysed to produce the member stiffness matrix (Ref. 6). The results of a typical calculation are shown in Fig. 2, where it can be seen that the use of imperfect two noded members has set off the appropriate buckling mode.

3. VARIABLE JOINT STIFFNESS

A long term aim of the work summarised in this paper has been to investigate the influences of joint size and bending continuity on the behaviour of shallow domes. To this effect, and because of the problems outlined in the previous section, numerical techniques have been developed to include the relevant joint properties in a

two noded member model. Extensive tests have been carried out on a number of domes of 8 metre span constructed with MERO joints (see Fig. 2) using two different member sizes to obtain experimental dome response data for different member-to-joint bending stiffness ratios. This work is presented in brief detail in Ref. 6 and will be more extensively reported in the near future.

4. GENERAL REMARKS

A great deal of work has been carried out since that reported in 1984 (Ref. 1) was completed. Unfortunately, in a general sense, not much progress has been made. This is because, although the two main program developments (imperfections and joint variable stiffness) perform well with simple examples, the programs in which they are incorporated fail to converge for many analyses of even moderate size. Therefore, the hoped for ability to numerically study the general effects on dome behaviour of imperfections, dome geometry, joint properties, and load patterns, by analysing many structures using a program extensively tested against a moderate number of experimental domes, has so far proved to be impractical.

On the positive side, the results that have been obtained in the last three years have generally supported the general conclusions reported in 1984; namely that the response of real domes is dominated by imperfections in node heights, and that the inclusion of realistic joint continuity gives reasonably shallow unloading paths. Also, although the computer programs have not so far proved to be practical for the analysis of a large number of domes, they have been capable of following particular experimental results with reasonable accuracy provided sufficient time has been available to sort out the numerical convergence problems associated with a particular dome. The realistic analysis of one-off domes can therefore be approached with some confidence.

Despite the rather barren returns gained so far from the investigations undertaken over the last three years, work is continuing at Cambridge to overcome the program difficulties noted in this report, and to assemble sufficient data to make reliable predictions of the general behaviour of shallow braced domes.

5. REFERENCES

1. R.E. McConnel, The Analysis and Testing of Some Single Layer Shallow Reticulated Domes, SSRC Proceedings, San Francisco, 1984.
2. T. See and R.E. McConnel, Large Displacement Elastic Buckling of Space Structures, Journal of the Structural Division, ASCE, Vol. 112, No. 5, May 1986.

3. I.M. Kani and R.E. McConnel, Collapse and Post-Collapse Analysis of Shallow Lattice Domes, Proceedings IASS Symposium, Vol. 3, Osaka, 1986.
4. I.M. Kani, A Theoretical and Experimental Investigation of the Collapse of Shallow Reticulated Domes. Ph.D. Thesis, University of Cambridge Engineering Department, February 1986.
5. W.H. Wittrick and F.W. Williams, A General Algorithm for Computing Natural Frequencies of Elastic Structures, Quarterly Journal of Mechanics and Applied Mathematics, Vol. XXIV, Part 3, 1987.
6. R.E. McConnel, F.A. Fathelbab and D. Hatzis, The Buckling Behaviour of Some Single Layer, Shallow Lattice Domes, Proceedings IASS Symposium, Vol. 13, Osaka 1986.

6. ACKNOWLEDGEMENTS

The work reported here has been carried out in close collaboration with both former and present research students.

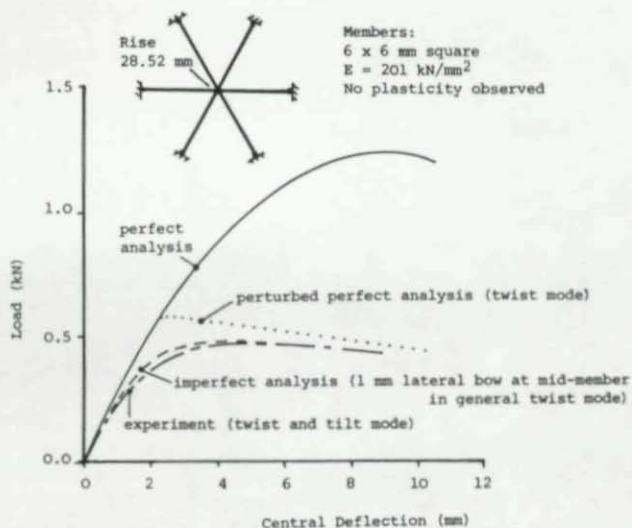


Fig. 1 Response of a Centrally Loaded Six Member Dome of 1000 mm Span.

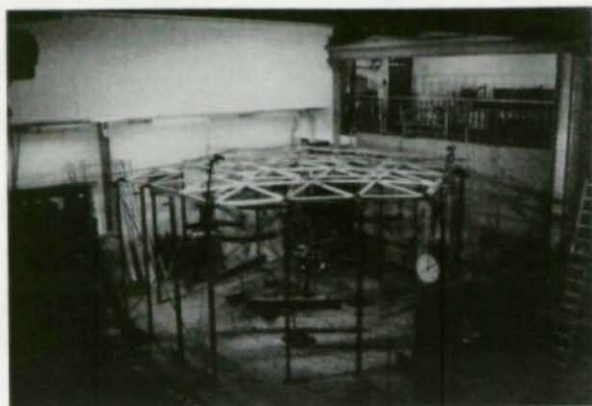
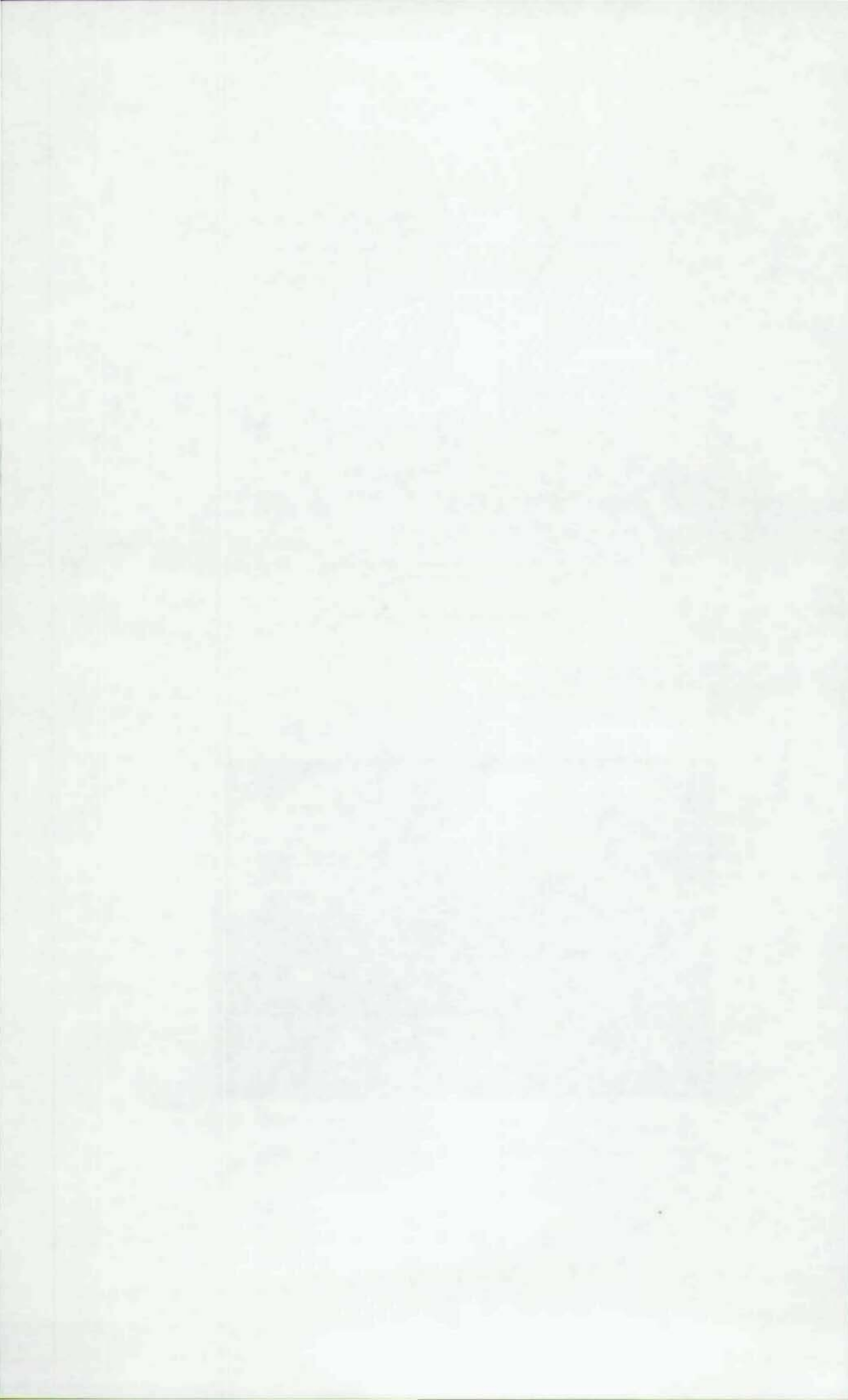


Fig. 2 90 Member Dome of 8 metre Span Under Test



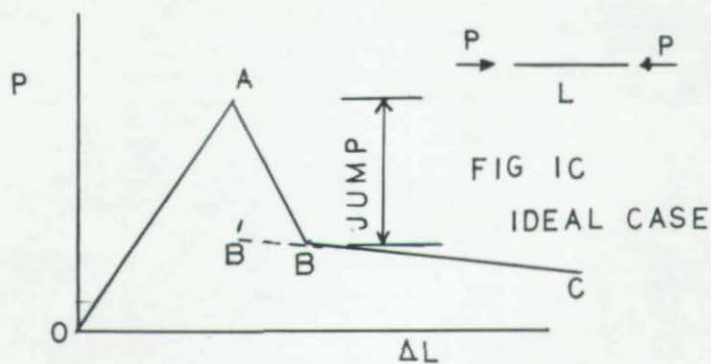
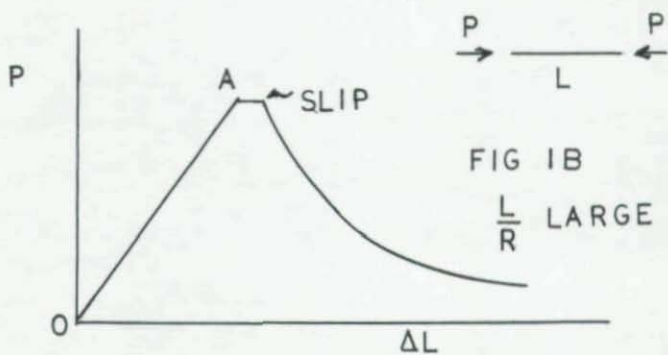
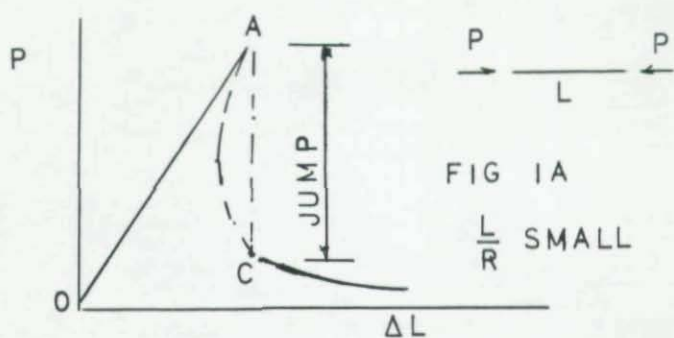
THE EFFECT OF STRUCTURAL STIFFNESS ON THE
PROGRESSIVE COLLAPSE OF SPACE TRUSSES

by Nicholas F. Morris
Manhattan College
Riverdale, New York 10471

INTRODUCTION

Space trusses are highly redundant structures. Hence one would expect them to be able to carry a substantial overload even after several members have failed either by yielding or buckling. Recent problems with constructed space truss structures (7) have lead to questions concerning their ability to carry load and the influence of redundancy on their overload capacity. Methods for the progressive collapse analysis of space trusses have been presented in (2,4,5,7, 8). In each reference except (8), the behavior of buckled members was modeled by following the unstable branch of the thrust-axial shortening curve and using the tangent modulus of this curve to define the member's negative post-buckling stiffness. While this approach appears to be reasonable, it overlooks the fact that in order for a member to follow the unstable branch of a stress-strain curve, the loading device must be stiffer than the member being loaded. Reference (8) errs in the other direction in that it is assumed that the member is always stiffer than the loading device so that jump instability always occurs.

A typical set of axial load-axial shortening curves is presented in Figure 1 (3,6,7,9). Such curves are usually linear along the rising branch OA and are assumed to be so herein. The situation after the buckling load is reached is the more interesting portion of the curve. Perfect columns, with low slenderness ratios can be expected to follow the curve as shown in Figure 1. There is a rapid drop off in load with increased axial shortening. Since the loading device which is unloading the specimen must be stiffer than the specimen, which is unlikely for a member with such a large negative tangent modulus as that which occurs at A, the unloading curve cannot be followed. The member must unload suddenly and the axial force must jump to the value at C. Curve b shows the typical curve for a member with some imperfections such as an initial deflection and applied transverse load, or a high slenderness ratio. There usually is some slip at constant load and then a negative axial load-axial shortening curve. Whether this curve is actually followed also depends on the stiffness of the loading device. If the stiffness of the device is greater than that defined by the negative tangent modulus at any point, the curve can be followed. If, however, the testing device is less rigid than the member, the axial force must jump to that portion of the load-deflection



curve where the tangent modulus is less than that of the loading device.

The loading device for an individual member in a space truss is the remainder of the structure. Therefore, one cannot determine the negative branch of the axial load-shortening curve unless one investigates the structure with the buckled member removed to determine the axial stiffness of the remaining structure against relative motion of the end joints toward each other. Herein, an attempt will be made to investigate the effect of this fact on the computation of the progressive collapse load of space trusses.

ANALYSIS

Three approaches to the computation of the collapse load are considered herein. In all cases, the member is assumed to follow the compressive axial load-deflection curve shown in Figure 1; the tensile curve is the usual ideal elastic-plastic curve. Unloading is assumed to be elastic. Non-linear geometry is included in the analysis of structure. With the exception of minor details, the method of analysis is described in (4). The variation from the previous method of analysis is presented herein.

The first approach completely neglects the effect of the surrounding structure on member post-buckling behavior. A buckled member is assumed to follow the compressive force-axial shortening curve. This is the traditional method for the computation of the progressive collapse load. Since this method does not assume any jump in axial force, it can be expected to yield an upper bound to the failure load. It is also the most simple analysis to carry out since the collapse load is computed with a single analysis.

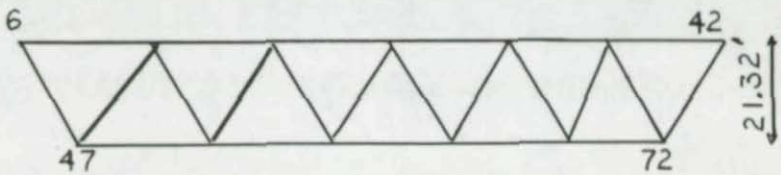
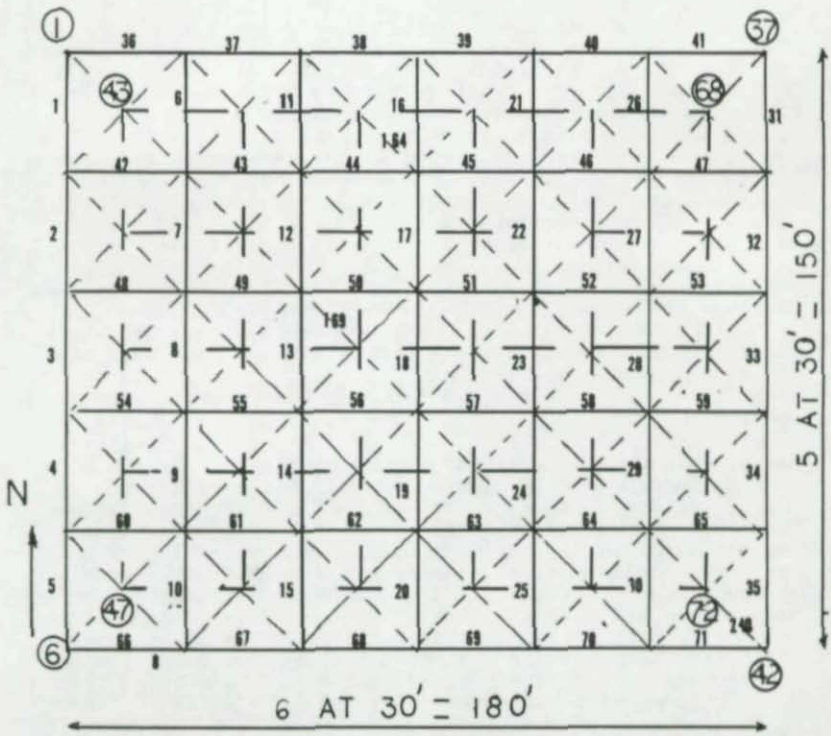
The second method of analysis is an interactive analysis. The structure is analyzed as in method one until the first member buckles. At this point, the nonlinear analysis is stopped. A linear analysis of the structure, with the buckled member removed, is carried out to determine the stiffness of the structure in the direction of the member. (This is accomplished by analyzing the structure subjected to unit loads at the end joints of the removed members and computing the relative movement of the joints). If the structure stiffness exceeds that of the bar on the unstable branch, the analysis is restarted with the buckled member following the curve AB. On the other hand, if the member stiffness is greater than that of the structure, the load in the member is lowered to B' and the analysis is restarted. The process is repeated when the next member buckles. A new linear analysis of the structure is carried out with the two buckled members removed to determine if member unloading is to occur along the negative axial force-shortening curve or by jumps to a new branch of the curve, B'C. The nonlinear analysis is restarted at this point and continues until the next member or

members buckle. Then the procedure is repeated. This approach is, admittedly, much more complicated than the first method of analysis. Nonetheless, it can easily be implemented. In addition, it should be noted that as members buckle, the structure's stiffness can be expected to drop off sharply so that once the analysis reveals that a jump will occur, it can usually be assumed that jumps will occur for each additional buckled member.

The third approach is a dynamic analysis. A member cannot jump from one equilibrium position to another one statically. Hence the jump load is an impact load on the structure. In addition, the structure which was in equilibrium under static load when the stiffness of the buckled member was defined by its positive elastic modulus must move to a new equilibrium position when that member has a stiffness defined by the negative tangent modulus along curve B'C. This can only be done dynamically. Therefore an analysis procedure similar to approach two can be carried out until it is determined that some buckled member must undergo a jump. A restart analysis is again carried out but the analysis, in this case, is a dynamic one. An impact analysis of the structure is carried out; a full period should be sufficient to determine whether additional members will buckle. If no new members buckle, the static analysis is continued until another member buckles and, if a jump occurs, another dynamic analysis is carried out. If any members fail during the dynamic analysis, it is assumed that these members have failed at the load level at which the original member which has undergone a jump has failed. A static analysis is continued until another member undergoes a jump, at which point a new dynamic analysis is carried out. The procedure is repeated until the collapse load is found.

NUMERICAL RESULTS

The preceding analyses were carried out for the double layered space truss shown in Figure 2. Figure 2 depicts a quarter plan of the first Hartford Coliseum roof (7). This structure was chosen because complete axial load-axial shortening curves were available for its members (7). No attempt was made to form an exact model of the roof. The roof as built had a design error in all east-west members; defective bracing made their effective length larger than the 15 ft assumed by the designer. No flaw existed in the north-south members. Herein it is assumed that all top chord members have this defect. This approach was followed because it was desired that the failure path be unknown at the start of the analysis. It should be noted that more than 50 different member types were employed in the model so space is not available to give the member details. The only support other than the symmetry conditions along lines 1-37, 37-42, 43-68 and 68-72 is a vertical support at the bottom node 51. Hence



the force distribution resembles the moment distribution in a flat slab. The design load is 70 psf on the top surface.

The results of the usual buckling analysis is presented in Table 1. As can be seen, the failure pressure is 62.24 psf which is 40 percent larger than the load at which the first member buckled. It is interesting to note that nonlinear behavior is not apparent from an analysis of the load-deflection curve for node 37 until the structure is at the failure state. Table 2 presents the analysis wherein jump instability is permitted. No jump occurs when member 31 buckles but jumps do occur at the buckling of all other members. Failure occurs at a pressure = 59.51 psf so the two analyses differ slightly for this structure.

It may seem surprising that the effect of jumps is not that large. The reason for this is the rapid unloading of buckled elements which reach the curve B'C in one or at most two load steps when no jumps are assumed. Therefore, the jump phenomenon has little influence on the structure's static behavior, at least for the structure under investigation.

Although a dynamic analysis at each load step wherein a member buckles can be time-consuming, there is no need to be so refined. If it is assumed that the ultimate failure path will be unchanged by any dynamic jump and that the effect of a dynamic analysis will be the same failure path at a reduced load level, the interactive analysis used to compute the structural stiffness at a buckled member can be used to estimate the influence of an impact load. The change in tension due to a unit unloading force is computed in this analysis. Since the change in force due to the jump in compressive stress is known, the static effect of the jump can be computed. Although the actual dynamic load factor is unknown, one would expect it to be around 1.20 to 1.60. Hence it is possible to estimate which members will buckle due to the dynamic effect of the jump instability. Using this approach it is seen that member 18 also buckles at a pressure = 49.00 psf. This has very little effect on the structure's overall behavior because the dynamic jump for this member is only around 42 kips. The critical load is $p = 54.24$ psf at which 3 members fail. This will cause a progressive failure of the structure and result in a failure pressure = 56.0 psf.

CONCLUSION

The numerical results obtained by the methodology introduced herein is insufficient to permit one to make broad generalizations. For the structure investigated herein, the difference between the two methods of static analysis is not large, leading one to conclude that interactive modeling need not be done for static failure analysis.

TABLE 1. USUAL BUCKLING ANALYSIS

p(psf)	w ₃₇	Buckled Members
43.76	.619	31
45.51	.645	26
47.24	.676	none
49.00	.726	21
50.76	.763	18
52.51	.851	13
54.24	.919	none
56.00	1.004	16,23,39,50
57.76	1.096	7,8
59.51	1.343	3,11,44,45,46,47,169
61.24	4.865	failure

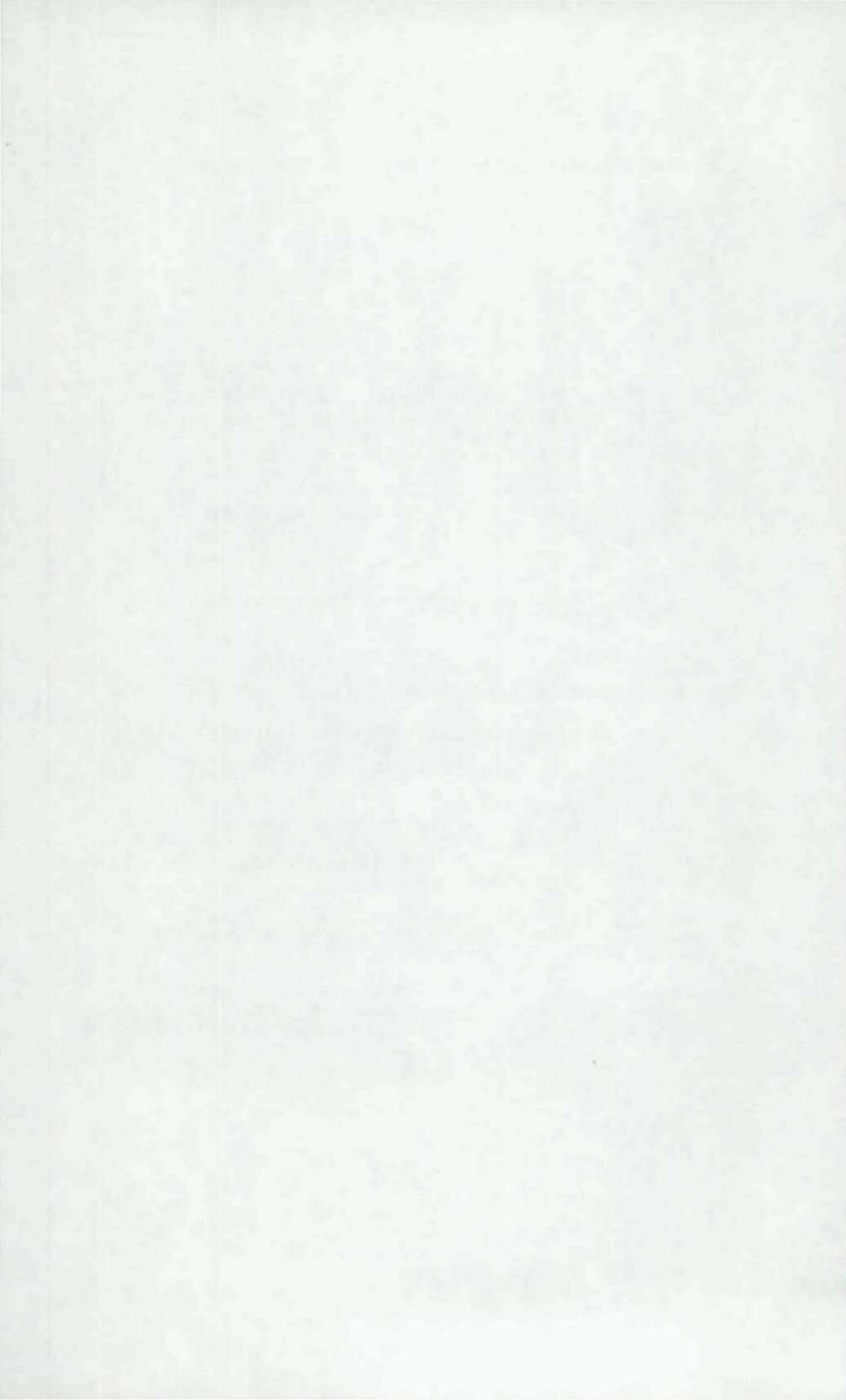
TABLE 2. INTERACTIVE BUCKLING MEMBERS

p(psf)	w ₃₇	Buckled Members
43.76	.619	31
45.51	.645	26
47.24	.694	none
49.00	.727	21
50.76	.816	18
52.51	.876	13
54.24	.966	16,39,50
56.00	1.137	7,8,44
57.76	1.439	2,3,4,11,23,164,169
59.51	8.401	failure

Although the influence of dynamic behavior is more pronounced, it must be admitted that the existence of a dynamic jump instability effect has not, to this writer's knowledge, been observed in any experiments on space trusses. Nonetheless, such jumps can be expected if the curves drawn in Figure 1 correctly describe the post-buckling curve. If the dynamic jumps postulated herein do not occur there must be some other mechanism acting which has not been hitherto considered.

REFERENCES

1. Golub, G. H., and Van Loan, C. F., Matrix Computation, The Johns Hopkins University Press, Baltimore, Maryland, 1983.
2. Hanaor, A., and Schmidt, L. C., "Space Truss Studies with Force Limiting Devices", Journal of the Structural Division, ASCE, Vol. 106, No. 11, Nov. 1980, pp. 2313-2329.
3. Kahn, L. F., and Hanson, R. D., "Inelastic Cycles of Axially Loaded Steel Members", Journal of the Structural Division, ASCE, Vol. 102, No. 5, May 1976, pp. 947-859.
4. Morris, N. F., "Buckling of Curved Space Trusses", Long Span Roof Structures, ASCE Symposium, St. Louis, Missouri, Oct. 1981.
5. Papadrakakis, M., "Inelastic Post-Buckling Analysis of Trusses", Journal of the Structural Division, ASCE, Vol. 109, No. 9, Sept. 1983, pp. 2129-2147.
6. Papadrakakis, M., and Chrysos, L., "Inelastic Cyclic Analysis of Imperfect Columns", Journal of the Structural Division, ASCE, Vol. 111, No. 6, June 1985, pp. 1219-1234.
7. "Report of the Engineering Investigation Concerning the Causes of the Collapse of the Hartford Coliseum Space Truss Roof on January 18, 1978", Lev Zetlin Associates, Inc., New York, 1978.
8. Smith, E. A., "Space Truss Nonlinear Analysis", Journal of the Structural Division, ASCE, Vol. 110, No. 4, April 1984, pp. 688-705.
9. Toma, S., and Chen, W. F., "Post-Buckling Behavior of Tubular Beam-Columns", Journal of the Structural Division, ASCE, Vol. 109, No. 8, Aug. 1983, pp. 1918-1932.



BEAM-COLUMN BEHAVIOR OF UNSTIFFENED FABRICATED STEEL TUBES

by

H.G.L. Frien

Ph.D. Candidate, Dept. of Civil Engineering, University of Toronto

P.C. Birkemoe

Professor, Dept. of Civil Engineering, University of Toronto

INTRODUCTION

The beam-column behavior of manufactured steel tubes has been well established, both analytically and experimentally. The automated production procedures produce a relatively high degree of accuracy in terms of cross-sectional shape and straightness. The size of these members, however, is limited to a diameter of about 300 to 400 mm. Larger cross-sections, up to 3 m in diameter, are required for structural applications such as offshore production platforms, and are typically fabricated from flat plate. Rolling and welding processes introduce significantly high levels of residual stress and geometric imperfection, which influence the load-deflection behavior and strength resistance of such members.

The column behavior [4,6,7,8,9,10,12,19,20] and the response under pure bending [14,18] of fabricated members have been studied experimentally and established by other researchers. The experimental beam-column behavior, however, has been largely done on manufactured rather than fabricated tubes [5,16,17]. The objective of this study was thus to establish experimental evidence on the strength and behavior of large scale fabricated tubes subjected to combinations of axial load and bending. Fabrication procedures as well as the induced residual stresses and geometric imperfections were measured to assist in subsequent analytical modelling. Extensive instrumentation and sophisticated load control permitted the close scrutiny of the behavior during loading, ultimate and post-buckling stages.

DESCRIPTION OF EXPERIMENT**Specimen parameters:**

All the tubes had a nominal diameter of 450 mm with wall thicknesses varying between 4.5 and 8.8 mm. In terms of the non-dimensional slenderness factor $\alpha = (E \cdot t / F_y \cdot D)$, all the specimens could be grouped into two categories, namely $\alpha \approx 7.5$ and $\alpha \approx 9.0$, representing a transitional region where local buckling begins to have an influence on the load resistance of members. Test specimens were made up from either two or four cans of 750 mm length each, with added extension tubes for the longer specimens.

TABLE 1 : Specimen Parameters

SPECI- MEN NO.	TEST TYPE	t [mm]	L [m]	Py stat. [MPa]	Fy dyn. [MPa]	$\alpha = \frac{E_t/F_D}{E}$ [-]	Py [kN]	Per [kN]	My [kNm]	Mp [kNm]	Mu [kNm]	MISMATCH as % of thickn. EXTENT, % of circumf.		INIT. ECC. [mm]
												WELD1 (4)	WELD2 (4)	
ST01	(a)	6.5	1500	304	320	9.74	2764	2764	-	-	-	52	11	-
ST02	(a)	6.5	1500	304	320	9.74	2764	2764	-	-	-	41	8	-
ST04	(b)	6.5	1500	304	320	9.74	2764	2764	308.0	392.1	363.5	13	3	18.5
ST05	(b)	6.5	1500	304	320	9.74	2764	2764	308.0	392.1	363.5	3	1	50.0
ST06	(b)	6.5	1500	304	320	9.74	2764	2764	308.0	392.1	363.5	23	14	25.0
ST07	(a)	4.5	1500	254	268	8.07	1603	1593	-	-	-	42	12	-
ST08	(a)	4.5	1500	254	268	8.07	1603	1593	-	-	-	32	14	-
ST09	(b)	4.5	1500	254	268	8.07	1603	1593	180.1	229.3	206.6	23	11	34.0
ST10	(b)	4.5	1500	254	268	8.07	1603	1593	180.1	229.3	206.6	44	9	33.5
ST11	(b)	4.5	1500	254	268	8.07	1603	1593	180.1	229.3	206.6	25	9	13.0
ST12	(b)	4.5	1500	254	268	8.07	1603	1593	180.1	229.3	206.6	26	7	50.0
ST13	(a)	7.3	1500	450	465	7.48	4513	4408	-	-	-	20	11	-
BC01	(c)	7.3	9880	450	465	7.49	4509	2850	484.2	627.3	559.5	44	25	14
BC02	(c)	7.3	9850	450	465	7.45	4529	2881	488.7	632.7	564.0	20	35	10
BC03	(c)	8.8	9825	450	465	8.93	5478	3551	591.3	767.7	701.9	27	35	20
BC04	(c)	8.8	9735	450	465	8.87	5513	3624	599.0	777.6	710.3	18	40	15
BC05	(c)	8.8	9645	450	465	8.83	5540	3686	605.3	785.7	717.2	8	10	25
BC06	(c)	7.3	9521	450	465	7.46	4523	2958	487.4	630.9	562.5	22	20	10
BC07	(d)	7.3	5000	450	465	7.46	4527	3927	488.7	632.3	563.6	11	10	15
BC08	(d)	8.8	4938	450	465	8.84	5531	4932	603.0	783.0	714.9	23	20	50
BC09	(d)	8.8	4870	450	465	8.85	5526	4941	602.1	781.2	713.4	9	20	50
BC10	(d)	7.3	4803	450	465	7.37	4583	4009	500.9	648.0	576.7	23	20	15
												11	15	14
												23	20	14
												11	15	10
												23	20	12
												11	15	10
												23	20	12
												11	15	10
												23	20	12
												11	15	10
												23	20	12
												11	15	10
												23	20	12
												11	15	10
												23	20	12
												11	15	10
												23	20	12
												11	15	10
												23	20	12
												11	15	10
												23	20	12
												11	15	10
												23	20	12
												11	15	10
												23	20	12
												11	15	10
												23	20	12
												11	15	10
												23	20	12
												11	15	10
												23	20	12
												11	15	10
												23	20	12
												11	15	10
												23	20	12
												11	15	10
												23	20	12
												11	15	10
												23	20	12
												11	15	10
												23	20	12
												11	15	10
												23	20	12
												11	15	10
												23	20	12
												11	15	10
												23	20	12
												11	15	10
												23	20	12
												11	15	10
												23	20	12
												11	15	10
												23	20	12
												11	15	10
												23	20	12
												11	15	10
												23	20	12
												11	15	10
												23	20	12
												11	15	10
												23	20	12
												11	15	10
												23	20	12
												11	15	10
												23	20	12
												11	15	10
												23	20	12
												11	15	10
												23	20	12
												11	15	10
												23	20	12
												11	15	10
												23	20	12
												11	15	10
												23	20	12
												11	15	10
												23	20	12
												11	15	10
												23	20	12
												11	15	10
												23	20	12
												11	15	10
												23	20	12
												11	15	10
												23	20	12
												11	15	10
												23	20	12
												11	15	10
												23	20	12
												11	15	10
												23	20	12
												11	15	10
												23	20	12
												11	15	10
												23	20	12
												11	15	10
												23	20	12
												11	15	10
												23	20	12
												11	15	10
												23	20	12
												11	15	10
												23	20	12
												11	15	10
												23	20	12
												11	15	10
												23	20	12
												11	15	10
												23	20	12
												11	15	10
												23	20	12
												11	15	10
												23	20	12
												11	15	10
												23	20	12
												11	15	10
												23	20	12
												11	15	10
												23	20	12
												11	15	10
												23	20	12
												11	15	10
												23	20	12
												11	15	10
												23	20	12

Test parameters:

Four types of tests were conducted:

- (a) Stub-column tests with fixed ends were done on five two-can specimens (length 1500 mm) (Fig.1(a)).
- (b) Five short columns, consisting of two cans each, with pinned ends, were subjected to an eccentrically applied axial load (Fig.1(b)).
- (c) Six 10 m long members, consisting each of a four-can test section and two 3.5 m long extension tubes, with spherical pinned ends, were subjected to an axial load and two equal lateral point loads, 2.4 m apart (Fig.1(c)).
- (d) Four 5 m long specimens, consisting each of a four-can test section and two 1.0 m long extension tubes, with spherical pinned ends, were subjected to an eccentrically applied axial load (Fig.1(d)).

Specimen fabrication:

Hot-rolled steel plate was cold-formed into tubular sections, the seams of which were butt-welded with a single pass full penetration weld, using an automated DC submerged arc process. Two or four cans were joined, with longitudinal welds staggered at 90° , with a hand-held Metal Inert Gas welding process. For the stub-columns and short eccentrically loaded columns, the ends were machined flat and parallel. For the 5 m and 10 m beam-columns, flanged extension tubes were welded to the four-can test sections.

During fabrication, data was recorded to determine the amount of distortion and residual strain induced by the longitudinal welds. Residual strains were measured with a mechanical extensometer on targets which were 100 mm apart and set around the circumference, on the outside as well as the inside of the tube. A profiling rig in combination with an automated data acquisition system recorded radius readings at set intervals around the perimeter of a tube. Complete surface profiles of single cans were obtained before and after seam welding to determine the distortions. Entire specimens were profiled before testing to obtain a complete record of initial geometry.

Testing procedure:

(a) Stub-column tests

A concentric axial load was applied to the two-can specimens with the 5340 kN universal testing machine of the Structures Laboratory, University of Toronto. The bottom loading fixture was a fixed pedestal whereas a spherical bearing transmitted the force at the top. Once the specimen was geometrically aligned for uniaxial load, the bearing was locked into position for the remainder of the test. 0.5 mm thick aluminum sheets were placed between the machined edges of the specimen and loading plates to smoothen contact unevenness. The loading was controlled manually, through adjustment of the hydraulic pressure. During the loading phase, the rate was maintained at approximately 50 kN/min, and a strain rate of 0.003/min during unloading. The post-ultimate behavior was followed to about 30% of the ultimate load.

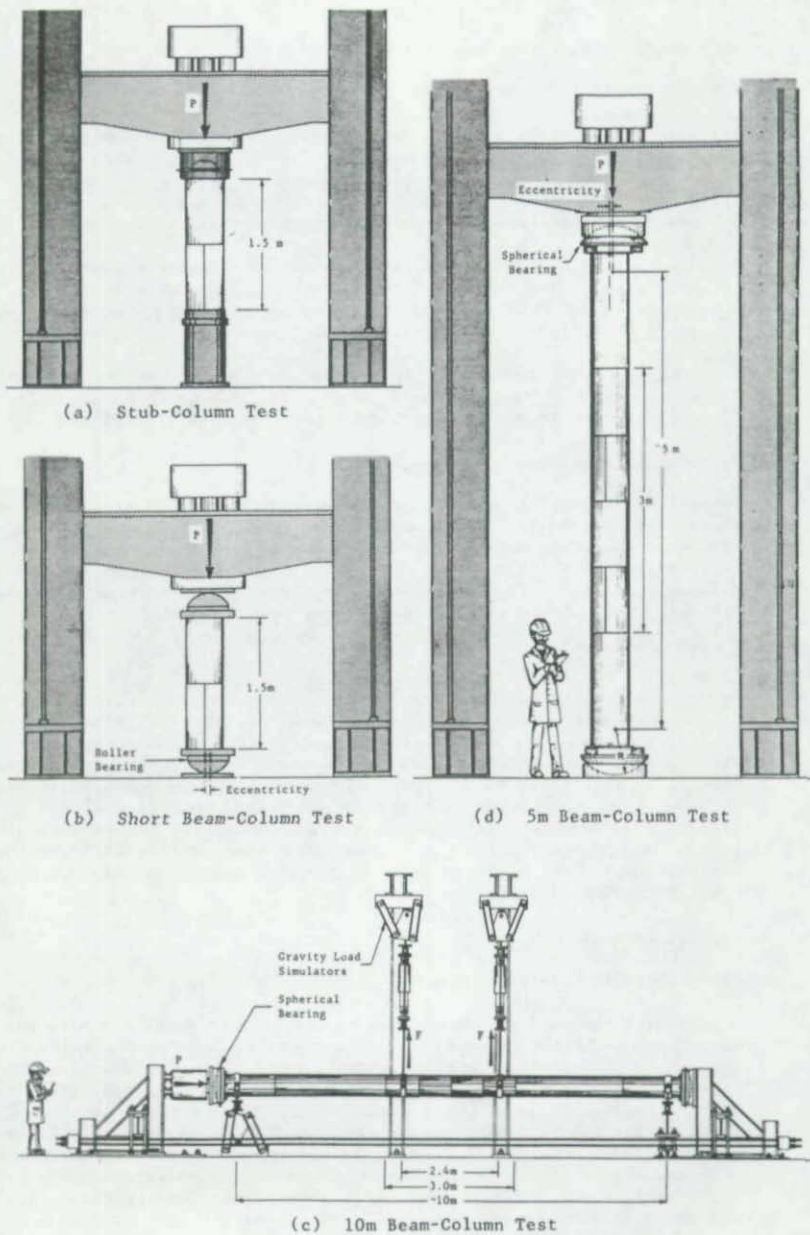


Fig. 1: Schematic Test Arrangements

(b) Short columns with eccentric load

Instead of fixed loading heads, hinged end bearings which allowed rotation about one axis were used. The specimens were positioned eccentrically to introduce a small moment in conjunction with the axial load. Testing proceeded as for the stub-columns.

(c) 10 m long beam-columns with lateral loads

The axial load was introduced through low friction spherical bearings with a manually controlled 10,000 kN actuator. After the predetermined axial load was reached, two equal lateral loads were applied with servo-controlled actuators while the axial load was kept constant. Lateral loads and reactions were introduced to the specimen through neoprene lined load collars. Translation of the load and reaction points was permitted by the use of gravity load simulators, thus avoiding any longitudinal force components. Except for the axial load, all load control and data acquisition was done with a computer controlled testing system.

(d) 5 m long beam-columns with eccentric axial load

These specimens were tested in the universal testing frame, similar to the short beam-columns. The same spherical bearings which were used for the 10 m specimens were employed here and the specimens were bolted to the loading plates at various eccentricities. Testing proceeded as for tests of the shorter beam columns.

In all the tests, one longitudinal seam weld was positioned to coincide with the maximum axial compression stress.

Instrumentation:

For all the specimens, load and stroke measurements, as well as the longitudinal strain distribution in the test section, at four locations around the circumference, were recorded. Diameter changes as well as lateral displacements were measured for the beam-column specimens ((b), (c) and (d)) at girth weld locations. Strain gages were positioned at strategic locations on the outside as well as the inside of the tubes to detect the onset of local buckling. Numerous displacement and strain measurements were taken to supplement the primary data records.

Specimen behavior under load:

All specimens exhibited a simultaneous yielding and buckling behavior at ultimate load with varying rate of decay after the ultimate load had been reached. In general, local yielding started around the girth weld long before a widespread yielded surface could be detected in the weld-free region. In the more slender specimens ($\alpha = 7.5$), some elastic buckling was observed before a plastic bulge developed over a localized area, in most cases opposite the junction of a longitudinal and girth weld. The more compact specimens ($\alpha = 9.0$) underwent a significant amount of yielding before a plastic buckle initiated the decay of resistance. The area engulfed by a buckle was considerably larger and buckles generally extended over the girth weld. In the 5 m and 10 m long specimens ((c) (d)), column buckling followed soon after a local buckle weakened the section. Lateral movement was rather abrupt (within a few seconds) due to the release of elastic energy in the specimen and reaction frames. A test in progress on a 10 m long beam-column is shown in Fig. 2.

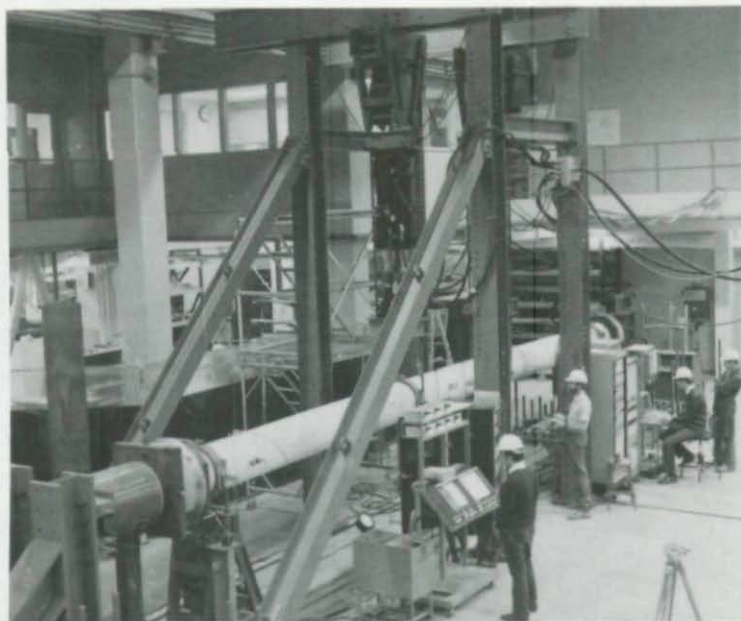
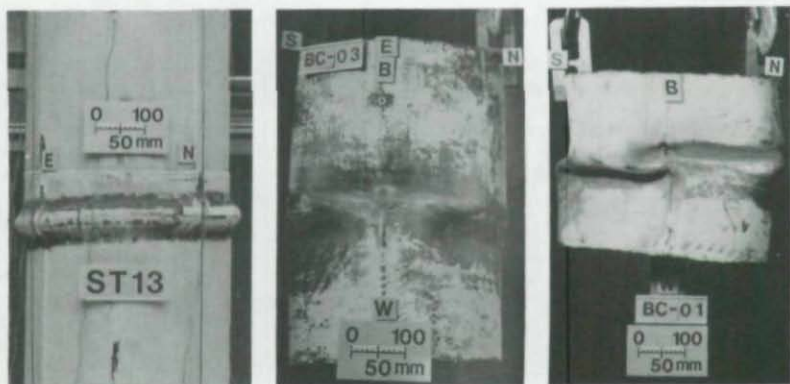


Fig. 2: 10 m Beam-Column Test



(a) Ring buckle

(b) Symmetric buckle

(c) Asymmetric buckle

Fig. 3: Typical Buckling Characteristics

Three distinct types of buckles could be observed, as shown in Fig. 3:

- (i) a single symmetric ring buckle that extended over the entire compression area. For the stub-columns, it extended around the full perimeter, which is often described as an "elephant foot" buckle.
- (ii) a symmetric alternating set of buckles with the initial buckle in the region of maximum compression, flanked by smaller buckles on either side.
- (iii) an asymmetric pair of buckles on either side of the maximum compression zone. A further set of smaller buckles often developed beside these.

In all tests, no significant end effects were observed. Only one 10 m long beam-column specimen (BC-06) failed at the load collar, but only after a higher than average stress level was reached in the remaining test region of the specimen.

RESULTS

Residual Strains

The maximum weld induced compressive residual strains in the longitudinal direction were found to be consistently about half the yield strain, and extended for about 1/8 of the circumference on either side of the weld, starting from the edge of the heat affected zone. The weld zone itself is generally believed to be strained beyond yield in tension. No significant difference was found in the strains on the inside and outside surface. A few selected strain gage readings confirmed the mechanically measured strains. (Fig. 4)

Distortions and Misalignment

Distortions caused by the longitudinal seam weld were the major reason for misalignment at the girth weld, and necessitated some cold forming and clamping to facilitate welding. A typical developed surface profile of a single can before and after welding is shown in Fig. 5.

The surface profile of a complete specimen, in Fig. 6, shows can deformations and misalignment at the girth weld, the extent of which is typically shown in Fig. 7. In Table 1, the misalignment in the compression region is given for all the girth weld locations.

Strength Interaction

The actual axial load and bending moment (including second order effects) at ultimate at a critical section are generally entered into a linear interaction formula of the type:

$$\frac{P}{P_y} + \frac{M_2}{M_y} \leq 1.0 \quad (1)$$

which restricts the member capacity to the point of first yield in the extreme compression fiber.

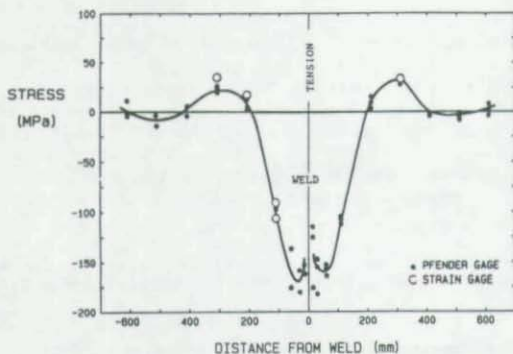


Fig. 4:
Residual Stresses
Induced by
Longitudinal Seam Weld

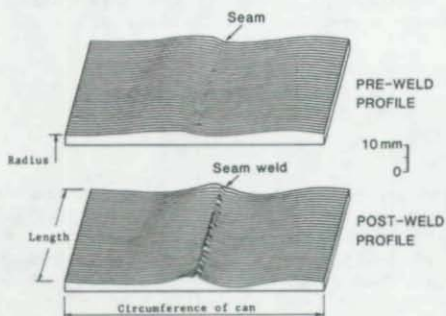


Fig. 5:
Distortions Resulting
from Seam Weld

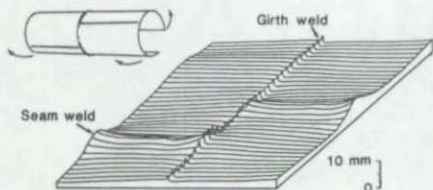


Fig. 6:
Total Distortion
After Girth Weld

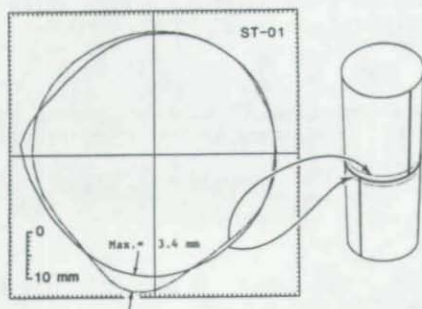


Fig. 7:
Girth Weld Mismatch
of Typical Two-Can
Specimen

TABLE 2 : Test Results

SPECI-MEN NO.	TEST TYPE	L/r	$\frac{a}{E_t/F_y D}$ [-]	P [kN]	d [mm]	M_1 [kNm]	M_2 [kNm]	$\frac{M_2}{M_1}$	$\frac{1-P/P_E}{1-P/P_E}$ [-]	STRENGTH INTERACT (1)	STAB. INTERACT (2)	$\frac{P}{P_y}$	$\frac{M_1}{M_y}$	$\frac{M_2}{M_y}$
ST01 (a)		-	9.74	2880	-	-	-	-	-	1.080	-	1.042	-	-
ST02 (a)		-	9.74	2840	-	-	-	-	-	1.043	-	1.027	-	-
ST03 (b)		9.7	9.74	2780	3.2	51.4	60.3	1.149	1.014	1.175	1.149	1.006	0.373	0.196
ST04 (b)		9.7	9.74	2300	2.4	115.0	120.5	1.012	1.012	1.071	1.152	0.832	0.373	0.391
ST06 (b)		9.7	9.74	2600	2.8	65.0	72.3	1.013	1.013	1.106	1.122	0.941	0.211	0.234
ST07 (a)		-	8.07	1720	-	-	-	-	-	1.125	-	1.073	-	-
ST08 (a)		-	8.07	1750	-	-	-	-	-	1.154	-	1.092	-	-
ST09 (b)		9.7	8.07	1485	2.1	50.5	53.6	1.011	1.011	1.153	1.179	0.926	0.280	0.298
ST10 (b)		9.7	8.07	1555	2.5	36.5	40.4	1.011	1.011	1.158	1.155	0.970	0.203	0.225
ST11 (b)		9.7	8.07	1640	1.4	21.3	23.6	1.012	1.012	1.161	1.134	1.023	0.118	0.131
ST12 (b)		9.7	8.07	1360	2.0	68.0	70.7	1.010	1.010	1.114	1.186	0.848	0.378	0.391
ST13 (a)		-	7.48	4450	-	-	-	-	-	1.015	-	0.985	-	-
BC01 (c)		63.9	7.49	1380	75.3	320.8	424.8	1.386	1.386	0.878	1.278	0.306	0.663	0.877
BC02 (c)		63.7	7.45	1202	127.5	309.4	462.6	1.312	1.312	0.910	1.137	0.265	0.633	0.947
BC03 (c)		63.3	8.93	1620	163.1	372.5	636.7	1.355	1.355	1.013	1.176	0.296	0.630	1.077
BC04 (c)		62.8	8.87	2826	112.9	133.1	452.3	1.786	1.786	0.944	1.114	0.513	0.222	0.755
BC05 (c)		62.2	8.83	2297	152.6	208.5	559.1	1.529	1.529	0.984	1.068	0.415	0.344	0.924
BC06 (c)		61.5	7.46	2154	96.4	179.9	387.6	1.666	1.666	0.969	1.261	0.476	0.369	0.795
BC07 (d)		31.3	7.46	3094	19.3	145.5	205.2	1.388	1.388	0.911	1.095	0.683	0.298	0.420
BC08 (d)		31.8	8.84	3747	32.6	176.1	298.3	1.375	1.375	0.932	1.049	0.677	0.292	0.495
BC09 (d)		31.4	8.85	2781	41.8	339.3	455.5	1.321	1.321	0.935	1.097	0.503	0.564	0.757
BC10 (d)		31.0	7.37	2199	25.6	268.3	334.6	1.311	1.311	0.848	1.065	0.480	0.536	0.648

$$(1) 2 \sin \left[\frac{\pi P}{4 P_{cr}} \right] + \left[\frac{M + P \cdot d}{M_u} \right]$$

$$(2) \frac{P}{P_{cr}} + \left[\frac{1}{1-P/P_E} \right] \frac{M}{M_u}$$

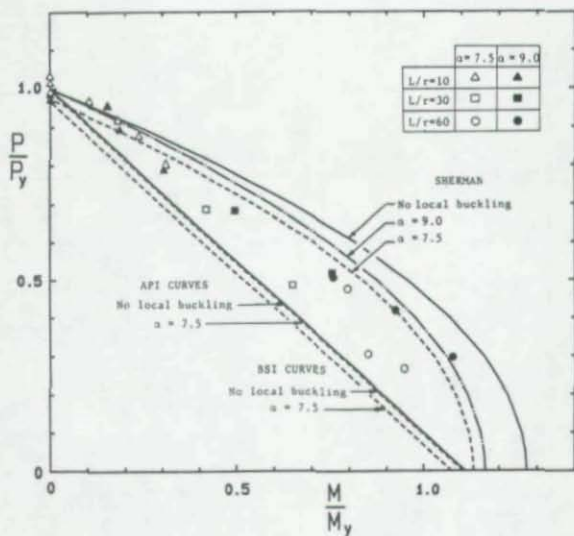


Fig. 8: Strength Interaction Curves

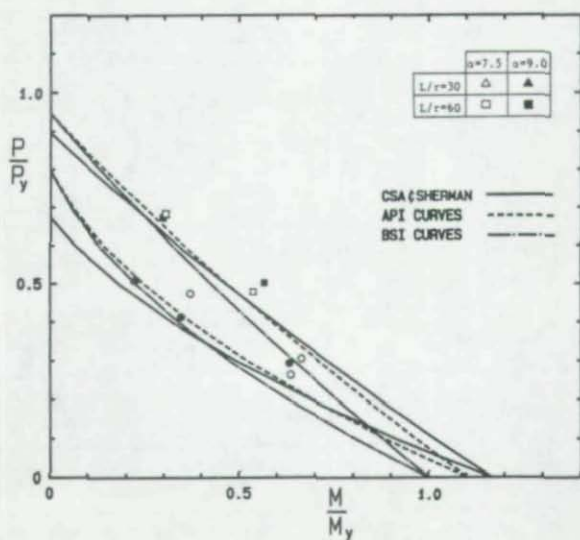


Fig. 9: Stability Interaction Curves

When full plastification of a section is regarded as the criterion for failure, the interaction formula becomes:

$$2 \sin^2 \left[\frac{\pi P}{4 P_y} \right] + \left[\frac{\pi M_2}{4 M_p} \right] \leq 1.0 \quad (2)$$

Both formulas are shown in the interaction diagram (Fig. 8) together with the test data.

As opposed to the pure axial load case where initial yield coincides with full plastification, the attainment of full plastic moment capacity requires compression strains far beyond yielding. The reduced load carrying capacity due to plastic local buckling is typified by a proposed set of reduced interaction curves [1,2,3,11,13], shown for the two section slenderness ratios tested.

Stability Interaction

The overall buckling of a beam-column is typically treated with an interaction of the form:

$$\frac{P}{P_{cr}} + \left[\frac{1}{1 - P/P_E} \right] \frac{M_1}{M_r} \leq 1.0 \quad (3)$$

The member slenderness is incorporated in the critical buckling load P_{cr} . The total moment is approximated by multiplying the first order moment M_1 with an amplification factor $1/(1 - P/P_E)$, while the moment resistance will generally incorporate local buckling reduction factors and may be based on the elastic (M_y) or plastic (M_p) moment capacity. Stability interaction curves from several popular specifications [1,2,3] are shown in Fig. 9, together with the test data from the 5 m and 10 m long beam-column experiments.

Load-deformation

For the purpose of uniformity the non-dimensionalized load parameter

$$\beta = M/M_y + P/P_y$$

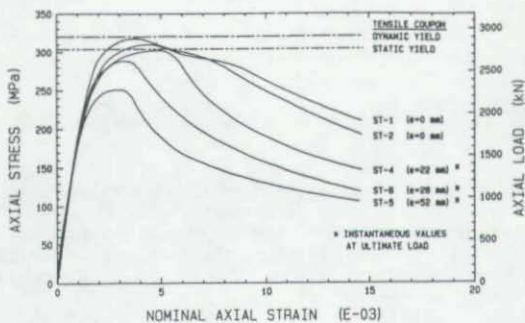
was plotted against the compression fibre strain. The value $\beta = 1$ represents the onset of yield in the extreme compression fiber. Typical load-deformation curves are shown in Fig. 10.

DISCUSSION AND CONCLUSIONS

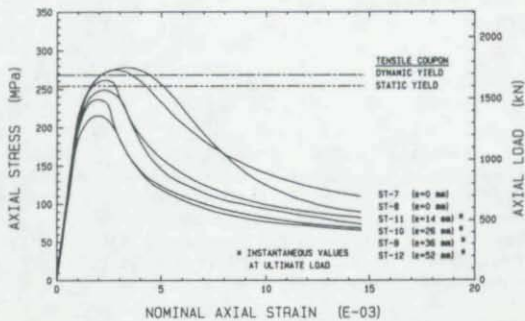
Within the scope of this experimental study, a few important points are highlighted here. While further evaluation of the data is underway, a few tentative conclusions can be made at this time.

Although fabrication procedures introduced significant imperfections in the tubes, no direct correlation was apparent between the imperfection level and the ultimate loads.

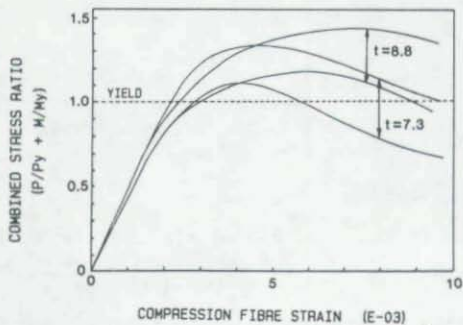
In considering the cross-sectional strength at the failure location, the stub-column specimens behaved as predicted, reaching the full yield load



(a) 6.5 mm Series



(b) 4.5 mm Series



(c) 5m and 10m Beam-Column Series

Fig. 10: Stress-Strain Behavior of Specimens

based on the coupon properties. With an increasing moment component, it became evident that full plastification could not be achieved.

The test results generally are lower than predicted by the strength interaction curves. The suggested strength mechanism compares well with experimental results of tubes subjected to pure bending [14,18]. The interaction between axial load and bending, however, may best be described with a linear relationship with the same reduced bending capacity as the limit for moments.

Two distinctive trends can be observed for the different slenderness ratios ($\alpha = 7.5$ and 9.0). The more slender specimens show a marked reduction from the predicted capacity with the exception of specimen BC-6, which failed at the load collar, rather than at one of the three girth weld locations.

The stability interaction equation (3) shows a reasonable agreement with experimentally observed capacities. The larger amount of scatter is expected since the second order moments are approximated with an approximate amplification factor.

An extensive analytical study is underway at the University of Toronto to model the behavior of fabricated tubular beam-columns and thus permit the extrapolation of the experimental results for more general geometric strength parameters.

NOMENCLATURE

D	Nominal outside diameter
d	Lateral member deflection at failure
E	Young's modulus, taken as 205,000 MPa
F _y	Coupon yield stress
L _y	Effective specimen length
M _p	Plastic moment capacity = F _y ·Z
M _r	Moment resistance $M_r = \phi M_u$
M _u	Reduced plastic moment capacity, due to local buckling
M _y	Yield moment = F _y ·S
M ₁	Applied bending moment (first order)
M ₂	Total bending moment (second order)
P	Applied axial load
P _{cr}	Axial buckling load
P _E	Euler load
P _y	Axial yield load
r _y	Radius of gyration
S, Z	Elastic, plastic section modulus
t	Wall thickness
α	Section slenderness E·t/F _y ·D
β	Load parameter
ϕ	Performance factor

REFERENCES (Alphabetically)

- [1] API Recommended Practice for Planning, Design and Constructing Fixed Offshore Platforms, API RP 2A, 12th Edition, Jan. 1981, American Petroleum Institute, Washington, D.C.
- [2] Code of Practice for Fixed Offshore Structures, BS 62345: 1982, British Standards Institution.

- [3] Canadian Standards Association, Steel Structures for Buildings-Limit States Design, CAN 3-S16.1-M84, ISSN 0317-5669.
- [4] Chen, W.F., and Ross, D.A., "Tests of Fabricated Tubular Columns", Journal of the Structural Division, A.S.C.E., Volume 103, ST3, March 1977.
- [5] Matsui, C., and Tsuda, K., "Strength and Behaviour of Circular Steel Tubular Beam-Columns", Proceedings of the International Conference on "Steel Structures - Recent Research Advances and their Applications to Design, Part 1, Budva, Yugoslavia, 1986, Hajdin, N., Sekulovic, M. (Ed.)
- [6] Ostapenko, A., and Gunzelman, S.X., "Local Buckling of Tubular Steel Columns", Proceedings, Methods of Structural Analysis, Volume 2, A.S.C.E., New York, N.Y., 1970.
- [7] Ostapenko, A., "Local Buckling of Welded Tubular Columns", Proceedings of the International Colloquium on Stability of Structures Under Static and Dynamic Loads, (Washington, D.C., May 1977), A.S.C.E., New York, 1977.
- [8] Ostapenko, A., and Marzulla, M.A., "Tests on Two High-Strength Short Tubular Columns", Proceedings of the 10th Offshore Technology Conference, Houston, Texas, May 1978.
- [9] Ostapenko, A., and Gunzelman, S.X., "Local Buckling Tests on Three Steel Large Diameter Tubular Columns", Proceedings of the Fourth International Conference on Cold-Formed Steel Structures, St. Louis, Missouri, June 1978.
- [10] Ostapenko, A., and Grimm, D.F., "Local Buckling of Cylindrical Tubular Columns Made Of A-36 Steel", Lehigh University Report No. 450.7, February 1980.
- [11] Plantema, F.J., "Collapsing Stresses of Circular Cylinders and Round Tubes", Report S.280, Nat. Luchtvaartlaboratorium, Amsterdam, The Netherlands, 1946.
- [12] Sato, J.A., "The Compression Behaviour of Unstiffened Fabricated Tubes", M.A.Sc. Thesis, Civil Engineering Dept., University of Toronto, 1985.
- [13] Sherman, D.R., "Inelastic Flexural Buckling of Cylinders", Steel Structures - Recent Research Advances and Their Applications to Design, M.N. Pavlovic (Ed.), Elsevier Applied Science Publishers, London, 1986.
- [14] Sherman, D.R., "Tests of Circular Steel Tubes in Bending", Journal of the Structural Division, A.S.C.E., Volume 102, ST11, Paper 12568, November 1976.
- [15] Sherman, D.R., "Inelastic Behaviour of Tubular Members", Preprint for Session No. 45, A.S.C.E., Chicago, 1978.
- [16] Sherman, D.R., "Post Local Buckling Behaviour of Tubular Strut Type Beam-Columns: An Experimental Study", University of Wisconsin - Milwaukee Report, June 1980.
- [17] Sherman, D.R., "Buckling Behaviour of Round Tubular Beam-Columns", Preprint of a paper presented at the A.S.C.E. Structures Congress, ST-16, Houston, Texas, October 1983.
- [18] Sherman, D.R., "Report on Bending Capacity of Fabricated Pipes", University of Wisconsin - Milwaukee Report, Feb. 1983.
- [19] Wilson, W.M., and Newmark, N.M., "The Strength of Thin Cylindrical Shells as Columns", Bulletin No. 255, Engineering Experiment Station, University of Illinois, February 1933.
- [20] Wilson, W.M., "Tests of Steel Columns, Thin Cylindrical Shells, Laced Column Angles", Bulletin No. 297, Engineering Experiment Station, University of Illinois, April 1937.

ULTIMATE BEHAVIOUR OF CIRCULAR TUBULAR MEMBERS

WITH

LARGE INITIAL IMPERFECTIONS

by

Jon Taby and Torgeir Moan

Division of Marine Structures, The Norwegian Institute of Technology,
The University of Trondheim

SUMMARY

The paper presents a method for calculating the load-displacement behaviour of tubulars with large initial imperfections, subjected to combined axial compression and bending moment.

Frame analyses are normally carried out with beam-column elements without accounting for the effect of local imperfections of the circularity of tubes. Effects such as local buckling of the cross section in the post-collapse region are neither considered.

Premature local buckling of the tube wall is normally avoided in structures made of unstiffened tubulars by choosing a sufficiently low D/t ratio or by use of a reduced yield strength. But even by taking this precaution, local buckling might occur if a dent is present. This is because abnormal imperfections are not accounted for by determining the safe D/t ratio given in codes.

In the method presented the effect of premature local buckling and buckling deformation of the cross section in the post-collapse region is accounted for. The method is assumed to be valid for any magnitude of initial imperfections in terms of overall beam deformation and local dent depth.

The theory is supported by a relatively large number of experimental results. Three series of tests with simply supported tubes, one series with tubes with clamped end conditions and one series with eccentrically loaded tubes have been carried out, 107 specimens in all.

The correlation between theoretical predictions and experimental results is discussed.

The method has been implemented on PC's as well as main-frame computers (VAX, IBM and NORD).

INTRODUCTION

To make decisions regarding safety and economy during design and operation, it is important to have knowledge about the ultimate strength after probable accidents have caused damage in form of large geometrical imperfections.

The verification of residual structural strength is in most cases done by means of linear methods. Especially for damaged trussworks such methods yield too conservative values. Methods which account for the geometrical and material non-linearities associated with load redistribution should therefore be applied.

However, such methods are normally based on ordinary beam-column elements without accounting for the occurrence of dents. Effect of further deformation of the cross-section in the post-collapse region are neither considered. Local buckling of the tube wall is normally avoided in structures made of unstiffened tubulars by choosing a sufficient low diameter to thickness ratio or by using a reduced yield strength. But even by taking this precaution, local buckling might occur if a dent is present because the safe D/t ratio or the reduction in yield strength found in the various design codes are not accounting for abnormal imperfections.

Rigorous analysis of dented tubes may in principle be carried out by means of non-linear finite element shell analysis; such analysis requires, however, a major investment of time and effort. Hence, simplified methods for calculating the strength of damaged tubular structures are needed.

Previous Work

The effect of damage on the behaviour of tubular members subjected to axial compression was first studied by Sith et al. /1/. They reported results from experiments with undamaged and slightly damaged tubular members. The damage was in the form of lateral bending and/or local denting. These results indicated a substantial loss of strength due to relatively small damages.

Later Smith /2/ presented a semi-empirical method to account for dents based on finite elements and empirical reduction factors for yield strength and material stiffness. The empirical factors were based on experimental results carried out at AMTE /1,3/ and in Trondheim /4/.

Shortcomings were, however, observed with respect to the post-collapse behaviour due to local buckling of thin-walled cross-sections.

Ellinas /5/ used the analytical model presented in Ref. /6/ in combination with ordinary beam column theory to evaluate ultimate strength of axially compressed tubes with denting and bending damages. Ellinas seems to be more interested in a lower bound solution, but the method seems to give different degree of under-estimation depending on tube geometry and degree of damage. It is found that the method corresponds quite closely to experimental results for slender tubes ($\bar{\lambda} > 0.6$). While for more stocky tubes ($\bar{\lambda} = 0.4$) the method gives rather conservative results at small initial deflections and non-conservative values at large initial lateral deflec-

tions. The under-estimation further increases with increasing dent depth; and decreases with increasing D/t ratio. A main reason for too low estimates for deeper dents may be the fact that the eccentricity acting at the short dented length is treated as if it was the amplitude of a sinusoidal initial lateral deflection curve over the whole member. Furthermore, this method only gives the ultimate load and may not be used effectively in a progressive collapse analysis.

Rashed and Taby /4,6,7/ developed during 1980 a simplified method for the computer program DENTA based on results from 24 dented test specimens. DENTA was designed to simulate partly damaged tubes where the damage had the form of a dent only. The effect of initial lateral deflection was not included. However, the method was later modified to include initial lateral deflections too /8/.

Present Work

The present paper deals mainly with the further development of the theory behind DENTA. From the experimental results carried out in ref. /8/ there were observed some discrepancy between experimental and theoretical results:

- Buckling strength of thick-walled tube were under-estimated by the present method.
- Buckling strength of thin-walled tubes were more influenced by premature local buckling of the tube wall than expected.
- The post-collapse strength was to a large extent influenced by increasing distortion of the cross-section during loading.
- In the case of restrained end supports it was found that effective buckling length of a dented tube differs from an undented one.

The refined method is based on a physically realistic, but simplified characterization of the dented length of the tube. The simplifications made have been justified by a large number of test results.

Experiments with 107 tubular specimens, with a various extent of damage have been carried out. The experimental result from these tubes have been the basis for the semi-empirical methods used for describing the interaction with premature local buckling and the increasing cross-sectional deformation in the post-collapse region.

Further, the validity of the method is demonstrated by comparative tests between experimental and theoretical results.

At the end of the paper, some parametric studies are carried out. The influence of dent depth, dent length, magnitude of overall bending damage and the location of the dent are examined.

BASIC OBJECTIVES OF THE THEORETICAL METHOD

The analysis model may be divided into four main modes of behaviour, namely (as shown in Fig. 1.):

- (i) Elastic behaviour up to first yield, P_y .
- (ii) Elastic-plastic behaviour up to ultimate load, P_u .
- (iii) Transition to fully plastic behaviour.
- (iv) Fully plastic post-collapse behaviour.

In the following the theoretical model is briefly described. This includes the idealization of the dented tube, the representation of premature local buckling and the growing cross-sectional deformation. For a more detailed description see ref /9/.

Idealization of a Dented Tube

As shown in Fig. 2 the member is modelled by three components; the dented length and the two parts adjacent to this.

The dented length is further divided into two part, namely the dented part of the cross-section and the undamaged part.

The dented part of the cross section is substituted by a force, F_d , which may increase to a maximum value which causes a yield hinge to be developed in the bottom of the dent. This maximum force, F_{dp} , is derived from a single flat, bent plate analogy. An empirical linear correction factor, C_{dp} , due to the restraining effect of the rest of the cross-section is introduced. Thick-walled tubes are by this simulated properly. F_{dp} may then be written as:

$$F_{dp} = C_{dp} \sigma_y D \alpha (\sqrt{4\eta^2 + t^2} - 2\eta) \quad (1)$$

where:

$$C_{dp} = 80 \cdot t/D \quad (2)$$

D - diameter to mid-thickness

t - wall thickness

σ_y - yield stress

η - the distance from the line of action of the force F_{dp} to the line at the bottom of the dent

$$= (\sin \alpha / \alpha - \cos \alpha) D/2 \quad (3)$$

$$\alpha = \arccos (1 - 2D_d/D) \quad (\text{see Fig. 2}) \quad (4)$$

D_d - dent depth

The neutral axis of the undamaged part of the cross section at the dented length is eccentrically located to the neutral axis of the undamaged circular cross-section. Normally the dented length is relatively short compared to the overall length and it's influence on the overall deflection during loading in the elastic region is normally small, of the order of 1% at first yield.

Loading up to first yield

The behaviour up to first yield is analyzed by two different methods depending on the boundary conditions:

- (i) In the case of simply supported tubes the load deflection relations are calculated analytically by means of a simplified amplification

factor, γ , to account for second order effects. This factor is approximately calculated as

$$\gamma = 1 + C_d / (P_{ER} - P) \quad (5)$$

where C_d is a correction factor to account for the location of the dent. P_{ER} is an approximate value for a reduced Euler load of a dented tube under the assumption of a sinusoidal buckling mode. The primary deflection to be amplified by this factor is the sum of the initial deflection and the deflection caused by the bending moment in the dented length caused by the eccentricity. The load level at first yield at most stressed fibre adjacent to the dent in the dented cross-section, P_y , is then found analytically.

- (ii) In the case of end conditions other than simply supported, a secant stiffness matrix is derived from the differential equation of the idealized dented column under the assumption of a sinusoidal bending damage. A tangential stiffness matrix is established and the analysis is performed in steps by incrementing the axial load $/10/$.

Premature local buckling

Interaction with premature local buckling is accounted for by replacing the yield stress, σ_y , with a critical local buckling stress, σ_c . The critical buckling stress is derived from a regression analysis which included results from 11 specimens. The method is based on "real" stress at a damaged cross-section and not a fictitious average stress derived from an intact cross section. Replacement of the yield stress by the critical buckling stress is performed during calculation of first yield and ultimate load. The critical local buckling stress may for members which are affected by plasticity be written as:

$$\sigma_c = \phi \sigma_y \quad (6)$$

where ϕ is an empirical function related to the structural slenderness and σ_y is the yield strength. Several slenderness parameters may be used. Here, the so-called reduced slenderness, $\bar{\lambda}$, is adopted for small imperfections (dents):

$$\bar{\lambda} = \sqrt{\sigma_y / \sigma_E} \quad (7)$$

where σ_E is the elastic shell buckling stress. One expression for ϕ as a function of $\bar{\lambda}$ may be obtained from a simple interaction approach, (Merchant-Rankine approach)

$$\left(\frac{\sigma_c}{\sigma_E}\right)^2 + \left(\frac{\sigma_c}{\sigma_y}\right)^2 = 1 \quad (8)$$

By combination of Eqs. (6), (7) and (8), the following result is obtained,

$$\phi = 1 / \sqrt{1 + \bar{\lambda}^4} \quad (9)$$

By definition:

$$\sigma_E = \rho \sigma_{C1} \quad (10)$$

where ρ is the knockdown factor and σ_{C1} is the classical buckling stress for cylindrical shells under axial compression given by:

$$\sigma_{C1} = 0.606 Et/R \quad (11)$$

An analytical expression for the knockdown factor, ρ , is obtained from Ref. /11/

$$\rho = 1 - \frac{C}{2} \left(\frac{\bar{w}}{t} \right) \left[\sqrt{1 - \frac{4}{C} \left(\frac{t}{\bar{w}} \right)} - 1 \right], \quad C = \frac{3}{2} \sqrt{3(1 - \nu^2)} \quad (12)$$

where \bar{w} is considered as an "effective" imperfection amplitude measured over a length $l = 4\sqrt{Rt}$.

From a regression it was found, /11/, that a best fit for cylinders with "normal" imperfections was obtained for

$$\bar{w} = 0.0022 \cdot 4\sqrt{Rt} \quad (13)$$

The imperfection parameter \bar{w} is not a physical quantity. However, by taking \bar{w} as the actual imperfection theoretical results compare well with experimental ones. Hence, Eq. (12) is adopted in the present theory in order to take "normally appearing imperfections" (small dents) into account. The minimum dent depth is set equal to w derived from Eq. (13).

The above formulation is developed on the basis of cylindrical shell theory valid for relatively small imperfections in relation to most frequent dent sizes. Consequently, it has been necessary to derive another expression for ϕ to account for larger dents.

To obtain an estimate for ϕ , a regression analysis have been carried out using experimental data from 107 tubes with different dents sizes and nominal geometries. However, in only 11 cases premature local buckling occurred. For each test specimen a value for ϕ was adopted for which theoretical and experimental ultimate load was equal ($\phi < 1$ in 11 cases). The tube parameters which might influence ϕ were judged to be D/t , E/σ_y and the dent depth expressed in terms of: $\sin(\alpha) + 1$. (see Eq. (4)).

A factor ϕ was derived,

$$\phi = \sqrt[3]{E/\sigma_y} (t/D [1 + \sin \alpha]) \quad (14)$$

and a regression equation of the form

$$\phi = a_0 + a_1 \phi + a_2 \phi^2 \quad (15)$$

was assumed and values of the coefficients a_0 , a_1 and a_2 were computed using a least-squares method to provide a best fit to the "true" value of ϕ . The equation finally obtained was

$$\phi = \begin{matrix} 11.095 \phi - 30.47 \phi^2 & \phi & < 0.164 \\ 1.0 & \phi & \geq 0.164 \\ 1.0 & \sqrt[3]{E/\sigma_y} (t/D) & > 0.08 \end{matrix} \quad (16)$$

The last term in Eq. (16) is overriding the two other if satisfied. This term is almost identical to what suggested by Ostapenko /12/ for undented tubes. He suggested a limit value of 0.07.

Fig. 3 shows Eq. (9) and Eq. (16) as function of the dent depth. The knock-down factor is calculated according to Eq. (12) and the imperfection parameter \bar{w} is substituted by the dent depth D_d and set equal to a min value according to Eq. (13). The curves are drawn for a tube with $D/t = 118.8$, $\sigma_y = 290$ MPa and $E = 2.07 \cdot 10^5$ MPa. For this particular tube, DnV App. C recommends a value of ϕ equal to 0.94 due to the high D/t ratio. As seen from the figure this is obviously not enough if the tube had a dent damage of about 0.02 times the diameter.

The curve derived from Eq. (16) implies an increasing buckling stress with increasing dent depth and may seem paradoxical. Nevertheless, it is logical since the theory used in DENTA accounts for a dent and is not using any fictitious average stress based on intact cross-section.

Fig. 4 shows the theoretical ultimate load compared to the experimental ones for the 11 tubes sensitive to premature local buckling before and after a reduction of the yield strength.

Elastic-plastic buckling and ultimate load

The method is based on equilibrium between internal and external forces while the stresses are kept within the yield surface. σ_y is replaced by σ_c if premature local buckling is likely to occur.

The lateral deflection is incremented until the axial load starts to drop at the level of the ultimate load, P_U .

The plastic deformation is assumed to be limited to a length equal to the dented length or the diameter, whichever is largest.

Deformation of the cross section in post-collapse region

Buckling of the tube wall in the post-collapse region is not a phenomenon addressed exclusively to initially dented tubes. This effect also influences the post-collapse behaviour of all tubular members, however, to a different extent; strongly in case of thin-walled tubes, and insignificantly to tubes with a D/t ratio lower than about 30.

For tubes with a D/t ratio above 60 it is assumed in DENTA that a certain degree of the (cross-sectional) deformation, dependent on D/t ratio, takes place during the transition from elastic-plastic state to a fully plastic one. The transition to fully plastic state is necessary in order to bring the tube to a condition which is consistent to the yield-hinge theory used for the post-collapse part of the analysis.

In the fully plastic state the rate of the further deformation is controlled by an empirical function and the current load condition. This function is derived from a regression analysis which includes results from 84 experiments. The buckling is treated as it should have been a dent which is growing deeper. The current dent depth is found possible to

describe as a function of the nominal geometry and the current relative load level). This is at least true if the bending of the tube is only caused by the axial compression load:

The growing dent depth D_{dg} , as function of post-collapse load may be expressed as

$$D_{dg} = D_d + G_1 f_{g1}(P, P_U, P_p) + G_2 f_{g2}(P, P_U, P_p) \quad (17)$$

where

D_d - dent depth at the beginning of the plastic post-collapse

$$G_1 = 0.00254 D/t + 5.093 \cdot 10^{-5} (D/t)^2 - 3.465 \cdot 10^{-7} (D/t)^3 - 0.03847 \geq 0 \quad (18)$$

$$G_2 = 3.056 (\sigma_y/E) (D/t) + 8.024 G_1 - 29.24 G_1^2 + 34.12 G_1^3 - 0.8525 \geq 0 \quad (19)$$

$$f_{g1} = D[(1 - P/P_p)^{2.0} - (1 - P_U/P_p)(1 - P/P_p)^{1.0}] \quad (20)$$

$$f_{g2} = D(0.25 - P/4P_U) \sin(1.57 (P_U - P)/P_U) \quad (21)$$

In Fig. 5 the effect of cross-sectional deformation on the load end-shortening behaviour is demonstrated and compared to experimental results. In this case the D/t ratio is as high as 78. However, the effect is also significant for D/t ratios as low as 40.

Post-collapse behaviour

The post-collapse behaviour is calculated by means of a yield-hinge theory introduced by Ueda et. al in Ref. /13/. The yield-hinge is inserted at the location of the most stressed cross section, most often the dented cross-section.

By this method the plastic interaction relationship between moment and axial force is regarded as a plastic potential describing the behaviour of the plastic hinge. The interaction relationship is influenced by the growing deformation of the cross section; and this effect is regarded when a tangential stiffness matrix is established. The post-collapse behaviour is then calculated by incrementing the axial load.

The plastic interaction curve for a dented tube is assumed to be expressed as:

$$\Gamma = M/M_p - B - \sin \gamma + 0.5 \sin \alpha = 0 \quad (22)$$

where:

$$B = (\sigma_{dp}/2\sigma_y) \sin \alpha \quad (23)$$

M - current moment

$$\gamma = \text{half the sector with tension} \\ = 0.5[\pi - \alpha + \alpha\sigma_{dp}/\sigma_y - \pi P/P_p] \quad (24)$$

$$\alpha = \text{half the dented sector (Eq. 4)}$$

$$\sigma_{dp} = \text{the maximum compressive stress in the dent} \\ = F_{dp}/(Dt\alpha) \quad (25)$$

$$M_p = \text{the theoretical fully plastic moment capacity} \\ = D^2t\sigma_y \quad (26)$$

EXPERIMENTAL INVESTIGATION

The primary geometrical parameter of a dented tube, besides the dent itself, is the D/t ratio. Therefore the tubes tested may in general in this context, be divided into three groups:

- "Thick-walled" tubes; tube with a D/t ratio lower than about 35. When the D/t ratio decreases below 35, the influence of a dent is decreasing substantially.
- "Normal-thick-walled" tubes; tube with a D/t ratio between 35 and 100. Above the upper limit, premature local buckling may be expected, especially if a dent is present.
- "Thin-walled" tubes; tube with a D/t ratio higher than 100. Tubes within this group are at least if a dent is present, likely to have their ultimate strength influenced by premature local buckling.

Several parameters may be used to classify types of tests. Here, the load- and boundary conditions are used for dividing the tubes into groups. In general three types of tests have been performed:

- (i) 69 tubes under central axial compression and simply supported end conditions. All tubes but 3 thin-walled ones among them, were subjected to damage in form of a dent or a combination of a dent and overall bending.
- (ii) 10 tubes under central axial compression and clamped end condition. All tubes in this category were subjected to a lateral load under fully clamped end condition (both axially and rotationally).
- (iii) 13 tubes under eccentric axial compression. All tubes were subjected to a combined overall bending and denting damage.

In order to have more ductile material without residual stresses, all the tubes, but four, were stress relieved. The four tubes not heat-treated had a diameter/thickness ratio of about 135 and a stress relieving process could easily affect their circular shape.

The overall bending damage and/or the dent were in all cases made by an indenter with a straight edge with a tip radius of about 5 mm. The dent was oriented 90° to the tube's axis.

Compression tests were carried out under displacement control in a hydraulic testing machine after initial measurements of diameter to mid thickness, D ; thickness t ; initial lateral displacement, δ_0 , and dent depth, D_d , were carried out.

Static yield stress, σ_y , was obtained from tensile specimens. No corrections for a possibly, higher yield stress in compression have been made.

In order to obtain static ultimate load, both tensile tests and the final compression test of the tubes were carried out at similar average strain rate of about $3 \cdot 10^{-3}$ /sec. Fig. 6 shows the arrangement for testing simply supported tubes.

Tables 1 - 5 summarize the main parameters of the tested specimens.

Simply supported tubes

Most of the tubes have been tested under simply supported end condition, with D/t ranging from 12 to 135. Tables 1 - 3 show dimensions and material properties.

In Fig. 7 experimental ultimate loads from 69 simply supported tubes are compared with theoretical predictions.

Clamped tubes

For undamaged tubes the effect of the boundary conditions is normally accounted for by use of an effective buckling length. In order to decide by which confidence a similar procedure could be used for dented tubes, 10 tubes with clamped end condition were tested /8/. Dimensions were chosen to cover a D/t range from 12 to 78. Table 4 shows dimensions and material properties of these tubes.

A lateral load simulating a colliding object was prior to compression test, applied centrally making a damage in form of a combination of dent and overall bending. The tube ends were prevented from both axial and rotational movement during this process.

Two methods have been used to predict the theoretical strength. In the first case by means of DENTA by simulating a clamped tube by use of simply supported tube with a buckling length equal to $l/2$. Thereafter by means of DENTA-2 where the real boundary conditions are taken into account /10/. By comparing both theoretical results with test results, /9/, it was found that a use of buckling length equal to $l/2$ gave conservative results. It seems to be two reasons for this:

- The effective buckling length: The true length between the two inflection points goes to zero when the stiffness at the dent approaches zero.
- The residual strength at the ends: The strength at the ends is the same in dented and intact cases.

In Figs. 8 and 9 theoretical results obtained with DENTA and DENTA-2 are compared to experimental results.

Eccentrically loaded tubes

13 tubes were loaded eccentrically with the eccentricity equal at each end, making an "S"-type moment along the tube. The eccentricity was so chosen for most of the tubes that the end moments caused a bending stress at ends equal to 20% of the axial normal stress. Specimens with load ratios of 10% and 40% were also tested.

Denting and bending damage was applied at different locations as indicated in Table 5. In some of the cases the dent was located at the tension side of the applied end moment. All tubes including those with a dent on the tension side of the end moment collapsed due to the dent. As shown in Fig. 10, theoretical calculations derived by DENTA-2 was in reasonable agreement with test results.

THEORY COMPARED TO EXPERIMENTS

The presented method have been used to analyze tubes tested at NTH. Fig. 11 shows that experimental ultimate loads compared well to theoretical ultimate loads. Fig. 12 presents test results compared with a characteristic strength defined as theoretical mean minus 2 st. dev. ($0.08 P_p$). As seen from the figure, only results for three tubes (which probably should have been disregarded) lay on the unsafe side.

CONCLUSIONS

The present study has addressed important aspects relating to the collapse behaviour of partly damaged unstiffened tubulars. In addition, interesting observations are made regarding cross-sectional deformation of tubulars in general. The effect of this deformation is important for progressive collapse analysis, especially if the structure is constructed of members with a diameter to thickness exceeding 50.

The study has also revealed a relatively large drop in collapse-load for relatively small dents in tubes subjected to premature local buckling.

A method is proposed to represent the behaviour of tubes with or without damage in form of a dent or lateral bending deformation or a combination of these. The method accounts for premature local buckling and cross sectional deformation in the post-collapse region.

The proposed theory is mainly based on a simplification of the physical behaviour of the dented area of a tube subjected to axial load and bending. Obtained results correlate well with 107 experimental tests conducted. However, premature local buckling, which affects the behaviour of thin-walled tubes, and post-ultimate rate of deformation of the cross-section are accounted for by using some of the experimental results to establish a semi-empirical approach.

The maximum bending to axial stress ratio which the theoretical model has been checked against, is that of a tube with reduced slenderness of about 0.8 and initial lateral deflection equal to $0.03 \cdot \lambda$. The model seems to

give, at least for tubes within the mentioned range, reasonable results for dent depths between zero and $D/2$.

ACKNOWLEDGEMENT

The work was made possible by grants and scholarship from the Norwegian Institute of Technology and support from the following institutions and companies:

- Anders Jahres Foundation for Scientific Research
- Aker Engineering A/S
- Det norske Veritas
- Norsk Hydro A/S
- Royal Norwegian Council for Scientific and Industrial Research
- Statoil
- SINTEF
- The Norwegian Maritime Directorate

REFERENCES

1. Smith, C.S., Kirkwood, W. and Swan, J.M.. "Buckling Strength and Post-collapse Behaviour of Tubular Bracing Members including Damage Effects". BOSS'79, 1979, pp. 303-326.
2. Smith, C.S.: "Assessment of Damage in Offshore Steel Platforms". Proc. of Int. Conf. on Marine Safety, Glasgow, Sept. 1983.
3. Smith, C.S., Somerville, W.L., Swan, J.W.: "Compression Tests on Full-Scale and Small-Scale Tubular Bracing Members Including Damage Effects". Dept. of Energy Report No. OT-R8079, Dec. 1980.
4. Taby, J. and Rashed, S.M.H.: "Experimental Investigation of the Behaviour of Damaged Tubular Members". Division of Marine Structures, Norwegian Institute of Technology, Rep. MK/R 92, Trondheim 1980. (Restricted).
5. Ellinas, C.P.: "Ultimate Strength of Damaged Tubular Bracing Members". ASCE Struct. Div. Vol 110, No. 2, 1984.
6. Taby, J., Moan, T. and Rashed, S.M.H.: "Theoretical and Experimental Study of the Behaviour of Damaged Tubular Members in Offshore Structures". Norwegian Maritim Research, Vol. 9, No. 2, 1981.
7. Rashed, S.M.H.: "Ultimate Strength and Post-Ultimate Strength Behaviour of Damaged Tubular Structural Member", Division of Marine Structures, Norwegian Institute of Technology, Report SK/R52, Trondheim 1980. (Restricted).
8. Taby, J.: "Experimental Investigation of the Residual Strength of Damaged Tubular Members". SINTEF report No. STF88 A87007, Trondheim 1984. (Restricted).

9. Taby, J.: "Residual Strength of Damaged Tubulars. Final report". SINTEF report No. STF71 A86068, Trondheim 1986.
10. Yao, T., Taby, J. and Moan, T.: "Ultimate Strength and Post-Ultimate Strength Behaviour of Damaged Tubular Members in Offshore Structures". 5th Internat. Symp. on Offshore Mechanics and Arctic Engineering (OMAE), Tokyo, Japan, April 1986.
11. Odland, J.: "On the Strength of Welded Ring Stiffened Cylindrical Shells Primarily Subjected to Axial Compression", Department of Marine Technology, The Norwegian Institute of Technology. Report No. UR-81-15, Trondheim, June 1981.
12. Ostapenko, A.: "Local Buckling of Welded Tubular Columns", Fritz Engineering Laboratory, Report No. 406.11, Lehigh University, Bethlehem, 1977.
13. Ueda, Y. et. al.: "Elastic-plastic Analysis of Framed Structures using the Matrix Method, 1st and 2nd reports". Journal of the Society of Naval Architects of Japan, Vol. 124 and 126, 1967-1968.

FIGURES

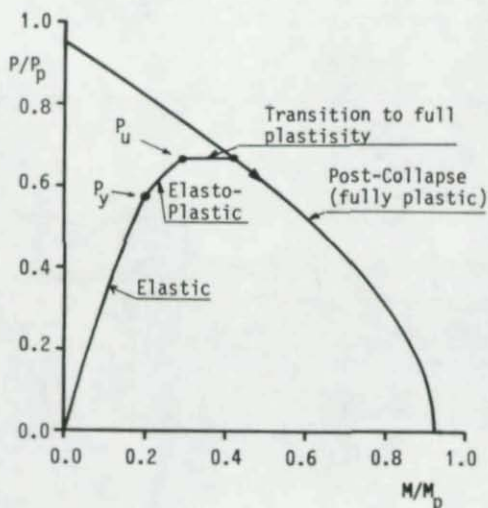


Fig. 1 Modes of behaviour in theoretical model

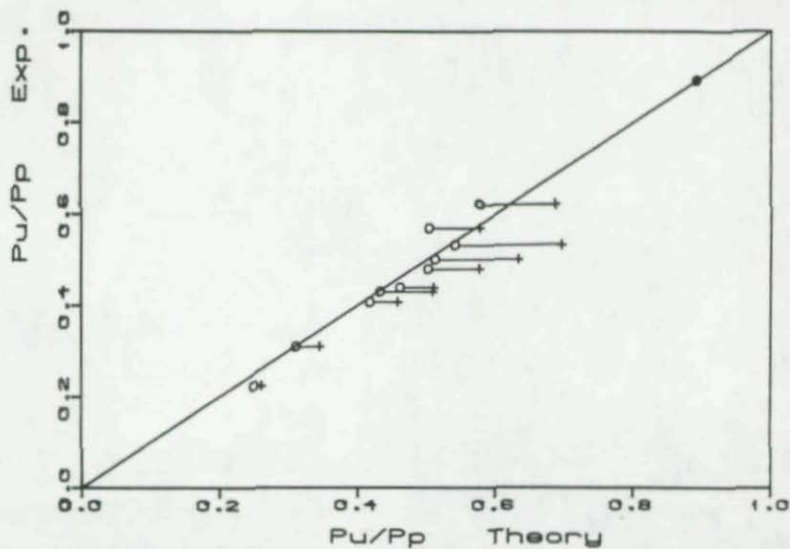


Fig. 4 Effect of correction with respect to local buckling

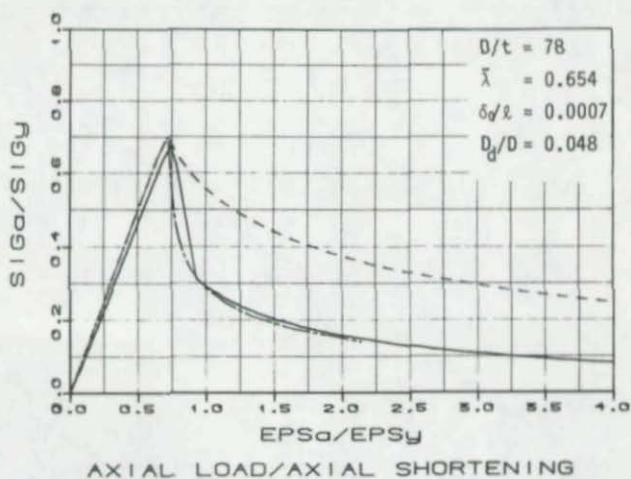


Fig. 5 Effect of cross-sectional deformation in post-collapse
 Experiment : ————
 Theoretical ignoring deformation: - - - - -
 Theoretical including deformation: - . - . - .

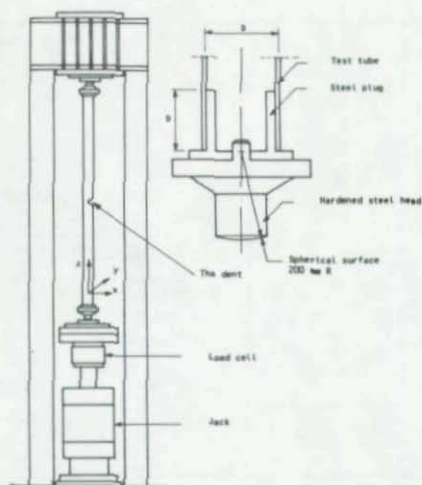


Fig. 6 Testing simply supported tubes.

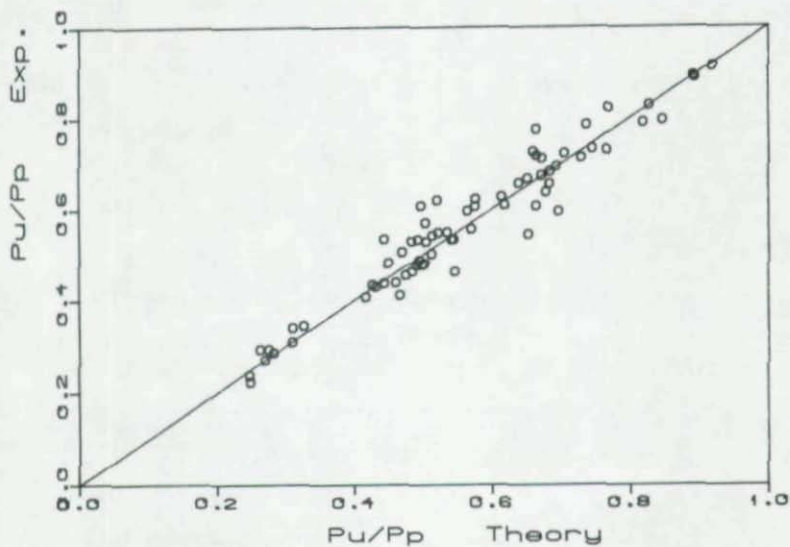


Fig. 7 Theoretical ultimate load compared to test results for simply supported tubes.

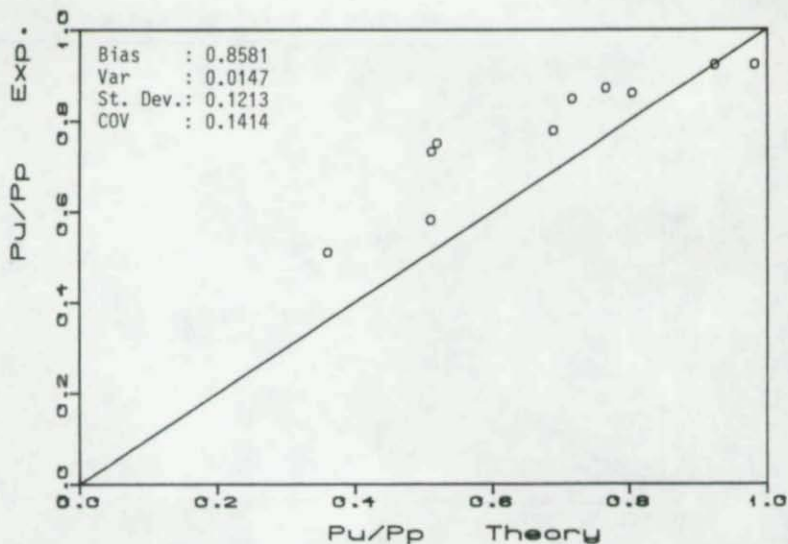


Fig. 8 Theoretical results (DENTA) compared to test results. Clamped end conditions. Assumed buckling length is $l/2$.

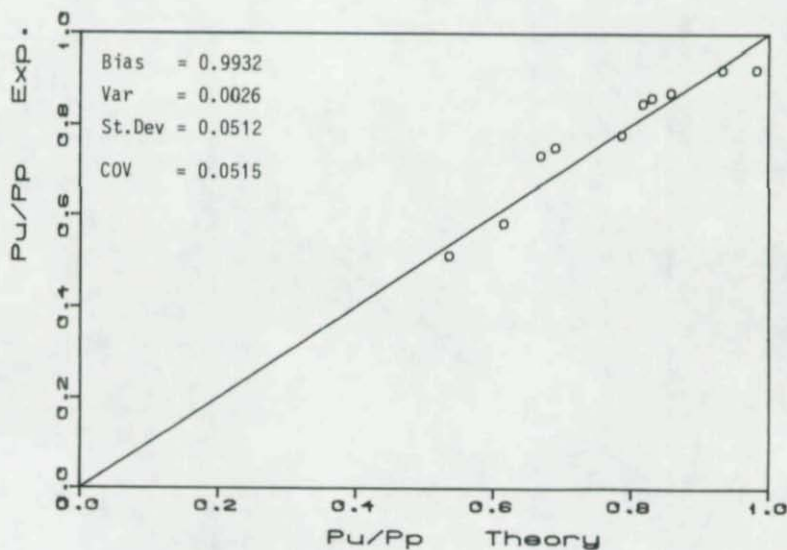


Fig. 9 Theoretical results (DENTA-2) compared to test results. Clamped end conditions.

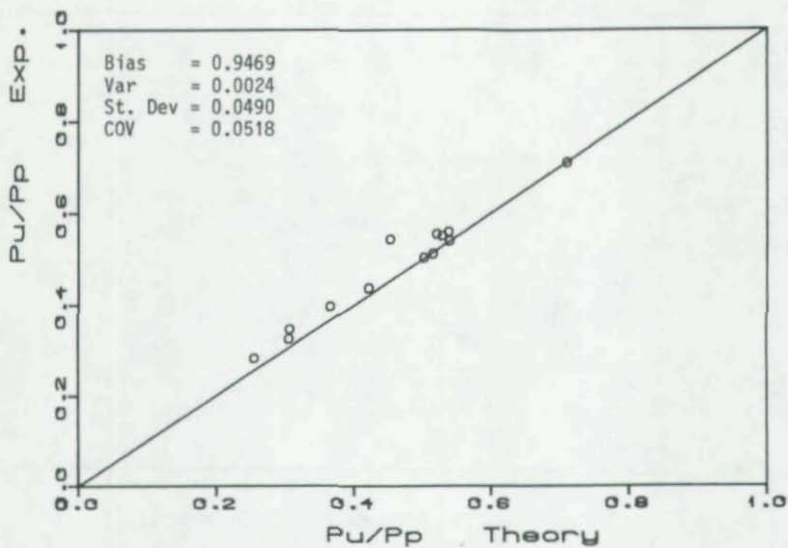


Fig. 10 Correlation between experimental and theoretical ultimate load for eccentrically loaded tubes.

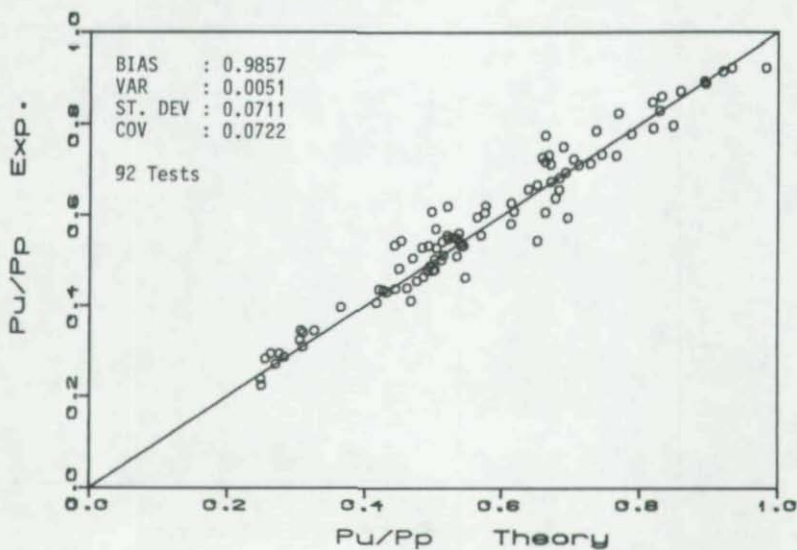


Fig. 11 All test results compared to theoretical results.

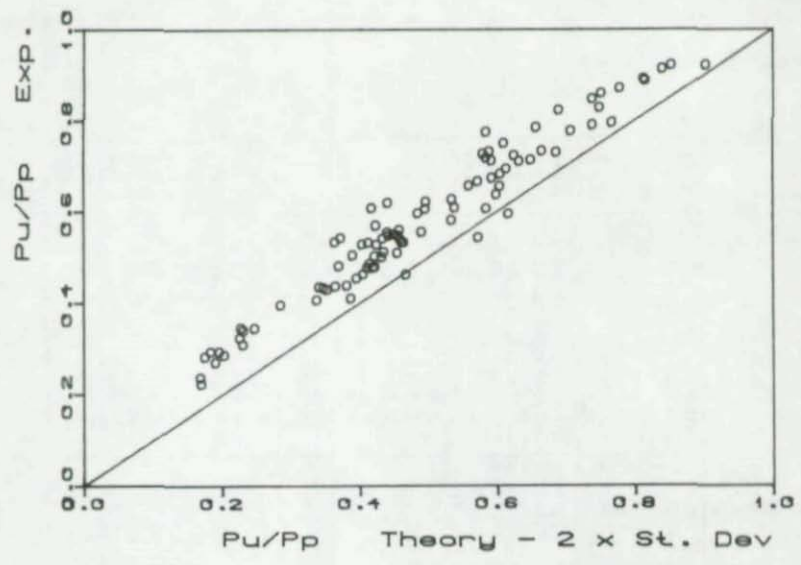


Fig. 12 Test results compared to characteristic strength.

Table 1

Spec. no.	Diam. to mid thickness D [mm]	Thick-ness t [mm]	Length l [mm]	Yield stress	Young's Modulus (assumed)*	D/t	Slender-ness l/r	Reduced slender-ness $\bar{\lambda}_k$	Max initial lateral deflection δ [mm]	Depth of Dent D _d /D
				σ_y [N/mm ²]	E [N/mm ²]					
IAI	123.11	2.04	3500	204	188000	60.35	80.40	0.843	2.59	.051
IAII	123.09	2.04	"	211	196000	60.34	80.42	0.840	6.41	.102
IAIII	123.15	2.04	"	207	203000	60.37	80.37	0.817	20.40	.204
IBI	122.64	2.50	"	250	211000	49.06	80.70	0.884	1.89	.051
IBII	122.68	2.51	"	230	198000	48.88	80.68	0.875	5.29	.102
IBIII	122.61	2.50	"	268	195000	49.04	80.72	0.953	20.90	.204
ICI	122.04	3.07	"	290	201000	39.75	81.09	0.981	2.00	.051
ICII	122.04	3.09	"	328	198000	39.50	81.09	1.051	7.21	.100
ICIII	122.03	3.06	"	256	198000	39.55	81.10	0.928	25.20	.207
IIAI	157.68	2.52	"	351	200000	62.57	62.78	0.837	0.81	.051
IIAII	157.64	2.52	"	351	197000	62.56	62.79	0.844	5.81	.102
IIAIII	157.65	2.52	"	314	194000	62.56	62.79	0.804	3.71	.020
IIBI	157.10	3.06	"	330	194000	51.34	63.00	0.827	4.20	.050
IIBII	157.07	3.07	"	233	194000	51.16	63.02	0.695	6.79	.102
IIBIII	157.02	3.06	"	258	194000	51.31	63.03	0.732	1.79	.020
IICI	156.05	4.06	"	470	207000	38.44	63.42	0.962	3.19	.055
IICII	156.13	4.10	"	457	207000	38.08	63.38	0.948	7.60	.103
IICIII	156.00	4.07	"	384	207000	38.33	63.44	0.870	2.59	.020
IIIAI	246.03	4.23	"	500	207000	58.16	40.23	0.629	2.10	.051
IIIAII	245.96	4.27	"	502	207000	57.60	40.24	0.631	3.50	.104
IIIBI	245.05	5.20	"	470	207000	47.13	40.39	0.613	0.21	.055
IIIBII	245.05	5.21	"	433	207000	47.03	40.39	0.588	7.00	.106
IIICI	244.35	6.02	"	472	207000	40.59	40.50	0.616	3.05	.052
IIICII	244.46	6.00	"	465	207000	40.74	40.48	0.611	6.41	.102

* Values equal 207,000 N/mm² are theoretical adopted because of dubious strain measurements

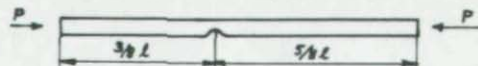


Table 2

Spec. no.	Diam. to mid thickness D	Thick-ness t	Length l	Yield stress σ_y	Young's Modulus (assumed)*	D/t	Slender-ness l/r	Reduced slender-ness $\bar{\lambda}$	Max initial lateral deflection δ_0	Depth of Dent D_d/D
	[mm]	[mm]	[mm]	[N/mm ²]	[N/mm ²]				[mm]	
IAIS	109.33	4.95	2000	362	207000	22.06	51.69	.688	7.02	0.0699
IBIS	109.33	4.92	"	362	"	22.19	51.69	.688	21.62	0.1292
ICIS	109.19	5.14	"	362	"	21.24	51.75	.689	11.42	0.1185
IDIS	109.11	5.11	"	362	"	21.34	51.79	.689	4.08	0.0628
IAIIS	105.99	8.40	"	475	"	12.61	53.20	.811	25.68	0.0543
IBIIS	105.88	8.53	"	475	"	12.41	53.26	.812	58.54	0.1335
ICIIS	105.99	8.41	"	475	"	12.59	53.20	.811	9.72	0.0591
IDIIS	106.25	8.03	"	600	"	13.22	53.09	.910	26.32	0.1206
IAS	118.47	1.51	"	383	"	78.15	47.74	.654	1.46	0.0480
IBS	118.48	1.51	"	458	"	78.41	47.74	.715	4.72	0.1266
ICS	118.47	1.52	"	478	"	77.89	47.75	.730	11.50	0.2168
IDS	118.52	1.51	"	430	"	78.44	47.73	.692	4.82	0.1146
IIAS	123.12	2.09	"	224	"	58.77	45.94	.481	2.52	0.0588
IIBS	123.19	2.09	"	224	"	58.75	45.91	.481	5.94	0.1157
IICS	123.17	2.07	"	228	"	59.42	45.92	.485	1.48	0.0652
IIDS	123.19	2.07	"	228	"	59.43	45.91	.485	4.32	0.1106
IIIAS	157.49	2.49	"	455	"	63.27	35.91	.536	1.12	0.0490
IIBS	157.44	2.50	"	455	"	63.10	35.93	.536	3.80	0.1025
IICS	157.46	2.49	"	470	"	63.14	35.92	.545	0.68	0.0602
IIDS	157.47	2.49	"	470	"	63.32	35.92	.545	3.20	0.1156
IVAS	202.03	1.50	3500	286	200000	135.14	49.00	.590	0.77	0.0431
IVBS	202.09	1.50	"	286	"	135.07	48.98	.590	0.00	0.0663
IVCS	201.98	1.50	"	286	"	134.38	49.01	.590	4.24	0.1070
IVDS	202.06	1.49	"	286	"	135.61	48.99	.590	7.60	0.2047

* Theoretical values adopted because of dubious accuracy of strain measurement



Table 3

Spec. no.	Diam. to mid thickness D	Thick-ness t	Length l	Yield stress σ_y	Young's Modulus (assumed)* [N/mm ²]	D/t	Reduced slender-ness $\bar{\lambda}$	Initial lateral deflection δ_0	Depth of Dent D_d/D	Supports during denting
	[mm]	[mm]	[mm]	[N/mm ²]	[N/mm ²]			[mm]	[mm]	
1AAA	118.74	1.00	2500	290	207000	118.74	0.710	1.48	0.00	-
1ABB	119.08	1.00	"	"	"	119.08	0.707	1.29	4.63	(A)
1ACB	118.80	1.00	"	"	"	118.80	0.709	4.35	6.97	(A)
1ACC	118.96	0.99	"	"	"	120.16	0.708	2.97	7.95	(B)
1ADB	118.92	1.00	"	"	"	118.92	0.708	2.95	11.72	(A)
1ADC	119.15	0.99	"	"	"	120.35	0.707	4.88	13.89	(B)
1AEC	118.89	1.01	"	"	"	117.71	0.709	17.8	25.70	(B)
1BAA	124.19	1.24	"	312	"	100.15	0.704	0.42	0.00	-
1BBB	124.30	1.25	"	"	"	99.44	0.703	1.16	4.95	(A)
1BCB	123.53	1.24	"	"	"	99.62	0.707	3.19	6.57	(A)
1BCC	123.92	1.24	"	"	"	99.94	0.705	1.88	7.36	(B)
1BDB	124.18	1.25	"	"	"	99.34	0.704	2.33	14.33	(A)
1BDC	124.37	1.26	"	"	"	98.71	0.703	4.02	13.48	(B)
1BEC	127.60	1.26	"	"	"	101.27	0.685	11.12	25.51	(B)
1CAA	133.55	1.47	"	295	"	90.85	0.636	0.79	0.00	-
1CBB	134.05	1.46	"	"	"	91.82	0.634	1.22	3.31	(A)
1CCB	133.89	1.51	"	"	"	88.67	0.635	0.97	8.30	(A)
1CCC	133.89	1.52	"	"	"	88.09	0.635	1.88	10.31	(B)
1CDB	133.81	1.42	"	"	"	94.23	0.635	4.72	15.63	(A)
1CDC	133.95	1.47	"	"	"	91.12	0.634	5.96	18.87	(B)
1CEC	133.59	1.53	"	"	"	87.31	0.636	21.81	31.12	(B)

* Theoretical values adopted because of dubious accuracy of strain measurement.

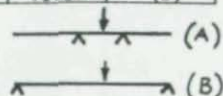
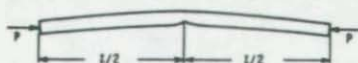


Table 4

Spec. no.	Diam. to mid thickness D	Thick-ness t	Length l	Yield stress σ_y	Young's Modulus (assumed)*	D/t	Slender-ness l_k/r	Reduced slender-ness $\bar{\lambda}_k$	Max initial lateral deflection δ_o	Depth of Dent D_d/D
	[mm]	[mm]	[mm]	[N/mm ²]	[N/mm ²]				[mm]	
IAIC	109.18	5.06	2000	362	207000	21.56	25.86	.345	1.36	0.0552
IBIC	109.36	4.95	"	362	"	22.10	25.84	.344	4.26	0.1042
IAIIC	106.04	8.24	"	600	"	12.88	26.59	.456	5.12	0.0503
IBIIC	106.01	8.25	"	600	"	12.85	26.60	.456	15.70	0.1114
IAC	118.47	1.51	3500	420	"	78.46	41.78	.599	6.69	0.1040
IBC	118.48	1.50	"	350	"	78.93	41.77	.547	14.46	0.1850
IIAC	123.21	2.10	"	213	"	58.67	40.17	.410	2.59	0.0501
IIBC	123.20	2.08	"	219	"	59.37	40.17	.416	6.79	0.1199
IIIAC	157.48	2.50	"	462	"	62.99	31.43	.473	2.66	0.0541
IIIBC	157.46	2.49	"	449	"	63.21	31.43	.466	6.76	0.1199

Buckling length, l_k , is set to $l/2$ when $\bar{\lambda}_k$ is calculated

* Theoretical values adopted because of dubious accuracy of strain measurement

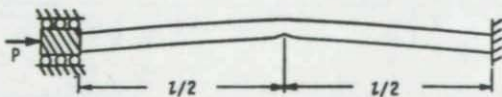
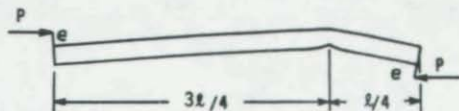
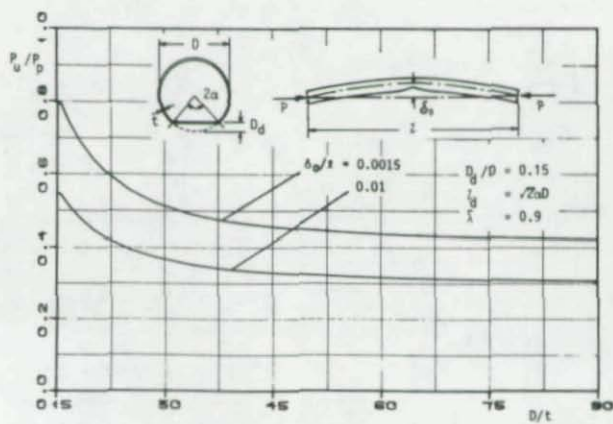
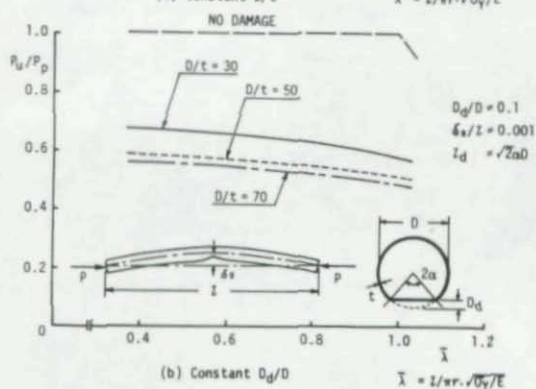
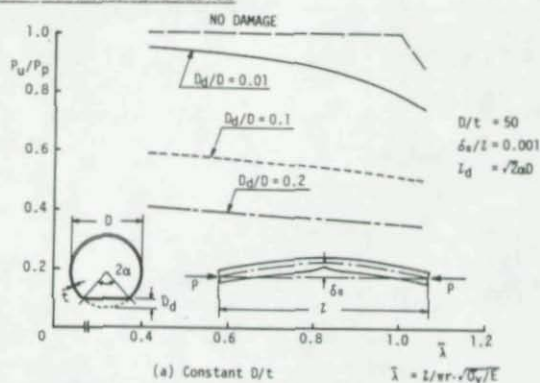


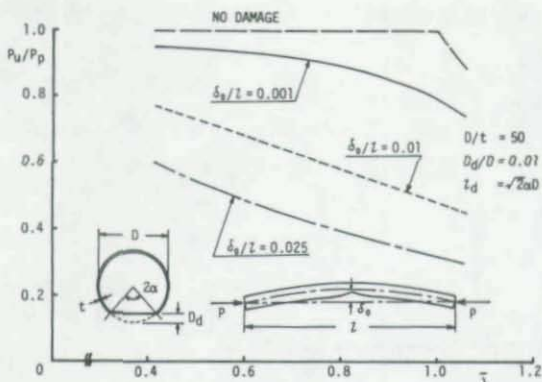
Table 5

Spec. no.	Diam. to mid thickness - D [mm]	Thick-ness t [mm]	Length l [mm]	Yield stress σ_y [N/mm ²]	Young's Modulus (assumed)* [N/mm ²]	D/t	Reduced slender-ness $\bar{\lambda}$	Initial lateral deflection δ_0 [mm]	Depth of Dent D_d/D [mm]	Eccentricities e [mm]	Place of dent	Bending to normal stress at ends σ_b/σ_a [%]
2AABB	122.57	2.57	2500	455	207000	47.69	0.8607	7.41	9.39	6.25	(A)	20
2BABB	122.58	2.57	"	454	"	47.70	0.8597	13.57	18.15	6.25	(A)	"
2CABB	122.59	2.57	"	443	"	47.70	0.8492	25.68	25.16	6.25	(A)	"
2ABBB	122.60	2.57	"	459	"	47.70	0.8643	-0.75	10.50	6.25	(B)	"
2BBBB	122.63	2.56	"	449	"	47.90	0.8546	7.39	17.14	6.25	(B)	"
2CBBB	122.61	2.56	"	444	"	47.89	0.8500	17.64	24.87	6.25	(B)	"
2ACBB	122.59	2.57	"	459	"	47.70	0.8644	4.00	10.16	6.25	(C)	"
2BCBB	122.58	2.58	"	442	"	47.51	0.8483	6.81	16.36	6.25	(C)	"
2CCBB	122.62	2.58	"	456	"	47.53	0.8613	14.33	23.20	6.25	(C)	"
2BCAB	123.07	2.05	"	452	"	60.03	0.8545	3.25	11.42	6.00	(C)	19
2BCCB	122.04	3.04	"	520	"	40.14	0.9241	4.12	11.58	6.00	(C)	"
2BCBA	122.64	2.55	"	448	"	48.09	0.8536	4.03	11.69	3.00	(C)	10
2BCBC	122.59	2.57	"	447	"	47.70	0.8530	3.98	10.86	12.50	(C)	40

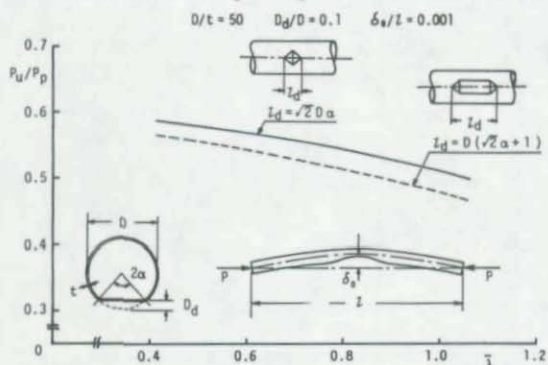
* Theoretical value adopted because of dubious accuracy of strain measurement



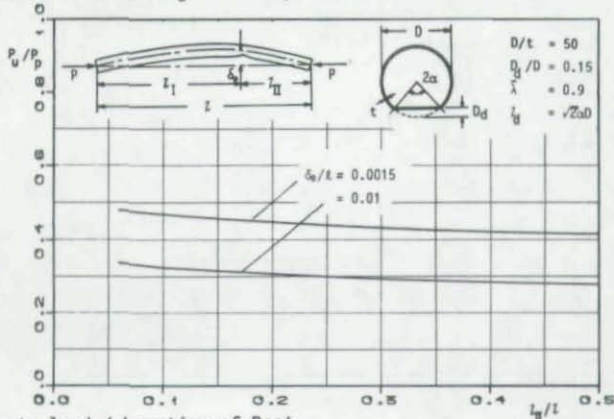




Influence of overall bending damage on compressive ultimate strength.



Influence of dent length on compressive ultimate strength.



ULTIMATE CAPACITY OF DAMAGED TUBULAR BEAM COLUMNS:
AN EXPERIMENTAL STUDY

by

I. Lotsberg* and P.C. Birkemo**

ABSTRACT

At the end of 1985 a project on experimental investigation of ultimate capacity of damaged tubular beam columns commenced at A/S Veritec in Oslo. This paper presents the goals of the study, and the experimental techniques which are being used. The purpose of the project is to determine experimentally the moment vs. axial force vs. rotation relationships for damaged tubular steel members. This information may then be used in the evaluation and verification of the residual strength of damaged offshore structures and to further develop and verify analytical models. The main test setup enables axial force and moment on the dented region to be specified and controlled simultaneously and independently. Computer controlled loading and displacement as well as computer based data acquisition are being used to obtain complete loading and collapse behavior of the dented region as well as the global member behavior.

* A/S Veritec, Hovik, Norway. 1986/87 Visiting Professor, Dept. of Civil Engineering, McMaster University, Hamilton.

** Dept. of Civil Engineering, University of Toronto.

**ULTIMATE CAPACITY OF DAMAGED TUBULAR BEAM COLUMNS:
AN EXPERIMENTAL STUDY**

by

I. Lotsberg

A/S Veritec, Hovik, Norway
1986/87 Visiting Professor, Dept. of Civil Engineering
McMaster University, Hamilton, Canada

P.C. Birkemoe

Professor, Dept. of Civil Engineering
University of Toronto, Toronto, Canada.

INTRODUCTION

Tubular members are used for the construction of jacket structures and other offshore structures such as jack-ups and certain types of steel gravity structures. Also deck trusses may be composed of tubular members.

The external loads in such structures are carried almost exclusively by axial forces in the members - compression or tension. The loadings which may influence the compression capacity of tubular beam-columns includes beams bending due to wave and current, frame bending due to global deformations, internal or external pressure and to a lesser degree torsion and shear.

The primary failure mode of members subjected to axial compression is column buckling. Local failure modes may, however, interact with the global member buckling depending on the geometry, material data and the loading. The detrimental effects of imperfections with respect to compression capacity is well recognized. Damage to tubular members in offshore structures will further reduce the compression capacity of tubular members. After damage has occurred the ability of the structure to withstand the functional and environmental loads is questioned. Also, repair of damaged members below water level is difficult and very costly. Therefore, decisions regarding acceptable damage in tubular members have to be made. After damage has been reported, it is important to be able to assess quickly and accurately the residual strength of the damaged member or the structure in order to take the precautions when necessary.

The purpose of the present project is to gain more experimental data on capacities of damaged beam columns which can be used in residual strength evaluations. Other researchers (Refs. 1, 2, 3, 4) have approached the damaged tubular problem in recent years from both theoretical and experimental standpoints. This study has been designed to provide data which is broadly applicable to analytical treatment and extrapolation, and which complements the reported experimental work of others.

In order to arrive at results practical for design verification it has been decided to describe the capacity of the dented region by forces and rotations related to sections of the tubular outside the damaged region, see Fig. 1. From the M-P- θ relations as shown schematically in Fig. 2, it should be possible to determine the residual strength of damaged beam-columns based on analytical methods, and it should also include enough data to perform a more advanced residual strength analysis of a platform accounting for the postbuckling behavior of the members using a finite element formulation.

The project commenced at A/S Veritec in Oslo at the end of 1985 and is planned to be finished within 1987.

SPECIMENS AND MATERIAL DATA

The relative geometry of the tubulars to be tested corresponds to that of typical members in jacket structures with D/t-ratios of 31 and 47. The diameter of the test specimens is 140 mm.

The dent (damage) depths are approximately $0.1 \times D$ and $0.2 \times D$. Three coupons (or specimens) from the end of each tubular will be tested to obtain a typical average cross-sectional yield stress. The specimens are tested at a strain rate of 10^{-5} /sec. At a strain of 0.002 the test is stopped at constant strain until a static stress level is reached. This procedure is repeated at a strain of 0.005. The lowest stable load recorded during the stop at a maintained strain is used to calculate the static yield stress.

The material used for the specimens is St52-N for D/t = 31 and St44-N for D/t = 47 corresponding to typical yield strengths used in offshore tubular construction members. Approximately 30 tubular member specimens will be tested in the current program.

The loading conditions are indicated in Table 1 for one type of specimen geometry. The axial load is to be kept constant while the specimen is subjected to an increasing moment caused by lateral loading.

TABLE 1: Loading conditions for one geometry

Test No.	Axial force P	Bending Moment	
		Compression in dent	Tension in dent
1	0	x	
2	0		x
3	P_2	x	
4	P_2		x
5	P_3	x	
6	P_3		x

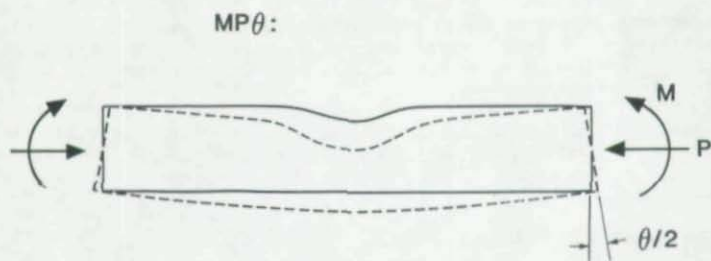


Fig. 1: Damaged part of tubular with M-P- θ definitions

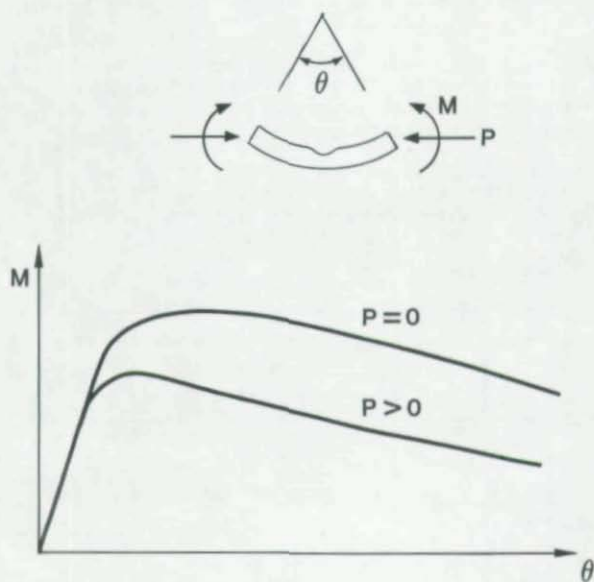


Fig. 2: Schematic M-P- θ curves

DENTING

Damage of the tubulars is simulated in a denting rig with the member fixed against end rotations but free to move longitudinally. This is achieved by supporting the member at a distance $L/4$ from its ends, where L is member length.

The member used for denting has a wedge shape with an edge radius of 20 mm. To achieve the specified dent depth the denting is performed in steps by loading and unloading in order to separate the elastic and permanent deformations. The dent width (in a plane normal to the member/loading plane) and the depth are measured during the denting process.

GEOMETRY MEASUREMENTS

A rig for geometry measurements has been constructed. The specimen is mounted in this rig in a vertical position and the surface shape of the tubular is measured using displacement transducers: a schematic representation of the rig is shown in Fig. 3. Measurements of the radial surface position are obtained around the circumference through a rotation of the tubular member in steps of 5 degrees. The ovalization and the out-of-straightness can then be calculated according to the procedure given in Ref. 5 for measurements of tolerances on shells.

TESTING OF ULTIMATE CAPACITY

A test rig has been designed where a constant axial load can be applied simultaneously with an increasing uniform bending moment over the central damaged region of the test specimen, see Fig. 4. The constant axial load is applied by means of a servo-hydraulic actuator operating in force control mode. The moment is created by the vertical hydraulic cylinders connected to gravity load simulators such that the transverse forces are acting normal to the axial load axis. The forces in these vertical cylinders are controlled manually.

The test progress is monitored through measurement of

- vertical displacements at the transverse load points
- horizontal displacements along the specimen
- rotations at the connections between the specimen and the lateral load actuators (inside the constant moment region)
- lateral (transverse) loads
- axial load

Through a computer based control/data acquisition system the force and moment in the dented region can be specified and controlled simultaneously or independently.

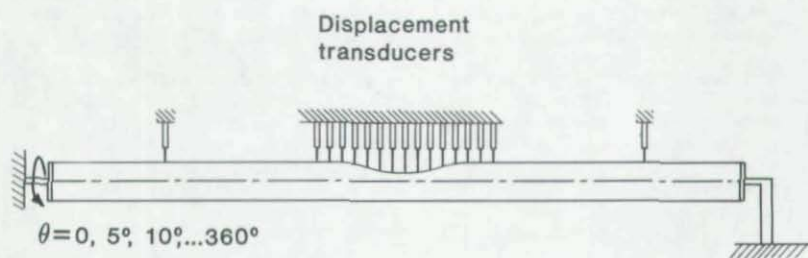


Fig. 3: Arrangement for geometry measurement

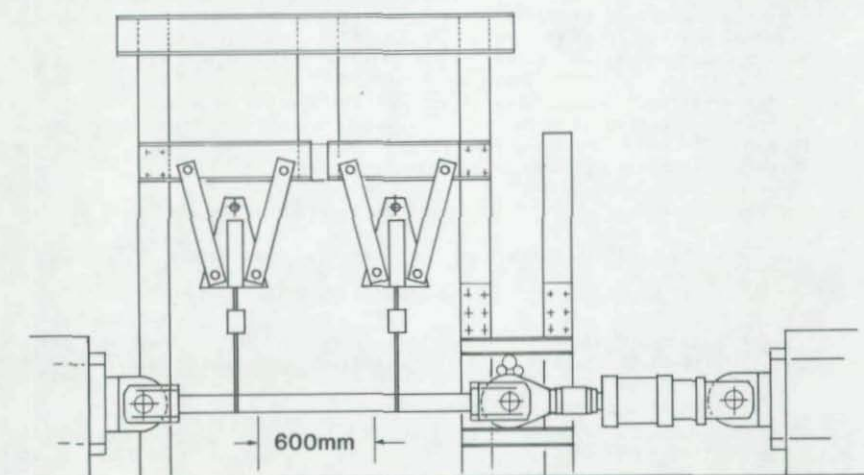


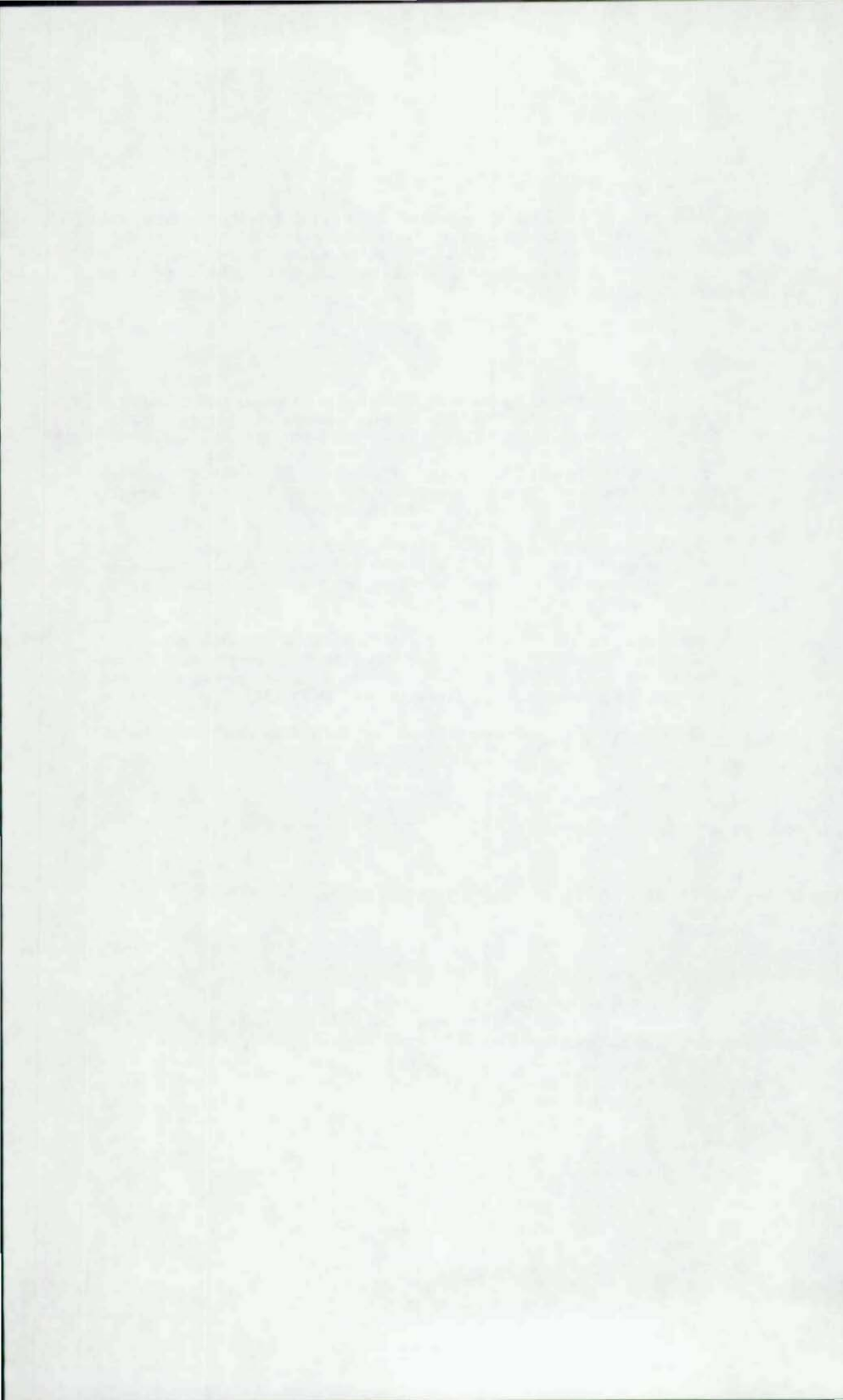
Fig. 4: Test rig

CLOSURE

The study described herein is supported by a joint industry program and is scheduled for completion during the current year. After a period of confidentiality, the results will provide valuable new data for a growing body of information used in the reliable safety assessment of damaged steel structures.

REFERENCES

1. Smith, C.S., Kirkwood, W. and Swan, J.W.: Buckling Strength and Post-Collapse Behaviour of Tubular Bracing Members Including Damage Effects. Behaviour of Offshore Structures, BOSS'79, London, 1979.
2. Smith, C.S., Sommerville, W.L. and Swan, J.W.: Residual Strength and Stiffness of Damaged Steel Bracing Members. Proceedings of Offshore Technology Conference, Houston, 1987.
3. Taby, J., Moan, T. and Rashed, S.M.H.: Theoretical and Experimental Study of the Behaviour of Damaged Tubular Members in Offshore Structures. Norwegian Maritime Research, Vol. 9, No. 2, 1982.
4. Yao, T., Taby, J. and Moan, T.: Ultimate Strength and Post-Ultimate Strength Behaviour of Damaged Tubular Members in Offshore Structures. 5th International Symposium on Offshore Mechanics and Arctic Engineering (OMAE), Tokyo, Japan, April 1986.
5. BS 5500 Specification for Unfired, Fusion-Welded Pressure Vessels. British Standards Institution, 1982.



STUDY OF CARRYING CAPACITY OF FABRICATED
TUBULAR COLUMNS UNDER AXIAL COMPRESSION

Xiao-Ming Yang, Guo-Zhou Wang and Shao-Fu Li
Department of Civil Engineering
Tsinghua University
Beijing, China

1. INTRODUCTION

Fabricated tubular columns are the basic elements of steel offshore platforms. This kind of column has a lot of advantages in mechanics, but it also has inevitable imperfections, because it involves a complicated manufacturing process. The manufacturing process of a fabricated tubular column includes three main steps: (1) Rolling from steel flat plate to form a cylinder; (2) Welding of the longitudinal seam of the cylinder to form a can; and (3) Transverse welding of the cans to form a long column. All the above steps may result in significant residual stresses and geometrical imperfections. These factors, as it is known, may have important effects on the ultimate strength and buckling behavior of axially loaded columns.

Therefore, it must be considered for a reasonable design of axially loaded columns that an actual column is geometrically and materially imperfect, and is also frequently subjected to bending moments resulting from unavoidable end eccentricities and support restraints. In the last decade, some research work on the buckling behavior of fabricated tubular columns have been done(8)(9). Despite these research efforts, the behavior of this kind of member is still not fully understood and samples of available test data are too small to reach a reliable conclusion for these columns. Up to the present, the design method of these columns is still based on empirical formulae. A need clearly exists for accurate and effective method of assessing the effects of all the factors that may affect the buckling behavior and ultimate strength of axially loaded fabricated tubular columns so as to lay the foundations for making the reasonable design curve of these columns.

Herein, an experimental and theoretical study on the buckling behavior and ultimate strength of fabricated tubular columns under axially loaded condition is carried out. In the experimental investigation some medium and long column tests and its corresponding tension coupon tests and stub column tests are completed. Based on finite difference principle and Newton-Raphson iterative technique, an elastic-plastic analysis method of beam-columns is advanced for the entire range of monotonic axial loading up to ultimate load including post-buckling unloading, and its corresponding computer program in FORTRAN is also developed. To demonstrate the validity of the computer program, comparisons between the computed results and tested results of steel columns are made. Using the computer program, systematical studies of the effects of longitudinal residual stresses and initial out-of-straightness imperfections on the ultimate strength and buckling behavior of fabricated tubular columns are completed and, finally, a reasonable column strength curve for this kind of column is obtained and compared with the current design curves specified in different design codes.

2. EXPERIMENTAL INVESTIGATION

The test program includes six medium and long column tests with slenderness ratio ranging from 43 to 72 and with diameter-to-thickness ratio of 50, three stub column tests with length of 500 mm, and thirty tension coupon tests. A diagram is shown in Fig.1 of the dimensions of the specimens as fabricated. All these tests were conducted in the Engineering Structure Laboratory, Tsinghua University, Beijing, China.

2.1 Tension Coupon Tests and Stub Column Tests

It is essential for the prediction of the buckling load and behavior of a medium or long tubular column to know the material properties. The material properties that have the most effects on the behavior of a steel tubular column are the modulus of elasticity, E , the yield stress, σ_s , and the stress-strain curve. Tensile specimen tests and stub column tests were conducted to obtain the material properties, respectively, in tension state and compression state.

(a) Tensile specimen tests : To obtain a statistical average value of material property, 30 tensile specimens that were taken from 5 flat plates, 6 specimens per flat plate, were tested. The size of the specimen and testing method of the specimen conformed to Chinese Standards (GB 228-76) (13). The test results of the statistical average values of the modulus of elasticity, E , and the yield stress, σ_s , are given in Tab.1. It also gives the corresponding values as contained in the mill report accompanying the flat plates. The typical stress-strain curve of the steel of tensile specimen is shown in Fig.2 and it is found that the stress-strain curve can be closely approximated by the elastic-perfectly plastic curve before strain hardening region is reached.

(b) Stub column tests : A stub column may be defined as a column long enough to retain the original magnitude of residual stresses in the section and short enough to prevent any premature failure occurring before the yield load of the section is reached. A stub column test is performed in order to obtain an average stress-strain curve for the complete cross-section which takes into account the effects of residual stresses. The stub column tests were conducted in a 500 ton compression testing machine and the test rig is shown in Fig.5. During the testing, the strains at midheight of the stub column were measured by electric resistance strain gages and the corresponding relative movements between the machine heads were also measured by electric dial gages. A typical stress-strain curve for stub column is shown in Fig.3. These stress-strain curves for stub columns are significant different from those for tensile coupon tests, which is due to the effects of residual stresses in the cross-sections of stub columns.

Good correlation is found between the results obtained from tension tests and stub column tests for the modulus of elasticity, E , and yield stress σ_s , which is given in Tab.1.

2.2 Residual Stresses

There are two major types of residual stresses in the fabricated tubular columns. They are circumferential residual stresses due to forming of a flat plate into a cylinder, and longitudinal residual stresses due to

welding of a cylinder into a can. The longitudinal residual stresses are believed to have more significant effects on the behavior and ultimate strength of a fabricated tubular column; hence, they must be considered in a reasonable theoretical analysis of beam-column. The longitudinal residual stresses in the cans were measured by a "slicing" technique(11). The distribution of the measured longitudinal residual stresses of these cans is shown in Fig.4. It is found that the curve can be closely approximated by following equation:

$$\sigma_r(\beta) = 1.0662 - 6.1227\beta + 9.3851\beta^2 - 5.9125\beta^3 + 1.6488\beta^4 - 0.1689\beta^5$$

in which β = radians rotating from weld; $\sigma_r(\beta)$ = nondimensional residual stresses. The curve in Fig.4 is similar to the curve of longitudinal residual stress distribution measured by D.A.Ross and W.F.Chen (1976)(12).

2.3 Long Column Tests

In the test program, six medium and long columns with overall length of 3m and 5m, each of which consists of three cans were tested to provide the data for check up the theoretical analysis.

As the initial out-of-straightness is one of the most important factors affecting the ultimate load of axially compressed columns, an extensive measurement of the initial crookedness of each column was carried out before testing. Typical specimen out-of-straightnesses are shown in Fig.6. To allow the column buckling in its weakest direction, two spherical bearings were used at both ends of the columns during testing. It also provides a real pin-ended condition which allows valuable information on column behavior to be collected. The testing rig is shown in Fig.5. The deflections at 7 sections in buckling direction were measured by electric dial gages, and the deflections in perpendicular direction were also measured at 3 of these sections. The strains in the same sections were also measured with electric-resistance strain gages. Before testing, alignment in which the center of each end of specimen is aligned with the center of the spherical bearing at that end was carefully made and the unintentional end eccentricities were measured by the measuring sets. The axial load was applied in increments and the static readings of column behavior were recorded.

The geometrical properties and collapse loads of medium and long columns are summarized in Table 2. In Fig.7, the test data recorded of ultimate load were given and compared with other test results of the same sort (8)(9), API design curve (6), ECCS/DnV-OS design curves (3)(4), and SSRC multiple curves (7). It is found that the test data here trend to the agreement with the test data obtained by former researchers and most of the test results are above the most of design curves.

3. THEORETICAL ANALYSIS

3.1 General

Because it is unavoidable for an actual column to have some imperfections such as initial crookedness, end eccentricities, residual stresses, end restraints and so on, which have, to varying degrees, effects on the buckling behavior of an axially loaded column, it is reasonable that

an actual column is analyzed as an elastic-plastic beam-column. An analysis of an elastic-plastic beam-column can be fall into two steps: (1) The generation of the behavior of a column segment, M-P- θ relations; (2) then, using this as input data, the load-deflection behavior of a beam-column is calculated and, therefore, the ultimate strength of the beam-column is also determined.

In this paper, a finite difference principle is first used to turn the equilibrium differential equation of beam-columns into an set of algebraic equations, which makes it easy to treat defferent end restraints and varying kinds of initial crookedness, and then a Newton-Raphson iterative technique is used to solve this set of equations. A general solution of elastic beam-column is also derived as initial state of the iterative process. The assumptions adopted in following theoretical derivation are as follows:

- (1) Plane section remains plane after the deformation.
- (2) The deflections are small and the slope angles in radian are negligible compared to unity.
- (3) The behavior of the material along the column has not deferences.
- (4) There are no occurrence of local buckling and twisting during loading.
- (5) There are no variations of residual stresses along the column.

3.2 Equilibrium Equation

Referring to the column shown in Fig.8, the equilibrium equation of a general beam-column can be derived as follows:

$$m = p(z + v + e_a) - c_a \theta_a - x(p(e_a - e_b) - (c_a \theta_a - c_b \theta_b)) \quad (1)$$

where p =compression load; z =deflection of column due to compression load; v =initial crookedness of the column; e_a, e_b =end eccentricities at end A, B; θ_a, θ_b =slope angles at end A, B; c_a, c_b =end restraint coefficients at end A, B; m =bending moment of the section at a distance x from the left end A of column. All the above quantities are nondimensional quantities and the dimensional quantities corresponding to above quantities are:

$$M = m \cdot Ms; \quad P = p \cdot Ps; \quad \theta = \theta \cdot \theta_0; \quad \theta_a = \theta_a \cdot \theta_0; \quad \theta_b = \theta_b \cdot \theta_0; \quad C_a = c_a \cdot Cs; \quad C_b = c_b \cdot Cs;$$

$$M_s = W \cdot \sigma_s; \quad P_s = A \cdot \sigma_s; \quad \theta_0 = Ms/EI; \quad \theta_{0a} = L \cdot \theta_0; \quad \theta_{0b} = L \cdot \theta_0; \quad C_s = EI/L;$$

$$Z = z \cdot q_k; \quad V = v \cdot q_k; \quad E_a = e_a \cdot q_k; \quad E_b = e_b \cdot q_k; \quad X = x \cdot L; \quad q_k = W/A.$$

where A =cross-sectional area; I =moment of inertia of the section; W =section modulus; L =length of beam-column.

3.3 General Solution of Elastic Beam-column

In the elastic range, the bending moment, m , has a simple relation with the curvature, ϕ , as follows:

$$m = \phi \quad (2)$$

and then it is easy to obtain the solution of the equation (1). If we define b^2 as:

$$b^2 = p/t \quad (3)$$

$$\text{where } t = \frac{I}{(\lambda_b \pi)^2}; \quad \lambda_a = \lambda/\lambda_s; \quad \lambda = L_s/r; \quad \lambda_s = \pi \sqrt{\frac{E}{\sigma_s}} \quad (4)$$

and express the initial crookedness, v , as:

$$v(x) = \sum_{i=1}^m a_i \sin(i\pi x) \quad (5)$$

the solution of an elastic beam-column can be obtained:

$$z(x) = \frac{1}{P \sin(b)} (z_a \sin(bx-b) - z_b \sin(bx)) + \frac{1}{P} (z_a(1-x) + z_b x) + u \quad (6)$$

where z_a , z_b are defined as:

$$z_a = z_p (D_1 c_a (b^2 e_b + c_b D_b) - (D_2 c_b - D_3) (b^2 e_a - c_a D_a)) \quad (7)$$

$$z_b = z_p (D_1 c_b (b^2 e_a - c_a D_a) - (D_2 c_a - D_3) (b^2 e_b + c_b D_b)) \quad (8)$$

and D_1, D_2, D_3, D_a, D_b , and z_p are given as follows:

$$D_1 = \sin(b) - b \quad (9)$$

$$D_2 = b \cos(b) - \sin(b) \quad (10)$$

$$D_3 = b \sin(b) \quad (11)$$

$$D_a = \pi \sum_{n=1}^m \frac{\alpha_n}{1 - \alpha_n} n a_n \quad (12)$$

$$D_b = \pi \sum_{n=1}^m \frac{\alpha_n}{1 - \alpha_n} n a_n (-1)^n \quad (13)$$

$$z_p = p \sin(b) / (D_1^2 c_a c_b - (D_2 c_a - D_3)(D_2 c_b - D_3)) \quad (14)$$

and $u = \sum_{n=1}^m \frac{\alpha_n}{1 - \alpha_n} a_n \sin(n\pi x)$ in which $\alpha_n = b^2 / (n\pi)^2$ (15)

In the case of pin-ended condition, the equation (6) becomes

$$z(x) = (e_a \sin(b-bx) + e_b \sin(bx)) / \sin(b) - (e_a(1-x) + e_b x) + u \quad (16)$$

3.4 Moment-Curvature Relations of Column Segment

In the elastic-plastic range, the equation (2) can not be true and, generally speaking, the bending moment m is a function of the stress-strain behavior of the material and the residual stresses in the section. To derive out a general moment-curvature relation of an arbitrary section considering arbitrary shapes of stress-strain curve and residual stresses in longitudinal direction, a general strain distribution of the cross-section is first derived as follows:

$$\epsilon = \rho f \sin(\alpha - \beta) + \epsilon_s + \epsilon_r \quad (17)$$

where ϵ = strain, ϵ_s = strain at centre of form, ϵ_r = residual strain, all the strain are non-dimensionalized with respect to the yield strain ϵ_s ; ρ = radial distance in the polar coordinates located in the centre of form of section non-dimensionalized with respect to $\rho_s = l/W$; α = angle between y-axis and the neutral axis; β = the angle in the polar coordinate located in the centre of form of the section.

A general stress-strain relationship in uniaxial stress test condition can be expressed by:

$$\sigma = G(\epsilon) \quad (18)$$

Substituting equation (17) into equation (16), the stress distribution in the section can be obtained as follows:

$$\sigma = G(\phi f \sinh(\alpha - \beta) + \epsilon_0 + \epsilon_r) \quad (19)$$

Thus, the generalized stresses: bending moments and axial force, are computed by:

$$p = \frac{1}{A} \int_A \sigma \, dA \quad (20)$$

$$m_y = \frac{1}{W} \int_A \sigma z \, dA \quad (21)$$

$$m_z = \frac{1}{W} \int_A \sigma y \, dA \quad (22)$$

The equations (20), (21), (22) and (19) give a general moment-thrust-curvature relationship of any section. As the M-P- ϕ curve usually cannot be computed by direct methods because of the nonlinear behavior of the stress-strain relationship, an iterative procedure must be applied to treat the nonlinear problem. The iterative procedure adopted in this paper is as follows:

- (1) Determine the following quantities:
 - * Range of the thrust, p , and its increment, dp
 - * Range of the curvature, ϕ , and its increment, $d\phi$
- (2) Set the load $p = p + dp$ for i th loop
- (3) Set the curvature $\phi = \phi + d\phi$ for j th loop
- (4) Get ϵ_0 from equation (20) by Newton-Raphson method
- (5) Substitute ϵ_0 and ϕ into equations (21), (22) to get m_y, m_z
- (6) Goto step (3) for $j+1$ th loop of ϕ
- (7) goto step (2) for $i+1$ th loop of p
- (8) Output the M-P- ϕ matrix

Based on the above algorithms, a computer program in FORTRAN, MCTAP, has been coded and the comparison of the computed results with analysis results of some sections has also been made. It leaves no doubt as to the validity of the computer program. Using the computer program, extensive studies of the effects of the longitudinal residual stresses and the direction of applied bending moment with respect to the longitudinal weld on the M-P- ϕ curves have been carried out. It is found that these factors have significant effects on the M-P- ϕ curves. The effect of residual stresses on M-P- ϕ curve is shown in Fig. 9 and the results computed in some directions are shown in Fig. 10-12.

3.5 Analyses of Elastic-Plastic Beam-Columns

As the moment-thrust-curvature relationship in plastic range behaves nonlinearly, recourse must be made to numerical methods to obtain the solution of the equation (1). Here, a finite difference principle is used to reduce the differential equation to a set of algebraic equations, and then a Newton-Raphson iterative technique is used to solve this set of equations.

The difference formulations used in the transformation of the differential equation to the set of algebraic equations are:

$$\begin{aligned}
 z_i'' &= \frac{1}{12h^2}(-z_{i-2} + 16z_{i-1} - 30z_i + 16z_{i+1} - z_{i+2}) & i=2,3,\dots,n-1 \\
 z_i'' &= \frac{1}{h^2}(z_{i-1} - 2z_i + z_{i+1}) & i=1,n \\
 z_i' &= \frac{1}{2h}(-3z_i + 4z_{i+1} - z_{i+2}) & i=0 \\
 z_i' &= \frac{1}{2h}(z_{i-1} - 4z_i + 3z_{i+1}) & i=n+1
 \end{aligned} \quad (23)$$

where z_i = deflection at i th node; h = constant, $x = ih$. Substituting the above difference formulations into the governing equation (1), a set of algebraic equations can be obtained as follows:

$$m(p, \phi_i) - p(z_i + v_i + e_a) + c_a \theta_a + ih(p(e_a - e_b) - (c_a \theta_a - c_b \theta_b)) = 0 \quad i=1,2,\dots,n \quad (24)$$

where

$$\begin{aligned}
 \phi_i &= -tz_i'' \\
 \theta_a &= tz_i' \\
 \theta_b &= -tz_{i+1}'
 \end{aligned} \quad (25)$$

Using Newton-Raphson iterative technique and considering equations (19)-(22), the set of equations (24) can be solved taking the elastic solution equation (6) as the initial values of the first iteration and then taking the interpolating values as the one.

Based on the above formulations, a computer program in FORTRAN, BCAP, has been developed and some of comparison between the medium and long column test results and the corresponding computed results are given in Fig.13-16. The further comparison of the results between test and computation is given in Fig.17. It is found that the identity between the both is good and the related coefficient equals 0.9896.

3.6 Column Strength Curves

Using the computer program, BCAP, some column strength curves of fabricated tubular columns are developed considering the longitudinal residual stresses in Fig.4 and 0.1% initial crookedness, and the results that are corresponding to different buckling directions of column with respect to the longitudinal weld are shown in Fig.18. It is found that the curve whose buckling direction is opposite to the longitudinal weld gives the lowest column strength. Therefore, it may be adopted as the design curve for the fabricated tubular columns. The suggested column strength curve can be closely approximated by the following equation:

$$p = \frac{1}{2\lambda_e^2} (1 + \epsilon_e + \lambda_e^2 \sqrt{(1 + \epsilon_e + \lambda_e^2) - 4\lambda_e^2}) \quad (26)$$

where $\epsilon_e = 0.1826\lambda_e$; $\lambda_e = \lambda/\lambda_s$, nondimensional slenderness ratio.

A comparison between the suggested curve and API design curve as well as SSRC multiple curves is shown in Fig.19. It is found that the suggested curve is significantly lower than the API curve and the SSRC curve "1" but higher than the SSRC curve "2". The comparison between the suggested curve and ECCS/DnV-OS curves is given in Fig.20 and it is shown that the suggested curve is close to the ECCS/DnV-OS curve "a" but slightly higher than it.

4. CONCLUSIONS

Experimental and analytical studies of the ultimate carrying capacity of axially loaded fabricated tubular columns have been made. An analysis method based on finite difference principle and Newton-Raphson iterative technique is used to compute the load-deflection curves of beam-columns for the entire range of monotonic loading up to ultimate load including post-buckling unloading. Based on this method, a computer program, BCAP, in FORTRAN has also been developed and its validity was demonstrated by the medium and long column tests, which are as a part of this study, and other test results. Using the computer program, accurate and systematical studies of the strength and behavior of real fabricated tubular steel columns, considering residual stresses, initial crookedness, end eccentricities and end restraints, can be carried out easily. From this paper, the following conclusions appear valid:

- (1) The test results of 6 fabricated tubular columns were consistent with the results of previous tests of the same sort and collapse strength of these columns is found to be mostly above the strength curves contained in API, ECCS/DnV-OS, and SSRC design recommendations.
- (2) By the computer program, BCAP, theoretical prediction of the strength and behavior of these test specimens was in good agreement with the experimental results and the comparison between the both is shown in Fig.17.
- (3) Using the computer program, the effects of longitudinal residual stresses on the $N-P-\phi$ curves and the column strength curves of fabricated tubular columns were studied and it is found that the longitudinal residual stresses and its location with respect to the buckling direction have considerable effects on these curves.
- (4) Among the above column strength curves, the one whose buckling direction is opposite to the longitudinal weld gives the lowest column strength, therefore, it may be adopted for the design of fabricated tubular columns. The suggested column strength curve can be closely approximated by the equation (26).
- (5) Comparisons between the suggested column strength curve and API, ECCS/DnV-OS, and SSRC curves are shown in Fig.19 and Fig.20. It is found that the suggested curve is close to the ECCS/DnV-OS curve "a" but slight higher than it.

5. REFERENCES

- (1) Ellinas, C.P., "Buckling of Offshore Structures, a state-of-the-art review of the buckling of offshore structures," First Edition, Granada Publishing Ltd, London, 1984.
- (2) Narayanan, R., "Axially Compressed Structures, stability and strength," First Edition, Applied Science Publishers Ltd, London and New York, 1982.
- (3) DET NORSKE VERITAS (DnV-OS) Rules for the Design, Construction and Inspection of Offshore Structures, Appendix C: steel structures, Høvik, Norway, 1982.
- (4) EUROPEAN CONVENTION FOR CONSTRUCTIONAL STEELWORK (ECCS) European Recommendations for Steel Construction, London: The Construction Press, 1981.
- (5) Dongsheng Qian, "The Carrying Capacity of Steel Compression Members," 1st. Ed. People's Railway Publishers, Beijing, 1980.

- (6) AMERICAN PETROLEUM INSTITUTE (API) Recommended Practice for Planning, Designing, and Constructing Fixed Offshore Platforms, API RP 2A, 13th Edition, Washington D.C., 1982.
- (7) Johnston, B.G., "Guide to Stability design Criteria for Metal Structures" Third Edition, John Wiley & Sons, New York, 1976.
- (8) Chen, W.F. and Ross, D.A., "Tests of Fabricated Tubular Columns," Proc. ASCE, Structural Division, Vol. 103, No. ST3, March, 1977.
- (9) Smith, C.S., Somerville, W.C., and Swan, J.W., "Residual Strength and Stiffness of Damaged Steel Bracing Members," Proc. OTC, Houston, Texas, 1981.
- (10) Toma, S. and Chen, W.F., "Analysis of Fabricated Tubular Columns," Proc. ASCE, Structural Division, Vol. 105, No. ST11, Nov., 1979.
- (11) Shao-Fu Li and Zhong-Min Wang, "The Measurement and Analyses of the Residual Stresses in Fabricated Tubular Columns," Research Report No. Civil-85-08, Tsinghua University, Beijing, China, 1985.
- (12) Chen, W.F. and Ross, D.A., "The Axial Strength and Behavior of Cylindrical Columns," Proc. OTC, Houston, Texas, 1976.
- (13) Chinese Standard (GB-228-76) "The Method of Tension Coupon Tests for Metals," Beijing, China, 1976.
- (14) Jun Hu, Guo-Zhou Wang, and Wen-Wei Zhao, "The Study of the Carrying Capacity of the Column with Welded Section under Axial Compression," Research Report No. Civil-85-01, Tsinghua University, Beijing, China, 1985.
- (15) Wen-Yuan Chen, Guo-Zhou Wang, and Wen-Wei Zhao, "The Study of the Carrying Capacity of the Column with Welded Section under Eccentric Compression," Research Report No. Civil-85-02, Tsinghua University, Beijing, China, 1985.
- (16) Wagner, A.L., Mueller, W.H., and Erzurumlu, H., "Design Interaction Curve for Tubular Steel Beam-Columns," Proc. OTC, Houston, Texas, 1976.

Table 1 Material Properties

	Yield Stress (kg/cm ²)	Modulus of Elasticity (kg/cm ²)
Hill Report	3290.0	-
Tension Test	3280.0	2.206E6
Stub Column Test	3189.0	2.195E6

Table 2 Long Columns: Derived Parameters and Collapse Loads

Specimen No.	Effective Length Lo (m)	L/r	λ_0	Collapse Loads (ton)	Collapse Stress (kg/cm ²)	Col. Strs. ----- Yie. Strs.
ZC-1	3.187	45.98	0.5644	77.1	3130.3	0.9544
ZC-3	3.187	45.98	0.5644	79.2	3215.6	0.9804
ZC-5	3.187	45.98	0.5644	75.4	3061.3	0.9333
C-1	5.187	74.84	0.9185	70.0	2842.1	0.8665
C-3	5.187	74.84	0.9185	72.8	2955.7	0.9011
C-5	5.187	74.84	0.9185	62.4	2533.5	0.7742

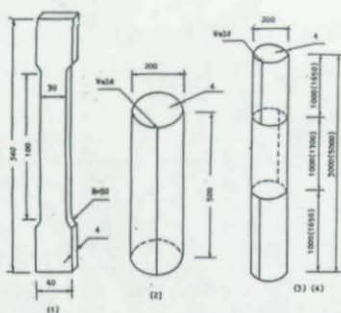


Fig. 1 Dimensions of Specimens (mm)

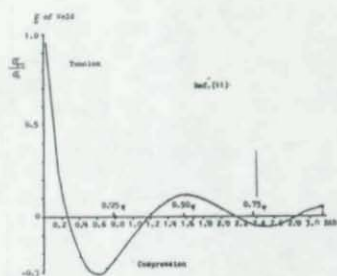


Fig. 4 Longitudinal Residual Stress Distribution

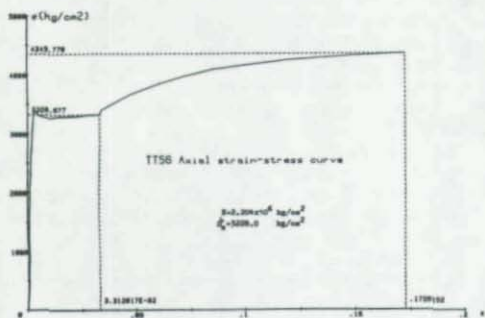


Fig. 2 Stress-Strain Curve of Tention Coupon

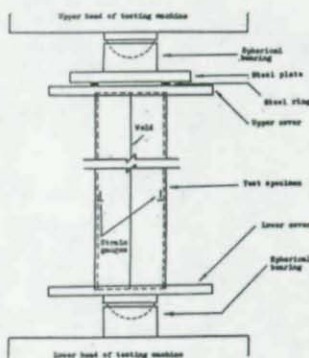


Fig. 5 Test Rig for Columns

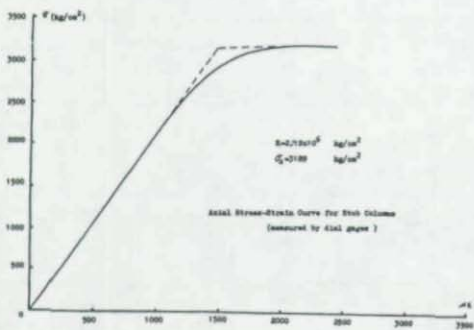


Fig. 3 Stress-Strain Curve of Stub Column

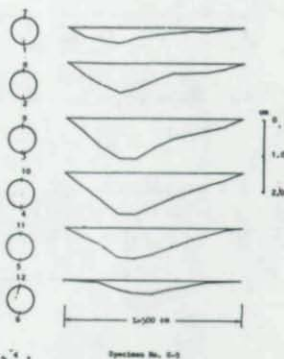


Fig. 6 Out-of-Straightness

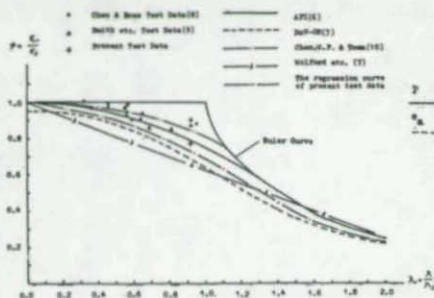


Fig. 7 Design Curves and Test Data for Fabricated Tubular Columns

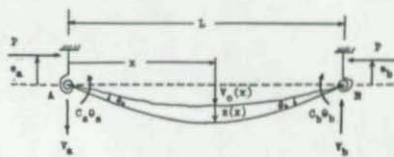


Fig. 8 Initial Crooked, End Restrained Column

End Restrained Column

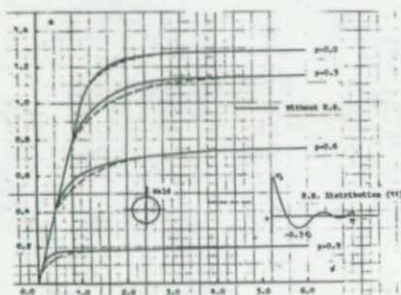


Fig. 9 M-P-Q Curves for Fabricated Tubular Columns

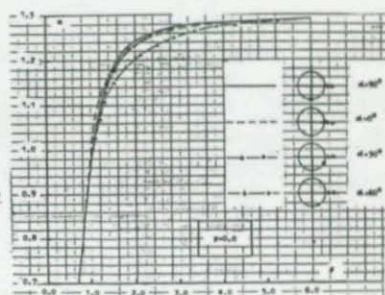


Fig. 10 M-P-Q Curves with Different Weld Locations

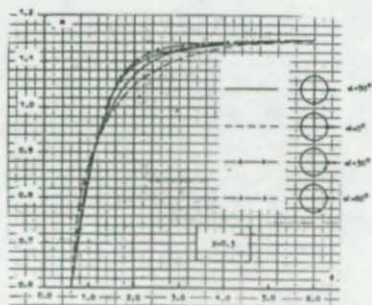


Fig. 11 M-P-Q Curves with Different Weld Locations

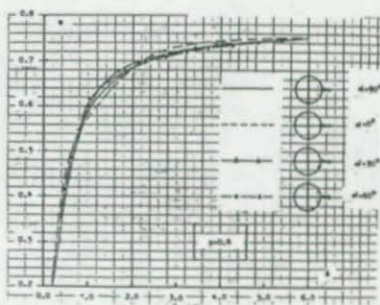


Fig. 12 M-P-Q Curves with Different Weld Locations

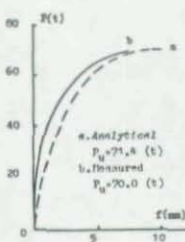


Fig. 13 Load vs. Deflection
-Specimen No. C-1

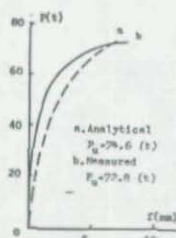


Fig. 14 Load vs. Deflection
-Specimen No. C-3

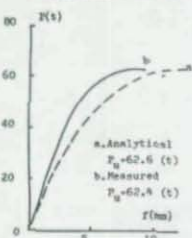


Fig. 15 Load vs. Deflection
-Specimen No. C-5

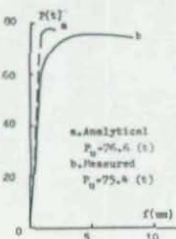


Fig. 16 Load vs. Deflection
-Specimen No. TC-5

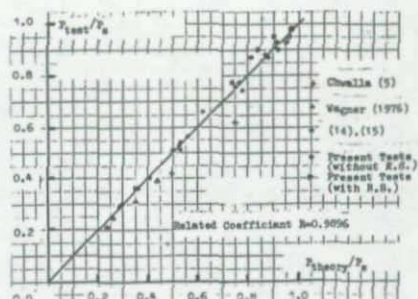


Fig. 17 Comparison of Ultimate Loads
between Experiments and Analyses

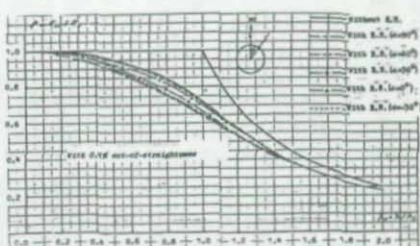


Fig. 18 Column Strength Curve with
Different Weld Locations

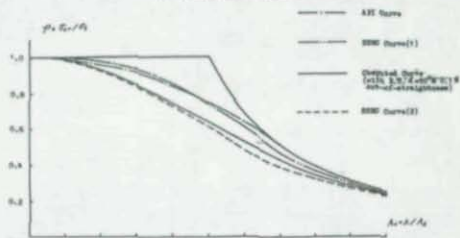


Fig. 19 Computed Column Strength Curves
Compared with API, SSRC Curves

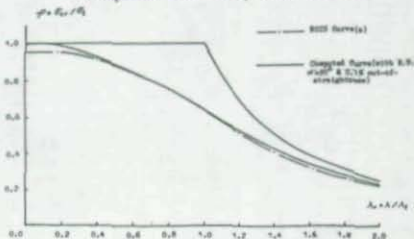


Fig. 20 Computed Column Strength Curve
Compared with ECSC Curve (a)

APPLICATION OF THE NUMERICAL INTEGRATION METHOD
TO STABILITY OF RING-STIFFENED CYLINDERS

John E. Goldberg, Professor Emeritus, Purdue University
Divaker V. Pathak, Consulting Engineer, Ypsilanti, Michigan

Introduction

This is a brief description of the Numerical Integration Method and its application to stability problems of ring-stiffened cylinders. The cylinder may have closed ends: spheroidal, paraboloidal, conoidal as well as flat; and the stiffeners may be internal or external and may have any practical profile including closed sections. In fact, the program which has been written for the stability problem includes a catalog of stiffening rings: flat, angle, jay, tee and flanged tee; and a catalog of closures; both of the catalogs can be readily expanded. Radial pressure and longitudinal loads are handled, and both of these may vary in the longitudinal direction.

The procedure and program are based on the first-order method, sometimes called the Numerical Integration Method, originated by Goldberg and Bogdanoff [1] for stress, stability and vibration analysis of shells of revolution. Two significant features of this method are its ability to handle shells of revolution of arbitrary shape with arbitrary variations of thickness and material properties, and its direct handling of all physically possible boundary conditions. For stability analysis, since only the lowest eigenvalue is required, the numerical integration method is coupled with an iteration procedure.

Theory

The governing equations are derived with the aid of classical shell theory. The stress-displacement relations and the differential equilibrium for a deformed shell in generalized orthogonal curvilinear coordinates are taken from Love [6] and the stress-strain relations are taken from Novozhilov [7]. The coordinates, s and θ , define points on the middle surface of the shell and on the middle surfaces of the stiffeners; with s and θ , respectively, being the distance along the meridional curve, and the angle between the meridional plane through the point and a reference meridional plane. The third coordinate, z , is the normal distance from the middle surface and is positive inward. It is convenient also to define the angle, ϕ , between the normal and the axis of the shell.

Taking the solution in the form consistent and generalized Fourier series, the basic partial differential equations are reduced to uncoupled sets of ordinary differential equations. It may be noted that the Fourier series representation is associated directly with the buckling and vibrational modes. In accordance with a basic principle of the Goldberg-Bogdanoff method, the differential equations are written in first-order form, which is particularly convenient for numerical integration, and in terms of physically meaningful variables: stress and moment resultants and displacements in the local coordinate directions.

The final form of the equations for an arbitrary circumferential wave number or index, n , is shown in Appendix II. The set of equations is of eighth order, consisting of eight first-order simultaneous ordinary differential equations. In symmetrical cases, n becomes zero and the set reduces properly and identically to sixth order.

Stability Problem

The stability problem is solved in two stages. The first stage, which may be called the prebuckling stage, determines the state of stress throughout the system due to symmetrically applied pressure and longitudinal loading distribution and a convenient unit or reference magnitude. The second stage, which may be called the buckling stage, determines the eigenvalue, which is the multiple of the unit or reference loading at which the system will buckle. The eigenvalue is obtained through the use of an iterative procedure (with which the names of Schwarz, Engesser, Vianello and Stodola are associated) in conjunction with the numerical integration method.

To apply the iterative procedure for a specific circumferential wave number, n , a geometrically admissible mode shape is assumed. The products of the prebuckling stress resultants and stress couples times the appropriate deformations of the assumed mode shape are taken as a distributed applied loading, and a new set of deformations is calculated by integrating the shell equations presented in Appendix II. A test for convergence is applied. If convergence to a desired degree has not been attained, the calculated deformations are normalized and the process is repeated until satisfactory convergence is attained.

Theoretically, the process has converged when the ratio of the previous displacements to the newly calculated displacements is uniform over all integration points. From a practical standpoint, a certain tolerance is acceptable and it can be assumed sufficient when the difference between the maximum and minimum deflection ratios does not exceed a specified percentage which may be set at the discretion of the analyst. The newly calculated displacements should not be normalized prior to calculating the deflection ratios. It is likely that the ratios behave erratically at points where the calculated normal deflection is small compared to the maximum calculated normal deflection. Consequently, when calculating maximum and minimum ratios at the end of one cycle, it is advisable to disregard the ratios for these points where the deflections are small. The entire procedure must be repeated for other values of n , the Fourier index number, until the lowest buckling load (multiple of the unit or reference value) is found. It should be noted that the computer calculates the deflections (by use of the differential equations) so that the deflection ratios can be calculated within the computer.

Computational Procedure

The differential equations, which are given in the Appendix, form a system of eight simultaneous first-order differential equations in the complete set of eight intrinsic variables. The intrinsic variables are the amplitudes of the three orthogonal displacements, the rotation in the

meridional plane and four stress resultants. With appropriate initial values of these variables, the equation may be integrated numerically using any stable technique such as the Runge-Kutta process, Adam's method or a predictor-corrector method. The problem, consisting of the set of equations together with appropriate boundary conditions at the initial edge, $s = 0$, and at the terminal edge, $s = s_t$, form a two-point boundary value problem. The problem, therefore, is transformed into a corresponding set of initial value problems by the technique described below. It is assumed that the system is of eighth order; however, with obvious changes, the technique may be applied to systems of higher order as well as of lower order such as the sixth-order system corresponding to the prebuckling state.

The process of transformation to an initial value problem is explained with the aid of the table which follows. Let p_5, p_6, p_7 and p_8 represent, in any convenient order, the initial values of the four variables which are specified, and let p_1, p_2, p_3, p_4 represent initial values of the remaining unspecified variables. Five solutions, numbered 0, 1, 2, 3, and 4 are constructed by numerical integration. For solution 0, the nonhomogeneous terms (loadings) in the differential equations are retained, and p_1, p_2, p_3 and p_4 are taken to be zero. For Solution 1 to 4, the nonhomogeneous terms and p_5 to p_8 are deleted; and the initial values of p_1 to p_4 are taken to have convenient arbitrary nonzero values and one and only one of these is retained for each solution.

Solution No.	Initial Values					Nonhomogeneous Terms
	p_1	p_2	p_3	p_4	p_5-p_8	
0	0	0	0	0	Include	Include
1	1	0	0	0	0	Delete
2	0	1	0	0	0	Delete
3	0	0	1	0	0	Delete
4	0	0	0	1	0	Delete

The correct solution is the sum of the nonhomogeneous solution (Solution 0) plus the linear combination of the homogeneous solutions (Solutions 1, 2, 3, 4) which satisfies the set of terminal boundary conditions. It should be noted that each of the five solutions (Solutions 0 to 4) yields terminal values for each of the eight intrinsic variables (displacements and stress resultants: $u, v, w, \beta, N_1, T, V, M_1$). Thus with p_j ($j = 1, \dots, 8$) denoting the initial values of the intrinsic variables as used in the heading of Table 1, let q_{jk}^m represent terminal values at $s = s_t$ obtained by integration in accordance with Table 1. The superscript m indicates the Solution Number, the subscripts j correspond to the subscripts in the heading of Table 1, and the subscripts k ($k = 1, \dots, 8$) define the list of variables from which the four variables for which terminal values have been specified. Also let f_k be the defined values.

To these definitions, add the definition a_1, a_2, a_3, a_4 are the factors by which the four homogeneous solutions must be multiplied to obtain the complete and proper solution. For example, let f_3, f_5, f_6 and f_7 be the values of the four intrinsic variables which are specified at the

terminus. Then the following equation can be written

$$\begin{Bmatrix} 0 \\ q_3 \\ 0 \\ q_5 \\ 0 \\ q_6 \\ 0 \\ q_7 \end{Bmatrix} + \begin{bmatrix} 1 & 2 & 3 & 4 \\ q_3 & q_3 & q_3 & q_3 \\ 1 & 2 & 3 & 4 \\ q_5 & q_5 & q_5 & q_5 \\ 1 & 2 & 3 & 4 \\ q_6 & q_6 & q_6 & q_6 \\ 1 & 2 & 3 & 4 \\ q_7 & q_7 & q_7 & q_7 \end{bmatrix} \begin{Bmatrix} a_1 \\ a_2 \\ a_3 \\ a_4 \end{Bmatrix} = \begin{Bmatrix} f_3 \\ f_5 \\ f_6 \\ f_7 \end{Bmatrix} \quad (1)$$

When the a 's have been calculated, a single and final integration of the equations with the nonhomogeneous terms included will provide the values at any location between $s = 0$ and $s = s_t$.

Alternatively, if the results of integrating the equations according to the table above had been stored for all of the intervening division points, these stored values may be multiplied by the calculated values of the a 's to obtain the values of all of the intrinsic variables at those points.

It is well known that, depending on geometry and wave number, the effect of conditions imposed at one end of a shell generally attenuate markedly with distance from that end. Under these circumstances the solution may be greatly damaged by round-off and truncation errors, and the matrix equation, Eq. (1), yields an undependable or perhaps totally incorrect set of values for the solution coefficients. An efficient technique for maintaining numerical stability has been devised [4,5] and has proved to be very useful, particularly so for stiffened shells.

The first step in using this technique is to divide the complete path of integration in the shell body into segments each of which is sufficiently short to preclude numerical instability. In the case of ring-stiffened shells, the points of attachment of the stiffeners should be taken as division points with one or more intermediate division points if needed for numerical stability. The next step is to construct five solutions, as listed in Table 1, for the first segment, which terminates at $s = s_1$. It is convenient to take the four components of displacement (u_1, v_1, w_1, β_1) to be p_1, \dots, p_4 . The terminal boundary conditions for Solution 0 (which retains the nonhomogeneous terms) are that the four components of displacement at s_1 are equal to zero; that is, the "edge" at $s = s_1$ is clamped. For each of the remaining four solutions, one displacement at $s = s_1$ is set equal to zero and the remaining displacements equal to zero. The boundary condition equation (at $s = s_1$) becomes

$$\begin{bmatrix} 1 & 2 & 3 & 4 \\ u & u & u & u \\ v & v & v & v \\ w & w & w & w \\ \beta^1 & \beta^2 & \beta^3 & \beta^4 \end{bmatrix} \begin{bmatrix} a_1 & v & w & \beta^1 \\ a_1 & a_1 & a_1 & a_1 \\ a_2 & v & w & \beta^2 \\ a_2 & a_2 & a_2 & a_2 \\ a_3 & v & w & \beta^3 \\ a_3 & a_3 & a_3 & a_3 \\ a_4 & v & w & \beta^4 \\ a_4 & a_4 & a_4 & a_4 \end{bmatrix} = \begin{bmatrix} 1 & 0 & 0 & 0 & -u^0 \\ 0 & 1 & 0 & 0 & -v^0 \\ 0 & 0 & 1 & 0 & -w^0 \\ 0 & 0 & 0 & 1 & -\beta^0 \end{bmatrix} \quad (2)$$

The elements of the first matrix and the last column of the third matrix are displacements at $s = s_1$ as given by the solutions of Eq. (1) with inputs as directed by Table 1. Premultiplication of both sides of Eq. (2) by the inverse of the first matrix provides the numerical values of the a^0 's.

The tractions at s_1 , the end of the first segment, can now be calculated for any prescribed set of the (four) displacements at that location. Thus, in particular, the tractions (N_1, T_1, V_1, M_1) which would exist if the first segment were clamped at $s = s_1$ are

$$\{F\}_1^0 = \{F\}_1^0 + [F]_1^1 \{a\}_1^0$$

or

$$\{F\}_1^0 = \begin{Bmatrix} N_1 \\ T_1 \\ V_1 \\ M_1 \end{Bmatrix} = \begin{bmatrix} N_1^0 & N_1^1 & N_1^2 & N_1^3 & N_1^4 & a_1^0 \\ T_1^0 & T_1^1 & T_1^2 & T_1^3 & T_1^4 & a_2^0 \\ V_1^0 + V_1^1 & V_1^2 & V_1^3 & V_1^4 & a_3^0 \\ M_1^0 & M_1^1 & M_1^2 & M_1^3 & M_1^4 & a_4^0 \end{bmatrix} \quad (3)$$

When arbitrary displacements, represented by the column vector $\{d\}_1$, are imposed at $s = s_1$, the tractions due only to these displacements are given by

$$\{F\}_1 = [F]_1^1 [A]_1 \{d\}_1 \quad (4)$$

in which $[F]_1^1$ is the 4×4 square matrix in Eq. (3) and $[A]_1$ is the 4×4 square matrix made up of the first four columns of the second matrix in Eq. (2). The total tractions at $s = s_1$ due to loading and displacements, $\{d\}_1$, imposed at the location are

$$\{F\}_1^* = \{F\}_1^0 + \{F\}_1 \quad (5)$$

Before proceeding to the second segment, the matrix $[A]_1$ and the vector $\{d\}_1$ are stored in the computer for use in future steps of the analysis.

Integration over the second segment proceeds in accordance with Table 1 where p_1, p_2, p_3, p_4 represent the displacements u, v, w, β and p_5, p_6, p_7, p_8 represent the tractions at s_1 obtained from the influence coefficients of the first segment. The nonhomogeneous solution for the second segment is constructed by setting the initial values of the displacements equal to zero, and taking the tractions as $\{F\}_1^0$. If there is a sharp change in direction at s_1 , the traction vector should be transformed appropriately. The four homogeneous solutions are taken as given in Table 1, and the initial values of the tractions are the vector $\{F\}_1$ from Eq. (4), transformed directionally if necessary. The initial values of the tractions used for the nonhomogeneous solution are stored as a vector, say $\{S\}_2^0$, and the initial values of the tractions used for the four homogeneous integrations are stored as the columns of a 4×4 matrix $[S]_2$ matrix

$[A]_2$ and vector $\{d\}_2$ are also stored.

Integration over the third and subsequent segments proceeds in the same manner as for the second segment until the last segment is reached. Matrices $[S]_m$ and $[A]_m$ and the vectors $\{S\}_m$ and $\{d\}_m$ are stored for each segment. The final^m segment may be handled in, essentially, the same manner as the preceding segments but taking account of the fact that the terminal boundary conditions are known.

Ring stiffeners may be located at any parallel circle of the shell but it is convenient to place a division point at that location. A stiffness matrix should be obtained for the junction edge and then added, after proper directional transformation, to the stiffness matrix of the "incoming" segment of the shell. It is advisable to due the integrations over the stiffeners by starting at the free edges of the stiffener and integrating toward the shell. If any of the stiffeners are identical, the homogeneous solutions for one stiffener may be used for all of the identical stiffeners.

References

1. Goldberg, J.E. and J. L. Bogdanoff, "Analysis of Coned Disks under Symmetric Conditions," Midwest Applied Science Corp., West Lafayette, Report 57-7, 1957.
2. Goldberg, J.E., J. L. Bogdanoff and D. W. Alspaugh, "Stresses in Spherical Domes under Arbitrary Loading Including Thermal and Shrinkage Effects," Proceedings of the Intl. Assn. for Shell Structures Symposium on Non-Classical Shell Problems, Warsaw, 1963, North Holland Publishing Company, Amsterdam, 116-135.
3. Goldberg, J.E. and J. L. Bogdanoff, "Static and Dynamic Analysis of Conical Shells under Symmetrical and Unsymmetrical Conditions," Proceedings of the Sixth Symposium on Ballistic Missile and Aerospace Technology, Los Angeles, 1961, Academic Press, New York, 219.
4. Goldberg, J.E., A. V. Setlur and D.W. Alspaugh, "Computer Analysis of Non-Circular Cylindrical Shells," Proceedings of the Intl. Symp. on Shell Structures in Engineering Practice, I.A.S.S., Budapest, 1965.
5. Goldberg, J.E., J. L. Bogdanoff and D.W. Alspaugh, "On the Calculation of the modes and Frequencies of Pressurized Conical Shells," Journal of Aircraft, AIAA, Vol. 1, No. 6 (1964), 372-374.
6. Love, A.E.H., A Treatise on the Mathematical Theory of Elasticity, Fourth Edition, Dover Publications, New York, 1944.
7. Novozhilov, V.V., Thin Shell Theory, Second Russian Edition, Translated by P. G. Lowe, P. Noordhoff, Ltd., Groningen, 1964.

APPENDIX I
Illustrative Examples

By way of illustrative examples, a part of the results for two sets of uniform cylindrical shells having hemispherical closures of the same thickness at both ends are presented. The radius of each shell is 10 inches and the spacing of the stiffeners for shells A2, A3, and B2 is 2.5 inches. Other geometrical properties are presented in the following table.

Shell	L	h	Ring Stiffeners				
			Type	m	b	d	h_s
A1	20	0.5	-	-	-	-	-
A2	20	0.5	Flat	9	-	1.0	0.5
A3	20	0.5	Tee	9	1.5	1.0	0.5
B1	5	1.0	-	-	-	-	-
B2	5	1.0	Flat	3	-	1.5	0.8

Dimensions are in inches

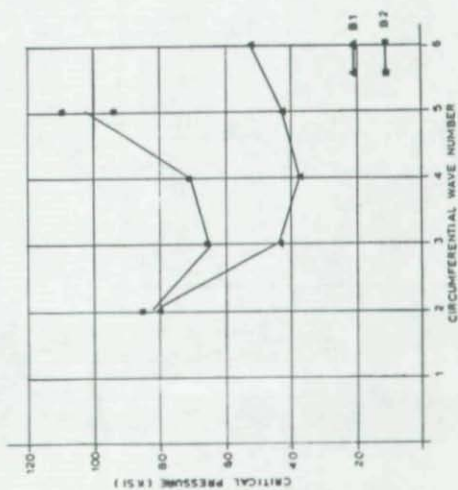
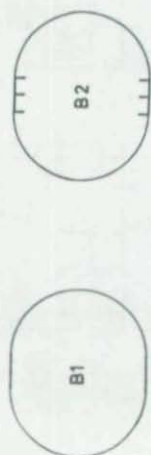
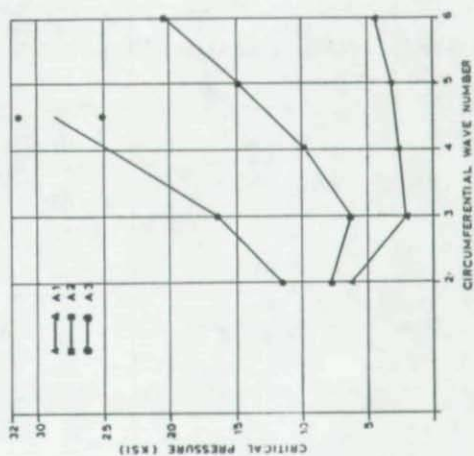
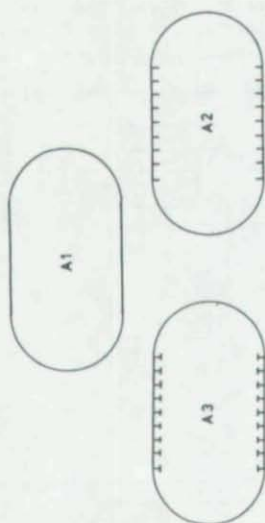
L = length of cylindrical body
h = thickness of cylinder and closures
m = number of stiffeners

b = flange width
d = web depth
 h_s = thickness
s

Shell A1				Shell B1			
Calc. Pressure, psi				Calc. Pressure, psi			
n	Maximum	Minimum	Diff., %	n	Maximum	Minimum	Diff., %
2	6,362	6,192	2.8	2	85,250	78,457	8.1
3	<u>2,961</u>	<u>2,926</u>	0.3	3	45,510	43,003	5.5
4	2,238	2,133	4.7	4	<u>38,473</u>	<u>37,143</u>	3.5
5	3,168	3,010	5.0	5	43,027	42,370	1.5
6	4,445	4,231	4.8	6	53,570	51,840	3.2
				7	66,717	65,017	2.5
				8	83,657	80,990	3.2
				9	103,321	99,437	3.8

Shell A2				Shell B2			
Calc. Pressure, psi				Calc. Pressure, psi			
n	Maximum	Minimum	Diff., %	n	Maximum	Minimum	Diff., %
2	7,964	7,915	0.9	2	85,507	81,673	4.5
3	<u>6,352</u>	<u>6,221</u>	2.1	3	<u>65,201</u>	<u>63,437</u>	3.7
4	9,830	9,605	2.4	4	81,920	79,937	2.4
5	14,809	14,270	3.6	5	109,160	93,807	14.0
6	20,411	19,535	4.3	6	140,407	104,993	24.6
				7	173,327	132,567	23.5

Shell A3			
Calc. Pressure, psi			
n	Maximum	Minimum	Diff., %
2	11,834	11,465	3.1
3	16,716	15,865	5.1
4	31,281	25,108	19.7



Appendix II
Detailed form of Equations (1)

1. Cylinder:

a. Differential equations

$$\frac{du}{ds} = \frac{H_1}{B} - vc$$

$$\frac{dv}{ds} = \beta$$

$$\frac{d\beta}{ds} = -\frac{M_1}{D} - vc$$

$$\frac{dv}{ds} = \frac{T}{C^*} + \frac{C}{C^*} \frac{nu}{a} + \frac{n^2}{3a} \frac{C}{C^*} \frac{n}{a} \frac{dv}{ds}$$

$$\frac{d(H_1a)}{ds} = -nT + \frac{2nh}{a} + \bar{H}_2(n \frac{dv'}{ds} - \beta')$$

$$+ \bar{H}_1 n \frac{d\beta'}{ds} + \bar{H}_2(n \frac{dv'}{ds} - \beta')$$

$$+ \bar{Q}_1 a \frac{d\beta}{ds} - Xa$$

$$\frac{d(Ta)}{ds} = V_2 + nH_2 + \bar{Q}_1 a(-\frac{n\beta'}{a} + \frac{1}{a} \frac{dv'}{ds})$$

$$+ \bar{Q}_1 a(-\frac{n\beta}{a} + \frac{1}{a} \frac{dv}{ds})$$

$$\frac{d(V_1a)}{ds} = -nV_2 - H_2 - \bar{H}_1 a \frac{d\beta'}{ds}$$

$$- \bar{H}_2(-\frac{n^2 w'}{a} + \frac{nv'}{a})$$

$$- \bar{H}_1 a \frac{d\beta}{ds} - \bar{H}_2(-\frac{n^2 w}{a} + \frac{nv}{a}) - Za$$

$$\frac{d(M_1a)}{ds} = 2nH + V_1a + \bar{H}_2(n \frac{dv'}{ds} - \beta')$$

$$+ \bar{H}_2(n \frac{dv}{ds} - \beta)$$

b. Auxiliary equations

$$c = \frac{nv}{a} - \frac{v}{a}$$

$$H_2 = vH_1 + Ehc$$

$$x = -\frac{n^2 w}{a^2} + \frac{nv}{a^2}$$

$$H_2 = vH_1 - \frac{Eh^3}{12} c$$

$$H = \frac{Ch^2}{6} (-\frac{n}{a} \frac{dv}{ds} + \frac{1}{a} \frac{dv'}{ds})$$

$$V_2 = -\frac{nM_1}{a}$$

2. Plate:

a. Differential equations

$$\frac{du}{ds} = \frac{H_1}{B} - vc$$

$$\frac{dv}{ds} = \beta$$

$$\frac{d\beta}{ds} = -\frac{M_1}{D} - vc$$

$$\frac{dv}{ds} = \frac{T}{C} + \frac{nu}{r} + \frac{v}{r}$$

$$\frac{d(H_1r)}{ds} = -nT + H_2 + \bar{H}_2 n \frac{dv'}{ds} + \bar{Q}_1 r \frac{d\beta'}{ds}$$

$$+ \bar{H}_2 n \frac{dv}{ds} + \bar{Q}_1 r \frac{d\beta}{ds} - Hr$$

$$\frac{d(Tr)}{ds} = -T + nH_2 + \bar{Q}_1 r(-\frac{n\beta'}{r} + \frac{nv'}{r^2})$$

$$+ \bar{Q}_1 r(-\frac{n\beta}{r} + \frac{nv}{r^2})$$

$$\frac{d(V_1r)}{ds} = -nV_2 - \bar{H}_1 r \frac{d\beta'}{ds} - \bar{H}_2(-\frac{n^2 w'}{r^2} + \beta')$$

$$- \bar{H}_1 r \frac{d\beta}{ds} - \bar{H}_2(-\frac{n^2 w}{r^2} + \beta)$$

$$\frac{d(M_1r)}{ds} = 2nH + H_2 + V_1r + \bar{H}_2 n \frac{dv'}{ds}$$

$$+ \bar{H}_2 n \frac{dv}{ds}$$

b. Auxiliary equations

$$c = \frac{nv}{r} + \frac{v}{r}$$

$$H_2 = vH_1 + Ehc$$

$$x = -\frac{n^2 w}{r^2} + \frac{v}{r}$$

$$H_2 = vH_1 - \frac{Eh^3}{12} c$$

$$H = \frac{Ch^2}{6} (-\frac{n}{r} \frac{dv}{ds} + \frac{nv'}{r^2})$$

$$V_2 = -\frac{2H}{r} - \frac{nM_1}{r}$$

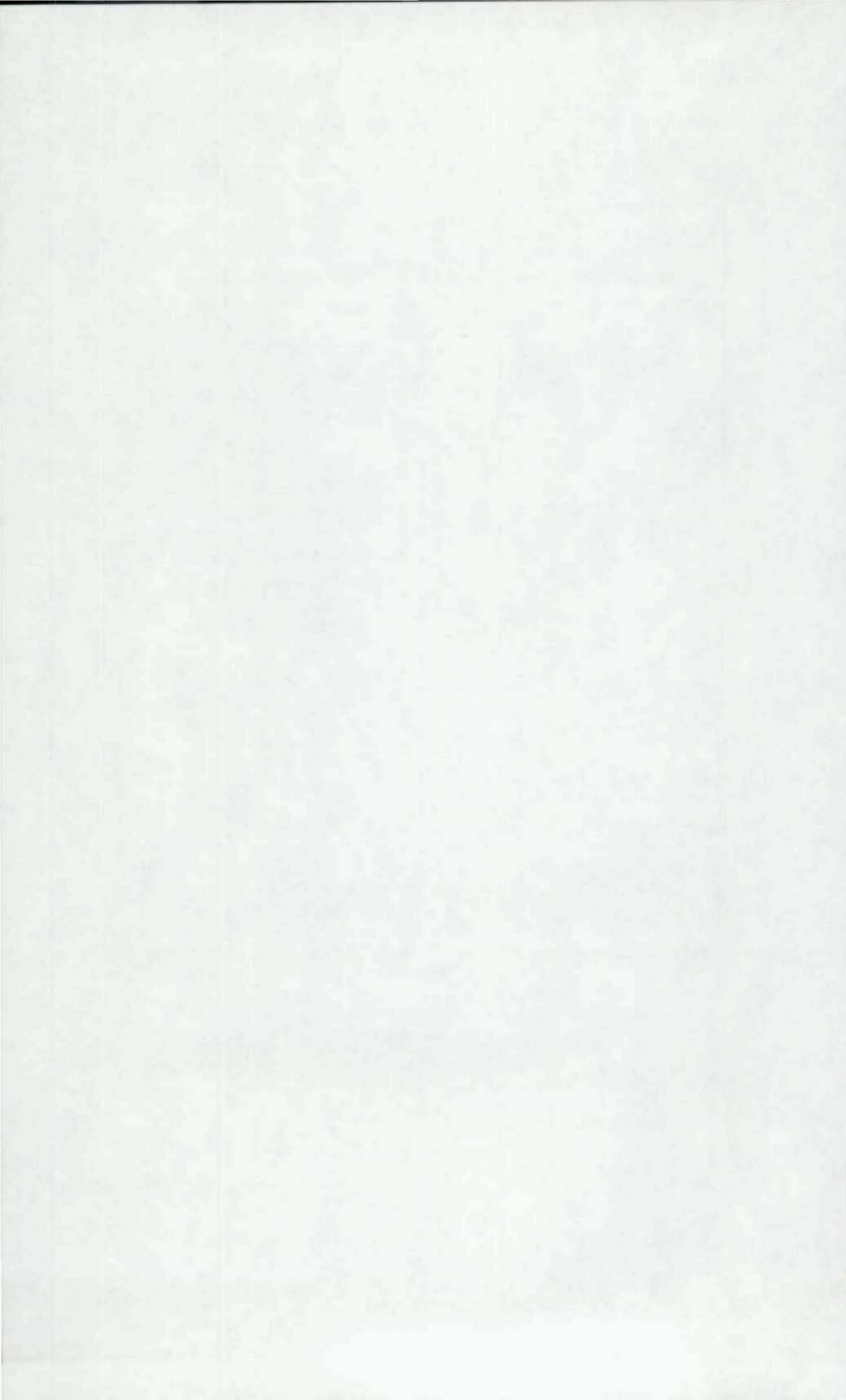
3. Definitions:

$$B = \frac{Eh}{1-\nu^2}$$

$$D = \frac{Eh^3}{12(1-\nu^2)}$$

$$C = \frac{Eh}{2(1+\nu)}$$

$$C^* = C(1 + \frac{1}{3}\nu^2)$$



RETROFITTING OF A LOCALLY BUCKLED TUBULAR COLUMN

A. Ostapenko and S.C. Apte
Department of Civil Engineering
Lehigh University
Bethlehem, PA 18015

ABSTRACT

Locally buckled or dented tubular columns in structures, such as offshore platforms, require a means for simple and quick repairs, even if only of a temporary nature. A study of repairing by stiffeners bridging over the local buckles is presented.

A short tubular column with local buckles from a previous test was reinforced with six stiffeners and then re-tested. Full capacity was regained from the 25% of the capacity after the local buckling test. The test specimen had a diameter of 0.585 m and $D/t=59.1$. The stiffeners were designed using a simple procedure and the AISC Specification(1978) limitations. The attachment to the buckled tube wall required no special fitting since the attachment points were outside the buckled portion.

The specimen was also analyzed by using the finite element program ADINA, and the stresses and the postbuckling behavior showed reasonable agreement with the test observations. The ultimate load, however, was somewhat lower than in the test, apparently because the computational yield stress was taken from the tensile coupon data and, thus, the increase due to strain hardening was not taken into account.

The repair system studied is proposed as a practical method for expedient retrofitting of locally buckled or dented structural tubulars.

1. INTRODUCTION

1.1. Background

Cylindrical tubular columns are commonly used in many structures such as, elevated storage tanks, transmission towers and offshore platforms. A sudden overload or impact by a ship may lead to the formation of local buckles and/or dents and to significant reduction of column capacity. Major repairs and/or replacement of the damaged columns for continued operation of the platform can be too time-consuming and not feasible under adverse weather conditions. Thus, a simple and quick method of retrofitting such columns in the field is needed; permanent repairs can be completed later when conditions permit.

A method for temporary retrofitting by welding a system of stiffeners to bridge over the local deformations is described here.

1.2. Previous Research

The use of a system of stiffeners was recently explored at Lehigh University.^{7, 8} The specimen was a locally buckled tubular column from a previous axial test.⁶ The repair system consisted of six stiffeners fabricated from steel plates and Tee sections, arranged symmetrically around the circumference and attached to the column by brackets using fillet welds.

An axial load test was conducted, but the load did not reach the full capacity of

this repair system because of the unforeseen failure by the yielding and fracture of the welds at the lower brackets.

1.3. Objectives of Present Research

The first objective of the research reported here was to repair and modify the specimen and retest it to determine the full strength of the retrofitted specimen. The specimen, then, was to be analyzed using a finite element program in the large-deflection elasto-plastic range. Then, the accuracy of the design procedure for the stiffeners used in the previous work was to be re-examined and any necessary corrections and/or modifications suggested as indicated by the results from the test and the finite element analysis.

2. EXPERIMENTAL WORK

2.1. Test Specimen

The original test specimen was fabricated from ASTM A36 steel. It was 1.22 m long with a diameter of 0.58 m and a plate thickness of 9.73 mm. The first axial test resulted in local buckles at the lower end of the specimen. Only the upper portion of 0.87 m remained straight and the overall length shortened to 1.1 m.⁶

The first attempt at retrofitting consisted of welding six stiffeners which bridged over the local buckles.^{7, 8} As shown in Figs. 1 and 2, the stiffeners were fabricated from a 150 mm x 25 mm flange plate and a Tee section cut from a W12x14 wide-flange section. The brackets at the ends of the stiffeners were 75 mm wide and 25 mm thick. The flange plates and the brackets were made of ASTM A 588 Grade 50 steel and the Tee section was made of ASTM A572 Grade 50 steel. All the connections were made by fillet welds. Due to the location of the buckles close to one end of the specimen, the stiffener connections to the column were different at the two ends. The axial capacity of the reinforced specimen was limited by the premature and unexpected yielding and fracture of the shear welds connecting the lower brackets to the tube wall and, thus, did not indicate the full amount of strength that could be regained through the use of stiffeners.

In the current program, in order to focus on the upper connection which was intended to represent a connection in a long column as it would exist in a full-scale structure, previous deficiencies were corrected by rewelding the fractured portions and tackwelding an additional base plate below each stiffener, thus fully supporting its overhang beyond the base ring through direct bearing as shown in Figs. 3 and 5. This ensured that the capacity would be controlled by the failure of the stiffener proper or of the tube wall at the upper end.

2.2. Test Setup and Procedure

The specimen was tested under axial compression in a 2500 ton (5,000,000 lb) capacity Baldwin hydraulic universal testing machine. The specimen was placed between a movable pedestal and the machine head with a layer of Hydro-Stone grout at each end of the specimen.(Fig. 5) A preload of 9 kN was applied to form level contact surfaces before the grout was allowed to set. The grout layers ensured a concentric and uniform application of the load to the specimen.

Three dial gages were used to measure the longitudinal deformation of the specimen. They were mounted around the specimen on the bottom pedestal with a fine wire leading from the dial gages to the magnets attached to the underside of the

machine head. The wire was yielded by hand to produce a straight and taut line, free of kinks. 137

With the ultimate capacity expected to be about 6300 kN, a load increment of 220 kN was used at the beginning to capture any initial adjustments in the load-deformation relationship and then increased to 445 kN. Later, as can be seen in Fig. 4, the load increments were reduced when the phases of yielding and failure approached. The loading was continued beyond the maximum of 6540 kN to more closely observe the failure pattern and the load-deformation relationship as the load continued to drop with increasing deformation. After the load had dropped to 4000 kN, the specimen was unloaded with load steps of 1335 kN.

3. TEST RESULTS

The ultimate capacity of the specimen was 6540 kN. This value is very close to the capacity of the original unbuckled specimen of 6580 kN.⁶

3.1. Axial Deformation

The plot of the load-vs-overall deformation (Fig. 4) shows an initial non-linear region up to the load of 890 kN. This can be attributed to the apparent redistribution of forces through the loading system. From 890 kN to 3780 kN, the plot is linear indicating an elastic behavior of the specimen. Then, it slightly deviates from linearity for the loads from 3780 kN to 4670 kN reflecting the initiation of yielding in the specimen. From this stage on, an increased load could not be sustained at the same level as it started dropping by 20 to 25 kN after each load increment. From the load of 4670 kN on, extensive deflection of the tube wall was observed. Finally, as the load reached 6540 kN, the specimen could not sustain the load for long. This was then considered to be the ultimate capacity of the specimen. Further loading of the specimen resulted in dropping of the load with a rapid increase of the deflection. Loading was continued in order to obtain the load-deformation relationship beyond the ultimate point.

After the load had dropped to 4000 kN, the unloading phase was started. Between 4000 kN and 1335 kN, the unloading curve is approximately parallel to the initial elastic range. Below 1335 kN, the curve is shallow, indicating reduced stiffness. The permanent plastic deformation was 35 mm.

3.2. Test Behavior

No visible changes were observed till the load reached 4000 kN. Then, the flaking of the whitewash on the surface and the appearance of yield lines in the upper web of the stiffeners near the brackets indicated the progression of yielding. The flaking was also observed in the spot welds connecting the stiffeners to the base plates. The yield lines had a pattern of a series of shallow arcs parallel to the longitudinal axis of the web. Each load increment in this range was accompanied by a slight drop-off.

Approximately above the load of 6320 kN, shallow bulges appeared on the wall near the upper connection of the stiffeners, and the bracket tops were pushed inside thus forming dents in the tube wall. More yield lines appeared on the stiffener web in the form of horizontal lines indicating high shearing stresses. As the loading continued, the dents in the tube wall became more and more pronounced and the yield lines continued to grow in the stiffener web and in the bracket at the upper end. Eventually, these deformations and the yielding in the tube wall made the specimen reach the ultimate capacity at the load of 6540 kN (Fig. 6).

At this time, cracks appeared in the weld between the stiffener web and the inner flange plate at the upper end. At one of the stiffeners the weld between the bracket and the tube wall cracked completely, thus separating the stiffener, whereas at other stiffeners, the cracks were slower to appear. These cracks were due to local shearing stresses induced in the upper web of the stiffeners and a complex effect of stress concentration and residual stresses.

As the test continued beyond the maximum load, the cracks and the dents increased and the load dropped off. See the crack at the top of the left stiffener in Fig. 6. A banging noise was heard when the load dropped to 4670 kN. It was probably caused by the fracture of the web at the upper end of one of the stiffeners. Further on, the weld on the lower bracket also cracked. The overall deformation increased as the specimen continued to crush without offering much resistance. The loading was stopped when the load dropped to 4000 kN which represented about 60% of the ultimate capacity.

4. FINITE ELEMENT ANALYSIS

4.1. Description of Analytical Model

Theoretical analysis of the specimen was made by using the finite element program ADINA.^{1, 2, 4} Non-linear material properties and large deformations were considered. Since the specimen was supposed to represent a locally buckled portion of a long column, as is the case in the field, the analytical model was assumed to be symmetrical with respect to the buckled portion of the tube with each half represented by the upper portion of the test specimen and with identical connection at both ends.

As the six stiffeners were identical in size and were symmetrically placed around the circumference of the tube, only one-sixth of the circumference with a stiffener at the center was discretized. This closely matched the actual behavior of the specimen as revealed by test results. Due to the symmetry in the longitudinal direction, just one half of the length was considered. To minimize local disturbances in the area of the stiffener attachments due to the applied loads, the loaded end was set at a sufficient distance (Fig. 2).

Four finite element models were explored to determine which would give a better correlation with test results.

The first three models had different types and numbers of elements in order to check their relative suitability. Since the variation in the results from these three models was less than 2%, Model 3, with a smaller number of elements but with a higher-order element type, was considered to be sufficiently accurate.

In these three models, the buckled portion of the column wall was discretized as a 'gap', and, thus, the contribution of the buckled wall was neglected. However, in view of the significant capacity of the specimen after local buckling revealed by the earlier test⁶, another model (Model 4) was prepared which considered the strength of the buckled wall.

Model 4 was identical to Model 3 except that the buckled portion of the wall was discretized by reducing the thickness of the bottom row of the wall elements and the 'gap' was closed by extending these elements to the line of support. Furthermore, the height of these elements was also reduced to match the length of the buckled portion. The reduction in thickness was proportional to the reduction of the capacity of the column after buckling in the original test. The reduced thickness was about 30% of the original thickness --- 2.8 mm versus 9.73 mm.

The modelled specimen portion was described in a cylindrical coordinate system. The top edge was free to move only in the longitudinal direction. The side edges were free to move in the longitudinal and radial directions, but, due to symmetry, not in the circumferential direction, nor could they rotate. Since the translational degree of freedom in the circumferential direction for one side of the model did not coincide with the global axes, the restraint was provided by using additional elements at each node of this side. A rigid beam element was connected on both sides of each node in the radial direction with only the translational degree of freedom along its axis released. This allowed the node to move freely in the radial and longitudinal directions, while the circumferential motion and the rotation in the horizontal plane were prevented (Fig. 7).

Similar rigid beam elements were also connected to the bottom end of the stiffener since this end also could move only in the radial direction. In Models 1, 2 and 3, the buckled portion, that is, the bottom edge of the tube wall was assumed to be free to move in any direction. In Model 4, the bottom edge was fully restrained.

4.3. Finite Element Types and Material Properties

In Models 1 and 2, the tube wall was discretized using 3-node, triangular, flat plate/shell elements (Element No. 6 in the ADINA element library).¹ Model 1 had 56 elements whereas Model 2 had 84 elements (Fig. 10). Models 3 and 4 (Figs. 11 and 12) used 28 9-node shell elements (No. 7) with 8 integration points. This is a higher order curvilinear element which better matches the cylindrical shape of the specimen.

For all four models, the material was assumed to have the idealized bilinear elastic-plastic relationship (Fig. 8) with von Mises yield criterion and isotropic strain hardening. The yield stress was set to 336 MPa, that is, the same as in the original test specimen, the modulus of elasticity to $E = 203,400$ MPa and the strain hardening modulus to $E_T = 210$ MPa.

The stiffeners and brackets were discretized using identical elements and material properties for all four models. (Fig. 13) The stiffener web and bracket were modelled using 2-D, plane stress elements (No. 2) and the flanges were modelled with 2-node, 3-D beam elements (No. 4). Models 1 and 2 used 3 elements for the bracket and 4 elements for the stiffener, whereas Models 3 and 4 used 5 and 6 elements, respectively. The yield stress was taken to be 345 MPa with $E = 203,400$ MPa and $E_T = 210$ MPa. This data is summarized in Table 1.

4.4. Loading

The loading was applied at the nodes of the top boundary as a series of equal axial forces. The loading increments were larger in the elastic range and smaller after the initiation of yielding as can be seen in Fig. 9.

5. RESULTS OF FINITE ELEMENT ANALYSIS

The behavior and ultimate loads of Models 1, 2 and 3 were computed to be essentially the same (in all three the buckled portion carried zero load). See Table 1. The ultimate load of 4115 kN for Model 3 increased by over 30% to 5625 kN after the model was modified to Model 4 by including the post-ultimate strength of the buckled portion of the tube wall. This gave a much better correlation with the test results, and Model 4 is used in further discussion.

5.1. Load-Deformation Relationship

A plot of the load-vs-longitudinal deformation computed for Model 4 is shown in Fig. 9. The relationship is linear up to a load of 2670 kN. In the load range of 2670 kN to 3560 kN, the plot deviates slightly from linearity. In this range, the tube wall portion near the bracket connection and the upper part of the web had started yielding.

Further loading resulted in extensive deformations and yielding in the tube wall and the web of the stiffener. At the load step which would have increased the total load to 5625 kN, there was no convergence within the prescribed number of iterations. This load was taken as the ultimate capacity.

5.2. Comparison with Test Results

The ultimate capacity of the specimen from the finite element analysis was 5625 kN, that is, 85% of the ultimate capacity obtained from the test on the original unbuckled specimen (6580 kN) or on the retrofitted specimen (6540 kN).

One possible reason for the lower computed capacity may be the use of the yield stress of 336 MPa obtained from the tensile coupons in the original test program.⁶ The actual yield stress in the fabricated specimen was probably higher due to cold-rolling and welding.

Another reason could be the finite element modelling of the connections. In the model, the connection between the bracket and the tube wall and the bracket and the stiffener was only at the nodes and not continuous as in the actual specimen. This might have affected the load transfer through the stiffeners and reduced their capacity.

However, the overall behavior of the analytical model was consistent with that of the test specimen. The deformation pattern of the tube wall near the bracket connection and of the stiffener (Figs. 14 and 15) was similar to that observed in the test. This included the bulging in the tube wall above the bracket connection, the bracket pushing into the wall to form a dent and the bending of the upper part of the stiffener. The stress pattern, that is, the development of bending stresses in the tube wall and of high shearing stresses in the stiffener web, was also consistent with the observations made on the test specimen.

6. COMMENTS ON THE REPAIR SYSTEM

6.1. Observations

Comparison of the test results indicates that the buckled specimen regained its full capacity through the use of the retrofitting system designed according to the AISC allowable stress method.³ This procedure is simple and quick enough to be applied to field problems and as such is considered satisfactory and accurate.

Although the designed stiffener system was unsymmetrical with respect to the buckles because of the location of these buckles on the test specimen, the same procedure can easily be used for a symmetrical case by making the connections at both sides of the buckled portion the same as the top connection in the specimen. This would represent the case of a longer column as would exist in the field.

6.2. Recommendations for Improvement

Even though the original column capacity was restored, the immediate post-ultimate strength in the test was drastically reduced by the fracture and opening-up of the joint between the web and the inner flange (see Fig. 6). To relieve the high shearing and tensile stresses in this area, it is recommended to weld an additional plate at the ends of the stiffeners.

It is proposed to design this plate to resist 50% of the bending moment developed about the inner corner between the bracket and the inner flange used as a pivot point during the transfer of the load.

For the specimen at hand, the plate size was worked out to be 75 mm wide and 12 mm thick and connected to the stiffener with a weld 260 mm long as shown in Fig. 16.

7. SUMMARY AND CONCLUSIONS

Locally buckled or dented tubular columns in offshore platforms need simple and quick repairs, at least, of temporary nature to restore their capacity. A simple system may be a set of stiffeners that bridges over the damaged portion of the member.

In a previous research, a short, locally buckled, tubular specimen was reinforced by a system of six fabricated stiffeners. However, in a compressive test performed on the specimen, the stiffener system failed prematurely due to the failure of the connections at one end.

In the current program, the specimen was repaired to strengthen the failed connections and then retested to determine its axial capacity. The ultimate capacity was found to be 6540 kN which is very close to 6580 kN, the capacity of the original unbuckled specimen.

A finite element analysis was performed on a model which represented a locally buckled portion of a longer column as would exist in the field. The ultimate capacity was found to be 5625 kN which represents 85% of the ultimate capacity from the test on the original unbuckled specimen or on the reinforced test specimen. The lower value of the ultimate capacity obtained from the analysis may be due to a higher value of the actual yield stress for the specimen because of the cold rolling and welding during its fabrication and due to the discontinuous analytical model of the connection of the stiffener to the column wall. However, the deformation and stress patterns in the analytical model were consistent with those of the test specimen.

It was concluded from the test results that the design procedure for the stiffeners was simple and adequate and that the finite element program ADINA can be used for more accurate analysis.

It is recommended that the post-ultimate strength can be improved by welding an additional plate at the ends of the retrofitting stiffeners.

8. ACKNOWLEDGMENTS

Financial support by the Department of Civil Engineering for the modification of the specimen and for the test is gratefully acknowledged. Dr. Irwin J. Kugelman is Department Chairperson. Thanks are also given to the staff of Fritz Engineering Laboratory for their assistance in conducting the test.

- ADINA Engineering, Inc., *ADINA Users Manual*, 71 Elton Avenue, Watertown, MA 02172, USA, 1981.
- ADINA Engineering, Inc., *ADINA-IN Users Manual*, 71 Elton Avenue, Watertown, MA 02172, USA, 1981.
- American Institute of Steel Construction, *Specifications for the Design, Fabrication and Erection of Structural Steel for Buildings*, Chicago, 1978.
- Bathe, K.J. (Ed.), "Nonlinear Finite Element Analysis and ADINA," *Journal of Computers and Structures*, Vol. 13, No. 5-6, 1981, .
- Larson, J.W., "Effect of Pinholes and Stress Relieving on the Behavior of Short Tubular Columns," Fritz Engineering Laboratory Report No. 354.501, Lehigh University, May 1985, (CE481 Report supervised by A. Ostapenko)
- Ostapenko, A., and Grimm, D.F., "Local Buckling of Cylindrical Tubular Columns Made of A-36 Steel," Fritz Engineering Laboratory Report No. 450.7, Lehigh University, February 1980.
- Wagner, D.C., and Kuzio, K.S., "A Repair System for Locally Buckled Tubular Columns," Fritz Engineering Laboratory Report No. 354.502, Lehigh University, May 1985, (CE211 Report supervised by A. Ostapenko)
- Wagner, D.C., and Kuzio, K.S., "A Repair System for Locally Buckled Tubular Columns," *The Welding Innovation Quarterly*, Vol. 11, No. 4, Fall 1985, pp. 18-20, Best of Program Award 1985

TABLE 1: Description of Finite Element Models

		MODEL 1	MODEL 2	MODEL 3/4
Tube Wall	Elem.Type Plate No. of Elem's	Plate 56	Shell 84	28
Stiffener	Web Elem.Type No. of Elem's	2-D Pl.Stress 4	2-D Pl.Stress 4	2-D Pl.Stress 6
	Flange Elem.Type No. of Elem's	2-D Beam 4	2-D Beam 4	2-D Beam 6
Bracket	Elem.Type 2-D Pl.Stress No. of Elem's	2-D Pl.Stress 3	2-D Pl.Stress 3	5
Results of Analysis	Ultim. Load	4090 kN	4115 kN	4115 kN /5625 kN

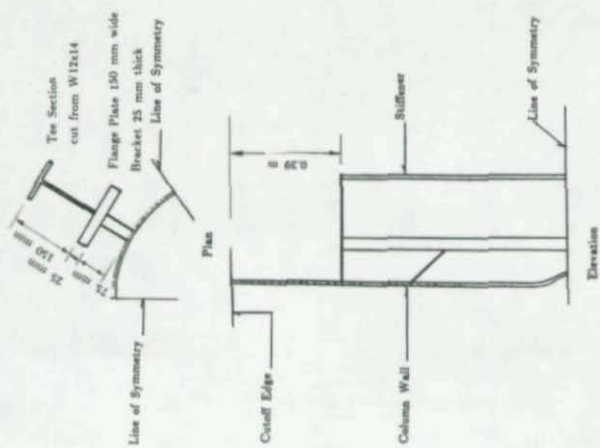
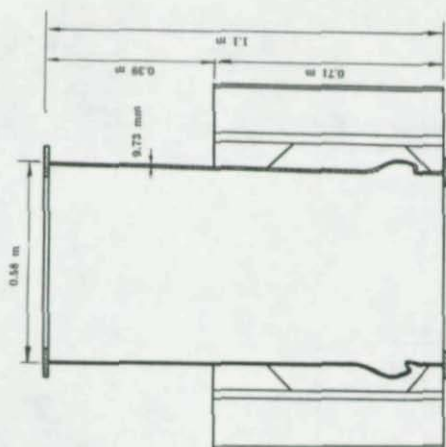


Fig. 2 Specimen Used in Analysis



For Cross Sectional dimensions of the stiffener see Fig. 2

Fig. 1 Existing Test Specimen

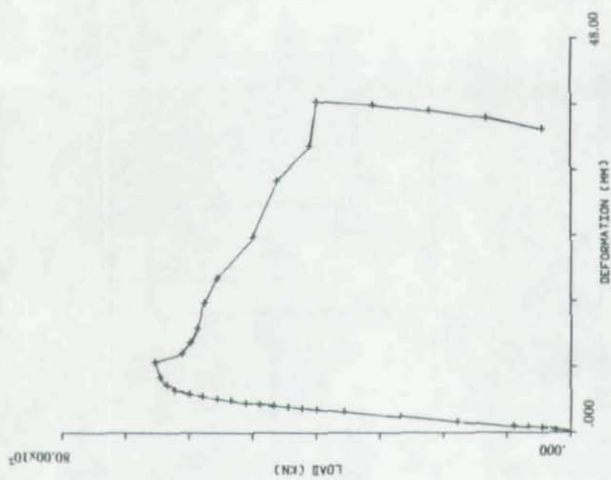


Fig.4 Load-vs-Overall Deformation (Test)

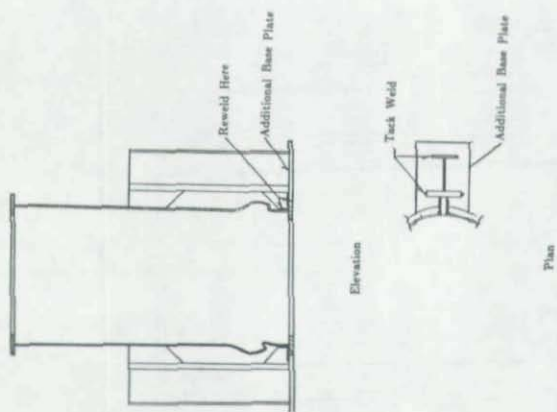


Fig.3 Modified Test Specimen

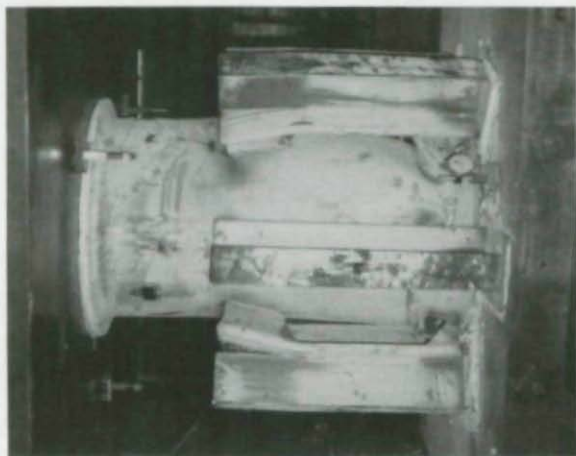


Fig.6 Specimen After Ultimate Load

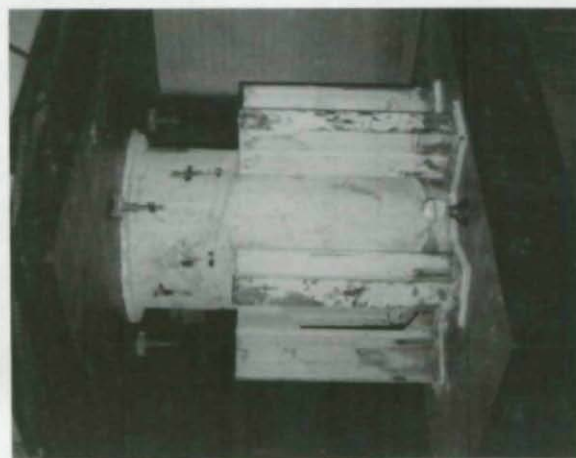


Fig.5 Specimen Before Loading

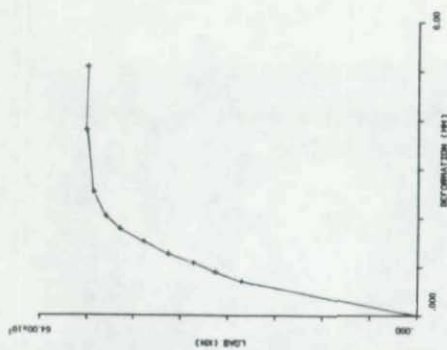


Fig. 9 Load-vs-Overall Deformation (Analysis)

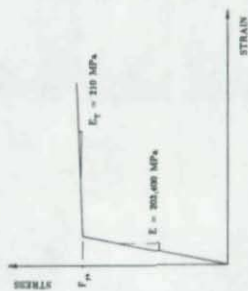


Fig. 8 Idealized Bi-Linear Relationship for Model Material

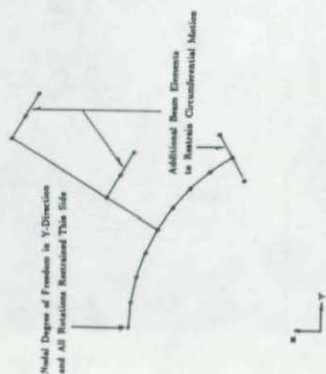


Fig. 7 Boundary Conditions

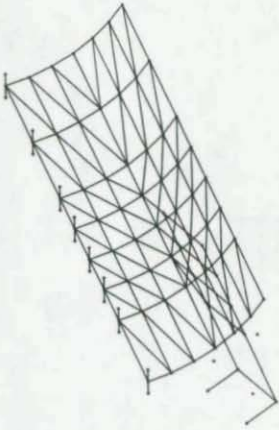


Fig.10 Mesh for Model 2

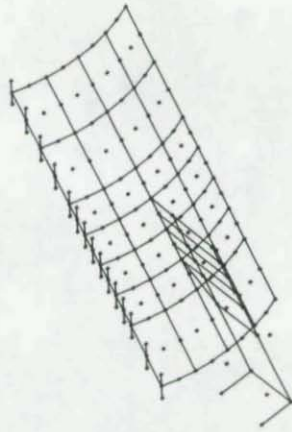


Fig.11 Mesh for Model 3

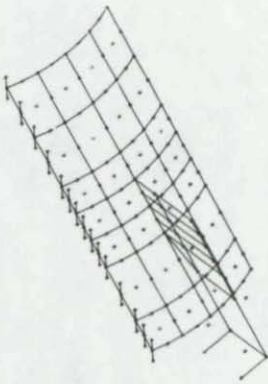
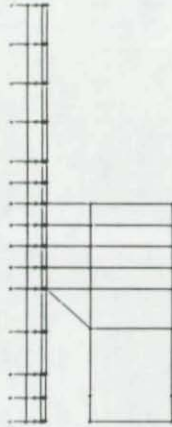


Fig.12 Mesh for Model 4

Fig.13 Mesh for Stiffener
of Model 4

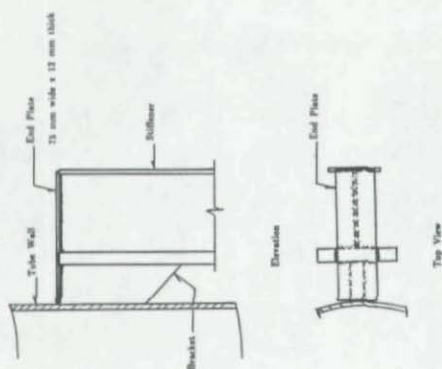
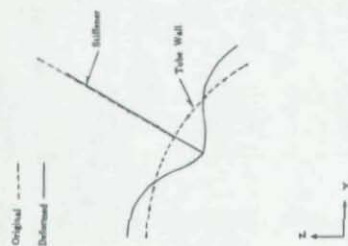
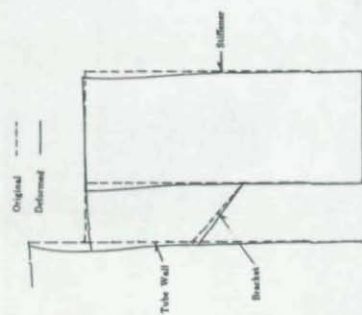


Fig. 16 Details of End Stiffener Plate

Fig. 15 Lateral Deflection of Tube Wall
at Top of Bracket (Ultimate Load)Fig. 14 Deformations in Stiffener
and Tube Wall at Ultimate Load

THE EFFECT OF ELASTIC SUPPORT AND SHEAR DEFORMATION

ON

STATIC AND DYNAMIC CHARACTERISTICS

Franklin Y. Cheng, Professor

C.P. Pantelides, Research Assistant

Civil Engineering Department

University of Missouri-Rolla

Rolla, MO 65401

INTRODUCTION

The theoretical analysis of the flexural vibration of beams was generally based on the Bernoulli-Euler theory with consideration of lateral inertia forces and bending deformations. Ever since Timoshenko pointed out that the effects of cross-sectional dimensions on the frequencies of beams could be significant (15), a considerable amount of research work based on Timoshenko's beam theory has been published. Early researchers studied the vibrations of Timoshenko beams with various boundary conditions (1,2,3,13). Later investigators employed the Timoshenko theory in developing numerical techniques for electronic computation such as consistent mass matrices and dynamic stiffness matrices by Archer (4) and Cheng (5), respectively. Cheng then extended his formulations for the frequency analysis of thin wall member grid systems (6), and for the response analysis of continuous beams and frames with various types of externally applied forces and foundation movements (7).

It has been well recognized that the axial force acting on a member can significantly affect the natural frequencies of that member. Djodjo studied the combined effects of axial loads and Timoshenko theory on the natural frequencies of beams (11). Howson and Williams investigated the combined effect based on both the analytical and experimental results (12). Cheng and his associates further extended his dynamic stiffness approach for plane frames of which the constituent members may have axial forces, transverse and rotatory inertia, and bending and shear deformations (7,8). He also studied the combined effects on the frequencies and responses of space structures based on the finite element approach (9).

The effects of elastic media on the flexural vibrations were examined by a number of researchers (11,14,18). Cheng employed the Bernoulli-Euler theory and the transfer matrix technique (17), to derive the dynamic stiffness and flexibility matrices for transverse and longitudinal vibrations (10).

This paper is an extension of Cheng's work of dynamic stiffness formulation to include elastic media of Winkler type, axial forces, lateral and rotatory inertia, and shear and bending deformations. Furthermore, the formulations presented herein consist of two new approaches as to how the shear component of the axial force is acting on a cross-section. In the first approach the shear component of the axial load is assumed to act perpendicular to the tangent line of the total slope which consists of the bending and shear slope; in the second approach the shear component of the axial load is acting perpendicular to the tangent line of the bending slope. The resulting stiffness coefficients and fixed-end forces are general and can be applied to large structural systems with the numerical procedures previously presented by the senior writer. In addition, the stiffness coefficients and the fixed-end force formulations are distinguished in the sense that the complex roots are not treated separately as solved previously in Cheng's work (5,8). These resulting formulations are expressed in terms of nondimensional parameters associated with the effects of lateral and rotatory inertia, axial force, elastic media, and shear and bending formations. When the individual effect is not considered then the associated parameter can be dropped. Numerical results are provided to show the significant effects of the individual parameters and that of the two approaches on natural frequencies, and dynamic response behavior.

BASIC DYNAMIC EQUATIONS

Consider the beam element shown in Fig. 1. The total slope $\partial y/\partial x$ is a combination of the bending slope, ψ and the shearing slope $\bar{\beta}$.

$$\frac{\partial y}{\partial x} = \psi + \bar{\beta} \dots\dots\dots(1)$$

The equilibrium equations for the free-body diagram shown in Fig. 1 yield

$$\frac{\partial V}{\partial x} = \rho A \frac{\partial^2 y}{\partial t^2} - w + qy \dots\dots\dots(2)$$

$$V = \frac{\partial M}{\partial x} - N \frac{\partial y}{\partial x} + \rho I \frac{\partial^2 \psi}{\partial t^2} \dots\dots\dots(3)$$

where $\rho = \bar{V}/g$, N = axial force, V = shear, M = bending moment, w = lateral load, q = foundation constant, A = cross-sectional area, g = acceleration of gravity, \bar{V} = weight per unit volume. From structural mechanics the bending moment, M of a Timoshenko-beam is

$$M = -EI \frac{d\psi}{dx} \dots\dots\dots(4)$$

in which E = modulus of elasticity and I = moment of inertia of cross-section.

Differential Equations Based on First Approach.—From Fig. 2 the shear component of the axial load N , on the cross-section is $N \sin(\frac{\partial y}{\partial x}) = N \frac{\partial y}{\partial x}$. Considering shear deformations

$$V + N \frac{\partial y}{\partial x} = \left(\frac{\partial y}{\partial x} - \psi \right) \phi \dots \dots \dots (5)$$

$$\phi = \frac{GA}{\lambda} \dots \dots \dots (6)$$

in which G = modulus of rigidity and λ = shear factor for cross-section.

By eliminating ψ and y from Eqs. 2-5, the following complete equations in y and ψ are obtained

$$EI \zeta \frac{\partial^4 y}{\partial x^4} + \rho(A + \frac{qI}{\phi}) \frac{\partial^2 y}{\partial t^2} + (N - \frac{EIq}{\phi}) \frac{\partial^2 y}{\partial x^2} - I\rho(\zeta + \frac{EA}{\phi}) \frac{\partial^2 y}{\partial x^2 \partial t^2} + \frac{\rho^2 IA}{\phi} \frac{\partial^4 y}{\partial t^4} + qy - \frac{I}{\phi} (\rho \frac{\partial^2 w}{\partial t^2} - E \frac{\partial^2 w}{\partial x^2}) - w = 0 \dots \dots \dots (7)$$

$$EI \zeta \frac{\partial^4 \psi}{\partial x^4} + \rho(A + \frac{qI}{\phi}) \frac{\partial^2 \psi}{\partial t^2} + (N - \frac{EIq}{\phi}) \frac{\partial^2 \psi}{\partial x^2} - I\rho(\zeta + \frac{EA}{\phi}) \frac{\partial^2 \psi}{\partial x^2 \partial t^2} + \frac{\rho^2 IA}{\phi} \frac{\partial^4 \psi}{\partial t^4} + q\psi \frac{\partial w}{\partial x} = 0 \dots \dots \dots (8)$$

where

$$\zeta = 1 - \frac{N}{\phi} \dots \dots \dots (9)$$

Differential Equations Based on Second Approach.—From Fig. 3 the shear component of the axial load N on the cross-section is $N\psi$, which can be expressed as

$$V + N\psi = \left(\frac{\partial y}{\partial x} - \psi \right) \phi \dots \dots \dots (10)$$

By eliminating ψ and y from Eqs. 2,3,4 and 10, the following differential equations in y and ψ are obtained

$$EI \frac{\partial^4 y}{\partial x^4} + \rho(Av + \frac{qI}{\phi}) \frac{\partial^2 y}{\partial t^2} + (Nv - \frac{EIq}{\phi}) \frac{\partial^2 y}{\partial x^2} - I\rho(1 + \frac{EA}{\phi}) \frac{\partial^2 y}{\partial x^2 \partial t^2} + \frac{\rho^2 IA}{\phi} \frac{\partial^4 y}{\partial t^4} + qvy - \frac{I}{\phi} (\rho \frac{\partial^2 w}{\partial t^2} - E \frac{\partial^2 w}{\partial x^2}) - wv = 0 \dots \dots \dots (11)$$

$$EI \frac{\partial^4 \psi}{\partial x^4} + \rho(Av + \frac{qI}{\phi}) \frac{\partial^2 \psi}{\partial t^2} + (Nv - \frac{EIq}{\phi}) \frac{\partial^2 \psi}{\partial x^2} - I\rho(1 + \frac{EA}{\phi}) \frac{\partial^2 \psi}{\partial x^2 \partial t^2} + \frac{\rho^2 IA}{\phi} \frac{\partial^4 \psi}{\partial t^4} + qv\psi - \frac{v\partial w}{\partial x} = 0 \dots \dots \dots (12)$$

in which

$$v = 1 + \frac{N}{\phi} \dots \dots \dots (13)$$

BASIC STATIC EQUATIONS

Differential Equations Based on First Approach.—Consider the beam element shown in Fig. 1, subject to a static axial load N and static lateral force w . As shown, the total slope, $\frac{dy}{dx}$, is a combination of the bending slope, ψ , and the shearing slope, $\bar{\delta}$,

$$\frac{dy}{dx} = \psi + \bar{\delta} \dots \dots \dots (14)$$

Because the time function is not considered, the slopes, shears, and moments sketched in Fig. 1 should now be expressed in total differential equation as shown in Eqs. 14, 15 and 16. The equilibrium conditions for the free-body diagram shown in Fig. 1 yield:

$$\frac{dV}{dx} = qy - w \dots\dots\dots(15)$$

$$\frac{dM}{dx} = V + N \frac{dy}{dx} \dots\dots\dots(16)$$

in which q = elastic media constant, V = shear, and M = bending moment. From structural mechanics

$$M = -EI \frac{d\psi}{dx} \dots\dots\dots(17)$$

The two approaches differ in terms of the assumed shear component of the axial load acting on the cross-section as shown in Figs. 2 and 3. In the first approach it is equal to $N \sin(\frac{dy}{dx}) = N \frac{dy}{dx}$; in the second approach it is equal to $N \sin \psi = N \psi$. For the first approach the force-deformation relationship of the shear may be expressed as

$$V + N \frac{dy}{dx} = (\frac{dy}{dx} - \psi) \frac{GA}{\lambda} \dots\dots\dots(18)$$

in which G = modulus of rigidity, A = area of cross-section, and λ = shear factor. From Eqs. 14-18, the following differential equations are derived

$$EI\zeta \frac{d^4y}{dx^4} + (N - \frac{EIq}{\phi}) \frac{d^2y}{dx^2} + qy + \frac{EI}{\phi} \frac{d^2w}{dx^2} - w = 0 \dots\dots\dots(19)$$

$$EI\zeta \frac{d^4\psi}{dx^4} + (N - \frac{EIq}{\phi}) \frac{d^2\psi}{dx^2} + q\psi - \frac{dw}{dx} = 0 \dots\dots\dots(20)$$

Differential Equations Based on Second Approach.—As shown in Fig. 3, the shear component of the axial load N acting on the cross-section is taken as $N\psi$ for which the force-deformation relationship is

$$V + N\psi = (\frac{dy}{dx} - \psi)\phi \dots\dots\dots(21)$$

Using Eqs. 15-17 and 21 yields the following differential equations

$$EI \frac{d^4y}{dx^4} + (N\psi - \frac{EIq}{\phi}) \frac{d^2y}{dx^2} + vqy + \frac{EI}{\phi} \frac{d^2w}{dx^2} - vw = 0 \dots\dots\dots(22)$$

$$EI \frac{d^4\psi}{dx^4} + (N\psi - \frac{EIq}{\phi}) \frac{d^2\psi}{dx^2} + vq\psi - v \frac{dw}{dx} = 0 \dots\dots\dots(23)$$

in which $v = 1 + N/\phi$.

SAMPLE STUDIES OF DYNAMIC CASE

Observation of the Frequencies based on the Two Approaches.—Presented herein is the effect of two approaches on the fundamental and higher frequencies of a typical simply supported beam. Using the first approach yields the following frequency equation

$$P1_n^2 = \frac{\phi}{2\rho I} \left\{ [n^2\pi^2(\zeta r^2 + s^2) + 1 + \frac{QL^2r^2}{\phi}] \right. \\ \left. - \sqrt{[n^2\pi^2(\zeta r^2 + s^2) + 1 + \frac{QL^2r^2}{\phi}]^2 - 4[n^2\pi^2s^2(\zeta n^2\pi^2 - \frac{N}{s^2\phi}) + \frac{QL^2r^2}{\phi}(n^2\pi^2s^2 + 1)]} \right\} \quad (24)$$

where n = mode number, $r^2 = I/(AL^2)$ (associated with rotatory inertia), and $s^2 = EI/(\phi L^2)$ (associated with shear deformations). When the shear deformations and rotatory inertia effects are ignored

$$PE_n^2 = \frac{1}{L^2} \left[n^4\pi^4 \left(\frac{EI}{L^2\rho A} - \frac{N}{n^2\pi^2\rho A} \right) + \frac{QI^2}{\rho A} \right] \quad \dots\dots\dots (25)$$

For the second approach, the frequency equation may be expressed as

$$P2_n^2 = \frac{\phi}{2\rho I} \left\{ [n^2\pi^2(r^2 + s^2) + \nu + \frac{QL^2r^2}{\phi}] \right. \\ \left. - \sqrt{[(n^2\pi^2(r^2 + s^2) + \nu) + \frac{QL^2r^2}{\phi}]^2 - 4[n^2\pi^2s^2r^2(n^2\pi^2 - \frac{N\nu}{s^2\phi}) + \frac{QL^2r^2}{\phi}(N^2\pi^2s^2 + \nu)]} \right\} \quad (26)$$

When the shear deformations and rotatory inertia are neglected, Eqs. 26 becomes identical to Eq. 25.

Using the parameters of $\mu = 0.25$ (Poisson's ratio), $\lambda = 1.5$, $\rho = 7829 \text{ kgm}^{-3}$, and $E = 212.95 \text{ kNm}^{-2}$, a plot of $P1/PE$ and $P2/PE$ versus N/NE is given in Fig. 4, for $q/q_e = 0$, and two slenderness ratios, $L/R = 40$ and $L/R = 20$. $P1$, PE and $P2$ are the natural frequencies of the first five modes from Eqs. 24, 25 and 26 respectively. NE is the fundamental Euler buckling load ($\pi^2 EI/L^2$). It may be observed that the Timoshenko theory has significant effect on a smaller L/R and a higher frequency and that the differences between $P1/PE$ and $P2/PE$ become significant for higher modes and for larger axial loads.

The ratios of $P1$ and $P2$ are given in Fig. 5 for the first five modes associated with $q/q_e = 0$. The figure shows that the first approach yields lower frequency than the second; the difference becomes more pronounced for higher axial loads and lower slenderness ratios.

SAMPLE STUDIES OF STATIC CASE

Parametric Studies of a Typical Beam-Column.—For a simply-supported beam-column on elastic media, one obtains the critical load N_{cr} associated with the first approach

$$N_{cr} = \frac{NE}{(1 + \frac{NE}{\phi k^2})} \left[k^2 + \frac{QL^2}{\pi^2} \left(\frac{1}{\phi} + \frac{1}{k^2 NE} \right) \right], \quad k = 1, 2, 3, \dots \quad (27)$$

where k is an integer corresponding to the number of buckling mode and NE is the Euler buckling load for a simply-supported column, ($NE = \frac{\pi^2 EI}{L^2}$).

Similarly, one may obtain the buckling load associated with the second approach as

$$N_{cr} = \frac{-[1 - \frac{QL^2}{k^2\pi^2\phi}] + [(1 - \frac{QL^2}{k^2\pi^2\phi})^2 + \frac{4}{\phi} (\frac{QEI}{4} + NEk^2 + \frac{QL^2}{k^2\pi^2})]^{1/2}}{2/\phi} \quad \dots\dots\dots (28)$$

When shear deformations are not included, $\lambda = 0$, then $1/\phi = 0$; Eqs. 27 and 28 yield the buckling load with bending deformations and elastic

media only. If no elastic media is present, $q = 0$, then Eqs. 27 and 28 become the buckling load expressions with both bending and shear deformations. It is worthwhile of noting that when the shear deformations are neglected, Eqs. 27 and 28 should be identical which can be obtained as follows:

$$N_{cr} = NE \left(k^2 + \frac{qL^2}{k^2 \pi^2 NE} \right) \dots \dots \dots (29)$$

A plot of Eqs. 27 and 29 is shown in Fig. 6, for comparison of the critical load with and without shear deformations. The critical load is expressed as a function of the elastic media constant, q , for a slenderness ratio, $L/R = 20$, and for the first three buckling modes ($k = 1, 2, 3$). The numerical data used for this figure are: $E = 29000 \text{ ksi}$ ($200 \times 10^6 \text{ kN/m}^2$), $A = 20 \text{ in}^2$ ($.012903 \text{ m}^2$), $I = 724 \text{ in}^4$ ($3.01315 \times 10^{-4} \text{ m}^4$), $\mu = 0.25$, $\lambda = 1.5$; where A = area of cross-section, I = moment of inertia of section and μ = Poisson's ratio. It is observed from Fig. 6 that the inclusion of shear deformations yields less buckling load, than that when it is ignored.

Figure 7 shows a plot for $L/R = 40$, with the same numerical data as given for Fig. 6. Comparing these two figures reveals that shear deformation effects are more important at low slenderness ratios. We may also note from Fig. 7 that second-mode buckling governs, for $q \geq 2.18 \text{ ksi}$ when shear deformations are included (point A), and $q \geq 2.44 \text{ ksi}$ if shear deformations are ignored (point B). The value of q for which a transition occurs from one buckling mode to another (points A and B in Fig. 6), can be obtained from Eq. 30 which is derived from Eq. 27

$$q_t = \left(\frac{\pi^2 EI}{L^4} \right) \left[\frac{k^2 (k+1)^2}{Z [2k^2 (k+1)^2 + (k+1)^2 + k^2] + 1} \right] \dots \dots \dots (30)$$

$$\text{in which } Z = \frac{NE}{\phi} = \frac{2\pi^2 n(1+\mu)}{(L/R)^2}$$

Figure 8, is a plot of the first three buckling mode shapes ($k = 1, 2, 3$) for $L/R = 60$ and 80 . It may be observed that the higher the slenderness ratio, the less the value of q_t at which a buckling mode changes.

Equation 30 can be used to determine the buckling load and its associated mode when q and the properties of the beam are known. The buckling mode-shape k , can be obtained first by solving Eq. 30, and then the buckling load N_{cr} can be obtained from Eq. 27. Numerical examples demonstrate these procedures as follows:

a. Using $L = 16 \text{ ft}$ (4.8768 m), $q = 5 \text{ ksi}$ (34474 kN/m^2), $E = 29000 \text{ ksi}$ ($200 \times 10^6 \text{ kN/m}^2$), $A = 32.9 \text{ in}^2$ (0.02123 m^2), $I = 719 \text{ in}^4$ ($0.29927 \times 10^{-4} \text{ m}^4$), $\nu = 0.25$, and $\lambda = 1.5$ we have $NE = 5582 \text{ kips}$ (24832 kN), $\phi = 254427 \text{ kips}$ ($1.13174 \times 10^6 \text{ kN}$). From Eq. 30, $k = 0.975$. Hence the first buckling mode will occur. Let $k = 1$, then Eq. 27 yields $N_{cr} = 24138 \text{ kips}$ (107371 kN). Similarly for the second approach Eq. 28 yields $N_{cr} = 24148 \text{ kips}$ (107415 kN).

b. Using $L = 32 \text{ ft}$ (9.7536 m), $q = 3 \text{ ksi}$ (20684 kN/m^2) and other information given above, we have $Ne = 1396 \text{ kips}$ (6208 kN) and $\phi = 254427 \text{ kips}$ ($1.13174 \times 10^6 \text{ kN}$). From Eq. 30 $k = 1.974$. Hence the second

buckling mode will occur. Let $k = 2$, from Eq. 27 we obtain $N_{cr} = 16669$ kips (74147 kN) for the first approach and from Eq. 28 $N_{cr} = 16677$ kips (74183 kN) for the second approach. It is seen that both approaches give similar answers. However they differ for low slenderness ratios as can be seen from Fig. 6 for $L/R = 20$. From Figs. 6, 7 and 8 we note that higher orders of buckling modes are possible for beam-columns with larger slenderness ratios.

OBSERVATION REMARKS

Comparison of the two approaches shows that the second approach gives higher natural frequency values and the difference increases with increasing axial load and decreasing slenderness ratio. Furthermore the two approaches result in different values for static stiffness coefficients. The effect of the elastic media (q-parameter) on the natural frequencies shows that q-values affect the fundamental frequency more than they affect the higher frequencies. The elastic media causes the frequencies to be increased. The effect of shear deformations and rotatory inertia becomes significant at higher modes.

The order of the buckling mode is affected by the magnitude of the elastic media. Depending on the beam-column properties, and the value of the elastic media constant, buckling may occur in a higher mode than the first. For given properties of the beam-column, the value of the elastic media constant, for which a transition from one buckling mode to a higher mode occurs, was derived. It was observed that the higher the slenderness ratio, the less the value of the elastic media at the transition point.

The two approaches yield different critical axial load for low slenderness ratios. When shear deformation is considered the critical axial load is reduced for both approaches, especially for beam-columns with low slenderness ratios.

ACKNOWLEDGMENTS

This work was partially supported by the University of Missouri-Rolla and the National Science Foundation.

APPENDIX I REFERENCES

1. Aalami, B. and Atzori, B., "Flexural Vibrations and Timoshenko's Beam Theory," AIAA Journal, 12, 1974, pp 679-685.
2. Abbas, B.A.H., "Vibrations of Timoshenko Beams with Elastically Restrained Ends," J. Sound and Vibration, 97, 1984, pp 541-548.
3. Anderson, R.A., "Flexural Vibrations in Uniform Beams According to the Timoshenko Theory," Transactions ASME, 75, 1953, pp 504-510.
4. Archer, J.S., "Consistent Mass Matrix for Distributed Mass Systems," J. Str. Div., ASCE, 89, 1963, pp 161-178.

5. Cheng, F.Y., "Vibration of Timoshenko Beams and Frameworks," J. Str. Div., ASCE, 3, 1970, pp 551-571.
6. Cheng, F.Y., "Dynamics of Prismatic and Thin-Walled Member Grids," Proc. of Application of Finite Element Methods in Civil Engineering, ASCE, 1969, pp 339-373.
7. Cheng, F.Y., Tseng, W.H., and Botkin, M.E., "Matrix Calculations of Structural Dynamic Characteristics and Response," International Proc. on Earthquake Analysis of Structures, 1970, Jassy, Romania, Vol. 1, pp 85-101.
8. Cheng, F.Y., and Tseng, W.H., "Dynamic Matrix of Timoshenko Beam Columns," J. Str. Div., ASCE, Vol. 99, ST3, 1973, pp 527-549.
9. Cheng, F.Y., "Dynamic Response of Nonlinear Space Frames by Finite Element Methods," Proc. Intern. Assn. for Shell Structures, Japan, paper 9-5; 1972, pp 817-826.
10. Cheng, F.Y., "Dynamic Matrices of Beams of Elastic Foundation," Proc. Inter. Symposium on Soil Structure Interaction, India, Vol. I, pp 203-208.
11. Djodjo, B.A., "Transfer Matrices for Beams Loaded Axially and Laid on an Elastic Foundation," Aeronaut. Quarterly, 20, 1969, pp 281-306.
12. Howson, W.P., and Williams, F.W., "Natural Frequencies of Frames with Axially Loaded Timoshenko Members," J. Sound and Vibration, 26, 1973, pp 503-515.
13. Huang, T.C., "The Effect of Rotatory Inertia and of Shear Deformation on the Frequency and Normal Mode Equations of Uniform Beams with Simple End Conditions," J. Applied Mechanics, 28, 1961, pp 579-584.
14. Lunden, R., and Akesson, B., "Damped Second-Order Rayleigh-Timoshenko Beam Vibration in Space - An Exact Complex Dynamic Member Stiffness Matrix," Intern. J. Numerical Methods in Engineering, 19, 1983, pp 431-499.
15. Timoshenko, S.P., "On the Correction for Shear of the Differential Equation for Transverse Vibrations of Prismatic Bars," Philosophical Magazine, Series 6, 41, 1921, pp 744-746.
16. Timoshenko, S.P., Young, D.H., and Weaver Jr., W., "Vibration Problems in Engineering," John Wiley and Sons, Fourth Edition, 1974.
17. Tuma, J.J., Cheng, F.Y., "Dynamic Structural Analysis," McGraw-Hill Book Company, 1973.
18. Wang, T.M., Stephens, J.E., "Natural Frequencies of Timoshenko Beams on Pasternak Foundations," J. Sound and Vibration, 51, 1977, pp 149-155.

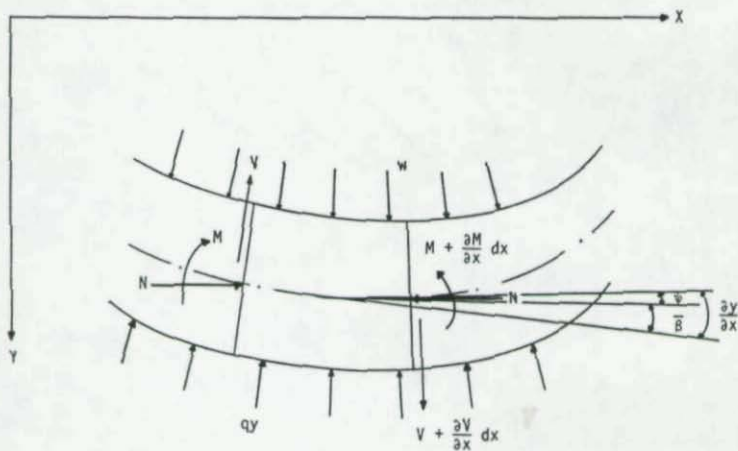


Fig. 1 -- Beam Element

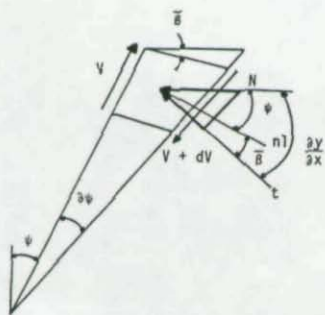


Fig. 2 -- Shear Component of Axial Load for First Approach

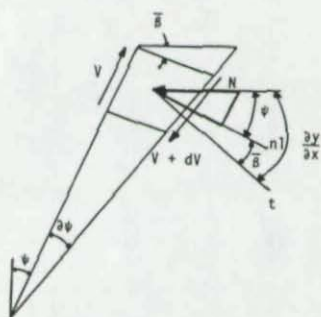


Fig. 3 -- Shear Component of Axial Load for Second Approach

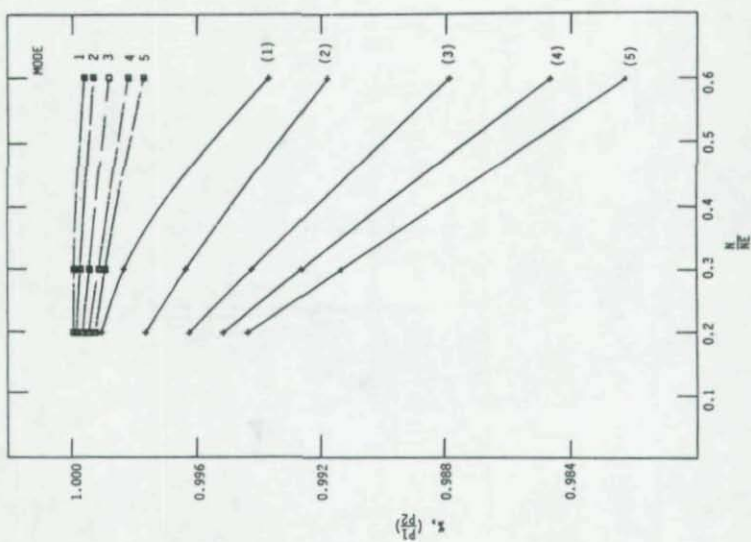


Fig. 5 -- Comparison of First and Second Approach Frequencies

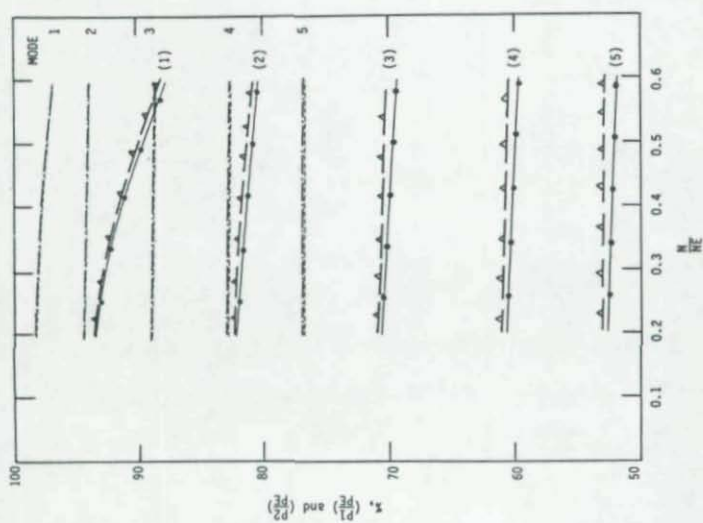


Fig. 4 -- Natural Frequencies Using First and Second Approach

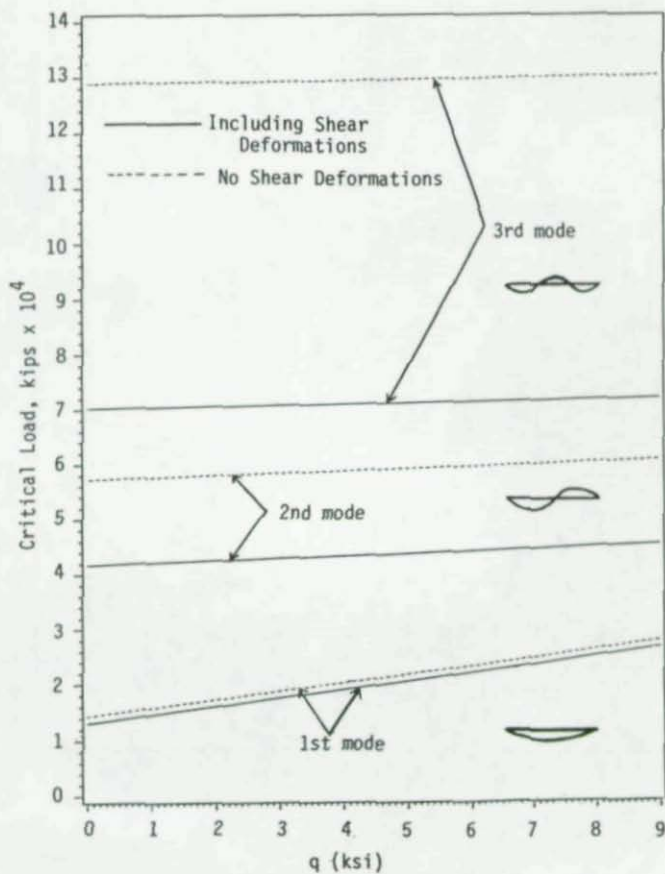


Fig. 6 -- Comparison of Critical Loads for $L/R = 20$

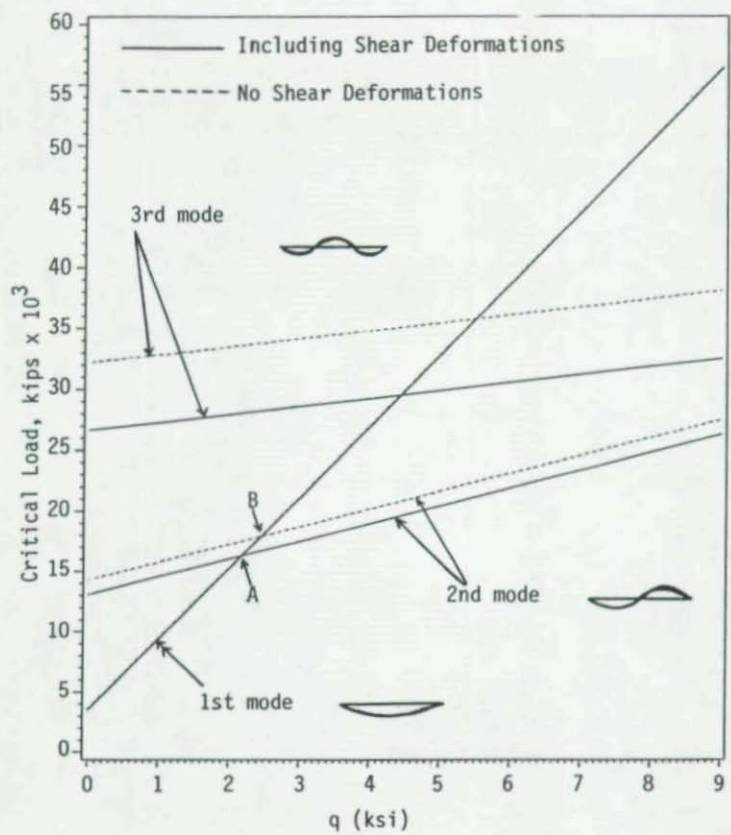


Fig. 7 -- Comparison of Critical Loads for $L/R = 40$

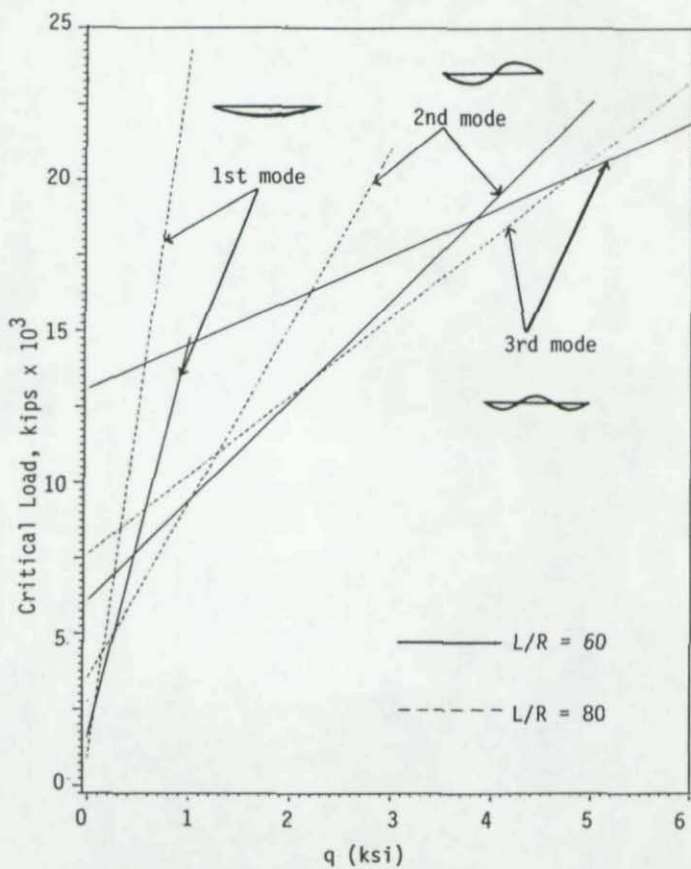
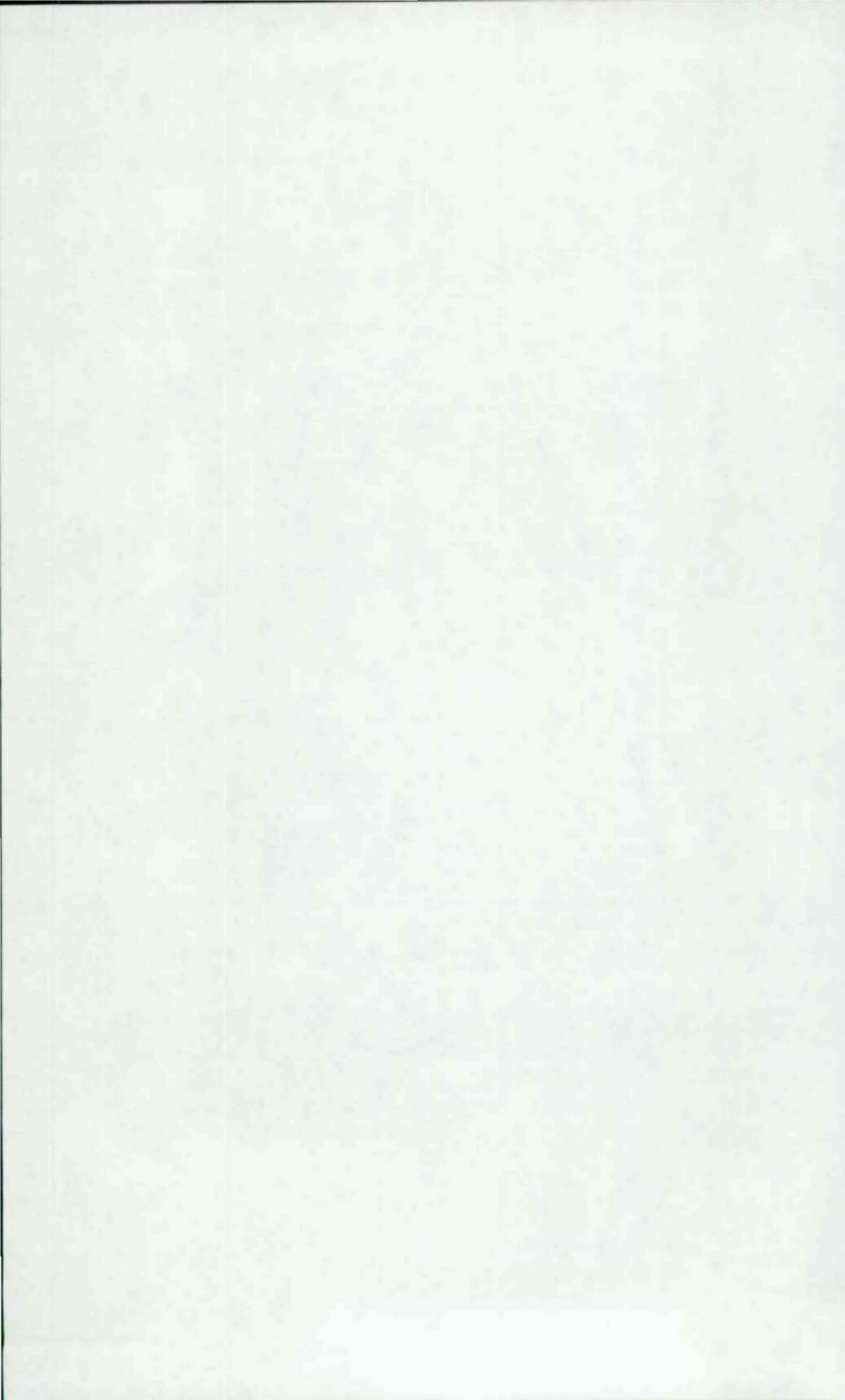


Fig. 8 -- Comparison of Critical Loads for $L/R = 60$ and $L/R = 80$



STUDY ON A STRUCTURAL STEEL FRAMEWORK DAMAGED
BY THE 1985 MEXICO EARTHQUAKE

Takao YAMADA, Kengo TAGAWA and Yuji NAKAMURA

Civil Eng. and Construction Dept., Nippon Kokan K.K.
2-1. Chome, Suehiro-cho, Tsurumi-ku, Yokohama, Japan

Koichi TAKANASHI

Institute of Industrial Science, University of Tokyo
7-22-1 Roppongi, Minato-ku, Tokyo, Japan

1. Introduction

The 19 September 1985 Mexico earthquake left many buildings in Mexico City that suffered various degrees of damage.

NKK participated in the construction of a steelmaking shop in Lazaro city near the epicenter and the structural steel framework of this shop was near completion.

This shop was not damaged as much as anticipated. However, anchor bolts and lateral bracing members were partially damaged.(9, 10)

The object of this paper is to present the elastic-plastic frame analysis method, applied to a computer program, and compare the computed results with observed damage, then study the reason why the damage was slight.

2. Response characteristics of observed earthquake

In the epicentral region, there was a network of strong motion observation instruments by National Autonomous University of Mexico (UNAM) and California State University(Fig. 1)(1).

A strong motion instrument set on bedrock at Villita near the site recorded earthquake acceleration as shown in Fig. 4.

The amplitude of the observed acceleration response spectra is shown in Fig. 8. The predominant period is 0.5 - 0.6 sec.

3. Building structure and outlines of damage

This building was designed according to the aseismatic design standards which provided that aseismatic design force coefficient distributes in inverted triangular shape of which the base shear coefficient is 0.2 in elastic design. Fig. 2 shows the building plan and damage of anchor bolts and bracing members.

In the transverse direction, which coincides with NS direction, the building is one-story with a three-span gabled roof frame having overhead cranes(Fig. 3). The lower part of the columns are lattice built-

up members and the upper part of the columns and beams are full web members. The bracing members are installed under a working deck.

Sectional moment of inertia of the upper part of the column is less than 10 percent of that value of the lower part, therefore input earthquake force of certain grid line frame can't be expected to distribute to another one, even assuming that plane rigidity of the roof is infinite.

Yield of anchor bolts, buckling of bracing members and breakages of clumping metals of crane rails were remarkably found in the transverse direction. Damage of end gables was slightly larger than that of inner grid line frames. (Figs. 26, 27)

In the longitudinal direction, the building has a braced frame structure, the columns are full web and the beams are built-up members. In this direction damage was negligible.

4. Simulated input acceleration for analysis

The site soil consists of sand and the model of the boring log is shown in Fig. 5. Shearing modulus is taken from Fig. 6, corresponding to N-value, assuming that the damping ratio is 5 percent. (2)

Site ground surface response was computed by means of inputting the observed Villita acceleration into bearing stratum layered 23 meters under the ground level, assuming that acceleration of bearing stratum is equal to the value of bedrock of Villita.

Simulated ground surface acceleration is shown in Fig. 7 and its acceleration response spectra in Fig. 9.

There are two peaks in the response spectra: the first predominant period is 1.1 - 1.4 sec, and the second period is 0.5 - 0.7 sec.

5. Elastic-plastic frame analysis method

(1) Beam-column element

Plastic stress and strain increments are derived mathematically from the plastic potential flow theory, assuming that relation between generalized stress and strain is perfectly plastic, and yield function expressed by generalized stress also represents the plastic potential. (3)

If the process of loading is continued after the yield point has been reached, a material work-hardens and the initial yield surface will change its form depending on the increasing plastic deformation. (3).

In order to describe work-hardening mathematically, two theoretical hypotheses are presented. One is isotropic work-hardening which presents the situation when the yield surface expands uniformly and retains its initial shape. (Fig. 10). The other is kinematic work-hardening which assumes that the yield surface undergoes a translation, like a rigid body without changing its initial form (Fig. 11).

Here Q is the generalized stress, $\bar{\alpha}$ denotes the translations of the center of the yield surface, and eX represents the plastic work done in the deformation process. ($0 \leq e \leq 1$).

W. Prager has proposed the following hypothesis:

$$d\bar{\alpha} = \bar{H} dg^P$$

where

$$d\bar{\alpha} = \text{increment of } \bar{\alpha}$$

$$dg^P = \text{increment of plastic strain } g^P$$

$$\bar{H} = \text{positive constant of kinematic work-hardening}$$

The strain increment vector lies in the exterior normal of the yield surface at the stress point. (Fig. 12)

Y. Ueda applied the plastic flow rule to the plastic hinge method and derived the elastic-plastic stiffness matrix of beam-column element(4). M. Hanai applied a kinematic work-hardening rule(5), then the authors added both isotropic and kinematic work-hardening rules to the stiffness matrix presented by Y. Ueda.(6)

In this study, yield function Φ for structural sections of beam-column elements subjected to thrust and bi-axial bending moments having a trapezoid section about the thrust load axis, is shown in Fig. 13, where

N = actual thrust load

N_p = full plastic thrust load

M_y, M_z = actual bending moment about y, z member axis

M_{py}, M_{pz} = full plastic bending moment about y, z member axis

β = parameter defines the yield surface form

(2) Bracing systems

The authors presented the numerical analysis methods of bracing systems subjected to repeated thrust loading by applying the open form stiffness to the plastic hinge method.(7)

In this analytical model, the brace is assumed to remain linear, whenever loaded in thrust, except for a central plastic hinge location.

Kinematic hardening and isotropic hardening rules are applied to the plastic hinge, and the plastic deformation is decided by the plastic potential theory, using the appropriate yield function Φ for the member section as shown in Fig. 14.

Fig. 15 shows the relation between thrust load N and displacement x of bracing systems subjected to alternating thrust load under constant displacement amplitude.

Fig. 16 shows the stress hysteresis process between thrust load N and bending moment M acting at plastic hinge. Numerals written in Fig. 15 and Fig. 16 represent the stress state of plastic hinge and correspond to each other. Each stress state is described as follows.

(i) STATE-0

Member is perfectly straight and performs elastic behavior.

(ii) STATE-1

Member buckles at the critical load, then plastic hinge is formed.

In this study, the author used the critical load proposed by Architectural Institute of Japan as shown in Fig. 17, where $\bar{\lambda}$ is a nondimensional slenderness ratio.(8)

(iii) STATE-2

Member is continuing plastic flow at plastic hinge under the condition of unloading compression force.

(iv) STATE-3, 3'

Member performs elastically under the condition that plastic hinge rotation is locked.

(v) STATE-4

Member performs similarly to STATE-2, except for yield function, direction of thrust load and plastic hinge rotation.

(vi) STATE-5

Member stress is pure tension and located at the corner point of yield function.

(3) Anchor Bolt

Bond stress between anchor bolt and concrete was originally eliminated by grease in construction. Restoring force-displacement characteristics of anchor bolt was modeled as a bi-linear tension yielding type. The yield strength N_p is calculated from the reduced effective sectional area.

6. Non-linear dynamic response analysis

We selected the 22th grid line frame as the typical frame in the transverse direction and replaced it with a lumped mass model presented in Fig. 18. To evaluate the effect of traveling crane girders, appropriate stiffness tie beams are installed within crane span AB and CD. In this case, crane loading is assumed to be empty.

Results of the eigenvalue are shown in Fig. 18. The first natural period is 1.28 sec. and the second is 0.62 sec. These periods eventually coincide with predominant periods of ground response spectra shown in Fig. 9.

In this analysis, \bar{H}/H and β are assumed to be 0.9 and 0.4, where H is sum of the isotropic and kinematic work-hardening coefficient and taken to be 1 percent of elastic stiffness (Fig. 12).

The input acceleration used in non-linear response analysis is a part of the simulated acceleration records and its duration time is 10 seconds. (Fig. 21).

Fig. 19 and Fig. 20 show the maximum absolute response accelerations and the maximum response displacements in horizontal direction, respectively. Values shown in parentheses are those of the structure of which the members are elastic and column bases are clumped perfectly. Compared with the perfect elastic response, non-linear response decreases to 30-40 percent in acceleration and 60-80 percent in displacement.

Figs. 23, 24 and 25 show the time history of the axial force ratio and the axial force-ductility ratio hysteresis of anchor bolts and bracing members respectively in (a) and (b).

Fig. 26 shows the bracing member of which the details are shown in Fig. 28, buckled about the weak axis out of the structural plane.

The N-M hysteresis at the plastic hinge of member B1 is shown in Fig. 29.

The maximum ductility ratio of members, computed from response analysis, is shown in Fig. 30. Ductility ratio of beam-column elements was less than 2.0, therefore this influence is negligible.

7. Comparison between analytical results and observed damage

Analytically computed ductility ratio μ_a of the anchor bolts at the intersection of the grid lines 22th and A was 4.62 - 6.77. (Fig. 30). Measured plastic elongation $\delta_p = 5\text{mm}$ (Fig. 2) and bolt length $l_b = 1110\text{mm}$, therefore the plastic strain $\epsilon_p = \delta_p/l_b = 0.0045$. Yield point $\sigma_y = 2.4 \text{ t/cm}^2$ and Young's modulus $E = 2100 \text{ t/cm}^2$, thus the yield strain $\epsilon_y = \sigma_y/E = 0.0011$. Therefore, observed ductility ratio μ_o becomes $\mu_o = 1 + \epsilon_p/\epsilon_y = 5.1$. As a result, ductility ratio of anchor bolts μ_a and μ_o coincide fairly well.

The bracing members buckled about the weak axis out of the structural plane, however plastic elongation was not measured in this damage investigation.

Notable damage of beam-column members was not observed.

8. Conclusion

The authors presented the elastic-plastic frame analysis method applied to a computer program and compared the computed results with the observed damage. The following conclusions can be derived.

- 1) Elastic-plastic analysis using our proposed numerical methods can simulate observed damage fairly well.
- 2) Compared with the perfect elastic response, the non-linear response decreases to 30-40 percent in acceleration and 60-80 percent in displacement.
- 3) In other words, seismic force decreases if the members possess enough plastic deformation capacity.
- 4) On the whole, damage is slight and negligible on repair.

9. Acknowledgement

We appreciate Prof. J. Prince et al of UNAM who supplied the observed accelerogram data. The authors wish to thank the many individuals who offered us information while preparing this report.

10. References

1. J. G. Anderson, J. Prince et al; Preliminary presentation of accelerogram data from the Guerrero Strong Motion Accelerograph Array. Preliminary Report GAA - 1A, October 10, 1985.
2. K. Ishihara; Basis of soil dynamics, Kajima Press.
3. W. Olszak, Z. Mróz, P. Perzyna; Recent Trends in the Development of the Theory of Plasticity. Pergamon Press.
4. Y. Ueda et al; Elastic-plastic frame analysis by matrix structural method. Trans. Society of Naval Architects of Japan, 124, pp.187 - 197, 1968., 126, pp.37-46, 1969
5. M. Hanai et al; Elastic-plastic analysis of steel structure subjected to repeated cyclic loadings. Trans. Architectural Institute of Japan, 214, pp.29-33, 1973.
6. T. Yamada, K. Takanashi and H. Tanaka; Experiments of miniature spherical tank substructures and elastic-plastic analysis. Proc. 29th Jour. Struct. Eng, pp.221 - 232, 1983
7. T. Yamada, K. Takanashi; Elastic-plastic analysis of bracing systems by plastic hinge method. Proc. 28th Jour. Struct. Eng, pp.153-164, 1982.
8. Architectural Institute of Japan; Plastic design standard for steel structures. 1975.
9. K. Tagawa et al; Reports Concerning Damages on Steel Structures Caused by the MEXICO Earthquake of 1985. Society of Steel Construction of Japan, Vol. 22, No. 237. 1986.7
10. T. Yamada, K. Kurabe, K. Tagawa; Study on a Structural steel framework suffered from the 1985 Mexico earthquake (Part 1, 2). Summaries of Technical Papers of Annual Meeting, Architectural Institute of Japan, 1986. C. Structures II. pp.1039-1042



Fig.1 Network of Strong Motion Observation Instruments

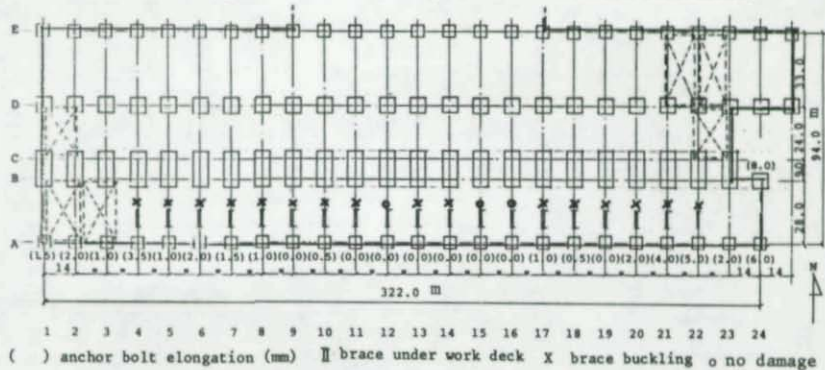


Fig.2 Building Plan and Outlines of Damage

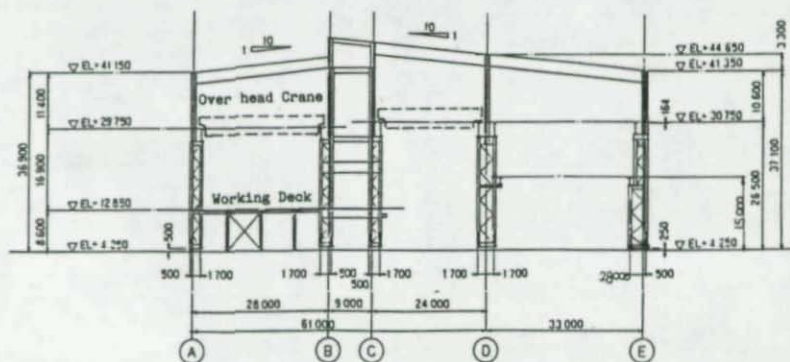


Fig.3 Structure in Transverse Direction

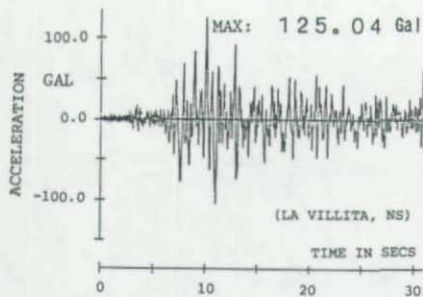


Fig. 4 Observed Acceleration

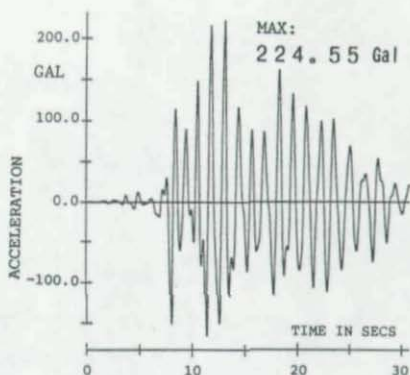


Fig. 7 Simulated Acceleration

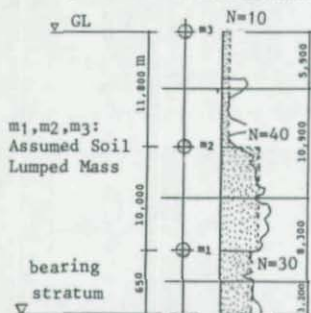


Fig. 5 Site Boring Log Model

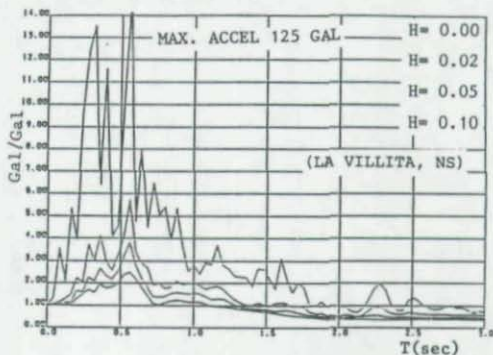


Fig. 8 Response Spectra of Observed Acceleration

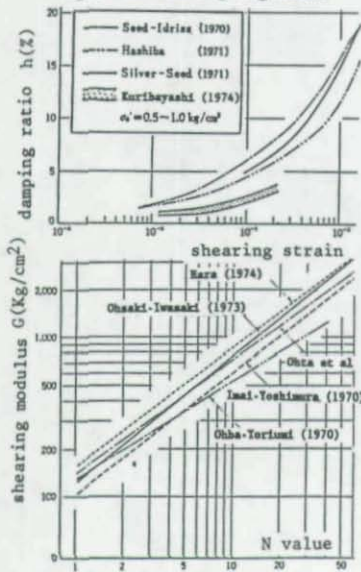


Fig. 6 Shearing-Model of Soil(2)

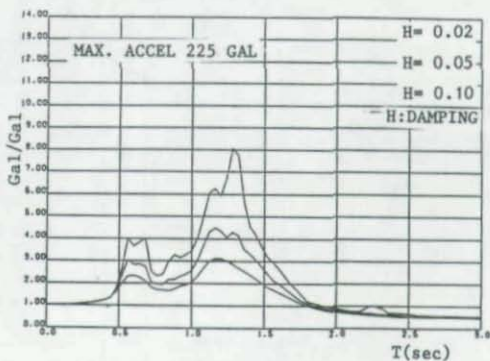


Fig. 9 Response Spectra of Simulated Acceleration

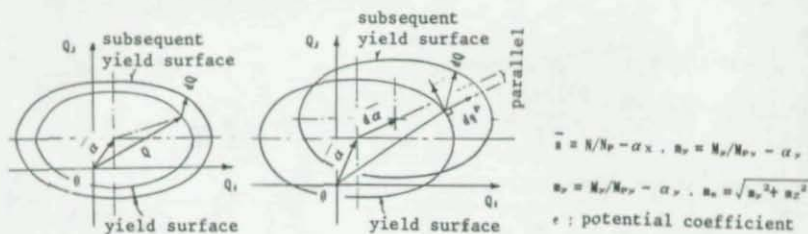


Fig.10 Isotropic Hardening Fig.11 Kinematic Hardening

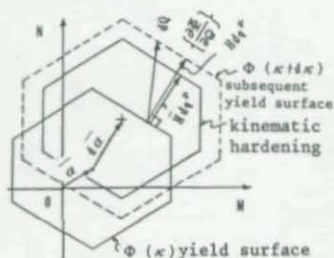


Fig.12 Strain Increment

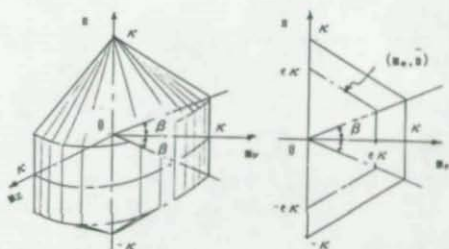


Fig.13 Yield Surface of Beam-Column Element

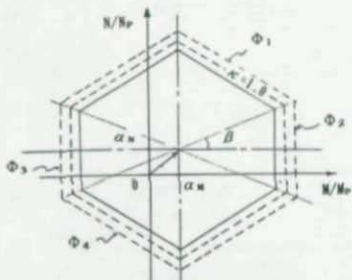


Fig.14 Yield Function of Bracing System

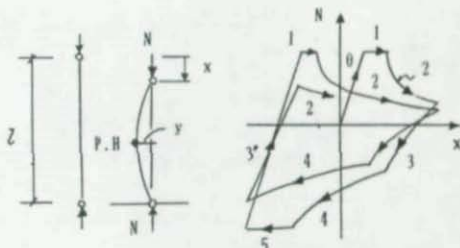


Fig.15 Restoring Force of Bracing System

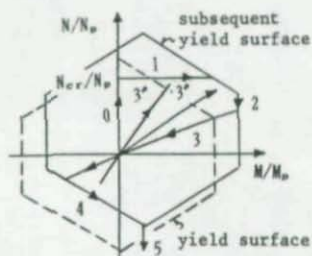


Fig.16 Stress Hysteresis of Plastic Hinge

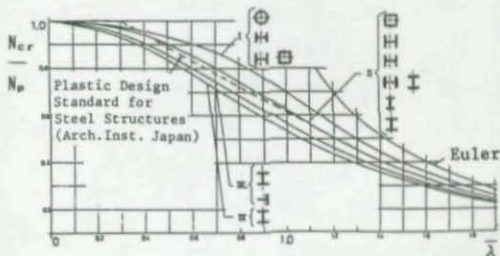


Fig.17 Critical Load of Simply Supported Column

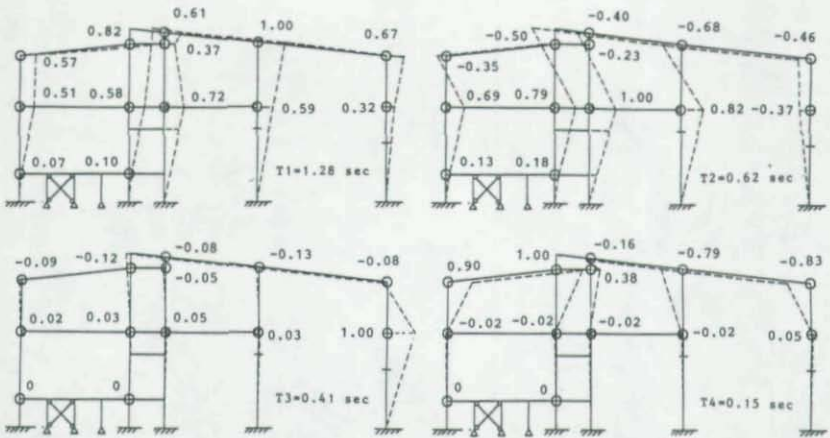


Fig.18 Results of Eigenvalue

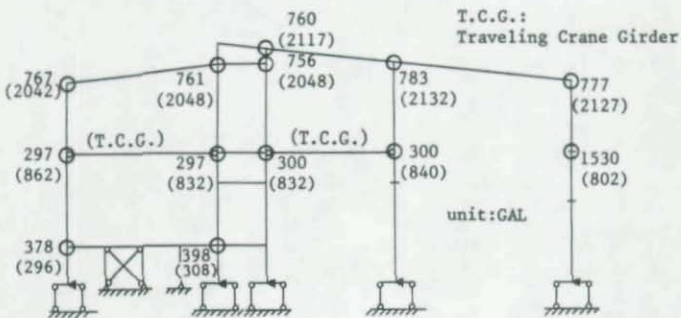


Fig.19 Maximum Absolute Response Acceleration

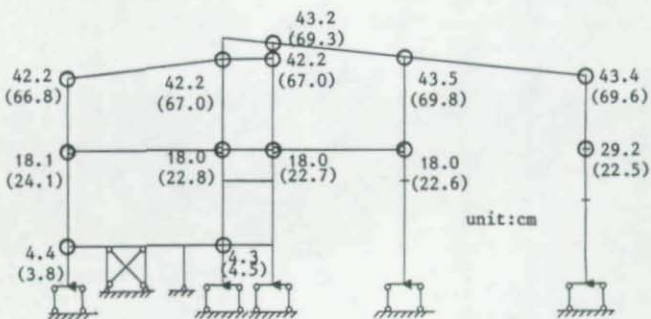


Fig.20 Maximum Displacement Response

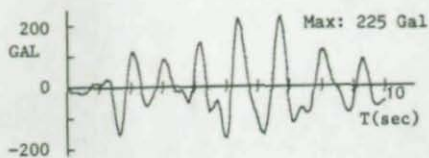


Fig.21 Input Acceleration for Analysis

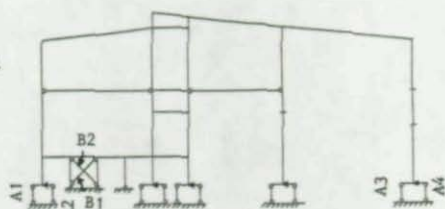


Fig.22 Abbreviation of Members

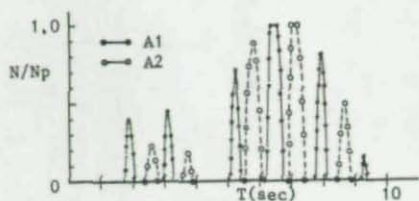


Fig.23(a) Force Ratio Time History of A1, A2

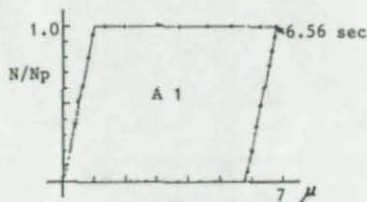


Fig.23(b) Force-Ductility of A1

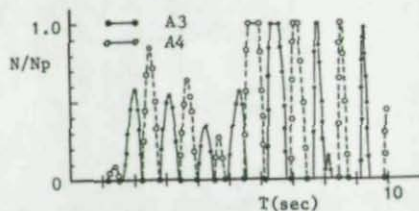


Fig.24(a) Force Ratio Time History of A3, A4

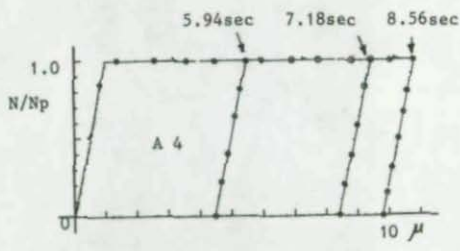


Fig.24(b) Force-Ductility of A4

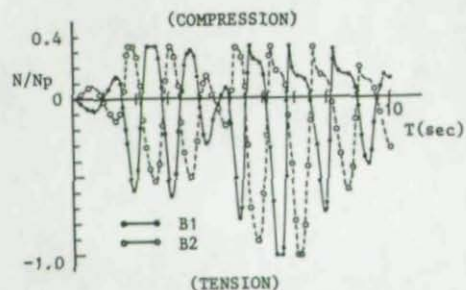


Fig.25(a) Force Ratio Time History of B1, B2

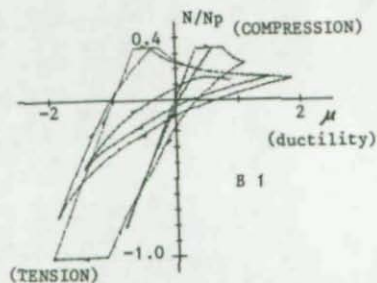


Fig.25(b) Force-Ductility of B1



Fig.26 Buckling of Bracing Member

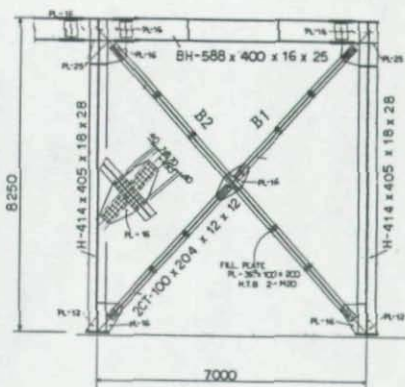


Fig.28 Detail of Bracing Members



Fig.27 Yield of Anchor Bolt

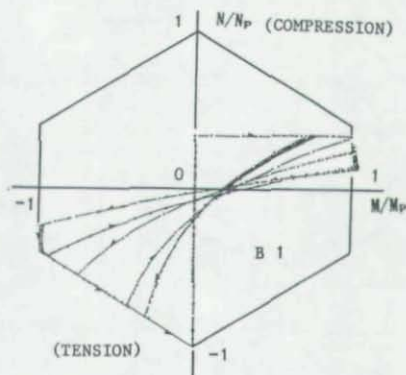


Fig.29 N-M Hysteresis of Plastic Hinge

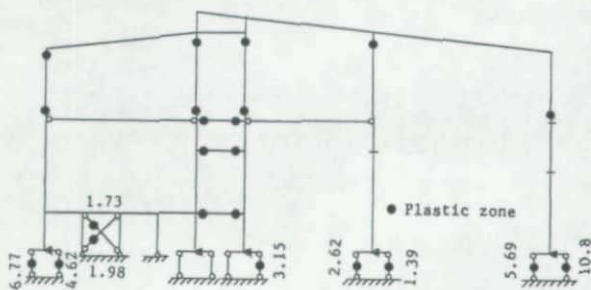


Fig.30 Maximum Ductility Ratio of Members

by

Subhash C. Goel and Xiaodong Tang
Department of Civil Engineering
The University of Michigan
Ann Arbor, Michigan

INTRODUCTION

In the current design practice concentrically braced structures are not considered as ductile structures. The non-ductile behavior of these structures mainly results from early cracking and fracture of bracing members due to local buckling in regions of plastic hinges which form during cyclic post-buckling deformations. The building codes recognize this fact and attempt to take care of this problem by specifying increased design forces for braced frames in general. This practice may not always result in safer structures, however, since the fracture life of less slender bracing members may be smaller than that of more slender ones. Furthermore, columns may also be subjected to buckling leading to possible collapse of some structures.

The above mentioned problems may be more critical in braced structures in which no backup ductile moment frames are provided. These structures are quite common and in spite of increased design forces they generally turn out to be more economical because of simple connections between the beams and columns. The problems associated with column buckling and early failure of bracing members in non-moment resisting braced structures during severe earthquake motions are studied in this paper. A practical and rational method for safe design of such structures is also presented.

The structure selected for this study is patterned after the six-story, full-scale test structure (shown in Fig. 1) with concentric K-bracing in one bay of the middle frame in the direction of loading, which was used in the U.S.-Japan Cooperative Earthquake Research Program. The floor plan, dimensions and gravity loads are kept the same, but this structure has no backup moment-resisting frames. Thus, the braced bay provides all the lateral force resistance for the entire structure.

FRAME F1

The structure is first designed in strict compliance with the requirements of current Uniform Building Code, 1982 edition [6], and allowable design procedure of the current AISC Specification [1]. W sections in A36 steel are used for beams and columns, and square structural tubes of A500 grade B steel for the bracing members. The connections of beams with columns are simple, non-moment type. The resulting member sizes of the braced frame are shown in Fig. 2. This frame which provides all the lateral force resistance for the entire

structure is designated as F1 in this study.

The inelastic response of Frame F1 is computed for the NS component of the 1978 Miyagi-ken Oki earthquake with the peak acceleration scaled to 500 gals (1 gal = 1 cm/sq. cm). This ground motion was also used in the final pseudodynamic test of the U.S.-Japan concentrically braced structure. Some response results of Frame F1 are shown in Figs. 3 and 4. DRAIN-2D program originally developed at UC Berkeley [6] and later enhanced at the University of Michigan [5,8] was used for this study. It is noticed from Fig. 3 that the horizontal displacements at upper three floors are quite large. Few plastic hinges formed in the beams and inspite of large displacements at the upper floors brace buckling occurred only in the second and third stories, Fig. 4. This figure also shows that plastic hinges formed at a number of locations in the columns even though the columns received only small moments from the bracing members. This indicates that columns in this frame were subjected to large axial forces which led to buckling in three of them, also shown in Fig. 4. Column buckling commenced as early as 4 seconds into the response. Buckling of columns resulted in large tilt of the frame in upper four stories as shown in Fig. 4.

Buckling of columns is perhaps the most significant and undesirable aspect of the response of Frame F1 resulting in large displacements at upper floor levels. Buckling in columns (local or overall) due to large axial force reversals may cause instability and complete collapse of braced structures under certain conditions. This aspect seems to have played an important role in the observed behavior of Pino Suarez buildings during the 1985 Mexico City earthquake [2].

FRAME F2

In order to eliminate the problem of column buckling during a severe earthquake motion the design procedure for columns was modified in Frame F2. In this frame the braces and beams were kept the same as in Frame F1. An upper bound on the required ultimate strength for the columns is calculated due to 1.3 times the design dead and live loads, and the vertical component of maximum compressive strength of the braces. The sections for columns in the braced bay were then selected according to the requirements of AISC Specification Part 2 (Plastic Design). This frame is called F2 and the member sizes are shown in Fig. 5. Increase in column sizes in the braced bay as compared with those in Frame F1 is apparent.

Response of Frame F2 to the same ground motion is shown in Figs. 6 - 8. It is noticed that inspite of formation of plastic hinges in beams as well as columns no buckling occurred in the columns. However, the braces in the second, third and fourth stories underwent cyclic buckling to the extent that they fractured quite early during the response. This caused very large drifts in those stories and large overall floor displacements. Inspite of this the structure

did not become unstable. The reason for this is that the columns in those stories could develop moments due to continuity in the stories where the braces did not fracture, thus, providing a second line of defense for the structure. Nevertheless, it is questionable whether the columns could remain stable under such large story drifts and associated plastic rotations.

The fracture criteria for the rectangular tube bracing members used in the analysis is rather simple and crude which is based on recent tests at The University of Michigan [3,7]. The detailed derivation of the criteria is given in Ref. 8. It is empirical in nature and can be expressed as follows:

$$N_f = C (KL/r) (b/d) / [(b-2t)/t]^2 \quad KL/r \geq 60$$

where,

N_f = number of equivalent cycles to failure

C = 262, an empirical constant

KL/r = effective slenderness ratio of the member

b/d = width to depth ratio of the section, and

$(b-2t)/t$ = clear width-thickness ratio of the flanges.

It should be pointed out that the width-thickness ratio of tubular bracing members used in Frames F1 and F2 meet the limit specified by the AISC Plastic Design criteria [1].

FRAME F3

It should be clear from the above fracture criteria that fracture life of tubular bracing members can be increased by using significantly smaller width-thickness ratios. Thus, the tubular bracing members of Frame F3 were designed by limiting the width-thickness ratios to $95/\sqrt{F_y}$, which is exactly half of that allowed by the current AISC Specification Part 2 [1]. For nominal yield strength of 46 ksi for A500 grade B steel this would amount to a limit of 14.

Modern building codes generally allow smaller design seismic forces for ductile structures while imposing "penalties" for less ductile structures or structural elements. According to the current Uniform Building Code buildings having ductile moment resisting space frames can be designed with a horizontal force factor of 0.67 or 0.8. For buildings in Seismic Zone Nos. 3 and 4, and for buildings with importance factor greater than 1.0 in Zone No. 2, all members in braced frames must be designed for 1.25 times the force determined otherwise. Since, the ductility of the bracing members in Frame F3 is ensured by using lower width-thickness ratios it was decided to delete the "penalty" factor of 1.25 in their design. The columns were designed by following the procedure as in Frame F2. The resulting member sizes for the braced frame F3 are shown in Fig. 9.

The computed response of Frame F3 is shown in Figs. 10 - 12. It is noticed that the horizontal floor displacements are much smaller than those of Frame F2. Plastic hinges formed in several beams and columns but no column buckling was

encountered. Cyclic buckling occurred in all braces. Axial deformation histories of some braces are shown in Fig. 12, which are quite severe. However, due to much more compact sections their integrity is ensured. Thus, it can be concluded that Frame F3 should perform satisfactorily when subjected to a severe ground motion such as the one used in this study.

CONCLUSIONS

Based on the results and discussion presented in this paper the following conclusions can be drawn:

1. Columns in braced non-moment resisting structures may be subjected to large forces causing them to buckle during a severe earthquake. It is necessary to check their buckling strength by an ultimate strength method such as the one suggested in this study.
2. The allowable width-thickness ratio specified by the AISC Specification for rectangular tubular bracing members should be reduced in order to increase their ductility and energy dissipation capacity for survival during a severe earthquake.
3. If the ductility of bracing members is ensured the design of concentric braced structures can be based on forces smaller than those specified by current building codes.

ACKNOWLEDGEMENT

This study was sponsored by the National Science Foundation under Grant No. ECE-8516866. The conclusions and opinions expressed in this paper are solely those of the authors and do not necessarily represent the views of the sponsor.

REFERENCES

1. AISC, "Specification for the Design Fabrication and Erection of Structural Steel for Buildings," American Institute of Steel Construction, Chicago, Ill., 1978.
2. Astaneh, A, "A Report on the Behavior of Steel Structures during September 19, 1985 Earthquake of Mexico City," Proceedings, Structural Stability Research Council Meeting, Washington, D.C., April 15-16, 1986.
3. Goel, S.C., "Seismic Stability of Braced Steel Structures," Proceedings, Structural Stability Research Council Meeting, Washington, D.C., April 15-16, 1986.
4. International Conference of Building Officials, "Uniform Building Code," Whittier, Calif., 1982.
5. Jain, A.K., and Goel, S.C., "Hysteresis Models for Steel Members subjected to Cyclic Buckling or Cyclic End Moments and Buckling," Report No. UMEE 78R6, Department of Civil Engineering, University of Michigan, Ann Arbor,

6. Kanaan, A.E., and Powell, G.H., "General Purpose Computer Program for Inelastic Dynamic Response of Plane Structures," Report No. EERC 73-6, University of California, Berkeley, Calif., April 1973.
7. Liu, Z., "Investigation of Concrete-Filled Steel Tubes under Cyclic Bending and Buckling," Doctoral Dissertation, Department of Civil Engineering, The University of Michigan, Ann Arbor, Michigan, March 1987.
8. Tang, X., "Seismic Response and Design Considerations of Braced Steel Structures," Doctoral Dissertation, Department of Civil Engineering, The University of Michigan, Ann Arbor, Michigan, April 1987.

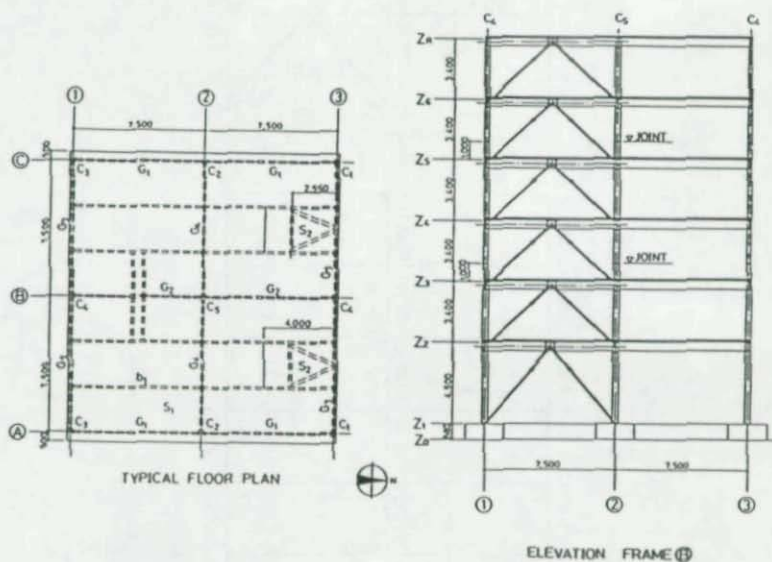


Fig. 1 U.S.-Japan Concentric Braced Structure.

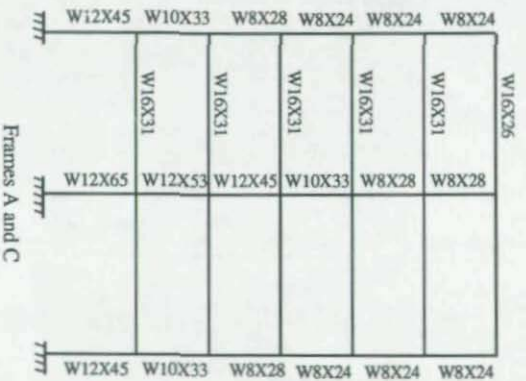
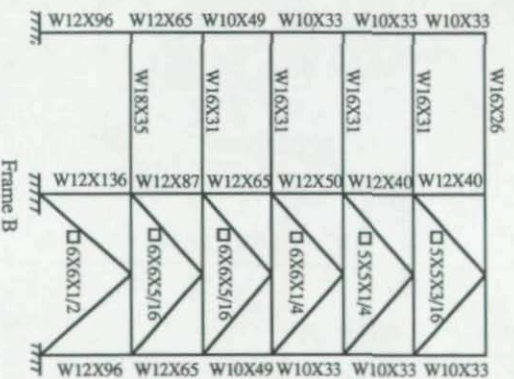


Figure 2 Member Sizes, Frame F1

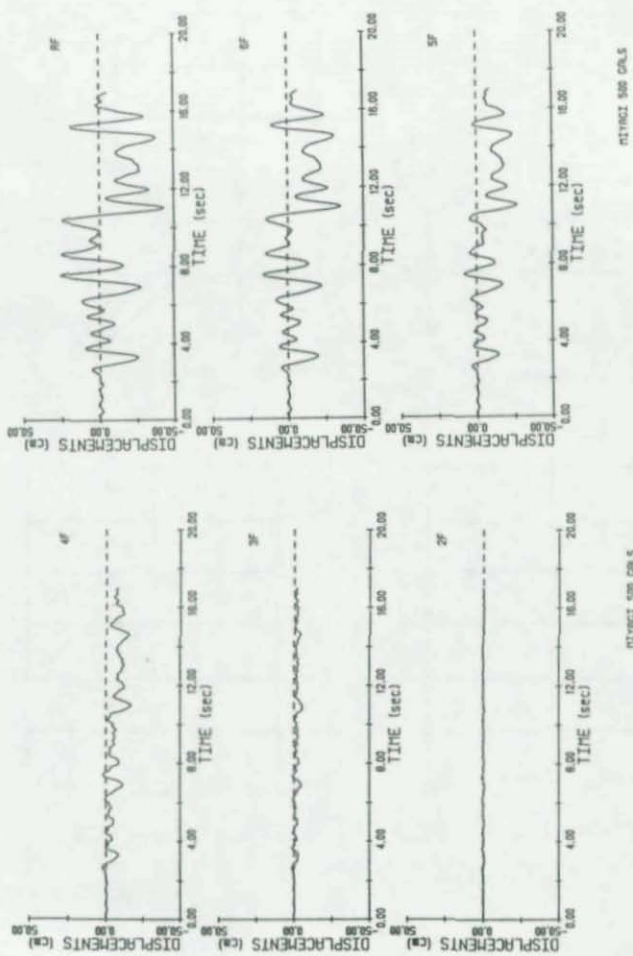


Figure 3 Horizontal Floor Displacements, Frame F1

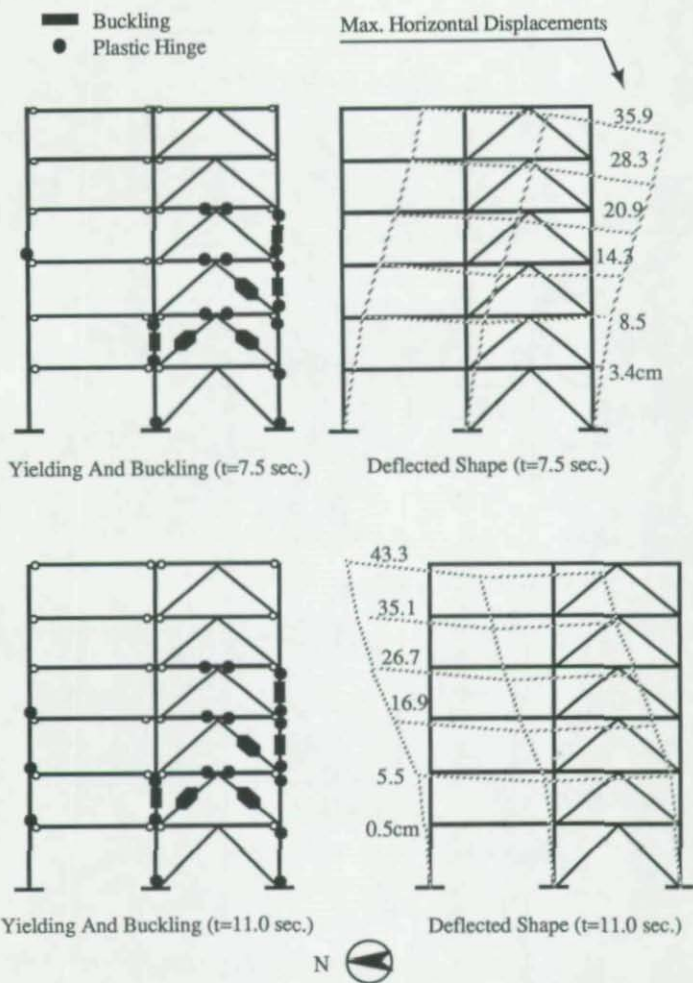


Figure 4 Yielding, Buckling and Deflected Shape of Frame F1 - Miyagi-Ken-Oki Earthquake

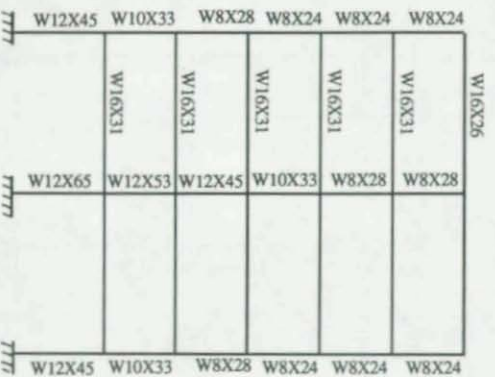
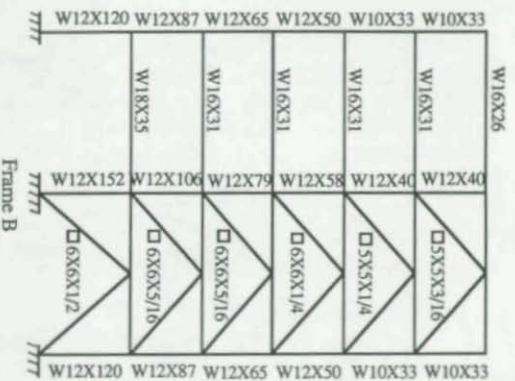


Figure 5 Member Sizes, Frame F2

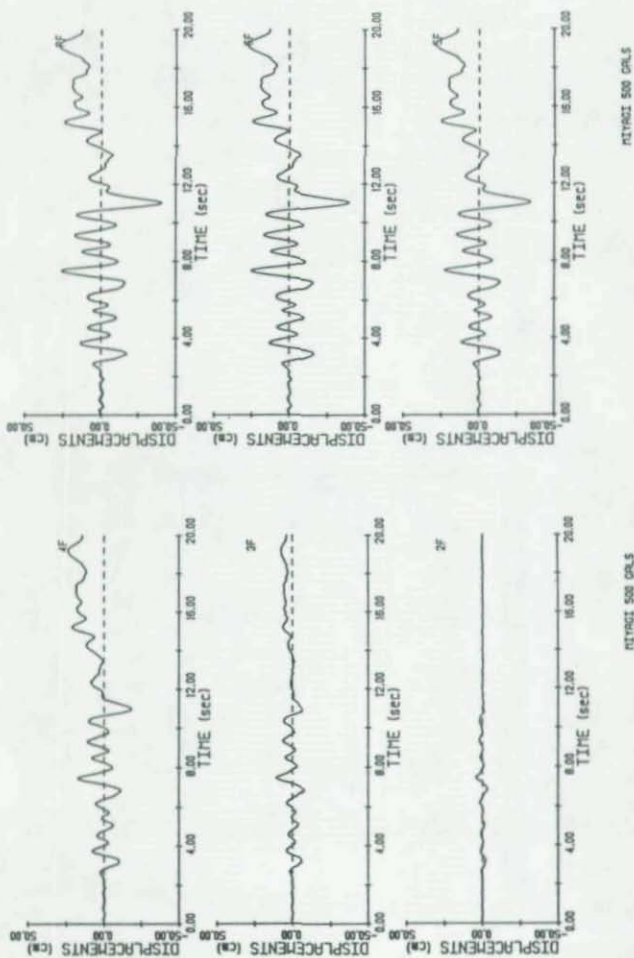


Figure 6 Horizontal Floor Displacements, Frame F2

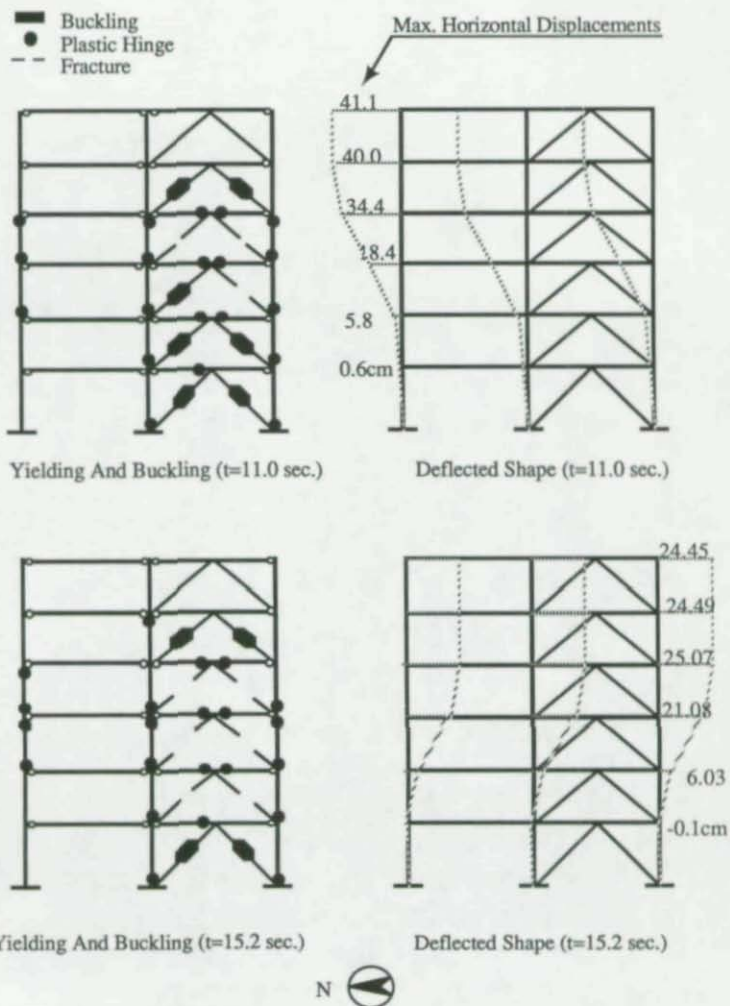
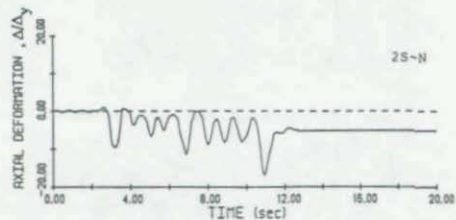
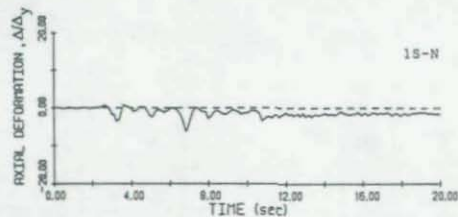
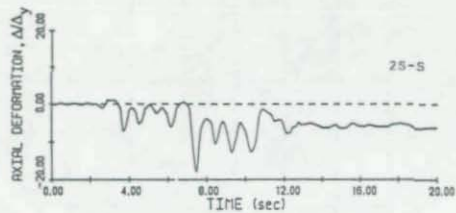
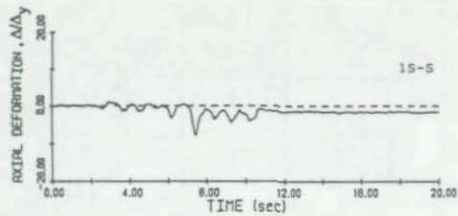


Figure 7 Yielding, Buckling, Fracture and Deflected Shape of Frame F2 - Miyagi-Ken-Oki Earthquake



MIYAGI 500 GALS

MIYAGI 500 GALS

Figure 8 Brace Deformation History, 1st and 2nd Stories, Frame 2

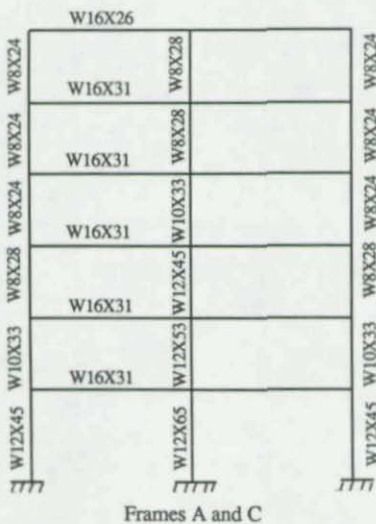
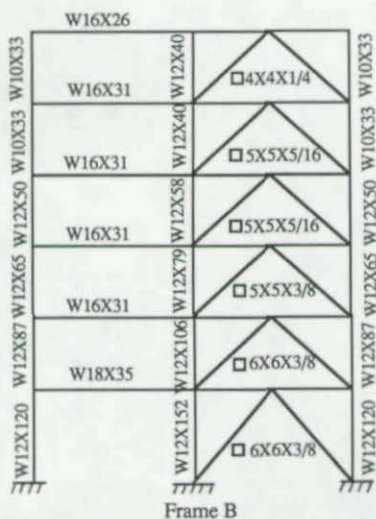


Figure 9 Member Sizes, Frame F3

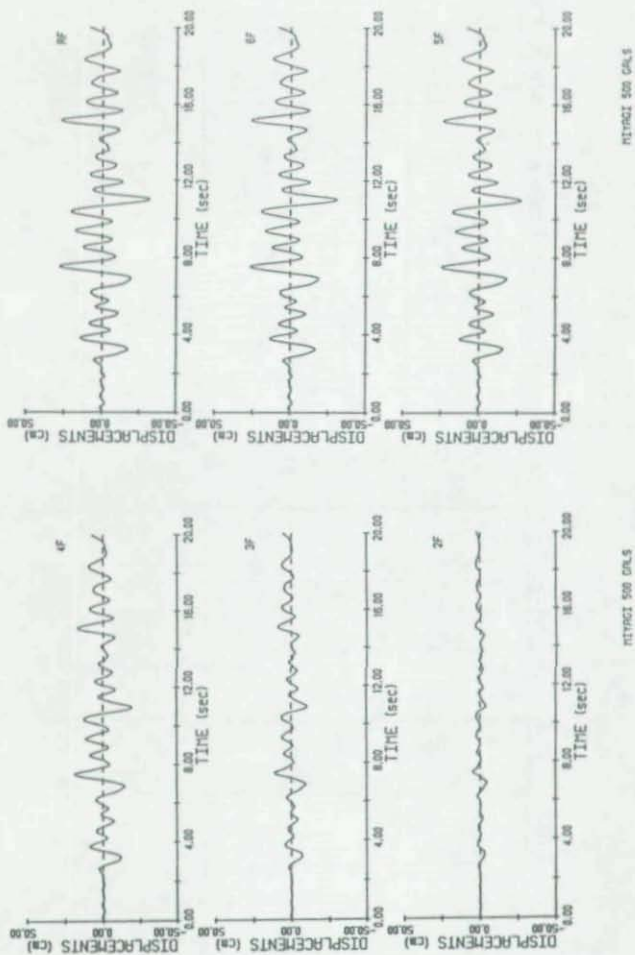


Figure 10 Horizontal Floor Displacements, Frame F3

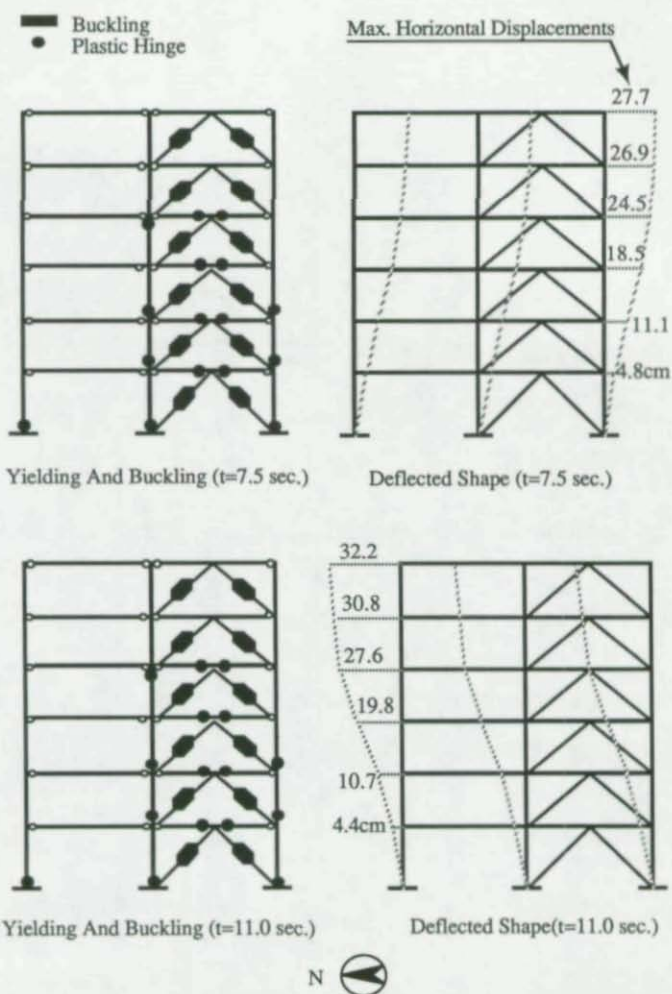


Figure 11 Yielding, Buckling and Deflected Shape of Frame F3 - Miyagi-Ken-Oki Earthquake

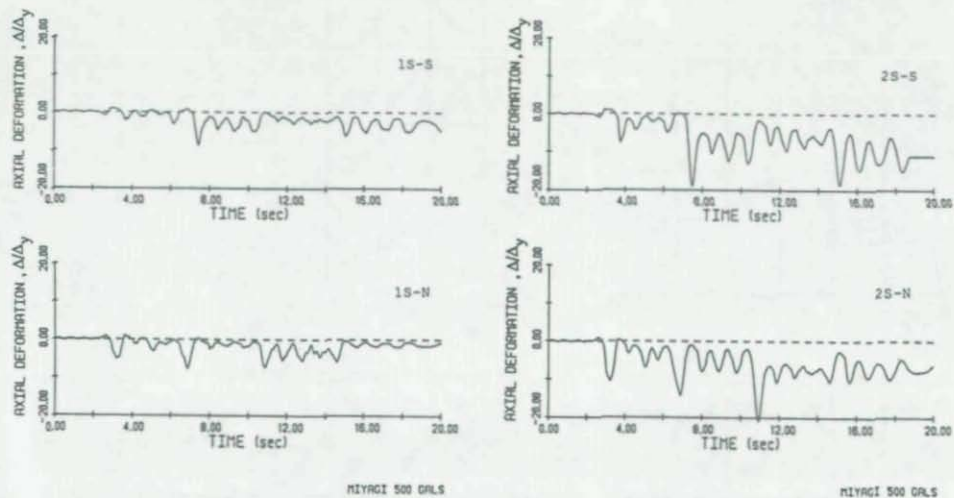


Figure 12 Brace Deformation History, 1st and 2nd Stories, Frame 3

COMPRESSIVE TESTS OF GUSSET PLATE CONNECTIONS

by J.J. Roger Cheng¹ and S.Z. Hu²ABSTRACT

The compressive behavior and buckling strength of thin-walled gusset plate connections were examined on the basis of an experimental investigation of full-scale diagonal bracing connections. Such connections are commonly used to transfer forces from a bracing member to the beam and column through the gusset plate. A total of 14 tests were run on six connection specimens. Plate thickness, geometric configuration, boundary conditions, eccentricity and reinforcement were considered in planning the tests. All of the tests failed in plate buckling except the tests with eccentricity which failed in bending yielding of the spliced plates. The test results were evaluated based on load and deformation data. An attempt was made to correlate the test results with the analytical studies using the finite element program BASP. The comparison is shown to be in reasonable agreement. Current design practices are discussed briefly and the methods are found to be very unconservative compared with test results.

INTRODUCTION

One of the most common methods of connecting two or more members together is by a gusset plate which is used to transfer forces from one member to another such as connections in trusses or braced steel frames. In the latter case, either tensile or compressive loads from a bracing member which is designed to resist horizontal forces are transferred to the beam and column through the gusset plate. The gusset plate is normally bolted to the bracing member, in which the spliced plate may or may not be used depending upon member geometry, and connected to the column and beam by bolts or welds. Fig. 1 illustrates such a connection. Although it is customary to assume that the bracing members in this arrangement are loaded only in their axial direction, the delivery of these loads will produce bending, shear and normal forces in the gusset plate.

Despite the popularity of this type of connection, the gusset plate has received relatively little attention in terms of strength, behavior and design investigation. Current design specifications only mention the design philosophy and no specific

¹ Assistant Professor of Civil Engineering, University of Alberta, Edmonton, Alberta, Canada, T6G 2G7

² Graduate Student in Civil Engineering, University of Alberta, Edmonton, Alberta, Canada T6G 2G7

formulas for evaluating the dimension and thickness of the gusset plate (AASHTO, 1983). The traditional method of gusset plate design (Gaylord et al., 1972) is primarily based on elastic analysis and uses beam theory to check the stresses at selected sections. It has been recognized that the applicability of the beam theory to the configuration of gusset plates is questionable. An alternative method is performed by evaluating the critical normal stress using Whitmore's effective width concept (Whitmore, 1952). The normal stress on this effective area should not exceed the allowable stress permitted by the appropriate specification.

Recently, a few studies have been conducted to determine the behavior and ultimate strength of gusset plate connections which aimed at providing a rational design method. A test was conducted by BJORHOVDE et al. (1985) to determine the ultimate tensile strength of a gusset plate used in a diagonal bracing connection. The physical tests done by BJORHOVDE et al. (1985) allowed RICHARD et al. (1983) to model gusset plate behavior using the finite element method. Based on these investigations, HARDASH et al. (1985) derived the block-shear concept of coped beam-to-column connections into the gusset plate loaded in tension. It was concluded that the governing block-shear model was to be the one incorporating tensile ultimate stress on the net area between the last row of bolts and a uniform effective shear stress acting on the gross area along the outside bolt lines. However, these studies did not address the problem of the compressive gusset plate connections, nor the related problem of gusset plate buckling.

Using compressive diagonal members increases the complexity of the connection. Common yielding stress analysis cannot represent the actual stresses because of load concentrations, warping of the plate section, local yielding and local eccentricity. All of these may cause buckling or crippling in the gusset plate adjacent to the diagonal member or to the spliced location. In addition, due to the uncertainty of boundary conditions, the prediction of buckling load becomes extremely difficult. Besides, compression stresses along free edges of gusset plates may cause local buckling and insufficient gusset plate thickness may cause unacceptable deformations in the connection. In order to avoid the local buckling along free edges of gusset plate, AASHTO (1983) limits the length of an unsupported edge of a gusset plate to a maximum of $930/\sqrt{F_y}$ times its thickness. It is assumed that the free edge behaves as a unit width column with a fixed-fixed boundary condition. From the previous discussion, it can be easily found that the above provision is oversimplified and very conservative.

A research project was undertaken by the authors to investigate the behavior of compressive gusset plate connections sponsored by the Canadian Steel Construction Council. This paper presents the results of the test phase of this project. The principal purpose of the tests was to provide experimental data

for the various design parameters so the ultimate goal of designing such a connection could be established. The test results will be compared with the analytical studies using the finite element program BASP and current design practices are briefly discussed.

EXPERIMENTAL PROGRAM

The experimental program was designed to represent the conditions of actual gusset plate connections. Thus, full-scale single gusset plate connections of a diagonal bracing member at the joint of a beam and a column as shown in Fig. 1(a) were used. The gusset plate was bolted to the bracing member by using spliced plates and then bolted to the column and beam through pre-welded end plates. The variables chosen for investigation are plate thickness, plate size, boundary condition, eccentricity and reinforcement. Two loading conditions, namely concentric and eccentric loadings, were used by arranging various positions of the spliced plates (see Fig. 4). To simplify the problem, thin plates were used in the test specimens. It was planned that most of the tests would fail in elastic buckling.

The test series consisted of six gusset plate specimens with varying plate thickness and plate size as given in Table 1. Two different thicknesses of splice plate used in each gusset plate specimen are also given in the Table. The detail of the two different plate sizes (850 mm x 700 mm and 850 mm x 550 mm) used in the test specimens are shown in Fig. 2. The gusset plate specimens were designed to be loaded in 45° by the bracing member. Plates C1 to C4 were loaded concentrically while plates E5 and E6 were loaded eccentrically. For comparison purposes, plates E5 and E6 have the identical cross-sectional properties as plates C1 and C3 respectively but have different loading conditions. The major material properties of the gusset plate specimens and the spliced plates are summarized in Table 2.

To simplify the test set-up, the gusset plate was loaded as shown in Fig. 3 and the forces that exist in the beam and column to balance the compressive load from the bracing member were neglected. A schematic test set-up is shown in Fig. 3. The test frame consisted of two W310 x 97 members as beam and column and one W250 x 58 acting as bracing member. The gusset plate was braced at the spliced plate locations as shown in Fig. 3 by tension bars and was allowed to move laterally by placing an additional pair of rollers underneath the test frame. The magnitude of the applied load and overall displacement of the specimens were monitored by the MTS test machine and a set of LVDTs and dial gages as shown in Fig. 4. Strain gages were placed in various locations of each specimen in pairs, one set on either side of the gusset plate, to measure the strain distribution. A pair of rosette gages was located on the gusset plate adjacent to the end of the spliced plate. For the specimens subjected to an eccentric load, a pair of strain gages was put on the spliced plate where a bending yield might occur.

Fourteen tests were run on the six specimens in order to best utilize the material. Eight concentric loading tests were run on plates C1 to C4, in which two tests were conducted for each plate. One, named "free case", allowed the bottom of the test frame free to move and the other, called "fixed case" did not allow movement. The test procedure was generally the same for plates C1 to C4. First, the specimen was tested in the free case and the test was terminated when the lateral displacement of the roller underneath the test frame became excessive, around 30 mm. Then the specimen sprang back to its original position when the load was removed. Stoppers were provided subsequently at the roller locations. A new test, fixed case, was then conducted until the maximum load was reached. Another six tests were performed on plates E5 and E6 with eccentric loading, in which three cases were tested for each plate and they were called "free without reinforcement", "free with reinforcement" and "fixed with reinforcement", respectively. The details of the three different cases were shown in Fig. 4. The test procedure followed the sequence of the above three cases. The first test was terminated when the maximum load was reached and unloading occurred or the lateral displacement of the rollers underneath the test frame became excessive, around 30 mm. In the second test the specimen was forced back to its original position and reinforcement was added at the spliced plate location and the specimen was reloaded, again, until it reached the maximum load. For the last case, fixed with reinforcement, the stopper was provided at the bottom of the rollers and the test procedure was the same as before.

TEST RESULTS AND GENERAL BEHAVIOR

The test results are divided into two groups: concentric and eccentric loadings. The concentric loading tests will be discussed first, followed by the eccentric loading tests. A summary of the highest measured applied loads, P_{max} , is given in Table 3.

Concentric Loading Tests

An examination of the reduced data showed that a plot of applied load versus critical lateral deflection reading gave the best representation of buckling phenomena of the test specimens. The final deflected shapes also afforded the best description of the failure due to plate buckling.

Because of the similarity of the behavior, only two plate specimens, C3 and C4 of which the thicknesses are 6.7 mm and 3.1 mm respectively, will be shown and discussed here. Two loading cases, free and fixed, will be discussed separately.

Free Case - All specimens failed as a result of overall buckling of the plates. The maximum deflection occurred at the roller locations. There was no yielding observed during the tests. The curves of applied load versus lateral deflection of the rollers

for the plate C3 and C4 are shown in Fig. 5. The curve for 6.7 mm plate, specimen C3, shows a typical plate buckling curve with a distinctive buckling load. For 3.1 mm plate, specimen C4, the curve gradually increases to the maximum load. This can be attributed to the large initial imperfection of the plate section which was induced by the end plate welding. The buckling shapes of the specimens C3 and C4 along two free edges and the center line of spliced plate were plotted in Fig. 6(a).

Fixed Case - The lateral translation of the test frame was prohibited in this case. The maximum deflection of the plates occurred at the mid-point of the longer free edge as shown in Fig. 6(b). Yield lines were observed on the spliced plate near the top of the gusset plate for both C1 and C3 due to the high axial load and the large lateral deformation of the gusset plate. A typical curve of load versus lateral deflection at the mid-point of the longer free edge is shown in Fig. 7(a). The load versus lateral deflection curve for test C4 as shown in Fig. 7(b) is different from other tests. The reason was that before reaching the maximum load two free edges of the plate were deflected in the opposite direction due to the large initial imperfection. After reaching its maximum load, the plate was forced to buckle in the same direction with a sharp decreasing load.

Eccentric Loading Tests

It is customary to neglect the eccentricity in designing gusset plate connections. However, some actual practice showed that the eccentricity may cause a significant reduction of the carrying capacity of gusset plates. Six tests run on two plate specimens, E5 and E6, also show the importance of the eccentricity. Due to the similar load-deflection curves and buckled shapes to the concentric loading tests, only the general behavior of three loading cases of the eccentric loading tests will be discussed below.

Free without Reinforcement - Both of the specimens failed by the yielding of the spliced plate. Yield lines were observed on the spliced plate at the last row of the bolts of the bracing member. The load decreased when the maximum load was reached. Permanent deformation was in the spliced plate after unloading.

Free with Reinforcement - Same specimens were stiffened and tested in the same boundary condition as the previous case to evaluate the effect of the reinforcement. Only one stiffener was provided for the plate E5 while three additional spliced plates were placed on the other side of the plate E6 (Fig. 4). The load carrying capacity of the specimens increased significantly which was approximately three times higher than previous case for plate E5 and six times for plate E6. However, both tests were unable to reach the loads of plates C1 and C3 in the free case. Again, the plate E5 failed due to the load exceeded the carrying capacity of the combined spliced plate and stiffener. For the

plate E6, the specimen failed in overall buckling of the gusset plate and no sign of yielding was found on the spliced plate. The maximum load of the test reached 89% of the plate C3 in the free case.

Fixed with Reinforcement - The same plates with the same stiffeners were used to perform another set of test with the stopper provided at the bottom the test frame. Both of the specimens failed in the loads less than the maximum loads of the plates C1 and C3 in the fixed case. Yielding in the spliced plate and stiffeners was observed during the tests. Sliding between the spliced plate and stiffeners also occurred for the plate E6.

DISCUSSION OF TEST RESULTS

The highest applied load of each test, P_{max} , is used for primary comparison and is summarized in Table 3. The corresponding load carrying capacity of each plate calculated according to the effective width concept (Whitmore, 1952) was also listed in the Table. As expected the effective width concept which is primarily based on the material strength of a gusset plate at the end of a bracing member gives much higher predicted values than the P_{max} . Since the test specimens were purposely designed to fail in plate buckling.

The computer program BASP which can handle plate buckling with stiffeners originally written by Akay et al. (1977) was used to compare with the test results. In the analysis, the gusset plates were assumed to be fixed at the boundaries of beam and column and fixed but allowing out-of-plane translation at the top of the plate for the free cases and fixed both rotation and translation for the fixed cases as shown in Fig. 8. The plates were idealized by two-dimensional finite elements while the thicker elements were used for the spliced plate locations. The applied loads were assumed uniformly distributed among the numbers of bolt on the gusset plate. The problems solved by this program are treated as a linear-elastic buckling problem. The results of the BASP are summarized in Table 3. The comparison with the test results is shown to be in reasonable agreement. However, large discrepancy exists for the free and fixed cases of the plate C1 and the fixed case of the plate C3. There are two major reasons. One is the simplified assumptions of the spliced plate thickness and uniform distribution of the applied load. The other is the yielding that occurred in the spliced plates due to the high axial load in the spliced plate and large lateral deformation of the gusset plate. The yielding reduced the rotational restraint at the spliced plate locations and consequently reduced the buckling capacity of the gusset plate. The analysis phase of this project which is in progress shows that the rotational restraint is a very important parameter for the buckling capacity of the gusset plate. The local buckling provisions of the AASHTO specification (1983) was calculated and shown in Table 3. The provisions yield very conservative results

as expected.

It was found from the tests conducted on the plates E5 and E6 that the eccentricity initiated the yielding in the spliced plate and eventually caused the failure of the connection. Thus, the beam-column formula of a rectangular cross-section (ASCE, 1971) was used to calculate the cross-sectional strength of the spliced plates at the conjunction of the bracing member and the gusset plate. Good correlation exists between the test results and the predicted values. The conservatism of the beam-column formulas applied to the fixed with reinforcement case of the plate E5 is because that the yielding in the spliced plate is not the final mechanism of the gusset plate. Comparing the cases with reinforcement to the cases without reinforcement indicates that the eccentricity could curtail the carrying capacity of gusset plates significantly. However, it also implies that the reduction of the strength could be minimized or even avoided by providing the sufficient stiffeners at the spliced plate locations.

SUMMARY AND CONCLUSIONS

The compressive behavior and buckling strength of thin-walled gusset plate connections were examined by an experimental investigation of full-scale diagonal bracing connections. The tests considered parameters such as plate thickness, plate size, boundary condition, eccentricity and reinforcement. A total of 14 tests were run on six connection specimens. Current design practices and finite element solutions were used to compare the test results. The following is a summary of the findings.

1. For the concentric loading cases that were examined, the primary failure mode for the free cases is overall buckling of the plate. The maximum deflection occurred at the roller locations. For the fixed cases, the failure is initiated at the free edges due to the local buckling of the plate. The maximum deflection occurred at the mid-point of the longer free edge.
2. Another type of failure may occur in spliced plate due to the existence of the eccentricity. This has been shown in the cases of free without reinforcement of the plates E5 and E6. The reduction of the strength may be significant.
3. The cases of reinforcement of the plates E5 and E6 shows that the reduction of the strength due to the eccentricity could be minimized by providing sufficient stiffeners at the spliced plate locations.
4. The effective width concept which is currently used in designing gusset plates was found to be very unconservative if the primary failure mode is the plate buckling. The local buckling provision adopted by the AASHTO appears to be very conservative and doesn't cover the various boundary

conditions.

5. The finite element solutions is shown to be in reasonable agreement with the test results. The beam-column formuluss of a rectangular cross-section gives reasonable prediction for the carrying capacity of the eccentrically loaded gusset plates.
6. The available design methods for compressive loaded gusset plates has been found to be inappropriate for determining the compressive behavior and failure of the gusset plate. The effects of variables such as thickness, size, boundary condition, etc. on the compressive strength of a gusset plate should be further investigated for the improvement of the existing design methods.
7. The requirement of the stiffeners for gusset plates and spliced plates should also be studied.

ACKNOWLEDGEMENTS

The experimental work presented herein was carried out at I.F. Morrison Structural Engineering Laboratory, Civil Engineering Department, University of Alberta. Financial support was provided by the Canadian Steel Construction Council and supplemented by the Natural Sciences and Engineering Research Council of Canada to J.J. Cheng under grant No. A4727. The guidance of the Project Coordinator, Mr. M.I. Gilmor, is greatly appreciated.

REFERENCES

1. Akay, H.U., Johnson, C.P. and Will, K.M., 1977. "Lateral and Local Buckling of Beams and Frames". Journal of the Structural Division, ASCE, Vol. 103, No. ST9, September, pp. 1821-1832.
2. ASCE, 1971. "Plastic Design in Steel - A Guide and Commentary", ASCE, Manual and Reports on Engineering Practice, No. 41, 2nd edition, pp. 128-137.
3. Bjorhovde, R. and Chakrabarti, S.K., 1985. "Tests of Full-Size Gusset Plate Connections", Journal of Structural Engineering, ASCE, Vol. 111, No. 3, March, pp. 667-684.
4. Gaylord, E.H. and Gaylord, C.N., 1972. "Design of Steel Structures", McGraw-Hill, New York, 2nd edition, pp. 139-141.
5. Hardash, S.G. and Bjorhovde, R., 1985. "New Design Criteria for Gusset Plates in Tension", Engineering Journal, AISC, Vol. 22, No. 2, 2nd Quarter, pp. 77-94.
6. Richard, R.M., Rabern, D.A., Hormby, D.E., and Williams, G.C., 1983. "Analytical Models for Steel Connections", Behavior of

Metal Structures, Proceedings of the W.H. Munse Symposium, Edited by W.J. Hall and M.P. Gaus, ASCE, May 17, pp. 128-155.

7. "Standard Specifications for Highway Bridges", 13 edition, 1983. The American Association of State Highway and Transportation Officials, Washington.
8. Whitmore, R.E., 1952. "Experimental Investigation of Stresses in Gusset Plates", Engineering Experimental Station, Bulletin No. 16, The University of Tennessee, Knoxville.

Table 1. Geometric Properties

Test Specimen	Thickness mm	Size mm x mm	Thickness of Splice Plate Used, mm
C1	6.70	850 x 550	13
C2	3.11	850 x 550	13
C3	6.70	850 x 700	13
C4	3.11	850 x 700	13
E5	6.70	850 x 550	8.1
E6	6.70	850 x 700	8.1

Table 2. Material Properties

Material Used	Elastic Modulus (MPa)	Static Yield Strength (MPa)	Ultimate Strength (MPa)
6.70 mm Gusset Plate	211,000	505	595
3.11 mm Gusset Plate	197,000	240	340
13.0 mm Splice Plate	205,000	260	420
8.1 mm Splice Plate	211,000	305	495

Table 3. Summary and Comparison of Test Results

Plate	Size	Load Case	P_{max} (kN)	Effective Width (kN)	BASP (kN)	AASHTO (kN)	Beam Column
C1	850x550x6.7	Free	441.7	1142	944	-	-
C2	850x550x3.1	Free	122.4	529	120	-	-
C3	850x700x6.7	Free	380.1	1142	382	-	-
C4	850x700x3.1	Free	89.6	529	43	-	-
C1	850x550x6.7	Fixed	914.0	1142	1314	137	-
C2	850x550x3.1	Fixed	140.6	529	152	43	-
C3	850x700x6.7	Fixed	678.2	1142	1083	137	-
C4	850x700x3.1	Fixed	145.5	529	130	43	-
E5	850x550x6.7	Free w/o Reinf.	80.4	1142	-	-	73.7
E6	850x700x6.7	Free w/o Reinf.	55.8	1142	-	-	73.7
E5	850x550x6.7	Free w/ Reinf.	232.8	1142	-	-	251
E6	850x700x6.7	Free w/ Reinf.	338.6	1142	-	-	518
E5	850x550x6.7	Fixed w/ Reinf.	392.5	1142	-	-	251
E6	850x700x6.7	Fixed w/ Reinf.	523.2	1142	-	-	518

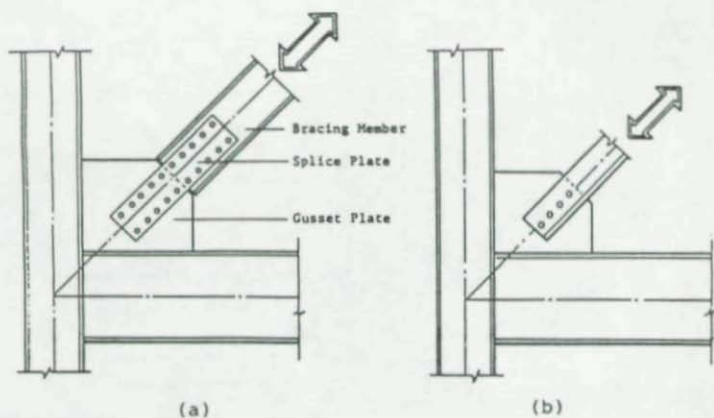


Fig. 1. Typical Gusset Plate connections of a Diagonal Bracing Member

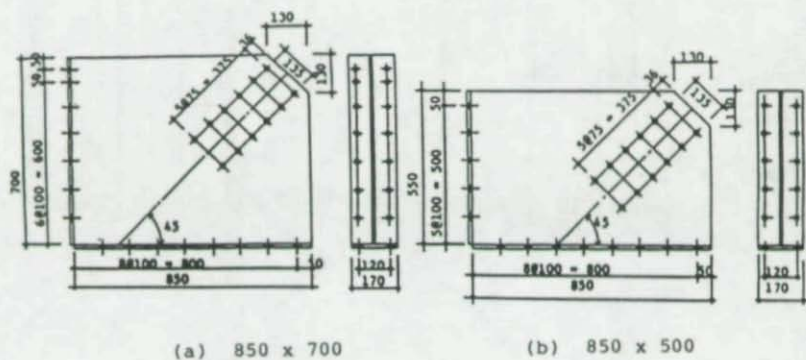


Fig. 2. Test Specimens

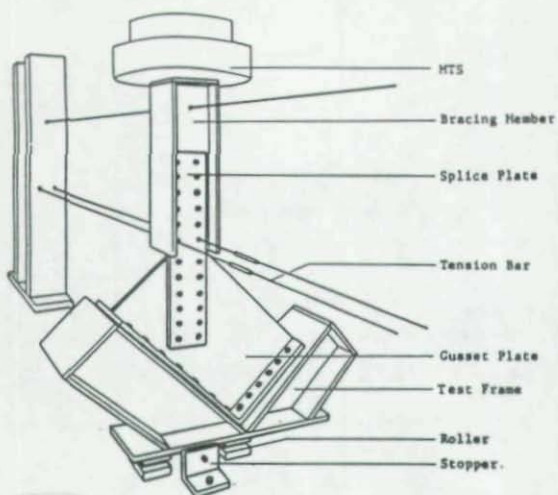


Fig. 3 Schematic Test Setup

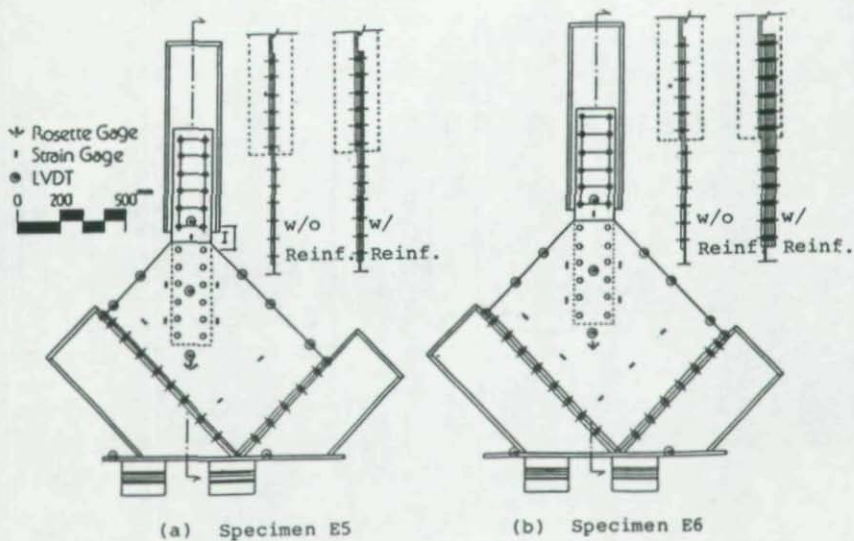


Fig. 4. Instrumentation and Splice Plate Details

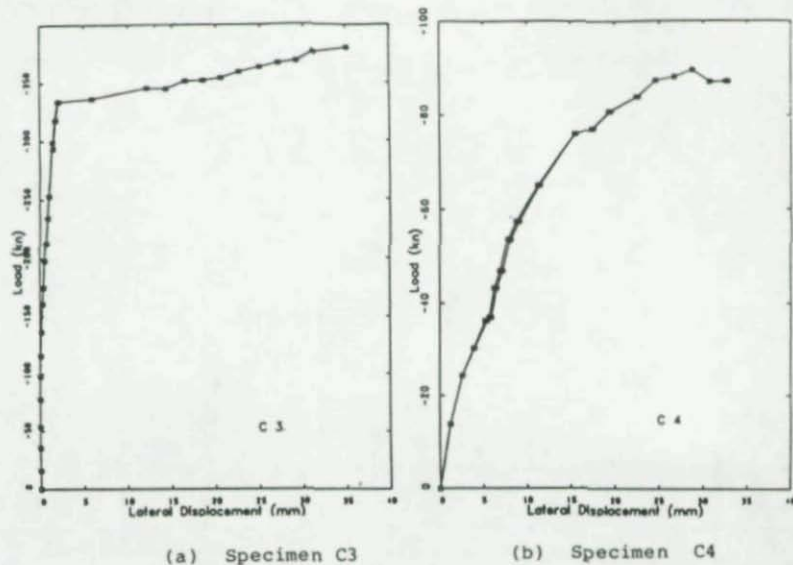


Fig. 5. Load-Lateral Displacement Curves for Free Cases

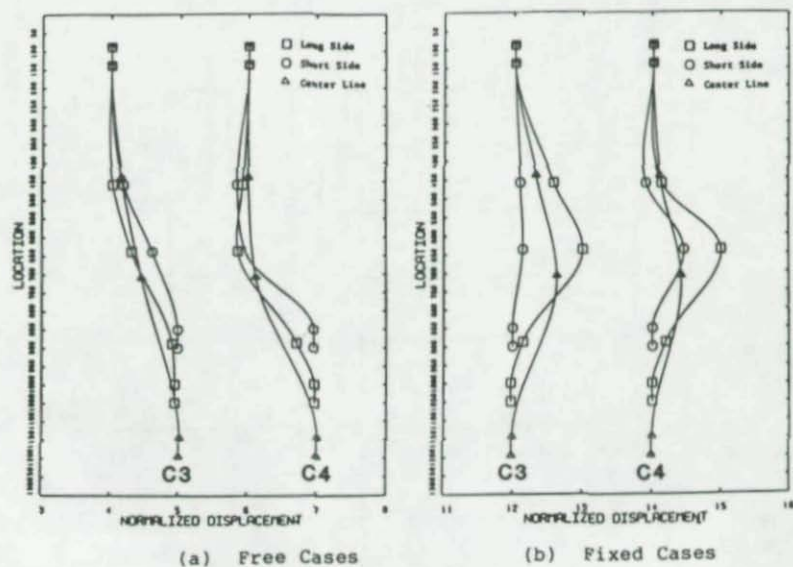


Fig. 6. Normalized Buckling Shapes

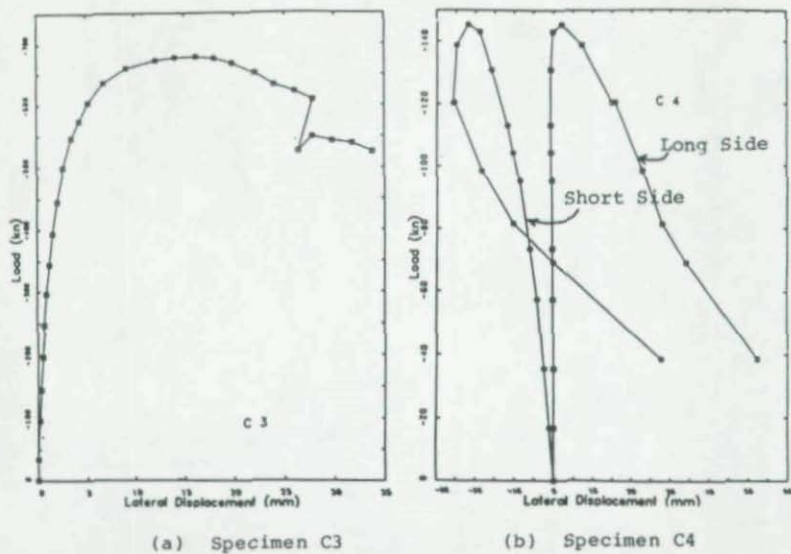


Fig. 7. Load-Lateral Displacement Curves for Fixed Cases

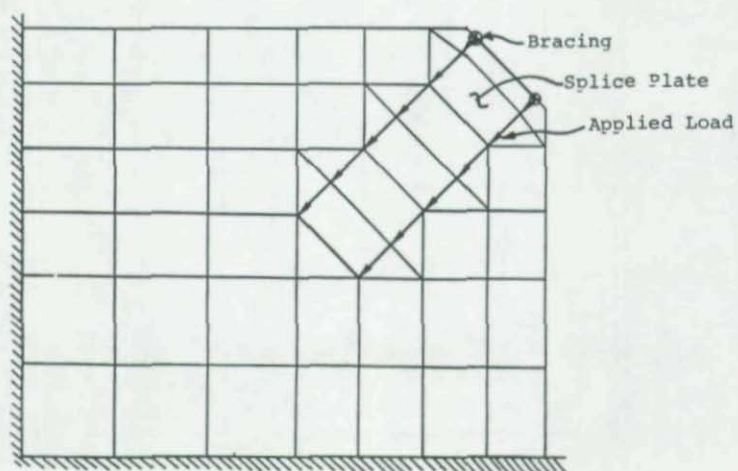


Fig. 8. Finite Element Model

CONCENTRIC AXIALLY COMPRESSED ANGLE COLUMNS—COMPARISON OF
EXPERIMENTAL AND CALCULATED FAILURE STRESSES

205

by

Murty K. S. Madugula and S. Mohan
Dept. of Civil Engg., Univ. of Windsor, Windsor, Ontario, Canada

ABSTRACT

The paper presents a review of the design practices of hot-rolled and cold-formed steel single and double angle members under concentric axial compression. Specifications of the American Institute of Steel Construction, American Iron and Steel Institute, American Society of Civil Engineers, Canadian Standards Association, Indian Standards Institution, and Standards Association of Australia are included in the review. Failure stresses computed according to the above specifications are compared with the available experimental failure stresses of concentric axially compressed hot-rolled and cold-formed single and double angles. A total of 269 hot-rolled and 22 cold-formed angle test results are included in the paper.

NOTATION

- a = distance between connectors in built-up angle compression member
 A = fully effective cross-sectional area of cold-formed angle
 A_e = effective area of cold-formed angle member in compression
 A_g = gross area of angle
 b/t = width-to-thickness ratio of angle leg
 C_r = factored compression resistance
 E = modulus of elasticity
 F_{cr} = critical stress at failure
 F_e = critical torsional or flexural-torsional elastic buckling stress
 F_{min} = critical elastic buckling stress, which is the least of the stresses for Euler flexural, torsional, and torsional-flexural elastic buckling
 F_y = yield strength
 F_{yeff} = effective yield strength in ASCE Manual No. 52
 $(KL/r)_m$ = modified slenderness ratio of built-up angle compression member
 $(KL/r)_o$ = slenderness ratio of built-up angle compression member acting as a unit
 Q = full reduction factor for slender angles in compression
 r_{min} = minimum radius of gyration of a component angle
 t = thickness of angle leg
 w/t = flat width-to-thickness ratio of angle leg
 ϕ = resistance factor
 μ = Poisson's ratio
 λ = non-dimensional slenderness ratio

INTRODUCTION

Angles are the most common structural shapes used in latticed electrical transmission towers and antenna-supporting towers. Angles are also extensively used in nuclear power plants as pipe supports. They are also used as chord and web members of trusses, as web members of long-span open-web steel joists, and as bracing members to provide lateral support

to the primary load-carrying members of a structure. Angles are easy to fabricate and erect because of the basic simplicity of their cross-section. They are classified as equal- or unequal-leg angles, single or built-up (i.e., compound) angles, hot-rolled or cold-formed angles. They can be plain angles, lipped angles or bulb angles, of steel or aluminium. Angles are loaded concentrically or eccentrically, axially or transversely, inducing stresses either below or beyond the proportional limit of the material. This paper deals with hot-rolled and cold-formed steel angles (without lips) under concentric axial compression.

REVIEW OF DESIGN SPECIFICATIONS

(a) AISC-LRFD specification for hot-rolled angles

Factored compression resistance for flexural buckling:

$$C_r = 0.85 A_g F_{cr} \quad (1)$$

$$\text{For } \lambda_c \sqrt{Q} < 1.5, F_{cr} = Q(0.658^{Q\lambda_c^2}) F_y \quad (2)$$

$$\text{For } \lambda_c \sqrt{Q} > 1.5, F_{cr} = \left[\frac{0.877}{\lambda_c^2} \right] F_y \quad (3)$$

$$\text{where } \lambda_c = \frac{KL}{r} \sqrt{\frac{F_y}{E}} \quad (4)$$

Angle sections should also be checked for torsional and flexural-torsional buckling as follows:

$$\text{For } \lambda_e \sqrt{Q} < 1.5, F_{cr} = Q(0.658^{\lambda_e^2}) F_y \quad (5)$$

$$\text{For } \lambda_e \sqrt{Q} > 1.5, F_{cr} = \left[\frac{0.877}{\lambda_e^2} \right] F_y \quad (6)$$

$$\text{where } \lambda_e = \sqrt{\frac{F_y}{F_e}} \quad (7)$$

in which F_e = critical torsional or flexural-torsional elastic buckling stress. If the width-to-thickness ratio does not exceed $76/\sqrt{F_y}$ (where F_y is the yield strength in ksi), the angle is non-compact and the value of Q is 1.0 for angle without lips. If b/t ratio exceeds $76/\sqrt{F_y}$, the angle is slender, and the value of Q for unstiffened angles is determined as follows:

When $76/\sqrt{F_y} < b/t < 155/\sqrt{F_y}$:

$$Q = 1.340 - 0.00447 (b/t) \sqrt{F_y} \quad (8)$$

When $b/t > 155/\sqrt{F_y}$:

$$Q = 15\,500/[F_y(b/t)^2] \quad (9)$$

(b) AISI specification for cold-formed angles

This is an allowable stress specification. However, in this paper, the factor of safety is taken as 1.0.

$$\text{For } F_{\min} > 0.5 F_y, F_{cr} = F_y(1 - F_y/4F_{\min}) \quad (10)$$

$$\text{For } F_{\min} < 0.5 F_y, F_{cr} = F_{\min} \quad (11)$$

F_{\min} is the least of the elastic flexural, torsional, and torsional-flexural buckling stress. For single angle sections with unstiffened flanges, F_{cr} shall be taken as the smaller of F_{cr} calculated from Eq. (10) or (11) and F_{cr} given by Eq. (12).

$$F_{cr} = \frac{\pi^2 E}{25.69(w/t)^2} \quad (12)$$

(c) ASCE Manual No. 52 - Recommendations for hot-rolled and cold-formed angles

(i) For $w/t < 80/\sqrt{F_y}$ (where F_y is the yield strength in ksi):

$$\text{If } KL/r < C_c, F_{cr} = \left[1 - \frac{1}{2} \left(\frac{KL/r}{C_c}\right)^2\right] F_y \quad (13)$$

$$\text{If } KL/r > C_c, F_{cr} = 286\,000/(KL/r)^2 \quad (14)$$

$$\text{where } C_c = \pi\sqrt{2E/F_y} \quad (15)$$

(ii) For $w/t > 80/\sqrt{F_y}$ (where F_y is the yield strength in ksi):

The values of $F_{y\text{eff}}$ given by Eq. (16) and (17) should be substituted for F_y in Eq. (13) and (15).

If $80/\sqrt{F_y} < w/t < 144/\sqrt{F_y}$:

$$F_{y\text{eff}} = \left[1.677 - 0.677 \frac{w/t}{(80/\sqrt{F_y})}\right] F_y \quad (16)$$

If $w/t > 144/\sqrt{F_y}$:

$$F_{y\text{eff}} = 9500/(w/t)^2 \quad (17)$$

(d) CAN/CSA-S37-M86 and CAN3-S16.1-M84 for hot-rolled angle members

These limit states design specifications use SSRC Column Curve 2 as the basic curve for determining the factored compressive resistance C_r of hot-rolled angles with b/t ratios not exceeding $\frac{200}{\sqrt{F_y}}$ (where F_y is the yield strength in MPa):

$$\text{For } 0 < \lambda < 0.15, C_r = \phi A F_y$$

$$\text{For } 0.15 < \lambda < 1.00, C_r = \phi A F_y [1.035 - 0.202\lambda - 0.222\lambda^2]$$

$$\text{For } 1.0 < \lambda < 2.00, \quad C_r = \phi A F_y [-0.111 + 0.636/\lambda + 0.087/\lambda^2] \quad (18)$$

$$\text{For } 2.0 < \lambda < 3.6, \quad C_r = \phi A F_y [0.009 + 0.877/\lambda^2]$$

$$\text{For } \lambda > 3.6, \quad C_r = \phi A F_y / \lambda^2$$

$$\text{where } \lambda = \frac{KL}{r} \sqrt{F_y/E} \quad (19)$$

If b/t ratio exceeds $\frac{200}{\sqrt{F_y}}$, singly symmetric angle sections with $t < 4.5$ mm

shall be designed according to CSA Standard CAN3-S136-M84 (cold-formed steel structural members); thicker sections must be designed by rational analysis.

(e) CAN3-S136-M84 for cold-formed angles

The factored compressive resistance

$$C_r = \phi A_e F_{cr} \quad (20)$$

where the compressive limit stress F_{cr} is obtained from Eq. (21) or (22), whichever is applicable:

$$\text{When } F_p (= 0.833 F_{\min}) > 0.5 F_y,$$

$$F_{cr} = F_y - F_y^2/4F_p \quad (21)$$

$$\text{When } F_p (= 0.833 F_{\min}) < 0.5 F_y,$$

$$F_{cr} = F_p \quad (22)$$

The factored compressive resistance of single angles is further limited as follows:

$$C_r = \frac{\phi(0.50)\pi^2EA}{12(1-\mu^2)(w/t)^2} \quad (23)$$

In Eq. (20) to (23), A , A_e , F_{\min} , w/t , ϕ and μ are as defined in the notation.

(f) Indian Standard IS:800-1984

This is an allowable stress specification. (In this paper the factor of safety is taken as 1.0.) The critical stress is calculated using the Merchant-Rankine formula. Width-to-thickness ratio (b/t ratio) is limited to $256/\sqrt{F_y}$ or 16, whichever is less (where F_y is the yield stress in MPa). If the b/t ratio exceeds this limit, the excess material shall be neglected in calculating the effective geometrical properties of the section.

$$F_{cr} = \frac{F_o F_y}{[(F_o)^{1.4} + (F_y)^{1.4}]^{1/1.4}} \quad (24)$$

where $F_o = \text{Euler critical stress} = \frac{\pi^2 E}{(KL/r)^2}$

(g) Standards Association of Australia AS:1250-1981

This is also an allowable stress specification. (In this paper, the factor of safety is taken as 1.0.) Critical stress is given by Eq. (25). Width-to-thickness ratio (b/t ratio) is limited to $208/\sqrt{F_y}$ (where F_y is the yield stress in MPa). When the value of b/t for any angle exceeds this limit, the critical stress is further limited to $0.833 F_y$.

$$F_{cr} = \left[\frac{F_y + (\eta+1)F_o}{2} - \sqrt{\left[\frac{F_y + (\eta+1)F_o}{2} \right]^2 - F_y F_o} \right] \quad (25)$$

where $\eta = 0.3(KL/100r)^2$

and $F_o = \text{Euler critical stress} = \pi^2 E / (KL/r)^2$

(h) Design Requirements for Built-up Angles

AISC and CAN3-S136-M84 specifications require the modification of the slenderness ratio for buckling about the built-up member axis. IS:800-1984 and AS:1250-1981 require a minimum of two interconnectors. Table 1 summarizes the requirements of various specifications regarding built-up angle compression members.

EXPERIMENTAL INVESTIGATIONS

The results of the following experimental investigations are included in this paper:

(a) Tests on Hot-rolled Angles

- (i) U.S. Bureau of Standards (1924):
Specimens with square ends (A1 to A10) - 10
Specimens with one bolt in each leg (D1 to E8) - 11
Specimens with two or more bolts in each leg (D11 to E32) - 37
- (ii) Ishida (1968):
Semi-killed high strength 'SHY' steel angle specimens:
75 x 75 x 6 mm size specimens (1A20 to C100 and 2A40 to S70) - 24
65 x 65 x 6 mm size specimens (D40 to 90) - 6
- (iii) Yokoo, Wakabayashi and Nonaka (1968):
90 x 90 x 7 mm size mild steel angle specimens (1020 to 1150) - 10
- (iv) Marsh (1971):
2 1/2 x 2 1/2 x 1/8 in. specimens (1 to 4) - length 24, 34, 64 and 74 in. - 4
2 1/2 x 2 1/2 x 3/16 in. specimens (5 to 8) - length 24, 34, 64 and 74 in. - 4
2 1/2 x 2 x 3/16 in. specimens (9 to 11) - length 24, 34, and 74 in. - 3
2 1/2 x 2 x 1/4 in. specimens (12 to 15) - length 24, 34, 64 and 74 in. - 4
2 1/2 x 1 1/2 x 3/16 in. specimens (16 to 19) - length 24, 34, 64 and 74 in. - 4

(v) Kennedy and Murty (1972):

Seventy-two hot-rolled angle struts, with both hinged and fixed end conditions were tested at the University of Windsor. To obtain a statistical average of the critical stress, three struts in each category were tested. Double angle struts had one intermediate connector at mid-length.

(vi) Short (1977):

Fourteen tests were carried out by Short on double angles arranged back to back (with 10 mm gap between them and connected together at 350 mm intervals) to investigate their buckling about the material axis (xx-axis), while thirteen tests were performed on double angles arranged back to back with 30 mm gap between them to investigate their buckling about the symmetric yy-axis.

(vii) Mueller and Erzurumlu (1983):

$3 \times 3 \times 1/4$ in. specimens - 4

(viii) Kitipornchai and Lee (1984):

The experimental program consisted of testing two series of pin-ended struts. For each strut size and length, two struts were prepared and tested to obtain an average failure load. A total of 42 angle struts were tested, comprising 14 single equal angle struts, 12 single unequal angle struts, 12 double equal angle struts, and 4 double unequal angle struts. Double angle struts had two intermediate connectors measuring 5 mm (gap) \times 25 mm \times leg length. For double unequal angle struts, long legs were connected.

(ix) Wilhoite (1986):

Details of seven post angles used in a full scale transmission tower test are given in Table 2.

(b) Tests on Cold-formed Angles(i) Chajes, Fang and Winter (1966):

Inelastic equal leg cold-formed angles - 6

(ii) Madugula, Prabhu, and Temple (1983):

$45 \times 45 \times 3$ mm specimens (S45-1 to 8) - 8

$65 \times 65 \times 4$ mm specimens (S65-1 to 8) - 8

COMPARISON OF EXPERIMENTAL AND CALCULATED FAILURE STRESSES

The experimental and calculated failure stresses for the test specimens described above are presented in Tables 3 and 4 for hot-rolled and cold-formed angles, respectively. The following comments apply to Tables 3 and 4:

(a) For U.S. Bureau of Standards test specimens, the following effective length factors are used:

(i) angles with square ends - no bolts: $K = 1/1.9$

(ii) angles with one bolt in each leg: $K = 1/1.3$

(iii) angles with two or more bolts in each leg: $K = 1/1.5$

(b) For double angle specimens S1 to S13 tested by Short (1977), the nominal slenderness ratio $(KL/r)_y$ was calculated from a radius of gyra-

tion based on a minimum separation of 8 mm between angles, although the bars as tested had a gap of 30 mm.

- (c) The calculated values for the test specimens by Marsh (1971) are based on the nominal yield stress of 44 ksi.
- (d) For hot-rolled angle test specimens having b/t ratio greater than $200/\sqrt{F_y}$ (where F_y is the yield stress in MPa) and thickness greater than 4.5 mm, failure stresses according to CAN/CSA-S37-M86 are not calculated.
- (e) The factor of safety is taken as 1.0 for failure stresses calculated from AISI, IS:800-1984 and SAA:AS 1250-1981.
- (f) For CAN/CSA-S37-M86 and CAN3-S136-M84, failure stress is obtained by dividing the factored compressive resistance C_r by the area of cross-section, i.e., resistance factor ϕ of 0.9 is included in the calculated values. If ϕ is taken as 1.0, the failure stresses will be 10/9 times the tabulated values.
- (g) The following double angle sections which did not satisfy the requirements of various specifications are treated as two single angles:
- (i) Double angle specimens which did not meet the requirements of ASCE Manual No. 52:
Short (1971): Specimens S1, 2, 3, 5, 6, 7, 9, 10 and 12.
Kitipornchai and Lee (1984): DAB.
 - (ii) Double angle specimens which did not meet the requirements of IS:800-1984:
Kennedy and Murty (1972): All double angle specimens.
Short (1977): S1, 2, 3, 5, 6, 7, 9, 10, 12 and 13.
Kitipornchai and Lee (1984): DAB.
 - (iii) Double angle specimens which did not meet the requirements of SAA:AS 1250-1981:
Kennedy and Murty (1972): All double angle specimens.
Short (1977): S1, 2, 3, 5, 6, 9, 10, 12 and 13.

CONCLUSIONS

A study of Tables 3 and 4 leads to the following general conclusions:

- (a) The failure stresses calculated according to ASCE Manual No. 52 are the highest and are the closest to the experimental failure stresses. (In a few cases, the calculated stresses even exceeded the experimental values.)
- (b) The stresses calculated according to AISC-LRFD and CAN3-S136-M84 are the lowest. *Safe conservative*
- (c) The requirements in some specifications regarding the maximum spacing and minimum number of interconnectors for double angle struts lead to unnecessarily conservative values.

ACKNOWLEDGEMENTS

The financial support for the preparation and presentation of the paper provided by the Natural Sciences and Engineering Research Council of

Canada under grant number All94 to the first author is gratefully acknowledged.

REFERENCES

1. American Institute of Steel Construction. "Load and Resistance Factor Design Specification for Structural Steel Buildings", Chicago, Illinois, September 1, 1986.
2. American Iron and Steel Institute. "Specification for the Design of Cold-formed Steel Structural Members", Washington, D.C., Draft Report, May 1986.
3. American Society of Civil Engineers. "Guide for Design of Steel Transmission Towers", Manual No. 52, New York, NY, Draft Revision, September 17, 1986.
4. Canadian Standards Association. "Antennas, Towers, and Antenna-Supporting Structures", CAN/CSA-S37-M86, Rexdale, Ontario, 1986.
5. Canadian Standards Association. "Cold-formed Steel Structural Members", CAN3-S136-M84, Rexdale, Ontario, 1984.
6. Canadian Standards Association. "Steel Structures for Buildings (Limit States Design)", CAN3-S16.1-M84, Rexdale, Ontario, 1984.
7. Chajes, A., Fang, P.J. and Winter, G. "Torsional-flexural Buckling, Elastic and Inelastic, of Cold-formed Thin-walled Columns", Research Bulletin 66-1, Dept. of Structural Engg., Cornell Univ., Ithaca, NY, 1966.
8. Indian Standards Institution. "Code of Practice for General Steel Construction", IS:800-1984, New Delhi, India, 1984.
9. Ishida, A. "Experimental Study on Column Carrying Capacity of 'SHY' Steel Angles", Yawata Technical Report No. 265, pp. 8564-8582 and pp. 8761-8763, Yawata Iron and Steel Co. Ltd., Tokyo, Japan, December 1968.
10. Kennedy, J.B. and Murty, M.K.S. "Buckling of Steel Angle and Tee Struts", Journal of the Structural Division, ASCE, Vol. 98, No. ST11, November 1972, pp. 2507-2522.
11. Kitipornchai, S. and Lee, H.W. "Inelastic Experiments on Angles and Tee Struts", Research Report No. CE54, Dept. of Civil Engg., Univ. of Queensland, St. Lucia, Australia.
12. Madugula, M.K.S., Prabhu, T.S. and Temple, M.C. "Ultimate Strength of Concentrically Loaded Cold-formed Angles", Canadian Journal of Civil Engineering, Vol. 10, No. 1, March 1983, pp. 60-68.
13. Marsh, C. "Buckling of Single Angles as Beams/Columns", Canadian Steel Industries Construction Council Project No. 712, 1971 (unpublished).
14. Mueller, W.H. and Erzurumlu, H. "Limit State Behaviour of Steel Angle Columns", Research Report of Civil-Structural Engg., Portland State University, Oregon, 1983.
15. Short, J. "The Buckling of Compound Members Consisting of Two Angles Stitch-bolted Together", Preliminary Report, Second International Colloquium on Stability of Steel Structures, Liege, April 1977, pp. 137-142.
16. Standards Association of Australia. "SAA Steel Structures Code", AS:1250-1981, North Sydney, NSW, Australia.
17. United States Bureau of Standards. "Results of Some Compression Tests of Structural Steel Angles", Technologic Papers of the Bureau of Standards, No. 218, Government Printing Office, Washington, D.C., 1924.

18. Wilhoite, G.M., Chairman, ASCE Task Committee on Updating Manual No. 52, private communication dated September 1, 1986.
19. Yokoo, Y., Wakabayashi, M. and Nonaka, T. "An Experimental Study on Buckling of Angles", Yawata Technical Report No. 265, pp. 8543-8563 and pp. 8759-8760, Yawata Iron and Steel Co. Ltd. Tokyo, Japan, December 1968.

TABLE 1

Built-up Angle Compression Members

Specification	Design Requirement
AISC-LRFD	<p>(a) $\frac{L}{r_{\min}}$ of component angle between fasteners } governing slenderness ratio of built-up member.</p> <p>(b) For buckling about built-up member axis producing shear forces in the connectors between individual angles, the slenderness ratio is modified as follows:</p> <p>(i) For snug-tight bolted connectors</p> $\left(\frac{KL}{r}\right)_m = \sqrt{\left(\frac{KL}{r}\right)_o^2 + \left(\frac{a}{r_{\min}}\right)^2}$ <p>(ii) For welded connectors and for fully tightened bolted connectors as required for slip-critical joints:</p> <p>With $\frac{a}{r_{\min}} > 50$:</p> $\left(\frac{KL}{r}\right)_m = \sqrt{\left(\frac{KL}{r}\right)_o^2 + \left(\frac{a}{r_{\min}} - 50\right)^2}$ <p>With $\frac{a}{r_{\min}} < 50$: $\left(\frac{KL}{r}\right)_m = \left(\frac{KL}{r}\right)_o$</p>
ASCE	<p>(a) $\frac{L}{r_{\min}}$ of component angle between stitch bolts } 0.75 times the governing slenderness ratio of the built-up angle member.</p> <p>(b) The maximum spacing of stitch bolts } 24 in.</p>
CAN/CSA-S37-M86 and CAN3-S16.1-M84	$\frac{L}{r_{\min}}$ of component angle between fasteners } slenderness ratio of built-up angle member.
CAN3-S136-M84	Modify slenderness ratio about built-up member axis.
	$\left(\frac{KL}{r}\right)_m = \sqrt{\left(\frac{KL}{r}\right)_o^2 + \left(\frac{a}{r_{\min}}\right)^2}$
IS:800-1984	<p>(a) $\frac{L}{r_{\min}}$ of component angles between fasteners } 0.6 times the governing slenderness ratio of built-up member or 40, whichever is less.</p> <p>(b) Min. no. of interconnectors = 2, equally spaced.</p>

SAA:AS 1250-1981

- (a) $\frac{L}{r_{\min}}$ of component angle between fasteners ≤ 0.6 times the governing slenderness ratio of built-up member or 50, whichever is less.
- (b) Min. no. of interconnectors = 2, equally spaced.

TABLE 2

Details of Post Angles - Full Scale Tower Test - Wilhoite (1986)

Specimen	Size (in)	KL/r	F _y (ksi)
1	3 1/2 x 3 1/2 x 1/4	84	55
2	3 x 3 x 1/4	78	58
3	5 x 5 x 5/16	76	57
4	4 x 4 x 1/4	76	61
6	5 x 5 x 3/8	81	56
7	4 x 4 x 1/4	70	52
8	4 x 4 x 1/4	45	52

TABLE 3 (follows Table 4)

TABLE 4

Comparison of Experimental and Calculated Failure Stresses for Cold-formed Angles

Test Specimen (1)	Experimental Failure Stress (ksi) (2)	Calculated failure stress (ksi) according to		
		AISI (F.S.=1.0) (3)	ASCE (4)	CAN3-S136-M84 ($\phi = 0.9$) (5)
(i) Chajes et al. (1966)				
A-I1	38.3	30.0	35.1	27.0
A-I2	38.3	34.5	39.3	31.9
A-I3	33.2	26.6	32.7	24.9
A-I4	33.2	26.5	32.4	24.6
A-I5	32.2	27.5	32.0	24.6
A-I6	22.5	24.5	26.3	22.7
(ii) Madugula et al. (1983)				
S45 - 1, 2	14.6	13.5	15.2	11.2
S45 - 3, 4	9.1	8.5	9.1	7.1
S45 - 5, 6	6.2	5.8	6.1	4.8
S45 - 7, 8	4.8	4.3	4.4	3.5
S65 - 1, 2	27.9	23.3	30.0	19.3
S65 - 3, 4	15.8	13.9	16.4	11.6
S65 - 5, 6	9.8	9.0	9.9	7.5
S65 - 7, 8	6.0	6.1	6.5	5.1

TABLE 3

Comparison of Experimental and Calculated Failure Stresses for Hot-rolled Angles

Test Specimen (1)	Experimental Failure Stress (ksi) (2)	Calculated failure stresses (ksi) according to				
		AISC-LRFD ($\phi=1.0$) (3)	ASCE (4)	CAN/CSA-S37-M86 ($\phi=0.9$) (5)	IS:800-1984 (F.S.=1.0) (6)	SAA:AS 1250-1981 (F.S.=1.0) (7)
(1) U.S. Bureau of Standards						
A1	40.0	24.7	33.8	---	32.4	31.1
A2	26.8	20.2	24.6	---	19.3	18.6
A3	10.75	10.8	11.5	---	10.7	9.3
A4	37.0	30.9	36.0	31.7	35.9	35.9
A5	36.0	30.2	33.7	27.9	32.0	32.8
A6	32.5	26.9	29.9	22.9	25.5	26.2
A7	25.0	21.1	24.5	16.7	19.2	18.4
A8	16.58	15.4	16.5	12.3	14.2	12.8
A9	10.75	10.8	11.5	9.5	10.7	9.2
A10	9.0	7.9	8.4	7.4	8.2	6.9
D1	13.82	11.3	12.1	---	11.2	9.7
D2	10.98	7.3	7.7	---	7.6	6.4
D3	11.62	11.3	12.1	9.8	11.2	9.7
D4	9.76	7.3	7.7	6.8	7.6	6.4
D5	13.7	11.3	12.1	9.8	11.1	9.6
D9	9.0	7.3	7.7	6.8	7.7	6.4
D10	6.13	5.0	5.4	4.8	5.5	4.5
E1	5.96	7.3	7.7	---	7.6	6.3
E2	4.53	5.0	5.4	---	5.5	4.4
E3	5.0	3.7	3.9	---	4.1	3.3
E8	3.93	5.0	5.4	4.8	5.5	4.4
D11	36.8	24.5	31.9	---	29.0	30.2
D12	26.05	21.3	25.8	---	20.5	20.0
D13	32.4	29.4	31.8	25.4	28.7	29.7
D14	29.9	22.2	25.7	17.9	20.3	19.8
D15	29.9	22.0	25.5	17.8	20.2	19.6
D16	22.7	15.1	16.1	12.1	14.0	12.5
D18	25.0	22.6	26.2	18.1	20.6	20.2

	(1)	(2)	(3)	(4)	(5)	(6)	(7)
D19		17.7	15.1	16.1	12.2	14.1	12.6
D20		19.9	15.1	16.1	12.2	14.0	12.6
D21		15.8	15.1	16.1	12.3	14.1	12.7
D22		41.0	25.1	35.6	---	35.8	31.1
D23		35.5	30.7	35.5	30.8	35.2	35.4
D24		36.0	32.2	34.9	30.3	34.7	34.8
D25		35.3	29.0	31.4	25.1	28.3	29.3
D26		35.5	34.0	35.6	30.9	35.4	35.5
D28		33.8	29.5	31.9	25.5	28.7	29.8
D31		36.0	32.4	36.7	31.8	36.4	36.6
D33		34.0	30.2	32.8	26.1	29.4	30.7
D34		38.0	33.8	36.5	31.7	36.2	36.4
D35		34.9	30.1	32.6	26.0	29.3	30.5
D36		41.8	36.3	37.4	32.3	37.0	37.3
D37		34.1	30.6	33.3	26.4	29.8	31.1
E10		14.25	14.8	16.1	---	13.8	12.4
E14		33.5	23.9	31.0	---	28.2	29.1
E17		30.0	28.8	31.1	24.9	28.2	29.1
E18		31.6	24.7	34.4	---	34.8	30.2
E19		22.8	21.0	25.2	---	20.2	19.7
E20		20.0	15.0	16.1	12.1	13.9	12.5
E21		37.5	24.6	34.4	---	34.4	29.9
E25		31.0	33.1	34.6	30.1	34.4	34.5
E26		30.2	24.1	30.9	---	28.4	29.4
E27		28.3	30.5	35.3	30.6	35.1	35.2
E28		27.9	29.3	31.7	25.3	28.6	29.6
E29		27.75	22.2	25.6	17.9	20.3	19.8
E30		31.7	34.0	35.7	30.9	35.4	35.5
E31		35.0	29.5	32.0	25.5	28.8	29.9
E32		28.82	29.5	32.0	25.5	28.8	29.9
(11) <u>Ishida (1968)</u>							
1A 20		57.2	46.4	62.5	---	62.5	53.2
40		56.3	44.9	58.5	---	55.6	53.2
50		50.6	44.2	55.5	---	50.2	53.2
60		44.7	43.8	51.9	---	44.3	50.5
70		40.4	40.2	48.1	---	38.9	43.7

	(1)	(2)	(3)	(4)	(5)	(6)	(7)
	80	37.2	35.6	42.9	---	33.5	36.3
	100	27.6	26.5	28.6	---	24.8	24.9
B	40	66.8	45.5	62.0	---	60.3	62.5
	50	60.5	45.2	58.6	---	52.3	62.5
	60	53.2	44.5	54.4	--	44.2	56.6
	70	45.2	41.5	49.3	---	36.5	46.8
	80	45.1	36.5	43.7	---	30.5	38.1
	100	30.0	26.7	28.6	---	21.6	25.7
C	40	54.4	45.4	60.5	---	57.3	55.2
	50	47.2	44.7	57.3	---	51.5	55.2
	60	42.9	44.2	53.4	---	45.3	51.9
	70	42.9	40.6	49.1	---	39.5	44.5
	80	37.7	35.8	43.6	---	33.9	36.7
	90	36.9	31.1	37.3	---	29.0	30.3
	100	27.3	26.5	28.6	---	25.0	25.1
D	40	58.5	46.9	59.1	---	56.1	53.8
	50	56.6	46.9	56.6	---	51.0	54.4
	60	48.1	45.5	52.8	---	44.9	51.3
	70	48.9	40.8	48.2	---	39.0	43.8
	80	40.9	35.9	43.0	---	33.5	36.3
	90	37.2	31.2	37.1	---	28.8	30.0
2A	40	48.1	42.3	54.2	---	51.9	48.9
	80	36.0	34.0	40.7	---	32.1	34.6
S	60	38.4	33.0	36.9	---	33.6	35.5
	70	38.1	31.5	35.0	---	30.5	32.3
(111)	<u>Yokoo et al. (1968)</u>						
	1020	42.1	34.7	43.5	---	43.5	36.7
	1040	42.1	34.0	41.6	---	40.5	36.7
	1060	40.9	33.6	38.4	---	34.7	36.7
	1070	41.6	32.2	36.3	---	31.3	33.5
	1080	37.6	29.5	33.9	---	28.0	29.4
	1090	33.3	26.7	31.2	---	24.8	25.4
	1100	31.4	23.8	28.2	---	21.9	21.7
	1110	27.2	21.1	24.9	---	19.3	18.6
	1130	18.9	15.9	16.9	---	15.1	13.9
	1150	14.2	11.9	12.7	---	12.0	10.7

	(1)	(2)	(3)	(4)	(5)	(6)	(7)
(iv) <u>Marsh (1971)</u>							
1	42.0	20.6	29.9	---	32.8	36.7	
2	35.3	20.3	28.0	---	23.8	34.2	
3	17.7	15.7	18.3	---	9.2	14.3	
4	13.6	12.3	13.1	---	7.0	10.9	
5	44.1	31.9	40.2	---	38.1	36.7	
6	35.1	31.3	36.4	---	31.5	33.7	
7	16.3	15.7	16.8	---	15.0	13.8	
8	12.8	11.8	12.5	---	11.9	10.5	
9	51.7	34.8	39.1	---	36.0	36.7	
10	39.6	29.1	34.1	---	28.2	29.8	
11	9.9	9.1	9.7	---	9.5	8.2	
12	40.2	36.3	38.9	31.5	35.7	37.9	
13	37.3	29.9	33.8	25.1	27.9	29.3	
14	13.1	11.7	12.4	10.5	11.8	10.4	
15	9.0	8.8	9.4	8.3	9.2	8.0	
16	28.1	30.7	35.6	---	30.3	32.3	
17	22.4	22.7	27.1	---	21.0	20.6	
18	6.8	7.1	7.6	---	7.6	6.5	
19	5.0	5.3	5.7	---	5.8	4.9	
(v) <u>Kennedy and Murty (1972)</u>							
SH1 - 1, 2, 3	33.1	27.5	32.3	---	23.0	29.4	
SH2 - 1, 2, 3	39.9	31.8	38.2	---	29.6	31.7	
SH3 - 1, 2, 3	37.5	23.8	31.2	---	23.3	36.3	
SH4 - 1, 2, 3	42.5	34.4	41.1	---	31.8	38.8	
SH5 - 1, 2, 3	40.7	36.4	42.4	---	34.5	38.5	
SH6 - 1, 2, 3	45.3	36.8	44.6	---	38.2	42.9	
SF1 - 1, 2, 3	44.3	34.4	41.4	---	33.1	39.6	
SF2 - 1, 2, 3	36.6	27.2	37.7	---	32.4	37.6	
SF3 - 1, 2, 3	42.9	37.8	41.6	32.5	36.3	40.1	
SF4 - 1, 2, 3	48.0	36.2	47.7	---	43.9	44.8	
SF5 - 1, 2, 3	53.2	42.0	53.9	---	51.1	49.1	
SF6 - 1, 2, 3	38.1	24.6	35.1	---	41.5	40.2	
DH1 - 1, 2, 3	32.4	22.2	32.1	---	13.0	11.8	
DH2 - 1, 2, 3	34.4	24.8	33.8	---	16.2	15.0	
DH3 - 1, 2, 3	38.0	27.3	36.9	26.2	15.7	14.7	

	(1)	(2)	(3)	(4)	(5)	(6)	(7)
DH4 - 1, 2, 3	41.6	41.6	32.5	41.9	---	22.0	22.1
DH5 - 1, 2, 3	46.1	46.1	37.9	47.2	---	28.6	30.6
DH6 - 1, 2, 3	40.0	40.0	23.3	35.4	---	29.4	37.8
DF1 - 1, 2, 3	43.1	43.1	31.0	44.5	---	32.8	36.0
DF2 - 1, 2, 3	36.5	36.5	25.6	40.4	---	33.9	36.3
DF3 - 1, 2, 3	41.0	41.0	35.2	43.7	36.9	34.7	37.9
DF4 - 1, 2, 3	45.4	45.4	34.0	49.9	---	42.9	43.5
DF5 - 1, 2, 3	53.2	53.2	40.2	55.2	---	49.8	47.6
DF6 - 1, 2, 3	42.1	42.1	23.8	36.8	---	46.5	43.1
(v1) Short (1977)							
A 1x	14.5	14.5	18.6	19.9	15.0	17.3	16.2
2y	13.6	13.6	18.5	19.9	---	17.1	16.1
3x	16.2	16.2	18.6	19.9	---	18.5	17.7
4y	16.8	16.8	18.7	19.9	---	18.5	17.7
5z	17.3	17.3	18.7	19.9	---	18.6	17.5
6x	23.1	23.1	25.1	30.6	---	24.3	24.5
7y	19.4	19.4	26.3	28.6	---	24.5	24.7
8z	20.3	20.3	25.5	30.3	---	24.3	24.2
9x	25.4	25.4	32.0	41.5	---	32.6	35.2
10y	25.2	25.2	35.0	42.2	---	33.0	35.7
11z	22.6	22.6	33.3	39.7	---	32.8	35.1
12x	31.2	31.2	37.7	49.9	---	43.0	48.6
13y	31.0	31.0	40.6	51.1	---	43.8	49.7
14z	28.9	28.9	37.3	46.2	---	42.3	47.2
S 1	18.0	18.0	10.6	9.5	---	9.6	8.6
2	18.7	18.7	13.9	9.5	---	9.6	8.6
3	20.5	20.5	15.7	9.5	---	9.6	8.6
4	23.8	23.8	17.2	19.9	---	18.3	17.5
5	22.6	22.6	15.2	13.7	20.6	13.2	12.1
6	23.2	23.2	20.0	13.7	---	13.4	12.3
7	25.2	25.2	22.6	13.7	20.7	13.3	24.0
8	26.7	26.7	24.6	30.6	---	24.0	24.2
9	32.6	32.6	23.7	21.3	---	19.3	18.6
10	36.4	36.4	28.2	21.3	-	19.3	18.6
11	35.5	35.5	31.9	40.9	---	32.2	34.8
12	39.5	39.5	35.0	37.3	37.4	28.9	30.4

	(1)	(2)	(3)	(4)	(5)	(6)	(7)
13		40.2	35.4	46.3	36.2	28.4	29.9
(vii) <u>Mueller and Erzurumlu (1983)</u>							
S2 HH 36-2		9.7	6.8	7.2	---	7.4	6.5
S1 HH 50-1		30.6	19.4	20.7	---	18.7	17.9
S1 HH 36-2		34.7	19.4	20.7	---	18.6	17.7
S0 BB 50-1		27.8	11.6	12.4	---	12.1	11.0
(viii) <u>Kitipornchai and Lee (1984)</u>							
SA1 - a, b		39.5	31.9	40.9	---	39.0	37.1
SA2 - a, b		41.0	31.7	39.6	---	36.7	37.1
SA3 - a, b		35.2	28.3	36.0	---	35.2	36.0
SA4 - a, b		32.3	28.1	34.4	---	31.9	34.3
SA5 - a, b		31.1	27.9	33.2	---	29.7	31.9
SA6 - a, b		33.0	26.7	32.8	---	30.6	32.2
SA7 - a, b		31.6	26.6	32.1	---	29.3	30.8
SA8 - a, b		38.6	32.0	36.2	---	32.8	34.9
SA9 - a, b		36.9	27.7	32.4	---	27.0	28.1
SA10 - a, b		35.3	29.8	32.4	---	31.3	33.8
SA11 - a, b		30.4	25.6	29.0	---	25.3	26.3
SA12 - a, b		36.5	28.8	31.5	---	29.8	31.9
SA13 - a, b		25.1	24.7	28.2	---	24.1	24.9
DA1 - a, b		33.0	26.1	32.7	---	30.5	32.4
DA2 - a, b		37.0	30.6	35.2	29.0	33.1	34.3
DA3 - a, b		38.0	29.1	36.0	---	33.0	34.0
DA4 - a, b		35.2	24.5	31.1	---	29.4	30.8
DA5 - a, b		35.2	27.1	33.5	---	30.8	31.5
DA6 - a, b		36.1	24.8	32.5	---	32.6	31.4
DA7 - a, b		35.2	26.7	35.1	27.1	30.1	32.0
DA8 - a, b		30.9	23.5	22.5	22.3	11.7	25.6
(ix) <u>Wilhoite (1986)</u>							
1		32.2	29.3	35.5	---	26.2	30.2
2		37.5	33.4	40.1	---	31.6	34.5
3		34.9	29.1	35.7	---	24.6	35.4
4		36.8	29.8	36.3	---	23.9	36.6
6		37.9	31.0	37.6	---	29.0	32.1
7		36.4	28.3	35.9	---	28.0	37.1
8		40.2	29.0	40.9	---	40.9	43.3

Murray C. Temple and Joo-Chai Tan
Department of Civil Engineering, University of Windsor
Windsor, Ontario N9B 3P4

INTRODUCTION

Double angles are frequently used as web members in trusses and as bracing members. Basically one of three configurations can be chosen if double angles are used and these are, as illustrated in Fig. 1, back-to-back, starred and boxed. The back-to-back configuration is used most frequently.

Each type of double angle has its advantages and disadvantages. Bolted connections in the back-to-back configuration make effective use of bolts since they are used in double shear whereas bolts in starred angles are in single shear. The only practical method of making a connection with boxed angles is by welding. Boxed angles make effective use of the material as the minimum moment of inertia is much greater than when the same angles are used in the back-to-back configuration. In an atmosphere where cleanliness is important, starred angles are advantageous since all surfaces are accessible for maintenance.

The back-to-back arrangement can be used with different types of chord members and hence the spacing between angles varies considerably. If the chord of the truss is a tee section, then the spacing between angles is relatively small. In other cases, however, the chord members consist of structural tubing which results in a spacing between angles that is relatively large and hence these double angles can be regarded as "widely spaced" angles. Fig. 2 illustrates widely spaced angles in the back-to-back configuration that are being used as web members in a truss.

Recent research (6, 7) on the interconnection of starred and boxed angle compression members indicates that two interconnectors, one at each of the third points, should be used in these double angle members to make them act as an integral unit. The Canadian Standard (4) and American Specification (1) require only one interconnector. Thus some concern has been expressed with regard to the interconnection of widely spaced back-to-back angles.

In this research project 44 widely spaced angles were tested. Two different column lengths were used but the angles were the same size. Most of the columns were tested with pinned ends but a few tests were conducted where the columns were pinned about the y axis and fixed about the x axis. The coordinate axes are shown in Fig. 3.

Four parameters were studied, which are:

- (1) the number of interconnectors,
- (2) the back-to-back spacing of angles,
- (3) the thickness of the interconnectors, and
- (4) the weld pattern used to connect the interconnectors to the angle.

(a) CSA Standard S16.1 (4). One of the reasons for conducting this research was to determine whether or not the requirements for the interconnection of double angles as contained in CSA S16.1 are adequate for the back-to-back arrangement. Clause 18.1.3 states that "Unless closer spacing is required for transfer of load or for sealing inaccessible surfaces the longitudinal spacing, in line, between intermediate bolts or clear longitudinal spacing between intermittent welds in built-up compression members shall not exceed the following, as applicable: (a) for compression members composed of two or more rolled shapes in contact or separated from one another by intermittent fillers, the slenderness ratio of any shape between points of interconnection shall not exceed the slenderness ratio of the built-up member. The least radius of gyration of each component part shall be used in computing the slenderness ratio of that part between points of interconnection with other component parts;"

The preceding can be expressed as

$$\frac{K_1 d}{r_z} \leq \frac{K_c L}{r_x} \quad [1]$$

where K_1 , K_c = the effective length factor of an individual angle and of the built-up section, respectively; d = distance between points of interconnection; r_z , r_x = minimum radius of gyration of an individual angle and of the built-up section, respectively (see Fig. 3); and L = the length of the built-up member. The geometric properties of the double angle back-to-back compression members made from equal leg angles are such that the mean value of the ratio $r_x/r_z = 1.56$ with a standard deviation of 0.01. These values were computed using the data for all the back-to-back double angles made from equal leg angles listed in the Canadian Institute of Steel Construction's Handbook of Steel Construction (3). With this relationship the minimum number of interconnectors required by CSA S16.1 can be calculated. Substituting $r_x/r_z = 1.56$ and $L/d = n+1$, where n = the number of interconnectors, into Eq. [1] results in a value of n of 0.56. Thus only one interconnector is required for a double angle back-to-back compression member made from equal leg angles.

(b) AISC Specification (1). This specification has the same requirements as CSA S16.1.

(c) DIN 4114 (5). There are two criteria used in this standard to determine the spacing of interconnectors. These are

$$\frac{d}{r_z} < 50 \quad [2]$$

or a minimum of two interconnectors at the third points, whichever gives the smallest spacing.

(d) BS 5950 (2). This standard has two requirements for the spacing of interconnectors which are

$$\frac{d}{r_z} < 50 \quad [3]$$

$$\frac{1.4d}{r_z} < \frac{K_c L}{r_x} \quad [4]$$

The minimum number of interconnectors, in addition to the end connectors, is two, so that the member is divided into at least three bays of approximately equal length. The interconnectors should be placed opposite each other at points of interconnection so that they form a cruciform, but this does not seem to be applicable to widely spaced angles.

(e) Example. Consider a back-to-back double angle compression member 96.0 in. long which consists of two 2 1/2 x 2 1/2 x 5/16 in. angles. The number of interconnectors required by each standard is:

(i) CSA S16.1 and the AISC Specification require only one interconnector, and

(ii) DIN 4114 and BS 5950 require three interconnectors.

If the length of the same member is reduced to 48.5 in. the number of interconnectors required by each standard is

(i) CSA S16.1 and AISC Specification still require only one interconnector, and

(ii) DIN 4114 and BS 5950 require two interconnectors.

(f) Interconnection of Double Angles With Fixed Ends About the Weak Axis. The interconnection requirements for double angles pinned about the y axis and fixed about the x axis were determined in accordance with CSA S16.1. Using Eq. [1] and a K_c of 0.65, as recommended by the CISC Handbook (3) as an approximation of the ideal fixed ended conditions, results in a requirement of two interconnectors for any back-to-back angle made from equal leg angles.

(g) Force and Moment Requirements in the Interconnector. Standards and specifications generally state force and/or moment requirements for "lacing" and "battens". Due to the arrangement and spacing of angles in a widely spaced double angle compression member it is unlikely that buckling will occur about the y axis which would be similar to buckling of a battened column, in which case the interconnector would behave like a batten. It is more likely that buckling will occur about the x-axis which is an Euler type of buckling. Thus the stitching on double angles does not, in general, behave as lacing or battens and might more correctly be termed an interconnector. Present practice is to use an interconnector of manageable proportions which is welded with a fillet weld to the angles.

EXPERIMENTAL PROGRAM

The experimental investigation consisted of tests on "intermediate length" and "slender" widely spaced double angles. Eighteen intermediate

length and 26 slender columns were tested of which 15 intermediate length and 23 slender columns were tested with pinned ends. The other six specimens, of which three were of intermediate length and three slender, were tested with end conditions which were pinned about the y axis and fixed about the x axis (see Fig. 3).

In order to reduce the number of variables the same size angles, $2\frac{1}{2} \times 2\frac{1}{2} \times 5/16$ in., were used for all tests. The length of the specimens were either 96 or 48.5 in. The back-to-back separation between angles was either 3 or 5 in., the outer dimensions of the structural tubing used to represent the upper and lower chords of the truss. The number of interconnectors was varied from zero to two. The interconnectors were 2 in. wide with a thickness of either $5/32$ or $3/8$ in. and a length to suit the back-to-back spacing of the angles. It is not suggested that the $5/32$ in. interconnector is a practical interconnector but the small thickness was selected as some concern was expressed as to whether or not the strains in a thicker interconnector would be large enough to be measured. The $5/32$ in. thick interconnectors were welded to the angles with a 0.1 in. weld while a $3/16$ in. weld was used with the $3/8$ in. thick interconnector. Most of the interconnectors were welded to the angles on three sides, a normal weld pattern, as shown in Fig. 4(a), but in a few cases the interconnectors were welded to the angles with welds on the inside only, a special weld pattern, as shown in Fig. 4(b). Strain gauges were attached to both faces of the interconnectors in order to determine the axial forces and bending moments in the interconnectors. Three different combinations of thickness of interconnector and weld pattern were used and these will be designated as follows:

(a) Type A - a $5/32$ in. thick interconnector with a normal weld pattern (see Fig. 4(a)).

(b) Type B - a $3/8$ in. thick interconnector with a normal weld pattern (see Fig. 4(a)), and

(c) Type C - a $3/8$ in. thick interconnector with a special weld pattern (see Fig. 4(b)).

Designation of Specimens. Each test specimen will be designated by a test series number. For example, 96.0B2.5.1 indicates that the column has a length of 96.0 in., had two type B interconnectors, there was a 5 in. separation between angles, and the last digit indicates that this was the first specimen of this type. In the case of 96.0SB1.3.1 the "S" indicates that the specimen was tested with special end conditions which were fixed about the x axis and pinned about the y axis (see Fig. 3).

Preparation of Specimens. The specimens in this study were fabricated from $2\frac{1}{2} \times 2\frac{1}{2} \times 5/16$ in. steel angles made from G40.21-M300W steel (44 ksi yield). The ends of the angles were welded to 6 in. long pieces of structural tubing made from G40.21-M350W steel (50 ksi yield). With the large dimension of the structural tubing placed horizontally a 5 in. separation between angles was obtained. With the large dimension vertical a 3 in. separation was achieved. The outer face of each piece of structural tubing contained two holes which were used to fasten the specimen to the knife edges. The initial out-of-straightness of each 96.0 in. specimen was measured at the mid-height and the quarter points prior to each test.

Loading System. Each strut was tested using the set-up shown in Fig. 5. The load was applied at the base of the column by means of a 100 kip capacity mechanical jack. The jack was placed in a frame which allowed the top of the jack to move freely in the vertical direction but prevented rotation of the ends of the specimen. The magnitude of the load was determined using a load cell. The strains in the interconnector were determined by using a strain indicator. The lateral displacements of each of the angles in both the x and y directions were determined with dial gauges located at mid-height of the specimen as shown in Fig. 6.

The regular end conditions, which are pinned-pinned, were obtained in the laboratory by using double knife edges. The knife edges allowed the column to rotate freely about each of the principal axes. The knife edges were arranged in such a manner that the effective length of the specimens about each of the perpendicular axes is the same. The double knife edges are illustrated in Fig. 7.

The special end conditions, fixed about the x axis and pinned about the y axis, were obtained by using a single knife edge.

RESULTS

The results for the 44 specimens are summarized in Tables 1 and 2. The factored compressive resistances were calculated in accordance with Clause 13.3.1 of CAN3-S16.1-M84 (4). The yield stress and modulus of elasticity, as determined from standard tensile tests, were taken as 49.3 and 29,560 ksi, respectively. The performance factor was taken as 1.0.

96.0 in. Specimens

These specimens, with a slenderness ratio of 126, can be classified as slender columns. The upper and lower limits of the slenderness ratio for slender columns for G40.21-M300W steel were given in a former standard as 200 and 96.1, respectively.

Zero Interconnectors. Since the individual angles are not interconnected, except at the ends, it can be assumed that each angle acts independently. The Euler buckling load for an individual angle when it buckles about the z axis (see Fig. 3) is 11.1 kips and hence 22.2 kips for both angles in the back-to-back double angle compression member. The Euler load for buckling about the minor principal axis of the combined cross section, the x axis, is 53.8 kips. The compressive resistance calculated in accordance with CSA S16.1, if the section met the interconnections requirements, is 44.7 kips. The experimental failure loads for the three specimens ranged from 40.9 to 42.9 kips, as listed in Table 1. Thus, as expected, the angles are neither pinned to the ends nor does the cross section act as an integral unit. The average failure load was 95% of the failure load as computed in accordance with CSA S16.1, but is only 79% of the Euler load.

The failure mode of the specimens was basically one of flexure about both the x and y axis, which is termed a "combined" failure. At failure the deflection in the y direction was about four times that in the x direction.

The results indicate that at least one interconnector, the number required by CSA S16.1, must be used.

One interconnector. With a back-to-back separation of 5 in. and one Type A interconnector, two of the three specimens had failure loads less than that specified by the standard. With one Type B interconnector, however, all three specimens had loads greater than that specified by the standard. With one Type B interconnector and a 3 in. separation, all failure loads were once again greater than that specified by the standard and were similar in magnitude to those obtained with a 5 in. separation.

In order to determine the effect of the weld pattern, five specimens were tested with a Type C interconnector. All failure loads were greater than that specified by CSA S16.1 and were of similar magnitude to those obtained with specimens which contained the normal weld pattern. Since this weld pattern does not offer significant rotational restraint to the angles, the conservative approach would be to avoid this weld pattern.

The double angles with double knife edges behaved consistently and buckled about the x axis, the weak axis of the entire cross section.

As shown at the end of Table 1, three specimens were tested with special end conditions, that is, fixed about the x axis and pinned about the y axis. Theoretically the specimens should have failed by buckling about the y axis at a load of 89.1 kips. In all cases the failure loads were greater than that specified but the failure mode was one of buckling about both the x and y axes. The failure load of 89.1 kips was calculated using an effective length about the x axis equal to 0.65 times the centre-to-centre distance between the structural tubes. Although CSA S16.1 requires two interconnectors for these columns only one was used in the tests and that seemed to be adequate.

Two Interconnectors. Three specimens with two Type A interconnectors and a 5 in. separation were tested. All had failure loads greater than that specified by CSA S16.1. With two Type B interconnectors and the same separation the failure loads were essentially equal to or greater than that specified. The average failure load of specimens with two interconnectors was essentially the same as that of similar specimens with one interconnector.

The failure mode was one of buckling about the x axis.

48.5 in. Specimens

These columns, which had a slenderness ratio of 64, can be classed as intermediate length columns since in a previous standard the upper and lower limits for intermediate columns made from G40.21-M300W steel were given as 96.1 and 20, respectively.

The results for these columns are given in Table 2. The failure loads of all specimens, except those with zero interconnectors, were greater than those specified in CSA S16.1. In these tests only the thicker interconnector, 3/8 in., was used because of experience gained from testing the slender columns with a 5/32 in. interconnector. Once again, changing the back-to-back separation from 3 to 5 in. or changing the number of interconnectors from one to two did not significantly effect the failure loads. The three specimens with a Type C interconnector and the special weld pattern had failure loads similar to

those specimens which used the regular weld pattern to weld the interconnectors to the angles.

The specimens with the special end conditions had failure loads equal to or greater than that specified in CSA S16.1.

The failure mode of the 48.5 in. specimens was the same as for the 96.0 in. specimens. With zero interconnectors and with the special end conditions, the failure mode involved buckling about both the x and y axis while specimens with one or more interconnectors failed by buckling about the x axis, the weak axis of the composite cross section.

Forces and Moments in Interconnectors

The strains measured in the interconnectors indicates that forces and moments are very small. The largest force of 0.9 kips and moment of 3.5 in.-kip were measured in Type C interconnectors but not in the same specimen.

CONCLUSIONS

The following conclusions can be made based on the preceding work:

(a) There is a great variation with regard to the design of the interconnectors for the back-to-back double angle compression members between North American and European standards.

(b) To satisfy the requirements of CSA S16.1 and the AISC Specification, only one interconnector is required at mid-height of any back-to-back double angle made from equal leg angles.

(c) Struts with zero interconnectors had a failure mode which involved buckling about both the x and y axes. Columns with one or more interconnectors consistently failed by buckling about the x axis, the weak axis of the composite cross section.

(d) Columns with one or more interconnectors had a failure load which is at least equal to and in most cases greater than the compressive resistance specified by CSA S16.1.

(e) Axial forces and moments in the interconnectors are very small.

(f) The weld pattern used to weld the interconnectors to the angles, whether welded on three sides or the inside only, did not affect the failure load. Conservatively, however, it might be best to use a normal weld pattern of weld on three sides of the interconnector.

(g) For back-to-back double angle compression members made from equal leg angles, only one interconnector at mid-height is required.

ACKNOWLEDGEMENTS

The authors would like to express their appreciation to the Natural Sciences and Engineering Research Council of Canada for the financial support provided for this research.

REFERENCES

1. American Institute of Steel Construction, Specification for the Design, Fabrication and Erection of Structural Steel for Buildings, Chicago, IL, November 1978.
2. British Standards Institution, Code of Practice for the Design of Simple and Continuous Construction for Hot-Rolled Sections, British Standard BS 5950-1985, British Standard Institution, London, 1985.
3. Canadian Institute of Steel Construction, Handbook of Steel Construction, Canadian Institute of Steel Construction, Willowdale, Ontario, 1985.
4. Canadian Standards Association, Steel Structures for Buildings (Limit States Design), Canadian Standards Association, 178 Rexdale Blvd., Rexdale, Ontario, CSA Standard CAN3-S16.1-M84, 1984.
5. Deutscher Normenausschuss, DIN 4114, German Buckling Specifications, Beuth-Vertrieb G.m.b.H., Berlin and Cologne, July 1952 (J. Jones and T.V. Galambos, trans.), Column Research Council, July 1957.
6. Temple, M.C., McCloskey, D.C. and Calabrese, J.M., "The Interconnection of Boxed Angle Compression Members", Proceedings of 1986 Annual Technical Session, Structural Stability Research Council, April 15-16, 1986, Washington, D.C.
7. Temple, M.C., Schepers, J.A. and Kennedy, D.J.L.K., "The Interconnection of Starred Angle Compression Members", Canadian Journal of Civil Engineering, Vol. 13, No. 6, December 1986.

TABLE 1. - RESULTS FOR 96.0 IN. SPECIMENS

TEST NUMBER	ACTUAL FACTORED COMPRESSIVE RESISTANCE, CSA S16.1 $C_{r,a}$ (kips)	EXPERIMENTAL FAILURE LOAD P_f (kips)	FAILURE MODE	$P_f/C_{r,a}$ (%)
96.OA0.5.1	44.7	42.9	Combined	96
96.OA0.5.2	44.7	42.9	Combined	96
96.OA0.5.3	44.7	40.9	Combined	92
96.OA1.5.1	44.7	42.0	x axis	94
96.OA1.5.2	44.7	46.1	x axis	103
96.OA1.5.3	44.7	44.1	x axis	99
96.OA2.5.1	44.7	49.9	x axis	112
96.OA2.5.2	44.7	49.9	x axis	112
96.OA2.5.3	44.7	47.0	x axis	105
96.OB1.5.1	44.7	51.9	x axis	116
96.OB1.5.2	44.7	51.0	x axis	116
96.OB1.5.3	44.7	47.0	x axis	105
96.OB2.5.1	44.7	55.1	x axis	123
96.OB2.5.2	44.7	44.1	x axis	99
96.OB2.5.3	44.7	49.9	x axis	112
96.OB1.3.1	44.7	49.0	x axis	110
96.OB1.3.2	44.7	48.1	x axis	108
96.OB1.3.3	44.7	51.0	x axis	116
96.OC1.5.1	44.7	49.9	x axis	112
96.OC1.5.2	44.7	47.0	x axis	105
96.OC1.5.3	44.7	47.0	x axis	105
96.OC1.5.4	44.7	48.1	x axis	108
96.OC1.5.5	44.7	48.1	x axis	108
96.OSB1.3.1	89.1	100.7	Combined	113
96.OSB1.3.2	89.1	98.0	Combined	110
96.OSB1.3.3	89.1	103.0	Combined	116

TABLE 2. - RESULTS FOR 48.5 IN. SPECIMENS

TEST NUMBER	ACTUAL FACTORED COMPRESSIVE RESISTANCE, CSA S16.1 $C_{r,a}$ (kips)	EXPERIMENTAL FAILURE LOAD P_f (kips)	FAILURE MODE	$P_f/C_{r,a}$ (%)
48.5A0.5.1	103.5	95.1	Combined	92
48.5A0.5.2	103.5	95.1	Combined	92
48.5A0.5.3	103.5	94.0	Combined	91
48.5B1.5.1	103.5	107.9	x axis	104
48.5B1.5.2	103.5	109.9	x axis	106
48.5B1.5.3	103.5	112.0	x axis	108
48.5B2.5.1	103.5	103.0	x axis	100
48.5B2.5.2	103.5	109.0	x axis	105
48.5B2.5.3	103.5	107.0	x axis	103
48.5B1.3.1	103.5	106.1	x axis	103
48.5B1.3.2	103.5	109.0	x axis	105
48.5B1.3.3	103.5	104.1	x axis	101
48.5C1.5.1	103.5	109.9	x axis	105
48.5C1.5.2	103.5	107.0	x axis	103
48.5C1.5.3	103.5	105.0	x axis	101
48.5SB1.3.1	129.4	136.0	Combined	105
48.5SB1.3.2	129.4	133.1	Combined	103
48.5SB1.3.3	129.4	133.1	Combined	103

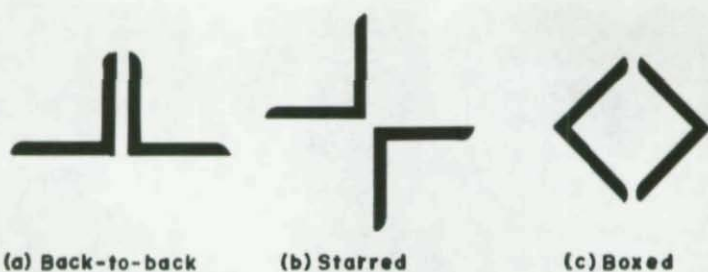


Fig.1 Arrangement of Double Angle

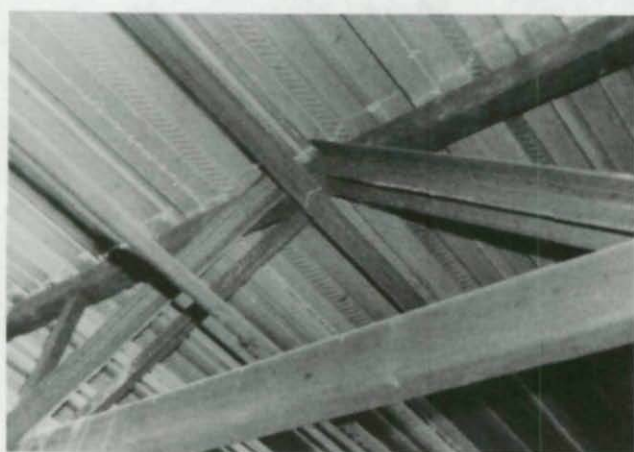


Fig.2 Back-to-back web members in a truss

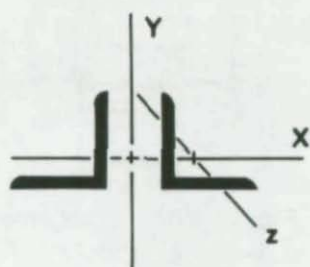
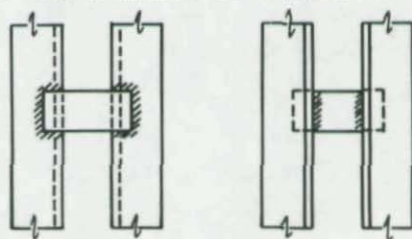


Fig.3 Coordinate Axes



(a) Normal

(b) Special

Fig.4 Weld Pattern

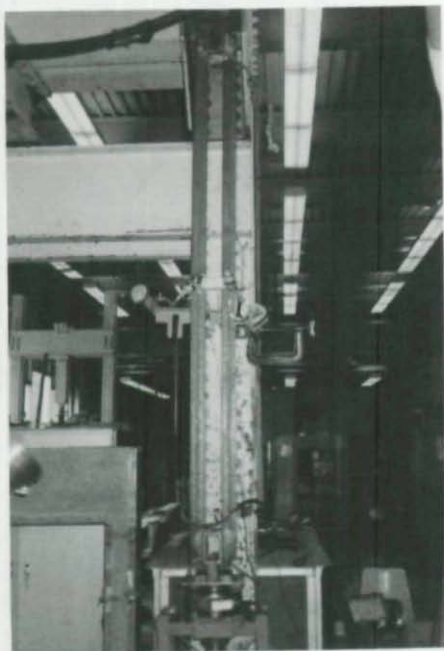


Fig. 5 Testing set-up for 96 mm specimens.

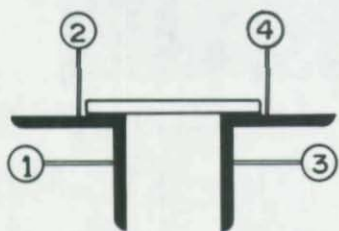


Fig. 6 The arrangement of dial gages.

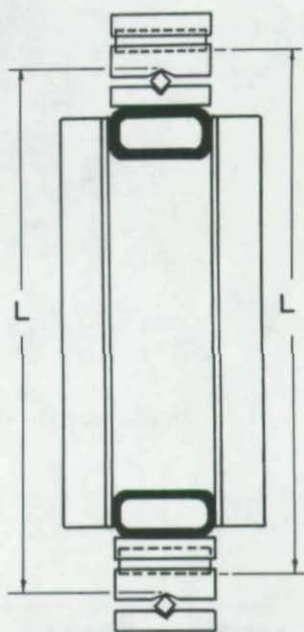


Fig. 7 The arrangement of double knife edges.

Zbigniew Mańko

Department of Civil and Environmental Engineering
Florida International University, Miami, Fl. 33199

ABSTRACT

This paper presents the results of experimental studies the aim of which was to determine the limiting load carrying capacities and the forms of stability loss in box spans. The studies were conducted for four schemes of loading on 12 models of such spans made of sheet brass. Relationships between the schemes of loading and the local forms of stability loss were found. Moreover, the load capacity of such spans was found to be greatly dependent on the deck stiffness and the character of the load. The kind of deck plate and the arrangement along the length of the span of such elements as diaphragms, cantilever ribs, webs, stiffening, etc., have a special influence on structures of this type. This paper presents also a comparison of the obtained results with the results obtained by the Finite Strips Method.

INTRODUCTION

The problem of the stability of a thin-walled construction (Klöppele et al. 1966; Massonnet et al. 1972) is currently the subject of widespread research, in consequence of numerous breakdowns, especially of steel spans of box bridges. The problem seems to be serious considering the numerous damages of steel bridge spans which were shown at the Xth and XIth IABSE Congresses (Tokyo 1976 and Vienna 1980) and at the Conferences of the Steel Construction (London 1973 and Moscow 1978). Some results are presented of research into the behavior of models of box spans under destructive loads. The purpose of the research was to determine the maximum load capacity of the spans and of the plate deck, as well as the character of the stability loss in this type of structure.

MODEL AND RESEARCH DESCRIPTION

All the models were one-span, free supported by a M63 brass plate of varying thickness for particular elements of the span. All the elements were joined by tin soldering. Transverse and longitudinal cross-sections as well as the detailed arrangement of dial indicators and strain gauges are shown in Fig. 1. The basic types of models were tested. Type I was a box with a plate deck in the shape of an orthotropic plate and it was stiffened with diaphragms. Type II differed from Type I in that it had no intermediate diaphragm. In Type III, the plate deck was an isotropic plate with closer diaphragm spacing than in Type I. Altogether, 12 models for four load schemes presented in Fig. 1 were tested. There were two models of type I - I1 and I2; three models of type II - II1, II2 and II3; and one model of type III - III1.

ragms had been cut out, six additional models of shorter span were built. The following three independent measuring systems were used in the tests:

1. A system which controlled and recorded the realized loads.
2. A system which measured unit strains, on the basis of which normal stresses in selected points of all the longitudinal ribs and in the upper and the lower plate could be determined.
3. A system which measured vertical and horizontal displacements in the longitudinal ribs, in selected points of webs, the deck and the lower plate.

Detailed arrangements of dial and strain gauges for each model are shown in Fig. 1, and a general view of the tests stand is shown in Fig. 2.

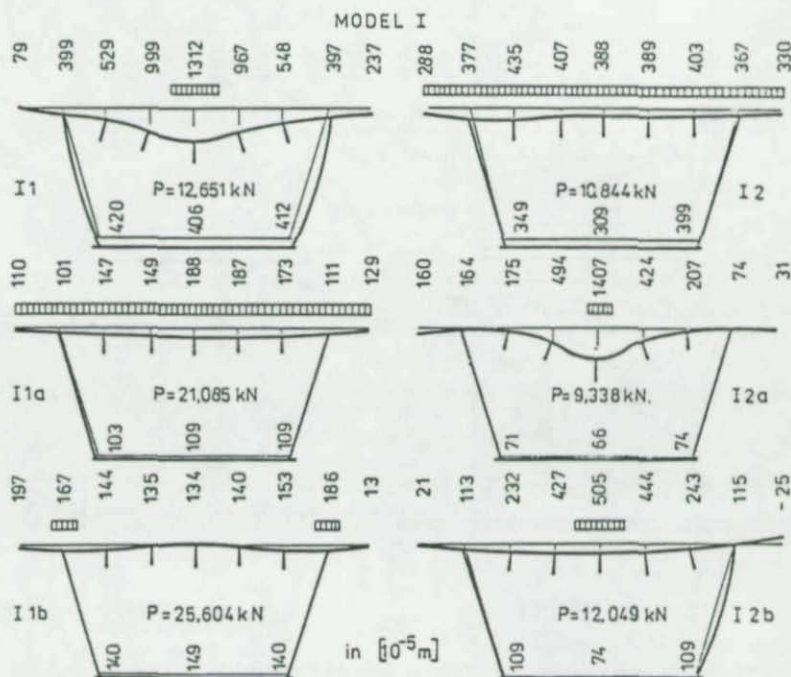


Fig. 3. Ultimate diagrams of the transverse cross-section displacements at the half-length of the spans of model I under destructive force action.

The models were subjected to loads monotonically increasing at every 0.25 kN up to the destructive force or ultimate strength. The destructive force or ultimate strength was defined as the value of the load at which local losses of stability in the deck or webs were accompanied by plastic deformation in these elements. In the case of large deforma-

tions, divisions of the material sometimes occurred, e.g. sheet puncture or cracking of welds.

TEST RESULTS

Some test results obtained from measurements made at the half-length of the spans are presented. The ultimate values of the cross-section displacements, under the destructive force for three types of models and various schemes of loading are shown in Fig. 3 for model I and in Fig. 4 for models II and III. Fig. 5 shows the relationship between (load) force P and the vertical displacement w of a selected cross-section point characteristic of all the models in half-span for the full range of loading, at every 1 kN, until destruction.

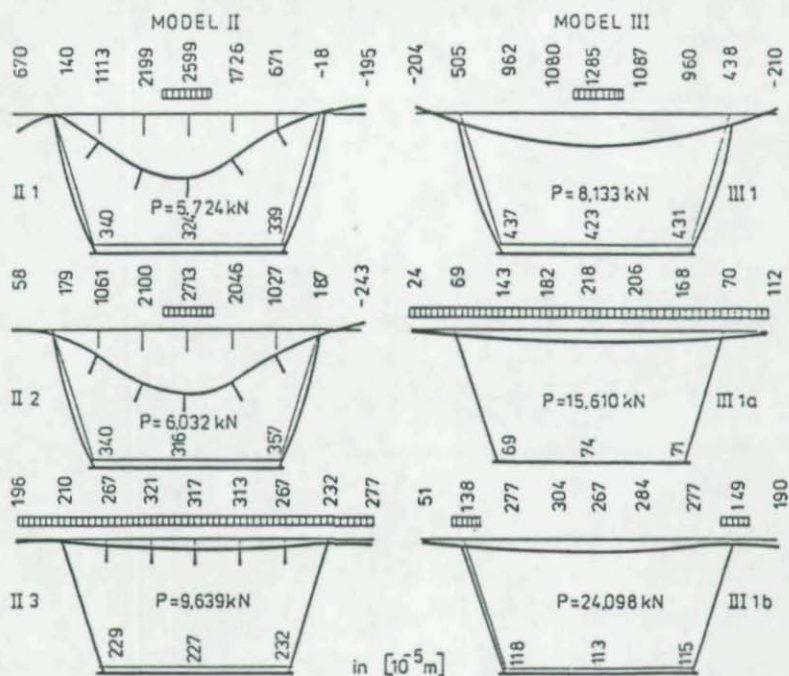


Fig. 4. Ultimate diagrams of the transverse cross-section displacements of the half-length of the span models II and III under destructive force action.

The characteristic points are: point 5 (the middle rib or the center of the plate) or point 8 (above the web of the box) depending on which element of the span had failed or been destroyed. Fig. 5 also shows the relationship $P = P(\xi)$ for point 5 of some selected models. The ultimate diagrams of the local forms of buckling (final forms of destruction) for all

the models and the loading schemes after unloading are presented in Fig. 6 (model I) and in Fig. 7 (models II and III). The view of the deck puncture in model I2a for loading scheme A is shown in Fig. 8. The antisymmetric form of the deck plastic strain in model I2b and the view of its convex web destroyed by scheme B loading are presented in Fig. 9 and 10 respectively. The view of model II destroyed by scheme B loading is shown in Fig. 11. Fig. 12 presents the view of the deck and web of model III1 destroyed by scheme B loading (symmetric form); and Fig. 13 shows model III1a destroyed by scheme C loading. Furthermore, the comparison of results obtained for model II (at 1 kN) with results obtained by Maňko et al. 1977-1980 and 1984-1985 with the finite strips method for four schemes of loading is presented in Fig. 14.

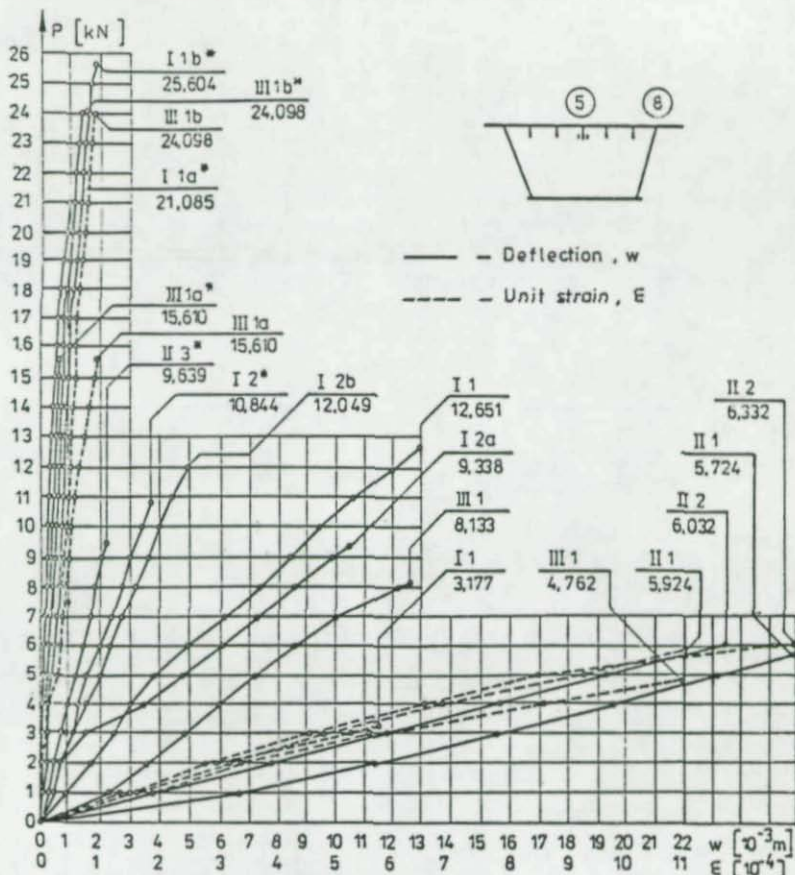


Fig. 5. Diagrams $P = P(w)$ and $P = P(\epsilon)$ for selected characteristic points 5 and 8 at the half-length of the span.

It was found that the deformation range of the load carrying plate varied according to the type of top deck plate (iso-orthotropic) and the kind of stiffening (with or without diaphragms). The range of strains for the load carrying plate deck is different. In spans with an orthotropic plate and diaphragms - model I - only three inter-diaphragmal sections clearly mate along the span length. However, in the case of local vertical loads in spans without diaphragms - model II - mating occurs along the whole span length but the displacements are considerably greater (Fig. 5). In isotropic plate span - model III - the deck sheet mates over the whole span length and considerable deflections are observed between the diaphragms in the directly loaded section. In case models II and III, mating of the cross-section between the webs is observed over the whole deck width, even at narrow loads (schemes A and B, Figs. 4 and 12) but deflections model III are greater. Spans lose their carrying capacity as a result of the local buckling of deck elements, ribs or webs, depending on the scheme of loading. The loss of stability in the case of loading schemes A and B is the results buckling of the middle

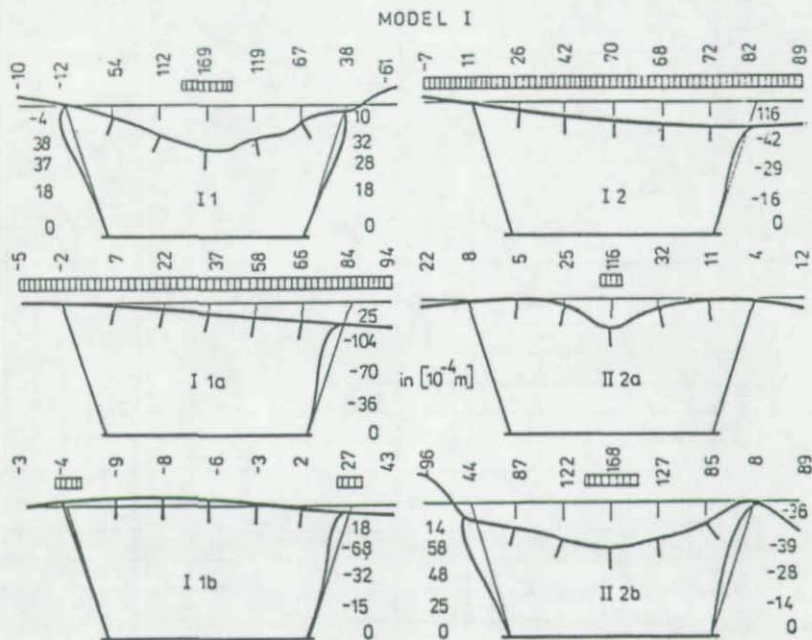


Fig. 6. Ultimate diagrams of the local forms of buckling in the cross-section at the half-length of the span for model I.

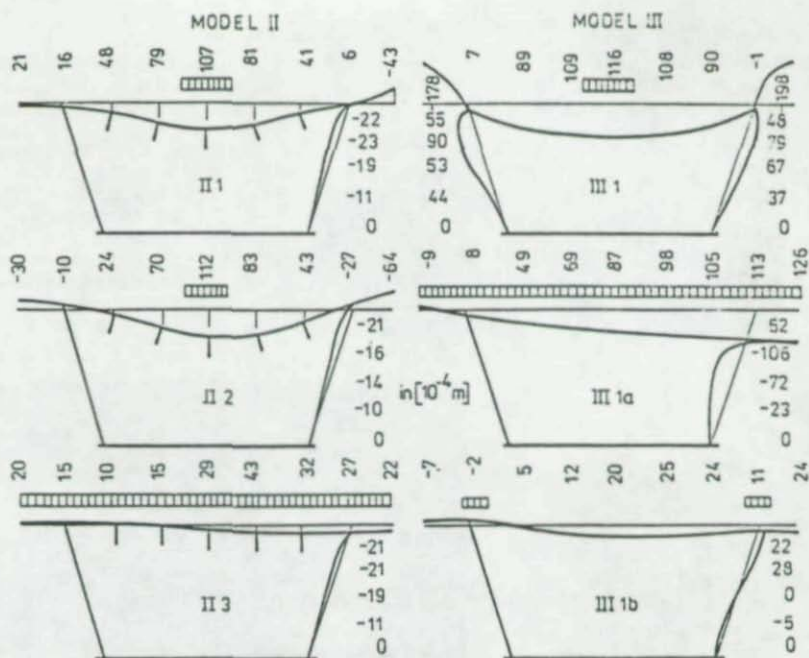


Fig. 7. Ultimate diagrams of the local forms of buckling in the cross-section at the half-length of the span for models II and III.



Fig. 8. View of the deck puncture in model I2a for scheme A loading.

rib or a puncture of the deck (scheme A - model I2a, Figs. 6 and 8); and in the case of loading schemes C and D, it is the outcome of the web buckling under loading, leading to cracking of the welds which join the webs to the deck plate.

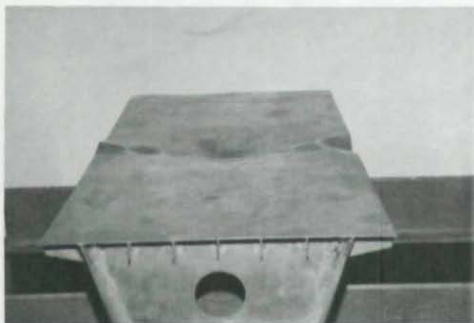


Fig. 9. View of the antisymmetric form of the deck plastic strain in model I2b under loading scheme B.

Fig. 10. View of the convex web in model I2b resulting from loading scheme B.

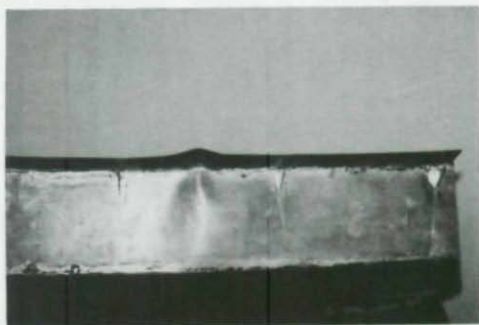


Fig. 11. View of model II destroyed by loading scheme B.

Buckling of a web occurred only in model II under scheme B loading (Fig. 11) and it was accompanied by a considerable sag in the directly loaded ribs. In the case, the increasing load causes the closing of the cross-section (reduction of the distance between the webs at the top of the span), which is attributable to the lack of intermediate diaphragms. It should

also be noted that the buckling of webs which results from loading according to schemes A and B develops symmetrically to the outside of the span, except for model I2b (Figs. 6 and 10), and the buckling which results from loading according to schemes C and D develops to the inside of the span.

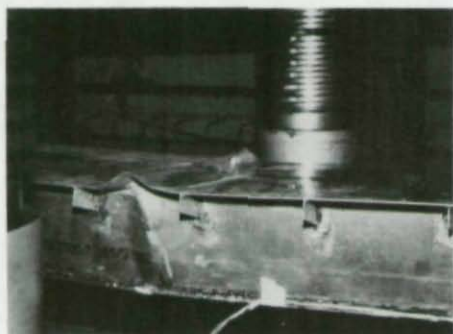


Fig. 12. View of the symmetric form of the destruction of model III1 under loading scheme B.

The unsymmetrical loss of stability by the webs could be caused by the eccentric positioning of the load or to inaccuracies in the construction of the models. Graphs of the relationship $P = P(w)$ and $P = P(\xi)$ have linear character for all the models. A change in the graph's slope occurred only in the case of model I2a, loaded according to scheme A, presumably premature failure of the middle rib (Fig. 5).

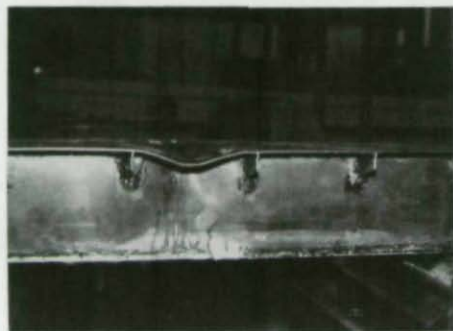


Fig. 13. Side view of model III1a destroyed by loading scheme C.

The greatest load capacities are achieved by the models in which the loads are transferred directly onto the webs (scheme D - models I1b and III1b), when the deck, irrespective of its type, is loaded by an evenly distributed load, and the highest values are reached by those models with orthotropic plates. At the same time, models of smaller span achieve load capacities, for the same loading scheme, which are similar to those of models of greater span (models I1 and I2b). However, the deflections of the first are smaller. For the same loading schemes, the deflections of the models with isotropic plates and those with orthotropic plates are almost similar (models

I1 and III1). For scheme B loading, the models without diaphragms (models II1 and II2) achieve about half the load capacity of those with diaphragms (model I1 and I2, Fig. 5).

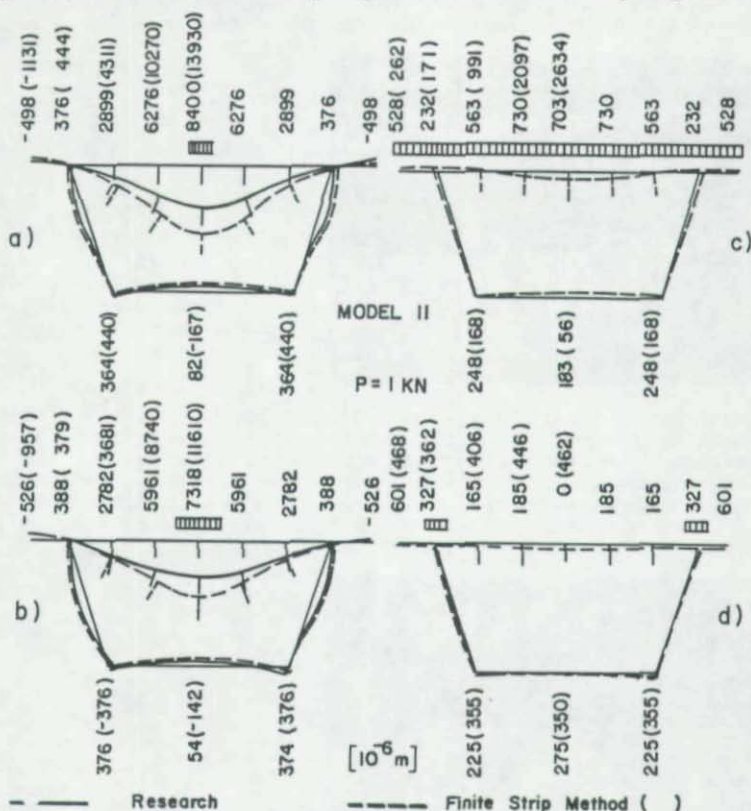


Fig. 14. Comparison of results obtained for the model II for four schemes of loading.

Studies of this scheme of loading conducted on two models gave results which were in close agreement (Fig. 4). At the same time, model II has a similar load capacity as the models with diaphragms (model I2) when loading scheme C is applied. The comparison of computational results and those obtained experimentally for model II has shown relatively high agreement of the results (Fig. 14).

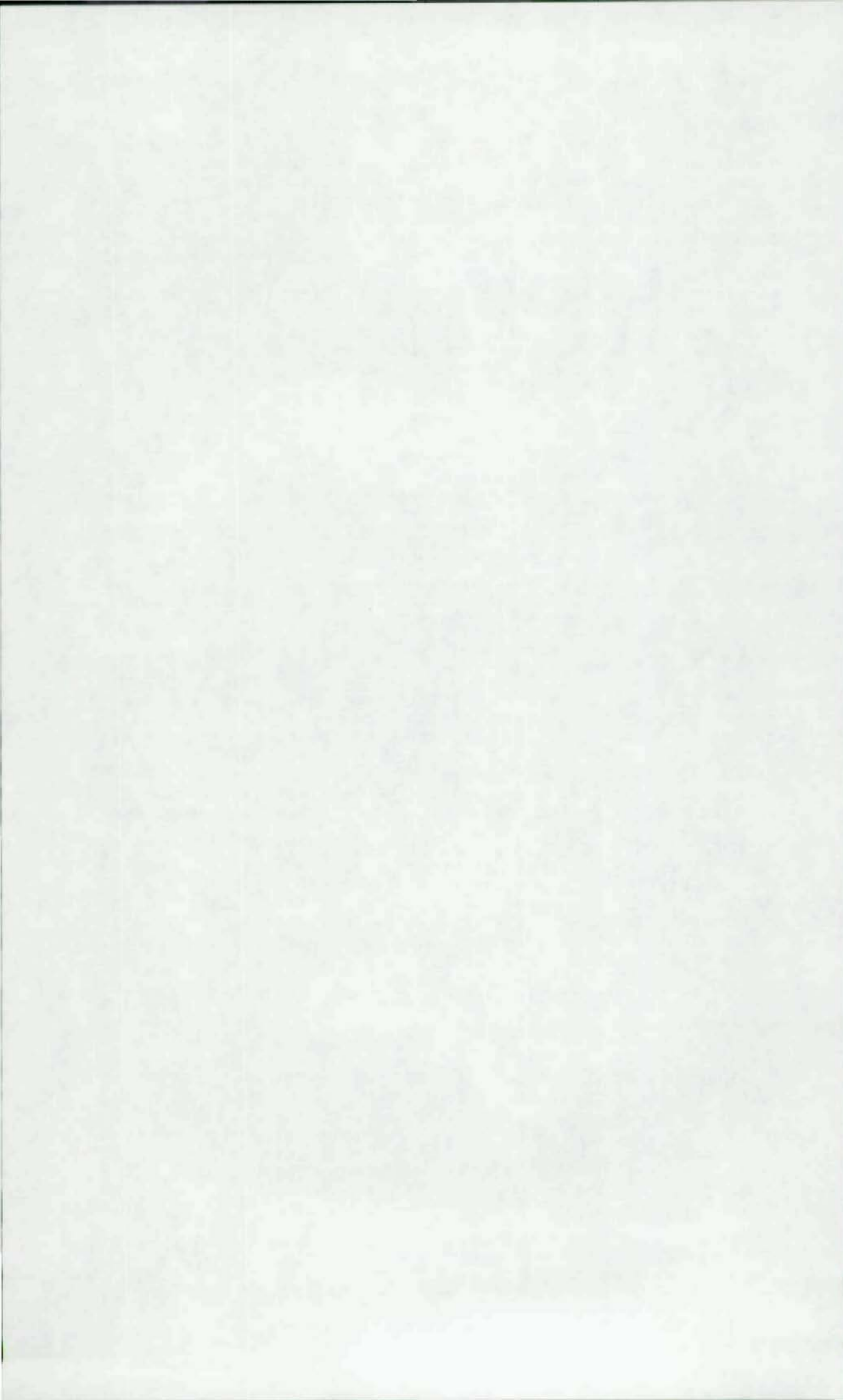
CONCLUSIONS

As a result of the studies conducted on the models of box spans, a relationship was found between the schemes of loading

and the local forms of stability loss. Deck stiffness and the character of the load have a decisive influence on the load capacity of box spans which is higher for models with an orthotropic plate and for loading schemes C and D. The kind of deck plate and the arrangement along the length of the span of such elements as diaphragms, cantilever ribs, webs, stiffening, etc., acquire special significance for structures of this type. Moreover, this paper presents a comparison of the obtained results with the results by the Finite Strips Method. This method can be successfully applied to constructions of this type for solving various analytical problems. The studies conducted so far represent the first stage of the work which is to tackle the above problems. Studies on large scale steel spans will be made in the future.

REFERENCES

- KLÖPPEL, K., SCHMIED, R., and SCHUBERT, J. 1966. Die Traglast mittig und aussermittig gedrückter dünnwandiger Kastenträger unter Verwendung der nichtlinearen Beultheorie. *Der Stahlbau* 35 (11), pp 321-337.
- MAIN TRENDS IN THE DEVELOPMENT OF STEEL STRUCTURES AND MODERN METHODS FOR THEIR FABRICATION. 1978. Final Report, IABSE Symposium, Sept.6-7, 1978, Moscow, USSR.
- MANKO, Z., and KMITA, J. 1977, 1978, 1979. The principles of construction and building of steel railway trestle bridges. Reports of the Civil Engineering Institute of Wroclaw Technical University, No. 66/77, 40/78 and 23/79.
- MANKO, Z., KMITA, J., and KLUK, K. 1980. Stabilität und Tragfähigkeit von Stahlkastenbrückenfelder. 11th Congress of the International Association of Bridge and Structural Engineering (IABSE). Aug.31-Sept.5, 1980, Vienna, Austria.
- MANKO, Z. 1984. Model investigation of steel box spans. *Proc. Instn. Civ. Engrs. Part 2*, 77, Dec., pp.491-500.
- MANKO, Z. Model investigation of steel box spans. Tenth Canadian Congress of Applied Mechanics, CANCAM'85, The University of Western Ontario, London, Ontario, Canada, June 2-7, 1985, pp.L5-L6.
- MASSONNET, CH., DEPRez, G., MAQUOI, R., MÜLER, R., and FONDER, G. 1972. Calcul des structures sur orlinsteur. *Analyse materielle des structures*. Vol. I, Paris, France.
- MASSONNET, CH. 1976. Progress in design of steel plate and box girders. Final Report, 10th Congress of the International Association for Bridge and Structural Engineering (IABSE), Sept.6-11, 1976, Tokyo, Japan, pp. 459-486.
- THE INSTITUTION OF CIVIL ENGINEERS. 1973. Steel box girders bridges. The Institution of Civil Engineers. London, England.



APPLICATION OF THE FINITE STRIPS METHOD TO STEEL BOX GIRDERS STABILITY ANALYSIS

Zbigniew Mańko

Department of Civil and Environmental Engineering
Florida International University, Miami, Fl. 33199

ABSTRACT

The paper presents the attempt to apply the Finite Strips Method to the analysis of the thin-walled simple-supported box girders. The possibility of the application of this method is connected with the construction of such structures characterized by the stable geometrical and physical properties along the analyzed span. The advantage of this method is that it makes use of functions orthogonal to the longitudinal approximation, leading to the separation of the equations of equilibrium for the particular harmonics. This allows for remarkable economy of calculations by comparison with the standard method of finite elements.

The main aim of this approach is the presentation of the analysis of buckling of such constructions under the arbitrary loads with the application of the Finite Strips Method and complex trajectories of the primary stress and interconnected buckling shapes. The examples of one and three-chamber box girders were treated for various loads schemes. The analysis of the results shows convergence depending on the number of strips and terms and the comparison with the other solution was made. Additionally the influence of orthotropy on the stability of such girders was taken into consideration.

INTRODUCTION

The stability of thin-walled construction is a problem which is presently the subject of wide research because of numerous breakdowns, especially of steel spans of box girders. The problem seems to be remarkable, considering the numerous damages of the steel bridge spans which was shown at Xth and XIth IABSE Congresses (Tokyo 1976; Vienna 1980) and at the Conferences of Steel Construction (London 1973; Moscow 1978). Solution methods have depended on the complexity of the particular structure, the nature of the loading and support conditions, the type of buckling considered and the required accuracy. The completely general method employs finite elements (Przemieniecki 1973; Zienkiewicz 1977). However, the well-known expansiveness of finite elements can make other methods competitive for particular types of structure and it is for this reason that the finite strips method has received attention (Cheung 1968 and 1976; Mańko 1975, 1978, 1980).

The paper presents the attempt to apply the Finite Strips Method to the analysis of the prismatic thin-walled simple-supported box girders. The possibility of the application of this method is connected with the construction of such structures, characterized by the stable geometrical and physical

properties along the analyzed span. The advantage of this method is that it makes use of the functions orthogonal to the longitudinal approximation, leading to the separation of the equations of equilibrium for the particular harmonics, which allows for remarkable economy of the calculations by comparison with the standard Finite Elements Method.

The main aim of this approach is to present the analysis of the buckling of such constructions under the arbitrary loads with the application of the Finite Strips Method and complex trajectories of the primary stresses and coupled buckling shapes (Graves Smith 1978; Plank and Wittrick 1974; Maňko et al. 1984 and 1985).

BOX GIRDERS DISCRETIZATION

Analyzed box girders (Fig. 1a and h) have been divided into a set of narrow longitudinal strips connected along the edges. Properties of each strip are assumed to be constant along the whole surface, they can be, however, various for particular strips. The strips are flat elements subjected to the forces active in the plane (plane state) and to bending (bending state). The state of the strain of the forces active in the plane is explicitly described by the composites u and v , and the state of strain by bending is described by w and parameter Θ (Fig. 1b). Behavior of the typical strip is described by the displacements being the local degrees of freedom on their edges in the set $q_i [i = 1, \dots, 4(M+N)]$; where M and N are numbers of the harmonics, expressed by the harmonic Fourier series in the longitudinal direction and polynomial linear functions for the plane state and of the cubic ones for the bending state in the transverse direction of the strip (Cheung 1968; Maňko 1975).

In the dimensionless co-ordinates $\varphi = y/l$ and $\eta = x/b$ corresponding displacement functions show as follows

$$u = f_{1m}(\eta) \sin(m\pi\varphi), \quad m = 1 \dots M, \quad (1)$$

$$v = f_{2m}(\eta) \cos(m\pi\varphi) + \lambda g(\eta) l(1/2 - \varphi), \quad (2)$$

$$w = f_{3n}(\eta) \sin(n\pi\varphi), \quad n = 1 \dots N, \quad (3)$$

where the functions f_{1m} , f_{2m} , f_{3n} , are given in details in the papers of Cheung (1968 and 1976) and Maňko (1975 and 1978). It can be showed relatively easily that the second term in the equation (2) allows for the equilibrium of the strips when the final stress σ_a is described by

$$\sigma_a = -\lambda g(\eta) E / (1 - \nu^2). \quad (4)$$

In this way, choosing suitable functions $g(\eta)$ for the strips, various systems of the longitudinal final stresses can be modeled for the construction as the whole. In order to obtain the non-conjugate equations of transformations between the global X , Y , Z (Fig. 1c) and local degrees of freedom, the nodes displacement u , v , w and Θ are assumed to be defined by the equations

$$248 \quad U = U_m \sin(m \pi \varphi), \quad (5)$$

$$V = V_m \cos(m \pi \varphi) + \psi (1/2 - \varphi), \quad (6)$$

$$W = W_n \sin(n \pi \varphi), \quad (7)$$

$$\Theta = \Theta_n \sin(n \pi \varphi), \quad (8)$$

where U_m , V_m , W_n , and Θ_n are the degrees of freedom in any nodal line while ψ is the value of $\text{ag}(\varphi)$ in the node. The complete collection of the global degrees of freedom is designated by $Q_j = [j = \dots, 2(M+N)J]$, where J is the number of the nodal lines. Compatibility then requires that for each strip, there is a linear relationship between q_i and Q_i of the form

$$q_i = T_{ij} Q_j, \quad (9)$$

where the transformation matrix T_{ij} is established by the procedures of the stiffness method of structural analysis (Cheung 1976; Zienkiewicz 1977).

Transverse load of the construction is distributed into components \bar{U} , \bar{V} , \bar{W} , \bar{M} (Fig. 1b) corresponding to the global displacements which are then developed into the same series as the displacements (Cheung 1968; Mańko 1975; Zienkiewicz 1977).

PRIMARY FORM OF THE TRAJECTORY OF EQUILIBRIUM

In order to obtain the equilibrium trajectory the total potential energy V of the deformed construction under a conservative load system in the function of the global degrees of freedom Q_i should be defined. This energy is composed of the internal strain energy U and the potential energy W of the loads. The internal strain energy for strip U_s is found from the result of equation

$$U_s = \frac{Et}{2(1-\nu^2)} \int_A [\epsilon_x^2 + \epsilon_y^2 + 2\nu\epsilon_x\epsilon_y + \frac{1}{2}(1-\nu)\gamma_{xy}^2] dA + \frac{Et^3}{24(1-\nu^2)} \int_A \{(\nabla^2 w)^2 - 2(1-\nu)[\frac{\partial^2 w}{\partial x^2} \frac{\partial^2 w}{\partial y^2} - (\frac{\partial^2 w}{\partial x \partial y})^2]\} dA, \quad (10)$$

where the strain components are defined according to the displacement by the following non-linear strain-displacement relations

$$\epsilon_x = \frac{\partial u}{\partial x} + \frac{1}{2} [(\frac{\partial u}{\partial x})^2 + (\frac{\partial v}{\partial x})^2 + (\frac{\partial w}{\partial x})^2], \quad (11)$$

$$\epsilon_y = \frac{\partial v}{\partial y} + \frac{1}{2} [(\frac{\partial u}{\partial y})^2 + (\frac{\partial v}{\partial y})^2 + (\frac{\partial w}{\partial y})^2], \quad (12)$$

$$\gamma_{xy} = \frac{\partial u}{\partial y} + \frac{\partial v}{\partial x} + [\frac{\partial u}{\partial x} \frac{\partial u}{\partial y} + \frac{\partial v}{\partial x} \frac{\partial v}{\partial y} + \frac{\partial w}{\partial x} \frac{\partial w}{\partial y}]. \quad (13)$$

In the expression enclosed in the square brackets of the equations (11-13) the displacements w and u together model the shapes of general (overall) buckling modes in the case when the nodal lines of structures are subject to remarkable displacements, the shape of the local buckling modes is modeled by w , while v has no considerable influence. The potential energy of the loads connected with the strip W_s is stated by the expression

$$W_s = -t \int_0^b [\sigma_y v_y]_{y=0}^{y=1} dx, \quad (14)$$

where σ_y is given by Graves Smith (1978) and Mańko et al. (1981, 1984, 1985). After doing the proper substitutions of the displacement functions (1-3) and integration the equation for V_s can be defined

$$V_s = -\lambda a_1 q_1 + \frac{1}{2!} (a_{1j} - \alpha c_{1j}) q_1 q_j + \frac{1}{3!} a_{1jk} q_1 q_j q_k. \quad (15)$$

So, the total potential energy of the construction according to the global degrees of freedom can be found by substituting the equations of transformation summing for the strips and adding the lateral loads potential energy ($-\Phi_p B_{p1} Q_1$), where B_{p1} are corresponding coefficients depending on the loads. Hence, one obtains

$$V(\lambda, \Phi_p, Q_1) = -\lambda A_1 Q_1 - \Phi_p B_{p1} Q_1 + \frac{1}{2!} (A_{1j} - \alpha C_{1j}) Q_1 Q_j + \frac{1}{3!} A_{1jk} Q_1 Q_j Q_k, \quad (16)$$

where

$$[i, j, k = 1, \dots, 2(M+N)J; p' = 1 \dots 4J]. \quad (17)$$

Use of the principle of the stationary potential energy minimization, the equilibrium paths can be found by differentiating V with respect to Q_1 and equating the obtained derivatives E_1 to zero. In this way the following equation is formed

$$E_1(\lambda, \Phi_p, Q_1) = -\lambda A_1 - \Phi_p B_{p1} + (A_{1j} - \alpha C_{1j}) Q_j + \frac{1}{2!} A_{1jk} Q_j Q_k = 0. \quad (18)$$

from which the required number of the non-linear equations are obtained for the unknowns Q_1 as functions of the load parameters λ and Φ_p .

The corresponding non-linear primary trajectories can be also obtained by means of perturbation (Croll et al. 1972) or

the other methods; but the paths got in this way are so very close to the linear in most practical cases the complications involved would not seem to be necessary. The present approach considers only the linear solutions obtained from equation (18) by taking into account the first three terms and solving

$$-\lambda A_1 - \Phi_p B_{p1} + A_{1j} Q_j = 0. \quad (19)$$

The solution of the equation (19) takes the general form

$$Q_1 = \lambda D_1 + \Phi_p E_{p1}, \quad (20)$$

in which the primary trajectories are produced by independently changing λ and Φ_p . Since the displacement functions (1-3) are orthogonal, the coefficients corresponding to the various harmonics are uncoupled, enabling solutions to be obtained with computational effort only linearly proportional to the number of harmonics considered.

THE SECONDARY EQUILIBRIUM PATH

For the sake of the simplicity of analysis, the construction behavior under the end load and constant lateral loads ($\Phi_p E_{p1}$) was solely examined. Then the corresponding primary path of equilibrium takes the shape

$$Q_1 = \lambda D_1 + F_1, \quad (21)$$

where $F_1 = \Phi_p E_{p1}$ (Eq. 19) are the initial displacements from the lateral loads. Supposing that the secondary path branches from the primary trajectory at λ_c , its displacements can be written as

$$Q_1^W = Q_1^P + \Delta Q_1, \quad (22)$$

where Q_1^P are the primary trajectory displacements for the same λ . The derivatives of potential energy V corresponding to the secondary path E_1^W can be obtained by substituting the equation (22) into (15)

$$E_1^W = E_1^P + (A_{1j} - \lambda C_{1j} + A_{1jk} Q_k^P) \Delta Q_j + \frac{1}{2!} A_{1jkl} \Delta Q_j \Delta Q_k, \quad (23)$$

where

$$E_1^P = E_1(\lambda, Q_j^P) = 0. \quad (24)$$

From the equation (24) one obtains displacements of the primary path, because it results from the definition ($E_1^P = 0$), that this is an equilibrium trajectory. Thus

$$E_1^W(\lambda, \Delta Q_j) = [A_{1j} + A_{1jk} F_k - \lambda(C_{1j} - A_{1jk} D_k)] \Delta Q_j + \frac{1}{2!} A_{1jkl} \Delta Q_j \Delta Q_k. \quad (25)$$

The secondary path can be described by means of the perturbation method (Croll et al. 1972) assuming that it branches off from the primary trajectory at the point $(\lambda, \Delta Q_1) = (\lambda_c, 0)$. Then, in order to state the increase along this trajectory arbitrary parameter ξ should be selected. When supposing λ and ΔQ_1 are analytic functions of ξ

$$\lambda = \lambda_c + \sum_r \lambda_{,r} \frac{\xi^r}{r!}, \quad (26)$$

$$\Delta Q_1 = \sum_r \Delta Q_{1,r} \frac{\xi^r}{r!}, \quad r = 1, \dots, R, \quad (27)$$

where

$$f_{,r} = \frac{d^r f}{d\xi^r}. \quad (28)$$

The secondary path is the equilibrium path ($E_1^W = 0$) for all the values ξ , and therefore all derivatives of the higher order E_1^W in relation to ξ at the branching point equal zero. Hence, the sets R of the perturbation equations can be derived as

$$[E_{1,r}^W](\lambda_c, 0) = 0, \quad (r = 1, \dots, R). \quad (29)$$

The equation (29) is sufficient in the aspect of number for stating the unknowns $\lambda_{,r}$ and $\Delta Q_{1,r}$ if ξ is taken as one of these unknowns. Thus if $\xi = \lambda$, then $\lambda_{,1} = 1$, $\lambda_{,r} = 0$ ($r > 1$) and there are then sufficient equations to obtain $\Delta Q_{1,r}$. Considering only the first set of the perturbation equations and differentiating the equation (25) one obtains the expression

$$[E_{1,1}^W](\lambda_c, 0) = [A_{1j} + A_{1jk}F_k - \lambda_c(C_{1j} - A_{1jk}D_k)]\Delta Q_{j,1} = 0, \quad (30)$$

which leads either to the trivial solution $\Delta Q_{j,1} = 0$ or to the indeterminable solution for the particular value of λ_c for which the following determinant equals zero

$$|A_{1j} + A_{1jk}F_k - \lambda_c(C_{1j} - A_{1jk}D_k)| = 0. \quad (31)$$

This is the standard problem of the eigenvalues and the smallest values λ_c of the $2(M+N)J$ satisfying the equation (31) states the critical load buckling of the given construction.

NUMERICAL EXAMPLES

On the basis of the algorithm presented, a calculation procedure in ALGOL-1900 was elaborated. The calculations were executed on the computer ODRA 1305 in the Computer Center of Wrocław Technical University. The applicability of the finite strips method to the analysis of more complex structures is

illustrated by the case of the thin-walled box girder shown in Fig. 1h and it was compared with the results given in the work by Graves Smith (1978). Critical (bifurcational) strains in the strip of constant thickness can be expressed in the form given by Timoshenko and Gere (1961)

$$\sigma_{cr} = \frac{N_{cr}}{t} = k \frac{\pi^2 D}{b^2 t}, \quad (32)$$

where k is the dimensionless coefficient dependent on the way of loading, conditions of support and length of plate's sides ratio.

One Box Girder Under Partial Web Loading

The analysis was made for the two linear loads, each of the length of l_1 , placed above webs symmetrically with the relation to the span's longitudinal axis (Fig. 1h). The calculation were verified and optimized by different methods which, among others, consisted in assuming the arbitrary number of strips p and the harmonics M (Fig. 1i). The results of buckling coefficients for the ratios $l_1/l = 0.25, 0.50$ and 1.00 are shown in Table 1.

Table 1. Comparison of the obtained results for one-cell girder

Load scheme	l_1/l	M	p	k		p	M	k		
				Smith	Mańko			Smith	Mańko	
1	0.25	7	4	-	3.351	12	5	-	3.327	3.392
			8	3.245	3.342		7	3.227	3.287	
			10	-	3.305		9	3.205	3.237	
			10*	-	3.292		11	3.200	3.201	
			12	3.227	3.287		19	-	3.196	
			16	3.220	3.215					
		20	3.216	3.198						
	0.50	7	8	-	2.423	16	1	-	2.732	
			16	-	2.412		5	-	2.487	
							9	-	2.410	
							19	-	2.406	
1.00	7	8	-	1.738	16	1	-	2.013		
		16	-	1.734		5	-	1.811		
						9	-	1.736		
						19	-	1.733		

* - the strip with higher order

Three-cell Box Girders Under The Arbitrary Load

The Finite Strips Method was also applied to the complicated thin-walled box girder given in Fig. 1a for different load schemes. Four load schemes were here analyzed (Fig. 1d,e,f,g). The first load was identical with the one in Example 1, the second load equaled half of it, the third formed

Table 2. Juxtaposition of the obtained results for three-chamber girder

Load scheme	M	p	k			p	M	k			
			0.25	0.50	1.00			0.25	0.50	1.00	
1	9	12	4.623	4.025	3.326	18	9	4.987	5.032	4.133	
		15	4.604	4.012	3.303			5	4.713	4.128	3.677
		18	4.591	4.001	3.292			9	4.591	4.001	3.292
		22	4.587	3.902	3.288			19	4.583	3.892	3.279
2	9	12	5.325	4.734	4.010	18	9	5.923	4.908	4.423	
		15	5.301	4.692	3.962			5	5.308	4.702	4.041
		18	5.282	4.668	3.939			9	5.282	4.668	3.939
		22	5.272	4.649	3.912			19	5.265	4.639	3.913
3	9	12	4.038	3.425	2.732	18	9	4.325	3.623	2.983	
		15	4.001	3.384	2.698			5	4.081	3.427	2.712
		18	3.980	3.361	2.669			9	3.980	3.361	2.669
		22	3.969	3.342	2.648			19	3.962	3.341	2.642
4	9	12	6.125	5.384	4.123	18	9	6.432	5.621	4.325	
		15	6.040	5.332	4.024			5	6.182	5.342	4.132
		18	5.981	5.299	4.001			9	5.981	5.299	4.001
		22	5.937	5.278	3.998			19	5.936	5.270	3.996

a uniform load placed along the whole width of the span, and the fourth was similar to the load according to the scheme 3 while its width occupied only the middle cell. The lengths of loads in the four load schemes were identical and equaled $l_1/l = 0.25, 0.50$ and 1.00 . The elasticity constants $E = 3.3 \text{ GN/m}^2$ and $\nu = 0.375$ were assumed as in the case of metaplex (Mańko 1975), and $E = 106 \text{ GN/m}^2$ and $\nu = 0.348$ as in the case of brass (Mańko et al. 1977, 1978, 1979, 1980, 1984 and 1985).

The results were analyzed according to the number of strips and the harmonics used in the solution. The influence of the number of strips p on the final result was analyzed firstly. Four different divisions were made of girder's elements into strips, distinguishing 12, 15, 18 and 22 strips (Fig. 1d,e,f,g). Assuming the divisions, considerably small influence of number of strips was found out on the final

result. Then, for the optimal divisions of box girder into 18 strips optimization was done according to the number of harmonics, 1, 5, 9 and 19 harmonics were assumed. Considerable fast stabilization was found out as convergence of results depending on the number of harmonics (terms). It can be stated that 9 terms are sufficient to assess the correct results of coefficient k . All the results of analysis were given in Table 2.

The Influence Of Material Orthotropy

The influence of material orthotropy on the stability of some one- and multi-box girders in compression was additionally analyzed. All the computed results (Fig. 2) are presented graphically, i.e. the dimensionless buckling stress is plotted against the dimensionless half wavelength of the buckling mode. As such results only give an indication of the effects of orthotropy on the buckling stress and the half wavelength values. No attempt has been made to directly illustrate the influence of orthotropy on the buckling mode. The procedure adopted for the illustrating the influence of the orthotropy on the structural response to compressive loading consists of comparing various orthotropic results with geometrically similar and equal weight, isotropic results for each type of one- and multi-box structures in turn (equal weight, isotropic results are obtained by reducing the plate thickness in the ratio of the densities of the isotropic and orthotropic materials). Fig. 2a shows a plot of the initial buckling stress against half wavelength μ of the buckle for the series of doubly symmetric, rectangular, brass boxes. This graph has been included for the sake of completeness, since it illustrates the influence of variations in the geometric parameters, rather than the material parameters, for particular structure.

In contrast to this, Fig. 2b illustrates the significant variations in the initial buckling stress that the material orthotropy may give rise to when the geometric parameters are maintained constant. Moreover, the superposition of the buckling curves for equal weight and geometrically similar brass boxes gives an indication of the structural efficiency of metaplexes - metaplex being approximately seven times lighter than brass. Furthermore, Fig. 2b confirms for multi-plate structures what is well known for single, specially orthotropic plates, namely, that material orthotropy has a significant influence not only on the initial buckling stress but also on the wavelength at which this occurs. Thus the initial buckling minimum stress value occurs at longer wavelengths for higher values of the longitudinal elastic modulus and this appears to apply throughout the results presented in this work. Since this computer program handles rather more complicated structural types than the other two examples, the computational times involved in producing the same quantity of results are rather more lengthy. Hence, more emphasis has been placed on demonstrating the versatility of the program and so results for number of different structural types are presented, somewhat at the expense of achieving concrete in-

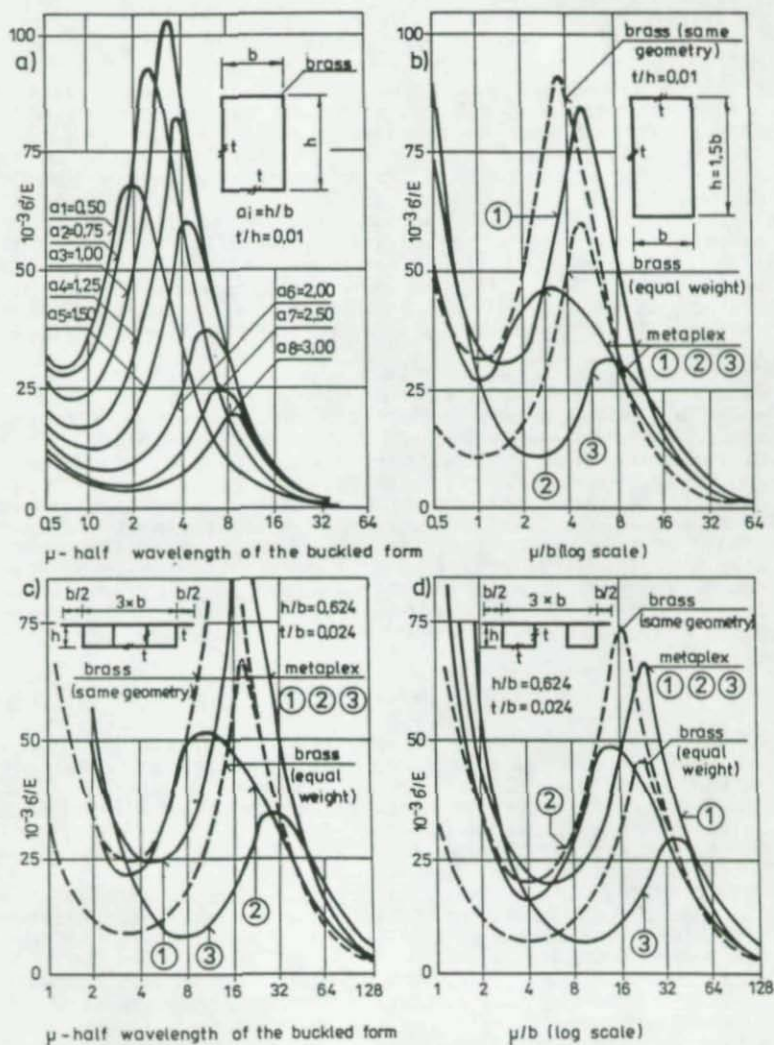


Fig. 2. Buckling stress-half wavelength curves for uniformly compressed, brass and metaplex, one rectangular box girders and three-cell box girders.

formation about the effects of orthotropy. These results for multi-box spans are presented in Fig. 2c and d. Once again the influence of orthotropy seems to be quite significant.

CONCLUSIONS

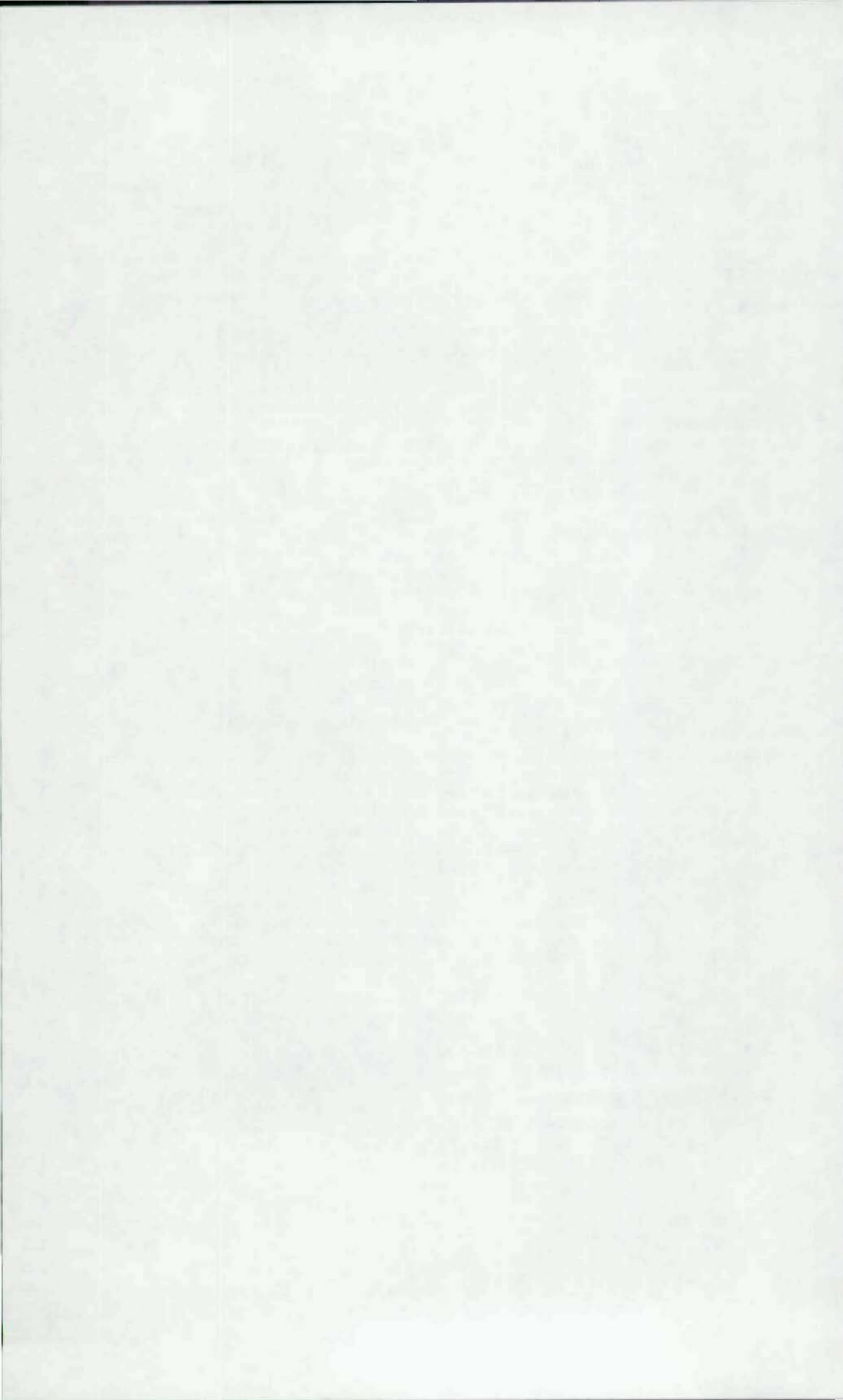
The presented numerical examples show that critical stress for complicated structures such as box girders can be effectively and with high accuracy calculated by means of the Finite Strips Method. The presented algorithm based on this method is an effective tool for box girder stability analysis. In relation to more general programs based on the method of finite elements the worked out program contributes to considerable decrease of calculation time. It is particularly seen in the case of structures simple-supported on both opposite edges. Still in each case the dimension of the matrix diminishes because of the generally small number of finite strips. It is consequently followed by the simplification of input data.

Graphs of initial buckling stress against the half wavelength of the buckling mode have been computed for a wide range of isotropic and orthotropic box girders in a state of uniform compression and under the arbitrary loads. By comparing the orthotropic results against the equal weight and geometrically similar isotropic results, it has been demonstrated that the material orthotropy can significantly alter both the initial buckling stress and the half wavelength at which buckling occurs. By use of this algorithm a relatively narrow strip matrix of construction is obtained. Hence, the expenditure of work for calculations is considerably smaller compared with the finite elements method, and moreover, only a few harmonics are necessary to obtain the proper results.

REFERENCES

- CHEUNG, Y.K. 1968. Finite strip method analysis of elastic slabs. ACE Journal of the Engineering Mechanics Division 94 (EM6), pp. 1365-1378.
- CHEUNG, Y.K. 1976. Finite strip method in structural mechanics Pergamon Press, London Oxford.
- CROLL, J.G.A., and WALKER, A.C. 1972. Elements of structural stability. Macmillan, London.
- GRAVES SMITH, T.R., and SRIDHARAN, S. 1978. A finite strip method for the buckling of plate structures under arbitrary loading. International Journal of the Mechanical Sciences 20 (10), pp. 685-693.
- MAIN TRENDS IN THE DEVELOPMENT OF STEEL STRUCTURES AND MODERN METHODS FOR THEIR FABRICATION. 1978. Final Report, IABSE Symposium, Sept. 7-8, 1978, Moscow, USSR.
- MAŃKO, Z. 1975. Statical analysis of chosen steel bridge spans. Reports of the Civil Engineering Institute of Wrocław Technical University, Wrocław, Poland, No. 5, p. 242, Ph.D. thesis, (in Polish).
- MAŃKO, Z. 1978. Statical analysis of box girders. Archiwum Inżynierii Łądowej XXIV (1), pp. 119-132 (in Polish).

- MAŃKO, Z., and KMITA, J. 1977, 1978, 1979. The principles of construction and building of steel railway trestle bridges. Reports of the Civil Engineering Institute of Wroclaw Technical University, No. 66/77, 40/78 and 23/79 (in Polish).
- MAŃKO, Z., KMITA, J., and KLUK, K. 1980. Stabilität und Tragfähigkeit von Stahlkastenbrückenfeldern. 11th Congress of the International Association for Bridge and Structural Engineering, (IABSE), Aug. 31-Sept. 5, 1980, Vienna, Austria.
- MAŃKO, Z. 1980. Spannungs- und Verformungszustand von Kasten-trägern. Bauplanung-Bautechnik 34 (20), pp. 79-81.
- MAŃKO, Z. 1980. Die Berechnung von Kastenbrückenfeldern. Der Stahlbau 49 (8), pp. 246-250.
- MAŃKO, Z. 1981. Application of finite strip method to the box girders buckling analysis. Proceedings of 5th Conference on Computer Methods in Structural Mechanics, May 6-9, 1981, Wroclaw-Karpacz, Poland. Scientific Papers of the Civil Engineering Institute of Wroclaw Technical University 28 (9) No. 2, pp. 37-43 (in Polish).
- MAŃKO, Z., and MAŃKO, B. 1984. Stability analysis of steel box girders. The Fifth Conference of the Mathematics of Finite Elements and Applications. MAFELAP 1984. Institute of Computational Mathematics, Brunel University, Uxbridge, Middlesex, U.K., May 1-4, 1984, pp. 43-44.
- MAŃKO, Z. 1984. Model investigation of steel box spans. Proceedings of the Institution of Civil Engineers 77 (2), Dec. pp. 491-500.
- MAŃKO, Z. and LEMAŃCZYK, M. 1985. Application of the finite strips method to the steel box girder stability analysis. Annual Conference and the 7th Canadian Hydrotechnical Conference of the Canadian Society for Civil Engineering, May 27-31, 1985, Saskatoon, Saskatchewan, Canada, Proceedings, Vol. 11A, pp.663-678.
- MAŃKO, Z. and LEMAŃCZYK, M. 1985. Application of the finite strip method to the steel box girders stability analysis. 10th Canadian Congress of Applied Mechanics. CANCAM'85, The University of Western Ontario, London, Ontario, Canada, June 2-7, 1985, pp. L3-L4.
- MASSONNET, CH. 1976. Progress in design of steel plate and box girders. Final Report, 10th Congress of the International Association for Bridge and Structural Engineering, (IABSE), Sept.6-11, 1976, Tokyo, Japan, pp. 459-486.
- PLANK, R.J., and WITTRICK, W.H. 1974. Buckling under combined loading of thin flat-walled structures by a complex finite strip method. International Journal of Numerical Methods of Engineering 8 (2), pp. 323-339.
- PRZEMIENIECKI, J.S. 1973. Finite element structural analysis of local instability. Journal of American Institute of Aeronautics and Astronautics 11 (1), pp. 33-39.
- THE INSTITUTION OF CIVIL ENGINEERS. 1973. Steel box girders bridges. The Institution of Civil Engineers, London, England.
- TIMOSHENKO, S.P., and GERE, J.M. 1961. Theory of elastic stability. McGraw-Hill, New York.
- ZIENKIEWICZ, O.C. 1977. The finite element method. Third Edition, McGraw-Hill, London.



SSRC 4th EDITION OF GUIDE -
CHAPTER ON STIFFENED CYLINDERS

Donald R. Sherman
University of Wisconsin-Milwaukee

INTRODUCTION

The primary purpose of this paper is to introduce the topic of stiffened cylinders and provide the background for the research and design papers that follow. A good way to accomplish this is to summarize what the SSRC Guide has to say about stiffened cylinders. The 3rd edition of the Guide was the first to have a chapter devoted to Cylindrical Tubes and Shells. In the 4th edition, this chapter has been updated as well as rearranged for clarity and to provide more definitive guidelines. As in other chapters of the Guide, the stability criteria are based on theory which has been empirically modified to agree with test data.

The seven sections of Chapter 14 can be divided into three topic groups; unstiffened cylinders, stiffened cylinders and interactive effects. Although much of the material on unstiffened cylinders forms the basis of the stability criteria for stiffened cylinders, this paper will be devoted to summarizing the two sections concerning the latter topic. Since the equations and detailed discussion appear in the Guide, only a qualitative summary will be provided.

Figure 1 defines the key terminology used with stiffened cylinders. Both ring and stringer stiffeners can be used alone or in combination on either the outside or inside of the cylindrical shell. Alternate terminology for the stiffeners are circumferencial and longitudinal. The stiffeners can be projecting plates or heavier sections such as angles, tees, channels or wide flange shapes. In modern fabrication, the stiffeners are welded to the shell, usually continuously although intermittent welds can be used. The bulkhead in Figure 1 is a diaphragm that keeps the shell circular where it is attached. Heavy rings or end closures can act as bulkheads for stability purposes.

RING STIFFENERS

Aside from column buckling under axial compression, ring stiffened cylinders fail in one of three modes:

1. Axisymmetric collapse of the shell between adjacent ring stiffeners. This mode is inelastic buckling and is characterized by accordion-shaped pleats around the circumference of the shell.
2. Asymmetric or lobar buckling of the shell between adjacent ring stiffeners. This is the elastic buckling mode as is characterized by two or more dimples around the circumference.

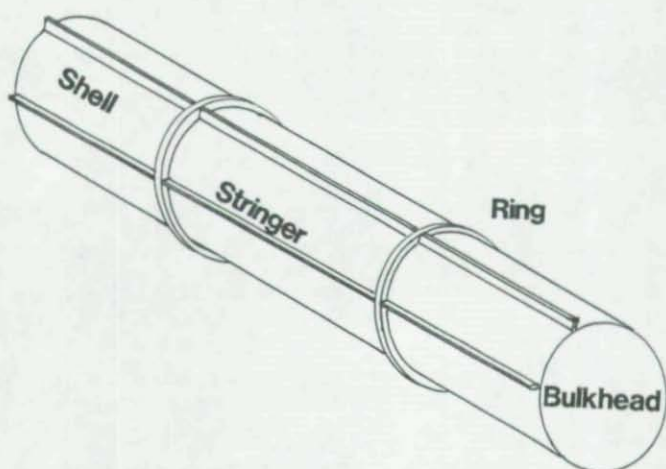


FIGURE 1 - TERMINOLOGY FOR STIFFENED CYLINDERS

3. General collapse characterized by large dished-in portions where both stiffeners and shell deflect together.

The first two instability modes are shell buckling and are governed by the criteria for unstiffened cylinders. These will occur if the rings have the stiffness and strength to act as bulkheads. The third mode occurs with lighter rings.

Ring stiffeners have little or no effect on column buckling. Therefore, they are used to enhance the local buckling strength. In order to accomplish this, they must be spaced closely enough so that length is a parameter in the buckling equations for the unstiffened shell between the rings. In the sections of the Guide dealing with unstiffened cylinders, groups of equations for critical loads are given for various loading conditions. A parameter that includes length defines the applicable range for each equation. One equation in a group applies to infinitely long cylinders where end boundary conditions do not effect the stability. The length parameter which defines when this equation is applicable also indicates a spacing above which ring stiffeners should have no influence.

Under axial loads, the implied critical length is $L/D < 1.22/\sqrt{D/t}$. This is an extremely short spacing relative to the critical length for pressure loads and would seldom be encountered in practice. Therefore, it can be concluded that ring stiffening is a very inefficient method of reinforcing a cylinder for axial loads or that the presence of rings will seldom influence the critical axial load.

For elastic buckling in flexure, the critical stress equations for axial loads are frequently used. This indicates that a very close spacing would again be required for rings to be effective. However, it is also known that ovalization is a factor in the buckling of cylinders due to flexure while it does not occur under axial loads. Therefore, rings may have more influence in flexural buckling, especially when it is inelastic. The boundary conditions for flexural buckling have not been thoroughly investigated so that specific recommendations for ring stiffeners are not given. However, it is believed that they would still need to be closely spaced and would be efficient only in regions of steep moment gradients.

The implied critical ring spacing for torsional loads is much larger than for axial loads, implying that this type of stiffener could be efficient. However, no information is available on the the interaction of shell and ring buckling. This is needed to determine the required stiffener size to act as a bulkhead. The lack of information could be due to the fact that torsional loading in thin cylinders seldom occurs in practice.

Ring stiffeners are most frequently used to increase the local buckling strength of cylinders subject to external pressure. Numerous studies of ring stiffened cylinder subject to pressure are cited and a history of criteria development is outlined in the Guide.

According to the solutions for unstiffened cylinders under external pressure, the critical spacing of rings is $L/D < 2.1\sqrt{D/t}$ for the hydrostatic loading case. The recommended equation for the critical buckling pressure involves the sum of a shell term and a ring term.

$$p_c = \frac{2E}{D/t} \frac{\lambda^4}{(n^2 + (\lambda^2/2) - 1)(n^2 + \lambda^2)^2} + \frac{E I_e (n^2 - 1)}{L_f R_o^2 R_c^2} \quad (1)$$

where

- $\lambda = \pi D / 2L_b$
- R_o = the outside radius of the shell
- R_c = the radius to the centroid of the ring and an effective width of shell
- I_e = moment of inertia of ring and effective width of shell
- L_f = center-to-center spacing of rings
- L_b = length between bulkheads or equivalent

n is the number of circumferential lobes existing at collapse and the correct value is that which produces the minimum critical pressure. For large stiffener spacings, there is little restraint to shell buckling and n is equal to 2. For closer spacings, the second term in Equ. 1 dominates. Equations are given in the Guide for determining the effective width of the shell.

The largest effective ring size is determined when the critical buckling pressure from Equ. 1 equals that for an unstiffened shell with a length equal to the ring spacing. Larger rings will not increase the critical pressure. The determination of the optimum ring size involves both an iterative solution for n and a trial solution for the size.

In some applications, there are a series of small uniformly spaced rings and at greater intervals there are heavier rings, also uniformly spaced. An empirical equation for the critical pressure when the buckling pattern includes both set of rings is recommended in the Guide. This is a complex equation to use and it involves applying Equ. 1 for both sets of rings. It can, however, be used to determine when the large rings will act as bulkheads.

Equ. 1 can be modified to account for inelastic behavior. For the shell term that is based on membrane stiffness, the value of E should be replaced by $\sqrt{E_s E_t}$, while in the ring term that reflects bending stiffness, E is replaced by the tangent modulus, E_t . In order to determine the tangent and secant moduli, the stress field at the stiffener and in the shell midway between stiffeners must be known. Equations for the

stress field are provided. The moduli are then determined from a representative stress-strain curve of the material. Charts in the ASME Boiler & Pressure Vessel Code can also be used to determine reduced moduli for different materials at various temperature. This procedure is illustrated for unstiffened cylinders and can be used for stiffened cylinders.

Imperfections can also effect the critical pressure for instability. An approximate equation for the bending stress in a ring due to out-of-roundness is given. Another type of stress is induced if the ring is initially tilted. When the sum of hoop stresses, the bending stress and the tilt induced stresses reaches yield, collapse in a general instability mode is likely to occur.

STRINGER STIFFENERS

Stringer stiffeners are very effective in increasing the axial load and bending capacity of cylinders. In addition to raising the critical stress for instability of the shell, they decrease the stress level by increasing the area and section modulus. They also influence the critical pressure but are not as efficient as ring stiffeners in this respect. Due to the large number of parameters involved when they are used with ring stiffeners and the multiple potential mechanisms of failure, it is difficult to achieve a universal set of design formulas substantiated by tests. Therefore, this section of the Chapter is limited to a general discussion of the methods that can be used to evaluate critical axial stresses and critical pressures.

For the case of axial compression, five failure modes are discussed:

COLUMN BUCKLING - The stringer stiffeners should be included in the calculation of the radius-of-gyration of the column cross section. If rings are also present, they have no effect.

LOCAL WITH SEVERAL STRINGERS - This mode usually occurs with closely spaced stringers and they can be treated as if uniformly distributed on the shell's circumference. Under this assumption, the stiffened shell is modeled as an equivalent orthotropic shell.

PANEL BUCKLING - If the stringers and rings (if they are present) are sufficiently rigid, the cylinder can be treated as a series of curved panels each of which is supported along four edges. If the panel is short and its curvature small, the panel buckles essentially as if it were a flat plate, which is treated in Chapter 4. For long panels or those with larger curvature, an estimate of the elastic buckling strength can be obtained by using the equations for moderately long unstiffened cylinders.

INDIVIDUAL STRINGERS - Buckling of individual stringers can be investigated by treating the stiffener and an effective width of shell as a column. The critical load of a typical stringer and effective shell skin is obtained by assuming it to behave as a column on an elastic foundation. Ring stiffeners act as the foundation, and depending on their spacing and area, the foundation is considered to be continuous or made up of elastic or rigid point supports.

LOCAL YIELDING - This is more of a stress analysis problem than a stability problem, but it must be given consideration.

Reference is made to Chapter 4 for a better understanding of stiffened plate behavior, which has some similarity to stringer stiffened cylinders in compression.

If stringers are spaced more closely than the buckling wave length of the shell, they will increase the critical pressure. Very little information is current available on this topic but test programs are currently underway to study the influence of size and spacing of stringer stiffeners on the critical pressure.

CONCLUSIONS

Ring stiffeners are used primarily to increase the critical external pressure while stringer stiffeners are most effective for axial compression and bending. A large volume of equations would be required to treat all the combinations of parameters and potential failure modes. The Guide recommends equations and details of procedures for determining critical pressures of ring stiffened cylinders. However, the treatment of stringer and combined stiffener arrangements and other loads is largely qualitative.

ON THE BEHAVIOUR OF DAMAGED AND INTACT STIFFENED CYLINDRICAL SHELLS

Patrick J Dowling and Beverley F Ronalds
Department of Civil Engineering
Imperial College, London, England

SUMMARY

This paper briefly summarises work at Imperial College on the inelastic buckling strength of ring-stiffened and stringer-stiffened cylindrical steel shells under axial and combined axial and pressure loading. It then concentrates on the most recent research relating to the denting of such shells and the residual strength of the damaged shells. The results of experimental programs and a new numerically based computer package, FINAS, have been used to validate simple analytically based methods. These are intended for use by designers to estimate the extent of damage caused by, say, a supply ship impacting the leg of an oil rig and thereafter to estimate the knock-down in strength of the damaged shell compared with that of the original undamaged or intact shell.

INTRODUCTION

Over a period of nearly ten years a number of studies have been undertaken at Imperial College concerning the ultimate load behaviour of stiffened cylindrical shells used in offshore structures. This work brought progressive developments in analytical techniques as well as in the fabrication and testing of small-scale models. Ring-stiffened, stringer-stiffened and orthogonally-stiffened shells have been tested under combinations of axial compression and external pressure loadings.

Early analytical work concentrated on inter-ring buckling of ring-stiffened shells, using a finite difference approach [1]. Subsequent numerical analyses have been undertaken using the finite element package, FINAS, which was developed at Imperial College. The inclusion of an eight-noded isoparametric shell element, and a compatible stiffener capable of representing any open-section stiffener with cross-section comprising rectangular elements, makes this package particularly suited to stiffened shell structures. In addition to FINAS several simpler mechanism approaches have been developed to model various aspects of shell behaviour. These analyses have been correlated with both FINAS and the test results.

The research programmes are very briefly outlined in the following sections with emphasis placed on the most recent results concerning the effect of local damage in the shells.

1. RESEARCH ON INTACT STIFFENED CYLINDERS

1.1 Longitudinally-stiffened Shells

Several test series have been undertaken on stringer-stiffened shells, firstly under concentric and eccentric axial compression, and later under combined axial and pressure loading. All models had either twenty or forty stringers for ease of fabrication. There were no intermediate rings (although strong rings were attached to each end) and thus the models represented one bay of an orthogonally-stiffened shell. Three bay orthogonally-stiffened models have been fabricated more recently and used in the damage tests discussed in a later section. The range of geometries chosen in the tests

ensured that failure occurred in different modes. Both local buckling of the shell between stringers and general buckling of the stringer-stiffened bay were produced experimentally.

Corresponding analytical work has concentrated on the local failure mode of the inter-stringer panels. A single stiffener between two adjacent half panels was modelled using the finite element package FINAS [1]. The centre-lines of the panels were assumed to be lines of symmetry, and symmetry was also invoked around the circumferential centre-line. Comparison between this model and test results can be seen in Fig. 1. Subsequently a parametric study was carried out on a range of geometries and loadings which produced local panel failures and the results of the study were used in a detailed examination of available design guidance.

In another approach a general collapse mechanism theory was established using rigid panel elements [1]. The method is closely parallel to the development of rigid-plastic finite elements. Correlation between the mechanism unloading curve for a curved panel and the corresponding FINAS results is shown in Fig. 2.

1.2 Ring-stiffened Shells

Two mechanism analyses have been developed for ring-stiffened shells [1]. The first looked at inter-ring panel failure under interactive loading while the second considered overall failure of the cylinder, including the rings, under predominant pressure loading. By combining the two mechanisms for a given size of stiffener, the point at which the two failure modes were predicted to be coincident could be obtained (see Fig. 3). Conversely, by varying the size of the stiffener, the optimum stiffener area required to just prevent overall buckling could be obtained. An example of a design chart produced in this way is shown in Fig. 4. Finite element analysis was used to validate the results and also to provide data beyond the range of applicability of the mechanisms (for example, in the geometrical ranges appropriate to elastic buckling). Two series of tests were also conducted to provide data under interactive loading.

2. DAMAGE TESTS ON STIFFENED CYLINDERS

Over twenty damage tests have been conducted on ring-stiffened [2-5] and orthogonally-stiffened [6-9] cylindrical shells in the slenderness range $133 < R/t < 267$. The damage was applied using a wedge-shaped indenter with a radiused nose, aligned perpendicular to the longitudinal axis of the cylinder. The indenter was positioned at different longitudinal locations in relation to the rings to generate both near-ring and mid-bay dents. Residual dent depths of up to 5% of the diameter were produced. The deformed shells were subsequently loaded in axial compression to determine the effect of the damage on their buckling behaviour. Analytical techniques have been developed for both the denting and compression phases of the tests.

2.1 Longitudinally-stiffened Shells

A plastic mechanism analysis of the denting process was developed in which the stiffened shell was divided into a number of imaginary longitudinal beams [8]. The beams become loaded as the dented area gradually increases and this load is carried in axial tension and bending. The analysis is compared with test data for an orthogonally-stiffened shell in Fig. 5. A step increase in load carrying capacity is predicted when the dent edge (as measured by φ_D) reaches a stringer. The symbol φ_P indicates when the intermediate ring stiffeners begin to deflect radially at a stringer position, which produces a small reduction in lateral stiffness.

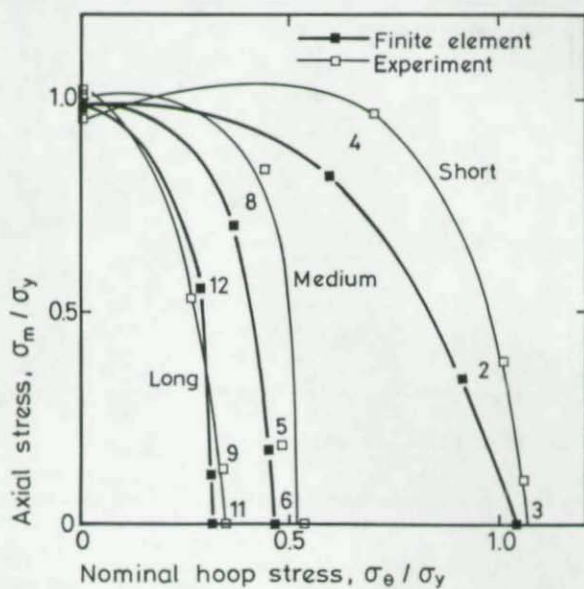


Fig. 1 Collapse strength under combined axial and pressure loading

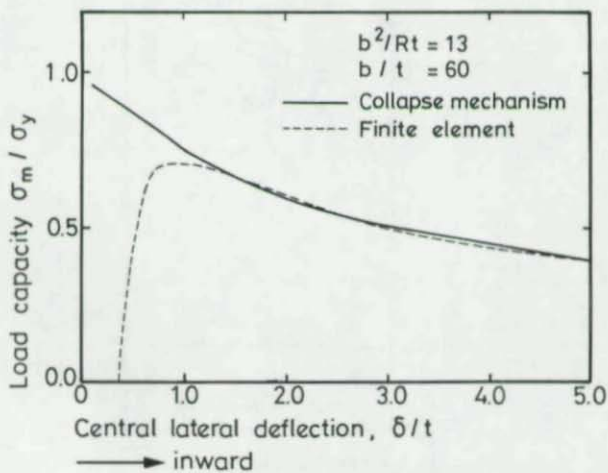


Fig. 2 Mechanism analysis of curved panel under in-plane load

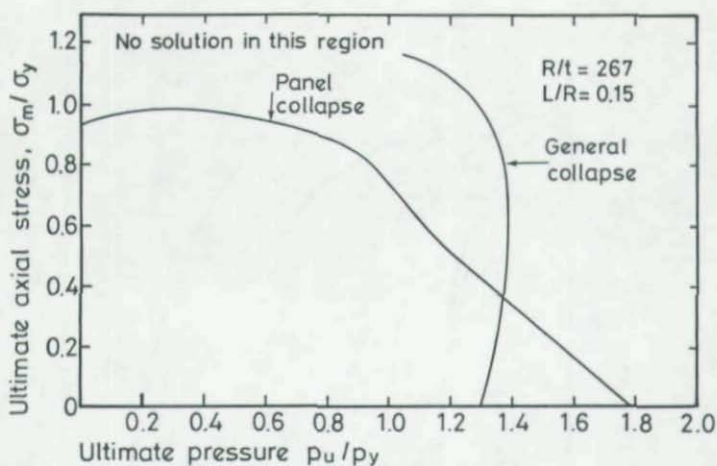


Fig. 3 Collapse strengths under combined loading for a particular stiffener geometry

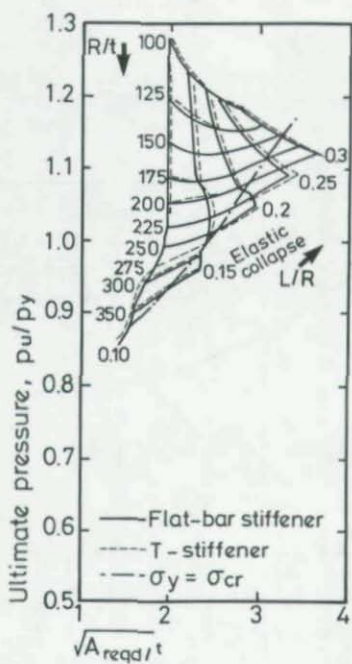


Fig. 4 Required ring stiffener area for hydrostatic loading

The thinner dashed line in the Figure is a membrane solution found by assuming that the tensile stress in the dented beam strips is at yield. This simple approximation compares well with both the more rigorous mechanism solution and the test points. The ends of the shells were restrained during denting by stiff end blocks, enabling membrane effects to become the dominant mode of lateral resistance. The actual development of membrane stresses in the dent zone during lateral loading is illustrated in Fig. 6.

In the compression tests the dent was found to carry very little longitudinal stress. This suggested an analysis of the axial response which simply neglected the damaged material [7]. The load was redistributed circumferentially to the effective arc of undamaged material, with the maximum stresses occurring immediately adjacent to the dent. The damaged cylinders failed when the maximum stresses attained the collapse strength of the intact shell geometry. This approach gave good correlation with the experimental results, as shown in Fig. 7. In this diagram the residual strength is drawn as a function of dent depth for three values of compression load eccentricity from the cylinder centre. The triangles represent test points for orthogonally-stiffened models in which the net load was applied a small distance away from the centre ($0.045 < ecc/R < 0.086$). Ring-stiffened cylinders were loaded concentrically ($ecc/R = 0$) and the results are marked using circles.

The most slender models fell below the predictions in Fig. 7 and the additional weakness was caused by the material next to the dent. This material, although "undamaged", had imperfections caused by its proximity to the dent. Firstly, it had significant radial distortion. Superimposed on the initial deflections formed during fabrication was an outward bulge produced under lateral loading to help relieve the circumferential shortening in the dent and to reduce the local circumferential curvature. Secondly, compressive stresses were generated here during denting (Fig. 6) and some residual stress may have remained after the lateral load had been removed. These imperfections were quantified for a typical ring-stiffened cylinder using FINAS and are discussed below.

2.2 Ring-stiffened Shells

For ring-stiffened shells the lateral loading process was modelled using finite element analysis [3]. The results gave a detailed picture of stresses and deformations during both loading and unloading and the latter enabled the residual state of the dented shell to be determined. Computed residual deflections and stresses are plotted in Fig. 8. The left side of the diagram shows the deflection profile around the circumferential centre line of the dent, to an exaggerated scale, and the right side shows the average longitudinal residual stresses at mid-panel. A peak outward bulge of approximately $0.12\delta_0$ occurred adjacent to the dent in a region of tensile residual stresses of up to $0.6\sigma_Y$. Compressive stresses of $0.3\sigma_Y$ occurred further round the circumference, combined with diminishing outward deflections which eventually became inward locally.

The compression tests of the damaged ring-stiffened shells were also analysed using FINAS [4,5], with good correlation being achieved. Fig. 9 compares the analysis and test results for a typical ring-stiffened model. A finite element prediction of the response of the corresponding undamaged geometry is included to show the stiffness and strength loss caused by denting.

These two numerical models were combined in a parametric study [5] of slender ring-stiffened shells in the range $300 < R/t < 500$, which was outside the scope of the tests. Experimental results had pointed towards an increase in sensitivity to damage for more slender geometries, (Fig. 7) possibly due to the dent deformations acting as a

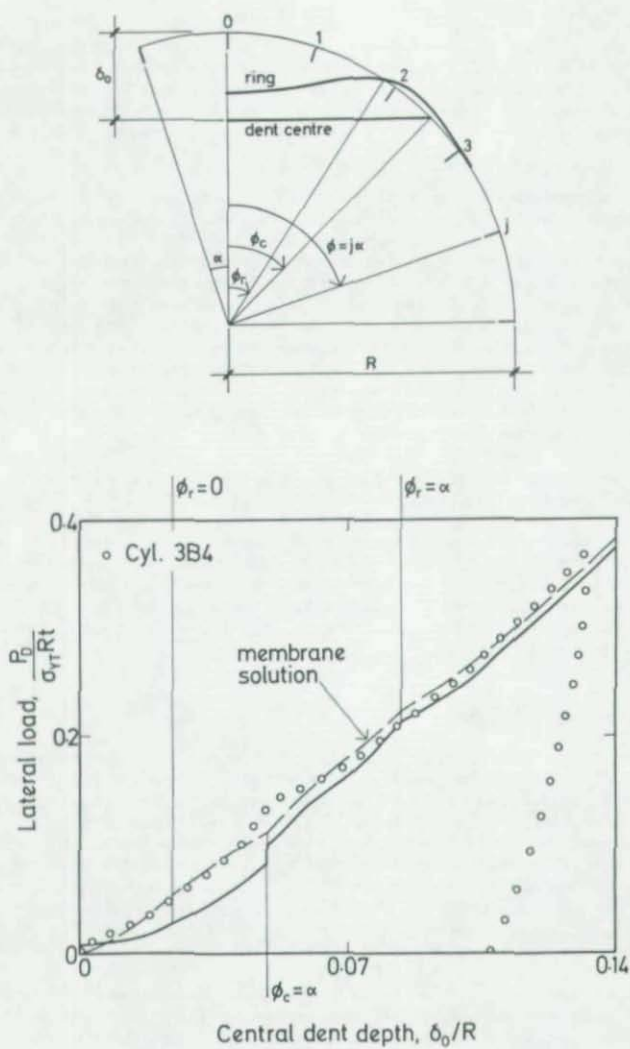


Fig. 5 Damage loading response of orthogonally stiffened shell

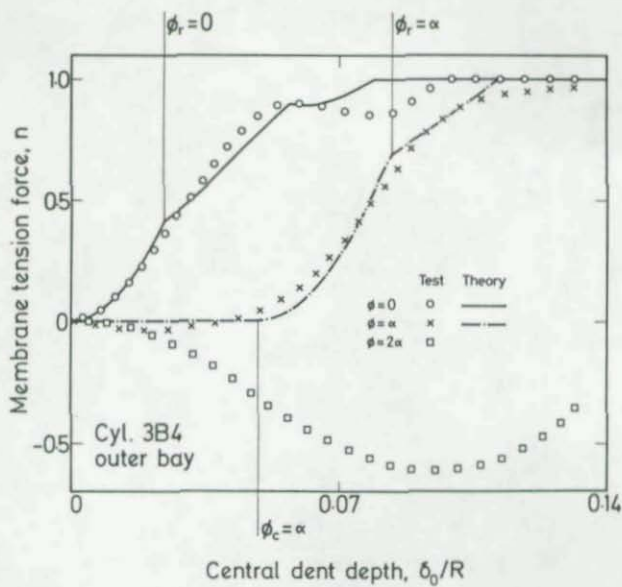


Fig. 6 Longitudinal membrane forces in dent zone

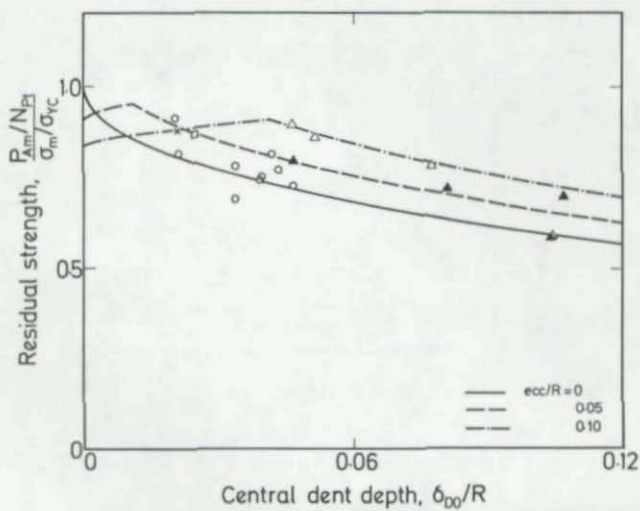


Fig. 7 Residual compressive strength of damaged shells

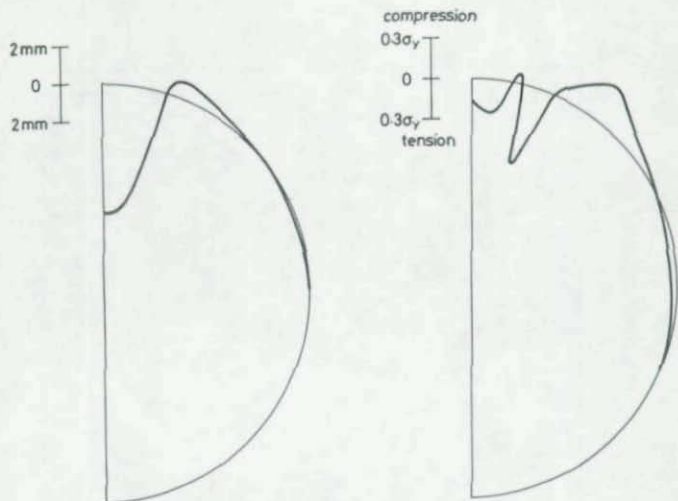


Fig. 8 Residual deformations and stresses after denting

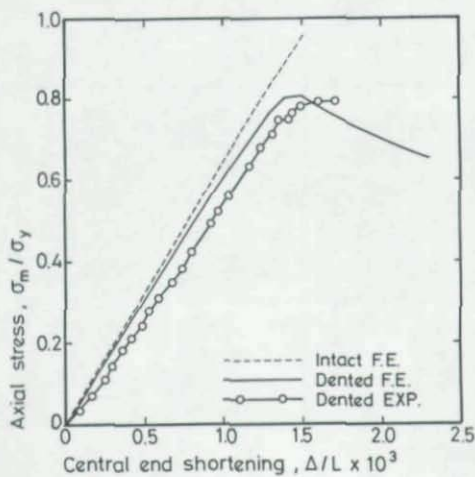


Fig. 9 Compression loading response of ring stiffened shell

sympathetic imperfection. The parametric study was intended to examine the implications of such a trend. Initially perfect shells were analysed to investigate the possible interaction between the dent form and different modes of collapse. Initially imperfect shells were also examined to enable an assessment of the effect of general imperfections to be made. Preliminary results indicated that there was little increase in the sensitivity to denting as the slenderness increased. The study showed that the simple effective section approach would still give good strength estimates in this slender range of geometries, with a 10% reduction in the predictions providing safe results. However further work is necessary to confirm the range of geometries in which these conclusions remain valid.

CONCLUSIONS

- a) New experimental and theoretical results are available to improve current design rules for stiffened cylindrical shells.
- b) A powerful numerical program, FINAS, has been produced to deal specifically with the non-linear inelastic buckling of stiffened shells and was used in the design of the first Tension Leg Platform.
- c) Verified simple new methods to predict the extent of damage to shells caused by impact are now available.
- d) A verified simple new method to predict the residual strength of damaged shells is also available.

ACKNOWLEDGEMENTS

The authors would like to acknowledge the contributions of all the research workers involved in the various programmes and also the help of the laboratory technicians who made the testing work possible. Of the testing described in the early part of the paper, the axial experiments were conducted at Imperial College while the interactive loading, including pressure, was carried out at the University of Surrey.

The authors are indebted to the various sponsors of the work, including the UK Science and Engineering Research Council, the UK Department of Energy, and the Norwegian Classification Society (DnV).

REFERENCES

1. HARDING J.E. and DOWLING P.J., Recent research on the behaviour of cylindrical shells used in offshore structures. *Steel Structures - recent research advances and their applications to design*, ed. Pavlovic M.N., 317 (1986).
2. ONOUFRIOU A. and HARDING J.E., Effect of impact damage on the residual strength of ring stiffened cylinders. *Proc. 5th. Int. OMAE Symp.*, Tokyo, ed. Chung J.S. *et al*, III, 315 (1986).
3. ONOUFRIOU A., ELNASHAI, A.S., HARDING J.E. and DOWLING P.J., Numerical modelling of damage to ring stiffened cylinders. *Proc. 6th. Int. OMAE Symp.*, Houston, ed. Chung J.S. *et al*, I, 281 (1987).
4. ONOUFRIOU A., HARDING J.E. and DOWLING P.J., Impact damage on ring stiffened cylinders. *Stability of Plate and Shell Structures*, Proc. Int. Colloq., Ghent, ed. Dubas P. and Vandepitte D., 493 (1987).

5. ONOUFRIOU A., Collapse of damaged ring stiffened cylinders. Ph.D thesis, Imperial College, University of London (to be submitted 1987).
6. RONALDS B.F. and DOWLING P.J., Finite deformations of stringer stiffened plates and shells under knife edge loading. *Proc. 5th. Int. OMAE Symp.*, Tokyo, ed. Chung J.S. *et al*, III, 323 (1986).
7. RONALDS B.F. and DOWLING P.J., Residual compressive strength of damaged orthogonally stiffened cylinders. *Stability of Plate and Shell Structures*, Proc. Int. Colloq., Ghent, ed. Dubas P. and Vandepitte D., 503 (1987).
8. RONALDS B.F. and DOWLING P.J., A denting mechanism for orthogonally stiffened cylinders. Submitted for publication.
9. RONALDS B.F. and DOWLING P.J. Local damage effects in cylinders stiffened by ring and stringers. *Steel Construction Offshore/Onshore Conf.*, London (April 1987).

A.C. Walker; S. McCall; M.K.Kwok
Department of Mechanical Engineering, University of Surrey,
Guildford, U.K.

INTRODUCTION

This paper presents the methodology of, and results from, a series of tests on ring stiffened cylinders which were initially subjected to simulated collision damage and then loaded to failure with a combination of external pressure and axial compression. These tests are one component of a research programme initiated and funded jointly by the UK Department of Energy and the Science and Engineering Research Council, Marine Technology Directorate. The research was a co-operative venture involving a number of Universities in the UK; coherence was maintained by the appointment of a Steering Committee and an industrial company (J.P. Kenny & Partners Ltd., London) to act as managers. Full details of the types of shells tested, the loading parameters and test results are contained in the final report ^(1,2) prepared by the managing company and the researchers.

The stimulus for the tests reported here comes from a requirement for engineers to be aware of the implications which minor damage may have for the strength of thin-walled stiffened shells which commonly form components in floating offshore structures. Whereas a large database exists for the strength of as-built shells there is relatively little information on the corresponding energy absorption and damage tolerance characteristics. A recent survey⁽³⁾ has shown that minor impacts are not rare events and so damage tolerance, etc., has considerable practical significance.

In the testing reported here, it was decided at the outset to impose the damage to the test shell using a knife edged indenter with its axis at right angles to the axis of the shell. In practice, of course, damage can be inflicted on a shell in a variety of ways; an attendant vessel may hit the structural member with its bow, stern or side. The vessel may be more or less structurally rigid than the shell and this absorbs more or less of the collision energy. It was considered here that the use of a rigid knife-edged indenter would inflict damage on the test shells which would tend to be more severe than the corresponding practical circumstances. This is open to debate but nevertheless the information obtained from tests on shells thus damaged will certainly give valuable insight to the behaviour of shells with other forms of damage.

DESCRIPTION OF TEST PROGRAMME

The geometries of the test shells are shown in Fig.1. The simulated damage, i.e. the dent, was imposed at mid-length of each shell, so that for the plain ring stiffeners the damage occurred on a panel, midway between two rings. The indenter was applied in the plane of a T-ring stiffener in the cases of shells R3 and R4. In the tests reported here, the shells were to be subjected to damage and then

loaded with a combination of external hydrostatic pressure and axial compressive loading until failure occurred. Table 1 presents the level of residual damage, i.e. dent depth, d_r , and the specified magnitude of the applied hydrostatic pressure.

TABLE 1. TEST PARAMETERS

Shell Code	Type	d_r (mm)	p (N/mm ²)
R1	Plain ring stiffeners	5.3 (9t)	0.5
R2	" " "	5.3 (9t)	1.0
R3	T-ring stiffeners	3.0 (5t)	1.0
R4	" " "	3.0 (5t)	0.5

where t is the thickness of the shell skin.

The T-rings of shells R3 and R4 were designed to have approximately the same value of second moment of areas as the plain ring in shells R1 and R2.

The shells had been manufactured using techniques developed in previous programmes of investigation into shell buckling. The fabricated shells were stress-relieved and attached to rigid end rings using a mixture of sand and Araldite. This has been found to give end conditions to the shell which very closely reproduce classical encastre conditions. The averaged material characteristics are given in Table 2.

All the shells had their initial imperfections measured and analysed statistically to provide a best-fit cylinder. The magnitudes of the imperfections in all the shells were found to be less than those corresponding to code tolerances. Details of these results are presented in Ref.1.

TABLE 2. AVERAGED VALUES OF MEASURED MATERIAL CHARACTERISTICS (N/mm²)

Shell Skin;	$\sigma = 387$, $E = 208 \times 10^3$; $\nu = 0.29$
Plain Ring Stiffeners	$\sigma^0 = 387$, $E = 208 \times 10^3$; $\nu = 0.29$
T-Ring Stiffeners	$\sigma^0 = 366$, $E = 205 \times 10^3$; $\nu = 0.29$

where σ is the tensile yield stress, E is Young's modulus and ν is Poisson's ratio.

The shells were all very extensively strain gauged, both for the denting tests and for the failure tests. A layer of brittle lacquer was also applied to the shells to provide information on the development of the damage region during the denting test. The failure tests were performed in a hyperbaric chamber in the University of Surrey; the chamber had the facilities to apply axial loading to the test shell and to permit strains and deflections to be measured during the test.

SUMMARY OF TEST RESULTS

The following is a very brief summary of the results of the various phases of the test programme

Shells R1 and R2

The results from the denting test in R1 is considered here, the results from the corresponding test on R2 were, within engineering accuracy, identical. Figure 2 shows the external view of shell R1 on completion of the denting tests; it may be seen from the crazing pattern in the brittle lacquer that the dent pattern extends through the ring stiffeners. Except for the small regions with no cracking, the shape of the dent boundaries was very similar to that observed on unstiffened shells⁽⁵⁾. This similarity is reinforced by the results in Fig. 4 which show that the relationship between the applied denting load, F , and the corresponding residual dent depth, d_r , i.e. that which remains when $F = 0$, can be predicted using an analysis developed for a plain shell⁽⁴⁾. It would seem that the plain stiffeners are subjected to very large values of tensile and compressive strains during the denting process, see Fig.4 for strain gauge layout and Figs. 5 & 6 for typical results. The gauges on the stiffener at the dent centre line show that even for very small values of indenter load, strain values well in excess of the material yield strain are induced. The gauges at position 13 show that for an indenter load up to 2kN the stiffener is subject to moderate values of compressive strains. At that load the yield strain is induced and the stiffener is quickly strained to a state where plastic tripping occurs. This local buckling of the stiffener is shown in Fig.7 which is a photograph of the interior of the shell R1 subsequent to its failure. It would appear from the results of the tests on R1 and R2 that this form of stiffener provides virtually no support to the shell in resisting lateral impact loading.

Shells R1 and R2 were each loaded in external pressure subsequent to the denting. Figure 8 is a recording of pressure vs. time for shell R1. It may be seen that at a pressure of 0.4 N/mm^2 the shell suffered a localised buckling, as indicated by the sudden drop in applied pressure due to the change in volume of the shell as it buckled. It is evident from Fig.9, that the stiffener was severely strained by the application of the pressure. When the strain level developed sufficiently beyond the material yield strain the ring stiffener developed a plastic mechanism and could no longer sustain increasing pressure loading. When the stiffener nearest the initial damaged region buckled due to the pressure, the loading on all the other stiffeners were required to carry considerably increased loading circumferentially, in the line of the original damage region. That they could not sustain this loading and buckled is evident from Fig.7. It may be surmised that if the shell had been longer and incorporated more plain ring stiffeners, they in turn would have collapsed in a "cascade" effect and the length of the buckle would be limited only by the provision of rigid ring stiffness or diaphragms.

Subsequent to this initial buckling, the shells R1 and R2 stabilised and were capable of carrying increased pressure loading. Shell R1 was pressurised to 0.5 N/mm^2 and, with this pressure held constant, was loaded in axial compressive loading until collapse occurred at $P = 29.6 \text{ kN}$. Shell R2 was subjected to slowly increasing pressure loading in an attempt to reach the specified pressure of 1.0 N/mm^2 . Collapse occurred at 0.55 N/mm^2 . It is evident from Figs. 10 - 12 that apart from the damage zone, which was very severely extended and deformed by pressure loading, collapse occurred due to inter-ring

buckling. In other words, it would seem that if the shell had not been damaged the strength of the rings would have been adequate to prevent general buckling. However, the plain ring stiffeners tested here were quite unable to provide the shell with strength to withstand the effects of the imposed damage.

Shells R3 and R4.

The denting tests on Shells R3 and R4 yield virtually identical results. Figures 13 and 14 show external and internal views of Shell R3 at the end of the denting test. Evidently considerable deformation has been imposed but there is no indication that local stiffener buckling had occurred. The development of the damage region appears to have been restricted by the ring stiffeners. Figure 15 shows the test results relating the applied denting load, F , to the corresponding residual dent depth, d_r , and compares them to values obtained from an analysis of a plain shell having the same radius and thickness as R3 but with a length of 48mm, i.e. the distance between the outer T-ring stiffeners. The T-ring stiffeners obviously have an important effect in supporting the shell against damage. This comment is supported by strain gauge results shown in Figs 17 and 18, the strains at position 1, see Fig. 16 on the inside face of the T-ring stiffener exceed yield but are much smaller than the strains recorded on the plain ring stiffness for the same position and corresponding load. None of the strains recorded in tests on the T-ring stiffeners shows any indication of local buckling. The longitudinal strains between the stiffeners exceed the yield strain, see Fig 18, as would be expected with the development of a plastic damage mechanism ⁽⁴⁾.

Subsequent to the denting test the T-ring stiffened shells were able to carry their specified pressure and were loaded to failure by applying a slowly increasing axial compressive loading in conjunction with a constant pressure. Figures 19-21 show the deformed state of the shells after collapse and it is evident that the damage zone had not extended significantly and that collapse was caused by inter-ring buckling.

Table 3 gives the collapse loads for the four shells considered here.

TABLE 3. LOADING STATES AT SHELL COLLAPSE

Shell code	Hydrostatic Pressure (N/mm^2)	Axial Compressive Load (kN)
R1	0.5	29.6
R2	0.55	-
R3	1.0	58.4
R4	0.5	123.0

CONCLUSIONS

One must be tentative in drawing conclusions from so few tests and in the absence of valid analytical models. However, it would seem evident that the T-ring stiffeners in R3 and R4 were very much more efficacious in resisting the effects of damage than were the plain ring stiffeners of R1 and R2. Indeed the latter seem to be quite valueless in that task while the T-ring stiffeners significantly increased the

damage tolerance of the shells and were able to sustain the specified pressure load in the damaged state. Another conclusion which may be drawn is that if, for any reason, plain ring stiffeners must be used it is vital that stronger ring stiffeners or diaphragms must be incorporated along the length of the shell to prevent disastrous buckling of the damaged zone occurring when the shell is subjected to quite low value of external pressure loading.

ACKNOWLEDGEMENTS

The authors gratefully acknowledge the support of the UK Department of Energy in funding the testing reported here.

REFERENCES

1. Cohesive Buckling Programme Report, UK Dept. of Energy, PED 8, 1987.
2. Walker, A.C., and McCall, S. Strength of Damaged Ring and Orthogonally Stiffened Shells. Report to UK Dept. of Energy, 1987.
3. Ellinas, C.P. and Valsgaard, S., Collisions and damage of offshore structures and State of the Art, Jour. of Energy Resources Tech., Vol. 107, p 297, 1985.
4. Kwok, M.K., and Walker A.C., Process of Damage in Thin-Walled Cylindrical Shells. Advances in Marine Structures, Elsevier and Applied Science, 1987.
5. Kwok M.K., McCall, S., and Walker A.C. The behaviour of damaged cylindrical shells subjected to static and dynamic loading. Proc. of Conf on Appld Solid Mechanics, Strathclyde Univ., 1987.

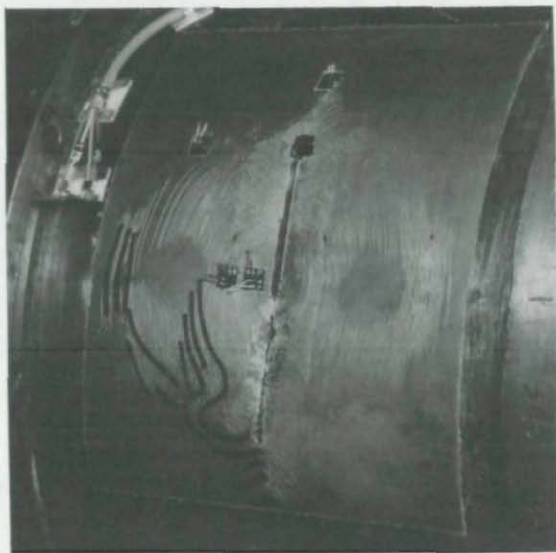
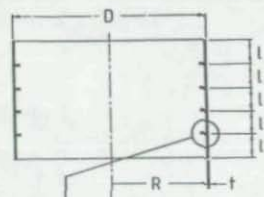


Fig.2

View of dent to external surface showing brittle lacquer crack distribution. R7.



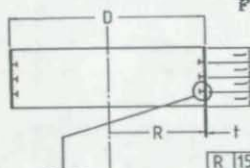
Shells R1 & R2

R/t	l/R	d_s/t_s
267	0.25	8

D	320
l	40
t	0.6
R	180
d_s	4.8
t_s	0.6

mm

Fig.1 Test Shell Geometries



Shells R3 & R4

R	159.8
t	0.6
t_1	0.84
t_2	0.6
b	6
d	3
l	24

R/t	l/R	b/t_1	d/t_2
267	0.15	7.14	5

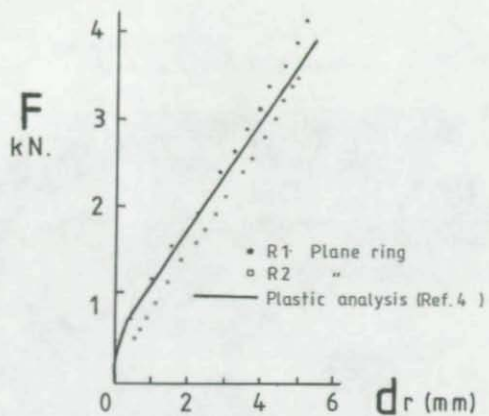


Fig.3

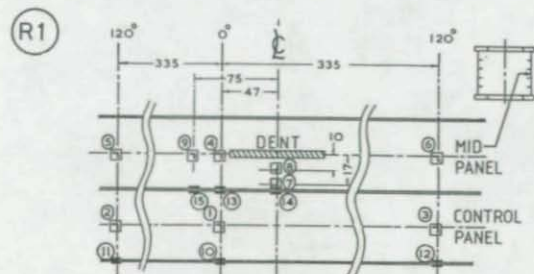


Fig.4

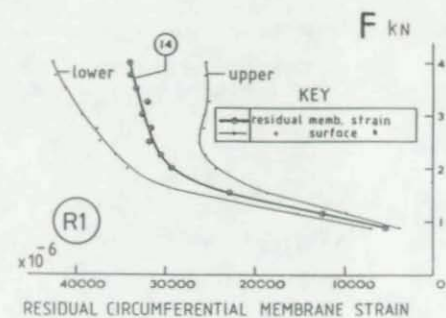


Fig.5

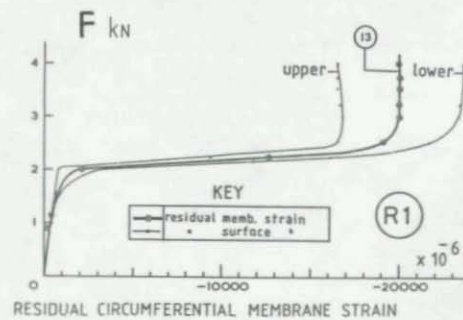


Fig.6

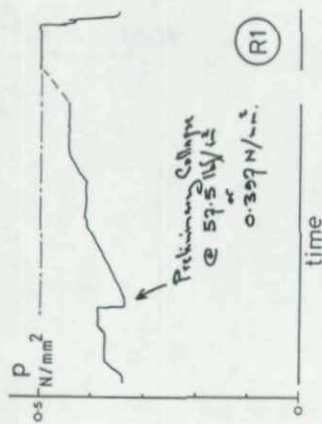


Fig.8 Recording of external pressure vs time

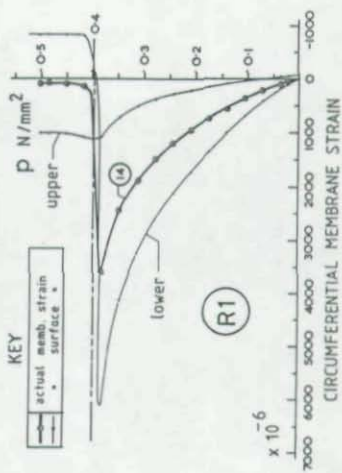


Fig.9 Pressure loading

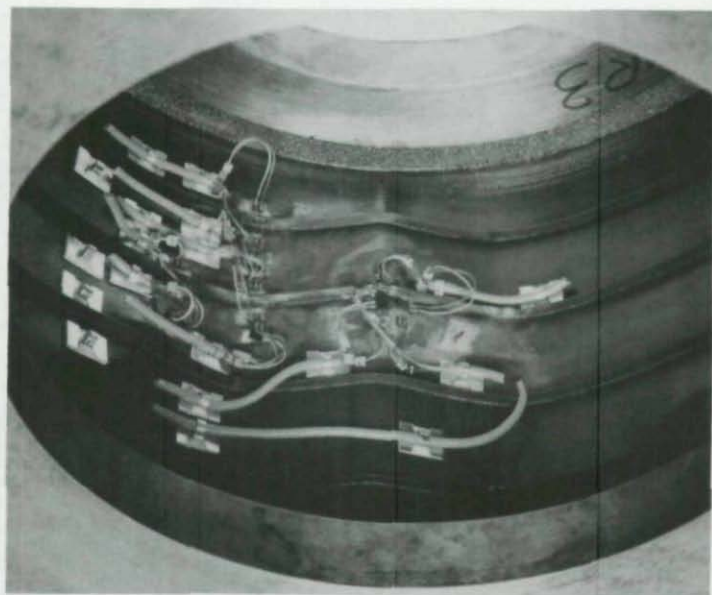


Fig.7 View of internal structural damage to shell at region of dent R1.

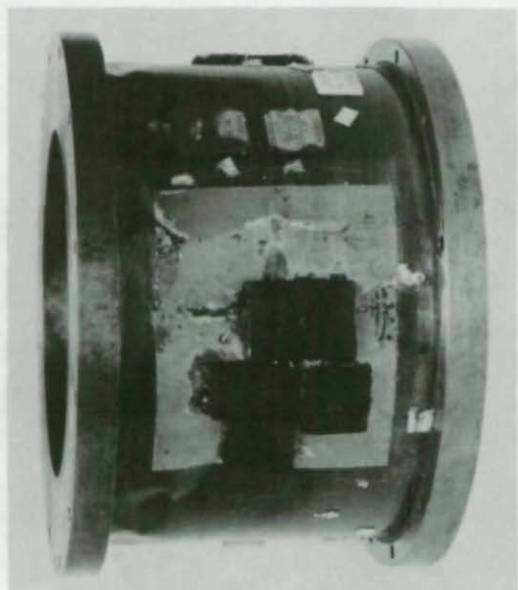


Fig. 10 External view of R1 at collapse

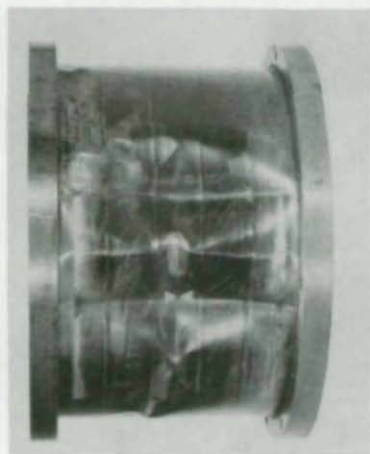


Fig. 11 External view of R2 at collapse

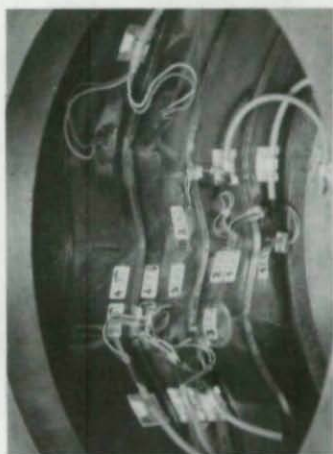


Fig. 12 Internal view of R2 at collapse

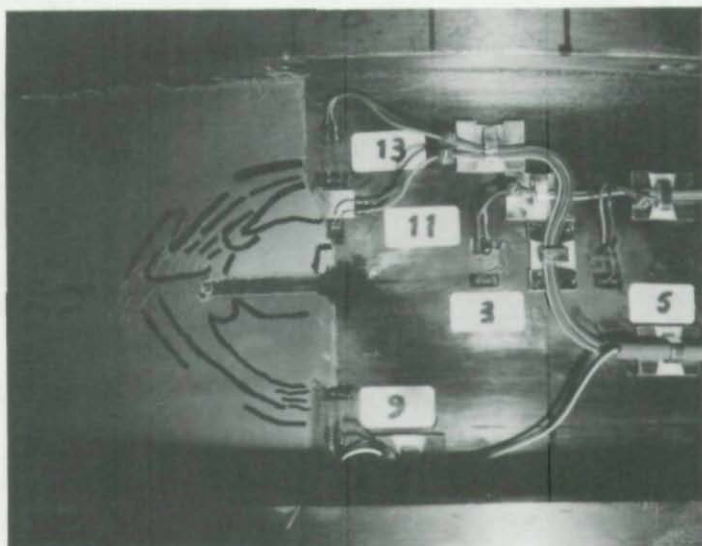


Fig.13 External view of damage on Shell R2.

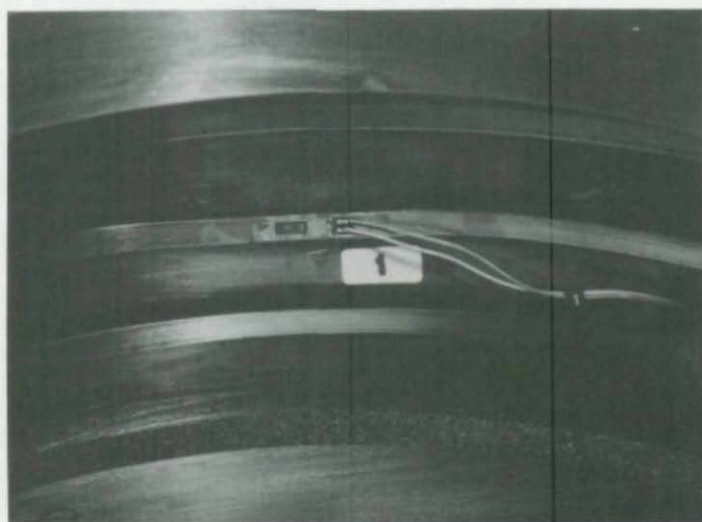


Fig.14 Internal view of damage on shell R3

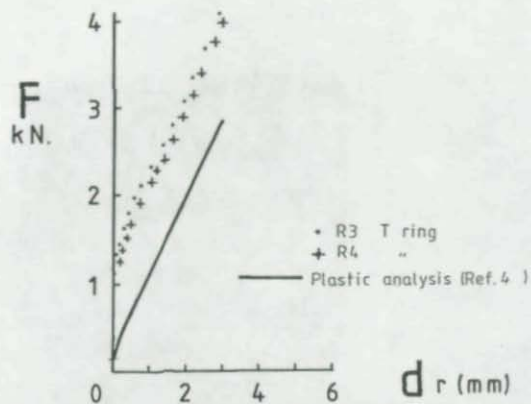


Fig. 15 Analytical and Test Results

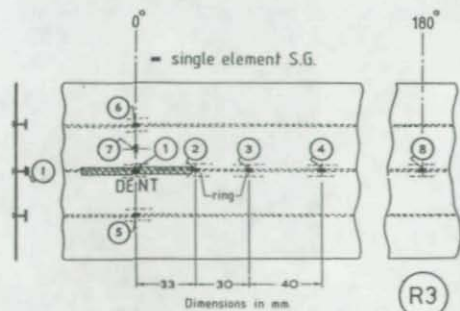


Fig. 16 Strain Gauge Layout

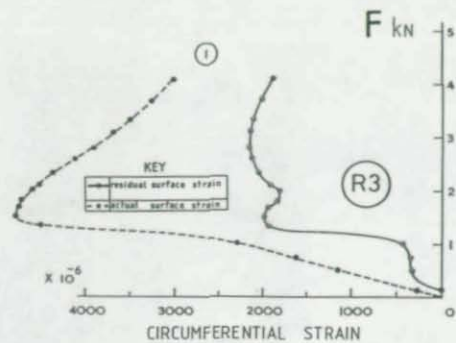


Fig. 17 Denting Test

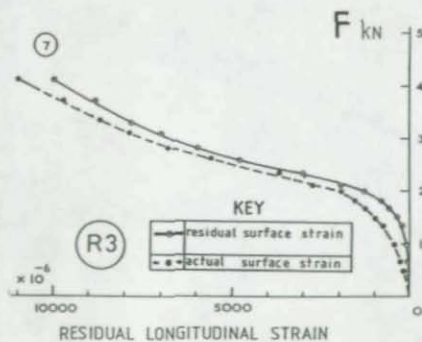


Fig. 18 Denting Test

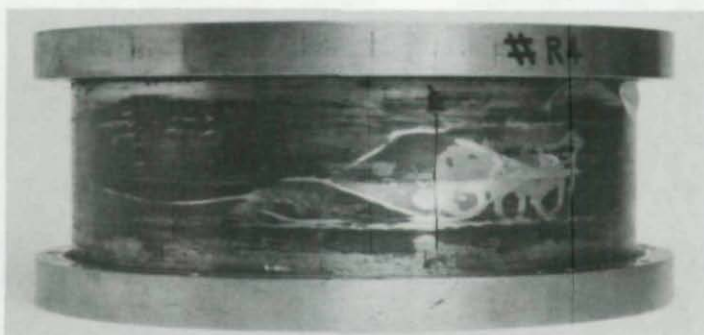


Fig.19 External view of R3 after collapse

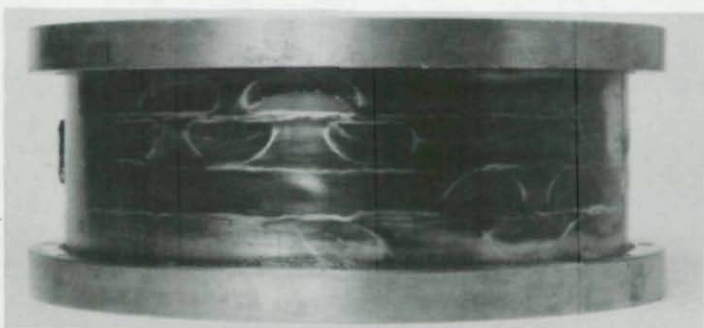


Fig.20 External view of R4 after collapse

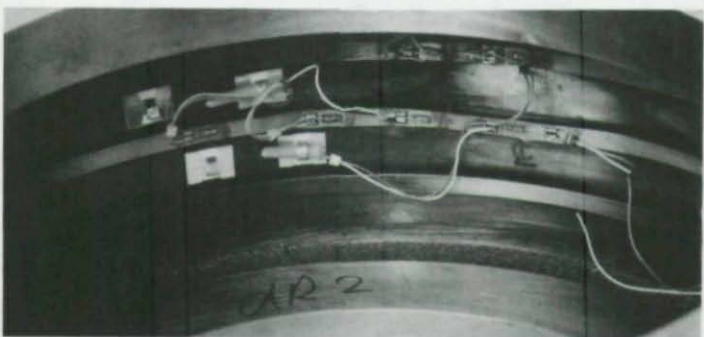


Fig.21 Internal view of R4 after collapse.

API BULLETIN 2U INTERACTION EQUATION FOR STIFFENED CYLINDERS
SUBJECTED TO AXIAL COMPRESSION AND EXTERNAL PRESSURE

C.D. Miller and J.F. Vojta
CBI Industries, Inc.
Research Laboratory
Plainfield, Illinois

SUMMARY

The offshore oil industry in the U.S. has developed a need for design rules for the buckling strength of cylinders having diameter/thickness ratios exceeding 300, and for ring and stringer stiffened cylinders. API Bulletin 2U is being prepared for this purpose.

One important portion of Bulletin 2U contains interaction equations to determine stability of cylinders under combinations of axial, bending, and external pressure loadings. This new interaction equation is of quadratic form, but its shape changes with stress magnitude, cylinder geometry, and buckling mode. It applies to a wide spectrum of geometries and vessel stiffening patterns.

This paper discusses the interaction equation, provides a brief guide to using it in Bulletin 2U, and presents comparisons of its predictions with numerous large scale model tests of fabricated stiffened and unstiffened cylinders. The paper is intended to present an understanding of this equation and its use, rather than attempt to promote or compare its strengths against other techniques.

INTRODUCTION

In recent years considerable interest has been focused on the buckling strength of stiffened cylindrical shells subjected to various combinations of axial and external pressure loading conditions. This is particularly true for the offshore oil industry where deep water drilling platforms such as tension leg platforms have become a reality. These require stability designs for cylinders with geometric parameters not previously tested or formulated to a sufficient degree.

In the United States the most commonly used rules for design of cylinders for offshore structures are those given by the American Petroleum Institute in API RP 2A (1). The rules are limited, however, to unstiffened and ring stiffened cylinders with diameter/thickness (D/t) ratios of 300 or less. Economical offshore designs, however, are now investigating ring and stringer stiffened cylinders having D/t values up to 1000.

Det Norske Veritas (2) updated its criteria for buckling strength evaluation in 1982. These rules can be applied to unstiffened, ring stiffened, stringer stiffened, or ring and stringer stiffened cylinders having larger D/t values. However, DNV emphasizes very close stringer spacing and other seemingly conservative techniques. These rules also appear to be inconsistent with more recent test results.

Tests have recently been performed to provide data for some of the missing parameter values. For example, buckling tests were reported (3) in 1983 on 66 large scale fabricated ring stiffened and ring and stringer stiffened cylinders with D/t ratios to 1000 and subjected to combinations of axial load and external pressure. Using the additional test data, the American Petroleum Institute will publish API Bulletin 2U (4) in April, 1987. This bulletin presents a design/analysis procedure based on semi-empirical formulations for evaluating the buckling strength of unstiffened, ring stiffened, stringer stiffened, or ring and stringer stiffened steel shells. It follows the design methods of ASME Code Case N284 (14) with modifications based upon tests and analytical studies conducted since 1979. Bulletin 2U is applicable to D/t ratios up to 2000 and uses a unique interaction equation to determine stability under general loading cases of combined axial load and external pressure.

The interaction equation in Bulletin 2U is of quadratic form but its shape changes with cylinder geometry, stress level, and buckling mode. This equation essentially covers the full spectrum of geometry and loading conditions anticipated for current designs in accordance with API Bulletin 2U. This paper will discuss this interaction equation, its use, and will compare it against some current test results.

API BULLETIN 2U STABILITY APPROACH

The general equations in Bulletin 2U to predict shell buckling stresses are (Eqs. 3-1 and 3-2 in Bulletin 2U):

$$F_{iej} = \alpha_{ij} \sigma_{iej} \quad (\text{for elastic shell buckling}) \quad (\text{Eq. 1})$$

$$F_{icj} = \eta F_{iej} \quad (\text{for "inelastic" shell buckling}) \quad (\text{Eq. 2})$$

where σ_{iej} is the theoretical elastic buckling stress based on classical linear theory and α_{ij} and η are reduction factors which account for the effects of imperfections, boundary conditions, residual stresses, and nonlinearity of material properties. The reduction factors were determined from test data. The subscripts (see nomenclature and Bulletin 2U) typically are as follows:

- i = denotes direction (and load); subscripts are ϕ , θ , x, h, r.
- e, c = denotes elastic or inelastic stresses, respectively
- j = denotes shell buckling failure mode (L = local shell buckling, B = bay instability, G = general instability)

The above equations are used to calculate predicted buckling stresses for the specific uniaxial load cases of axial load only (F_{xej} and F_{xcj}), and radial external pressure only (F_{rej} and F_{rcj}). Factors of safety and other such design considerations can be entered into the design by methods discussed in Bulletin 2U.

The calculation of uniaxial stresses F_{xcj} and F_{rcj} are made separately for each of the shell buckling modes (local shell buckling ($j = L$), bay instability ($j = B$) or general instability ($j = G$)). Other modes (stringer tripping or column buckling), are controlled by other checks in the bulletin. Design techniques are also presented to preclude interaction between the buckling modes.

API BULLETIN 2U INTERACTION EQUATION

Having calculated F_{xcj} and F_{rcj} for each selected buckling mode, interaction equations can now be used to determine the failure stresses for various combinations of axial load and external pressure. Based on Ref. 5 it was deemed reasonable and conservative to treat stresses from full section bending as equivalent membrane axial stresses. Section 6 of API Bulletin 2U provides the rules for use of the interaction equations.

For cases involving net axial tension combined with hoop compression a bi-linear stress envelope is used. This will not be further discussed.

For the more common cases involving net axial compression combined with hoop compression, a special quadratic failure envelope is utilized. The axial stresses are normalized by the predicted uniaxial failure stress F_{xcj} , while the hoop stresses are normalized by the predicted uniaxial hoop stress F_{rcj} . The end points of the curve are both equal to -1.0 (sign convention discussed later). Load combinations lying inside the curve are considered acceptable, those outside are unacceptable. The interaction curve is:

$$R_a^2 - cR_aR_h + R_h^2 = 1.0 \quad (\text{Eq. 3})$$

where:

$$R_a = F_{\phi cj} / F_{xcj}$$

$$R_h = F_{\theta cj} / F_{rcj}$$

c = coefficient dependent on cylinder stiffening configuration, load magnitude, and buckling mode

$F_{\phi cj}$ and $F_{\theta cj}$ = coincident failure stresses in the axial and hoop directions (after applying modification factors $K_{\phi j}$ and $K_{\theta j}$)

Investigations (6,7) of various ring stiffened model tests noted that the form of the interaction curve tends to flatten out for elastic buckling and approaches the elliptical Hencky-von Mises failure curve for highly inelastic buckling. When this occurs, higher compressive axial stresses can occur under combined loads than for axial load alone. Expanding the approach to ring and stringer stiffened cylinders, the coefficient c in Eq. 3 was thus formulated to better predict the shape.

Figure 1 demonstrates various forms of the interaction curve which result from varying "c" in Eq. 3. When $c = +1.0$, the Hencky-von Mises curve results. When $c = 0$, a circle results. When $c = -1.0$ the curve has become quite flat. The hypothetical case of $c = -2.0$ would be a straight line.

API Bulletin 2U suggests the following formulae for determining "c".

- 1) Unstiffened and Ring Stiffened Cylinders (both shell buckling modes, $j = L, G$)

$$c = \frac{F_{xcj} + F_{rcj}}{F_y} - 1.0 \quad (\text{Eq. 4})$$

- 2) Stringer Stiffened and Ring and Stringer Stiffened Cylinders
 a) Local buckling mode ($j = L$)

$$c = \frac{0.4 (F_{xcj} + F_{rcj})}{F_y} - 0.8 \quad (\text{Eq. 5})$$

- b) Bay instability and general instability modes ($j = B, G$)

$$c = \frac{1.5(F_{xcj} + F_{rcj})}{F_y} - 2.0 \quad (\text{Eq. 6})$$

where F_y = effective yield stress (use the greater of F_{ys} , F_{xcj} , or F_{rcj})

For design/analysis purposes the interaction curve can be used many ways. As one example, assume a geometry has been decided and we want to determine what maximum net axial load (N_ϕ) that can be sustained for a selected pressure load (N_θ). Assume local buckling is considered ($j = L$). The steps are:

- 1) Determine F_{xCL} and F_{rCL} for geometry by Eqs. 1 and 2 and methods in Section 4 of Bulletin 2U.
- 2) Calculate c from Eqs. 4, 5, or 6. Generate interaction curve by Eq. 3 ($-R_a$, $-R_h$ quadrant) using end points $(-1.0, 0)$ and $(0, -1.0)$
- 3) For $N_\theta = pR_o$, calculate $F_{\theta CL} = -\frac{pR_o}{t} \cdot K_{\theta L}$ where $K_{\theta L}$ adjusts for the effect of ring stiffener on shell
- 4) Calculate desired $R_h = F_{\theta CL}/F_{rCL}$
- 5) From interaction curve find corresponding R_a value; calculate $F_{\phi CL} = R_a/F_{rCL}$
- 6) Calculate maximum net axial load, N_ϕ

$$N_\phi = F_{\phi CL} \cdot t \cdot K_{\phi L}$$

where N_ϕ = maximum net axial load (axial plus bending)

$$N_\phi = \frac{P}{2\pi R} + \frac{M}{\pi R^2}$$

COMPARISON OF INTERACTION EQUATION WITH TEST RESULTS

Comparisons between interaction Eq. 3 and a variety of test results will now be presented. The test results cover a wide range of geometries, stiffener spacing, load ratios, and shell buckling modes. In addition the test models were fabricated cylinders utilizing rolled plates and welded joints. Some models were stress relieved while others were not. The plasticity factor (η in Eq. 2) accounted for either possibility.

The following interaction equation curves and test points have both been normalized by actual uniaxial stress values. This tends to isolate

the comparison from ongoing changes in formulation and techniques for calculating F_{xc} and F_{rc} . It should also be noted that during tests it is generally quite difficult to uniquely depict shell buckling modes for local buckling and bay instability. These modes occur as an ongoing series of small waves forming over a range of loads or pressures. The test points shown here generally relate to the first such depicted sign of the respective shell buckling mode.

In the comparison plots that follow, test results plotted outside of the interaction curve denote an underprediction; those falling inside depict an overprediction.

Figure 2 shows results from short unstiffened tubular columns under various combinations of axial load, external pressure, and bending moment (8). There were four values of D/t , ranging from $D/t = 31$ (Group 1) to $D/t = 74$ (Group 4). These are short stocky columns which have net axial plus bending stresses approaching (or slightly exceeding) the yield stress. The uniaxial hoop stresses, however, vary from about $0.5 F_y$ to $1.0 F_y$. The uniaxial stresses are shown for reference purposes. For these cases the interaction curves are approaching the Hencky-von Mises curve. The interaction curve appears to predict the results moderately well. In all but Group 1 the deviations are underpredictions of the actual strength. It might also be noted that for these cases the cylinders were capable of sustaining axial loads near, or above, yield stress levels for R_h values up to about 0.8.

Tests by Sherman (9) showed that for cylinders with D/t values less than 48 the buckling stresses related to bending are higher than axial. Bulletin 2U conservatively neglects this effect.

Figure 3 shows results for axial and external pressure loaded ring stiffened cylinders (3, 10, 11). Groups 1, 2, 3, 4 (Ref. 10) were for local buckling failure loads (ring stiffeners intentionally overdesigned) with D/t values from 48 to 96, $M_x = 8.8$ to 24.1, and two different strength materials. These stocky models were designed for uniaxial hoop stresses to range from about $0.5 F_y$ to $0.9 F_y$ with high axial only stresses. Group 6 (Ref. 11) is for local buckling of a thinner shell with moderately short ring stiffener spacing ($D/t = 1000$, $M_x = 6.01$). Group 1-4 is for stress relieved models (3) having a thin shell with a short ring stiffener spacing ($D/t = 600$ and $M_x = 3.4$). In Figure 3 the correlation is again reasonably good, with the better predictions seemingly occurring for the more elastic thin shell cases.

Figures 4 and 5 present comparisons of the interaction equation with the results of a series of 44 tests of ring and stringer stiffened cylinders for Conoco/ABS, et al (Ref. 3). A follow-up series of tests has also been performed, but the results are not available for release at this time. The tests presented here were made on large scale fabricated models (diameters of 28.5 inches to 75 inches) having generally elastic behavior and the following ranges of parameters: $D/t = 380$ to 1000, $M_x = 6.9$ to 17.9, $M_\theta = 2.2$ to 6.0 and various combinations of axial load and external pressure. Two nominal material yield strengths were used (50 ksi and 80 ksi) and most of the models were stress relieved. Welding sizes and procedures were closely scaled to actual conditions, and typical shell imperfections were also incurred during fabrication. All models exhibited

local buckling and bay instability (pressure cases only) but none failed by general instability where ring collapse would be involved.

Figure 4 shows the comparisons for the local buckling mode while Figure 5 presents the comparison for the bay instability mode. It should be noted these are all slender shells with large D/t values. The larger axial F_{xc} (relative to uniaxial hoop F_{rc}) indicates the strengthening effects of stringer stiffeners. The values of "c" are all negative indicating a curve which is flatter than the circular shape ($c = 0.0$). Considering the wide range of parameters, the correlation appears to be very good for both Figures 4 and 5. However, there is a lack of data points at the higher axial stress levels. The follow-up tests should furnish some of this missing data.

DISCUSSION OF INTERACTION EQUATIONS

There are numerous test results for welded steel cylindrical shells for either axial compression alone or external pressure alone. Most of these are for unstiffened or ring stiffened cylinders. Except for the Conoco/ABS tests, there is very little published data available for almost any form of stringer stiffened or ring and stringer stiffened cylinders. It is not surprising, then, that there are numerous forms of interaction equations in existence. The intent of this paper is simply to present the form to be used in API Bulletin 2U and to show some of its correlations with test data. As further test data becomes available further refinement of the methods is expected.

Some methods currently in use are: (i) linear, as per the ECCS code (12), (ii) circular, as per the DNV code (2), (iii) linear/quadratic, as suggested by Odland (13) and (iv) variable quadratic, as discussed in this paper. The linear and circular forms are essentially the same as Eq. 3 when $c = -2.0$ and $c = 0.0$ respectively. The linear case is obviously the most conservative.

Almost all of the methods are intended to be lower bound predictors and safety factors will be applied to obtain allowable stresses.

CONCLUSIONS

The interaction equation presented here can be applied to a wide spectrum of cylindrical shell sizes, stiffener spacing, and combinations of axial, pressure, and external pressure loading conditions. Reasonably good correlation was shown for numerous fabricated steel scale models representative of those in the offshore industry and other fields involving stability design/analysis of cylindrical sections.

NOMENCLATURE

Note: The terms not defined here are uniquely defined in the sections in which they are used.

- i subscript denoting direction and load
 - ϕ - longitudinal direction and any load combination
 - θ - hoop direction and any load combination
 - x - longitudinal direction and axial compression load only ($N_{\theta} = 0$)
 - h - hoop direction and hydrostatic external pressure ($N_{\phi}/N_{\theta} = 0.5$)

	r	- hoop direction and radial external pressure ($N_\phi = 0$)
j		subscript denoting buckling failure mode
	L	- local shell buckling
	B	- bay instability
	G	- general instability
b		stringer spacing measured as arc length along shell mid-thickness
D		centerline diameter of shell
	F_{icj}	predicted inelastic shell buckling stress for fabricated shell
	F_{iej}	predicted elastic shell buckling stress for fabricated shell
	F_y	yield stress of material
	F_{ys}	static yield stress of material (zero strain rate)
	$K_{\phi j}$ and $K_{\theta j}$	axial and hoop stress adjustment factors, see API Bulletin 2U
	L_r	ring spacing
M		applied bending moment across full cylinder cross-section
M_x	L/\sqrt{Rt}	
M_θ	b/\sqrt{Rt}	
N_ϕ		axial load per unit of circumference
N_θ		circumferential load per unit of length
p		applied external pressure
P		applied axial load
R		radius to centerline of shell
R_a	$F_{\phi cj}/F_{xcj}$	
R_h	$F_{\theta cj}/F_{rcj}$	
R_o		radius to outside of shell
t		thickness of shell
α_{ij}		capacity reduction factor to account for the difference between classical theory and predicted instability stresses for fabricated shells
n		plasticity reduction factor which accounts for the nonlinearity of material properties and the effects of residual stresses.
σ_{iej}		theoretical elastic instability stress

PARTIAL GLOSSARY - BUCKLING MODE TERMS

Bay Instability	Simultaneous lateral buckling of the shell and stringers with rings remaining essentially round
General Instability	Overall collapse of the combined shell and stiffening system including lateral buckling of ring stiffeners
Local Buckling	Buckling of shell plate between stiffeners without significant stiffener distortion

REFERENCES

1. American Petroleum Institute, "Recommended Practice for Planning, Designing and Constructing Fixed Offshore Platforms", API RP 2A, Fifteenth Edition, October 22, 1985.
2. Det Norske Veritas, "Rules for the Design, Construction, and Inspection of Offshore Structures", Appendix C, 1977 (Rev. 1982).
3. Vojta, J.F. and Miller, C.D., "Buckling Tests on Ring and Stringer Stiffened Cylindrical Models Subject to Combined Loads", Final Report, Contract No. 11896, Vol. I - Main Report and 3-Volume Appendix, CBI Industries, Inc., April 1983.

4. American Petroleum Institute, "Bulletin on Stability Design of Cylindrical Shells", API Bulletin 2U, to be published April 1987.
5. Stephens, M.J., Kulak, G., and Montgomery, C.J., "Local Buckling of Thin-Walled Tubular Steel Members", Proceedings of Third International Colloquium on Stability of Metal Structures, Toronto, Canada, SSRC, May 1983, pp. 489-508.
6. Miller, C.D. and Grove, R.B., "Collapse Tests of Ring Stiffened Cylinders Under Combinations of Axial Compression and External Pressure", ASME, PVP Conference, Chicago, Illinois, July 20-24, 1986.
7. Det Norske Veritas, "Buckling Strength Analysis", Classification Notes, Note No. 30.1, July 1982.
8. Kiziltug, A.Y., Grove, R.B., Peters, S.W. and Miller, C.D., "Collapse Tests of Short Tubular Columns Subjected to Combined Loads", Final Report, Contract No. UI-851604, CBI Industries, Dec. 1985.
9. Sherman, D.R., "Flexural Tests of Fabricated Pipe Beams", Third International Colloquium on Stability of Metal Structures, Toronto, Canada, May 1983.
10. Eder, M.F., Grove, R.B., Peters, S.W. and Miller, C.D., "Collapse Tests of Fabricated Cylinders Under Combined Axial Compression and External Pressure", Final Report for API PRAC Project 82/83-46 and CBI Contract 21738, CBI Industries, Inc., Research Laboratory, Plainfield, Illinois, February 1984.
11. Miller, C.D., "Summary of Buckling Tests on Fabricated Steel Cylindrical Shells in USA", Buckling of Shells in Offshore Structures, Edited by Harding, Dowling and Agelidis, Granada, London, Sydney, New York, 1982, pp. 429-472.
12. European Convention for Constructional Steelwork, Publication 29, "European Recommendations for Steel Construction: Buckling of Shells", Second Edition, 1983.
13. Odland, J., "Buckling Resistance of Unstiffened and Stiffened Circular Cylindrical Shell Structures", Norwegian Maritime Research, Vol. 6, No. 3, 1978, pp. 2-22.
14. American Society of Mechanical Engineers, Boiler and Pressure Vessel Code Case N-284, "Metal Containment Shell Buckling Design Methods", Nuclear Code Case Book, 1986.

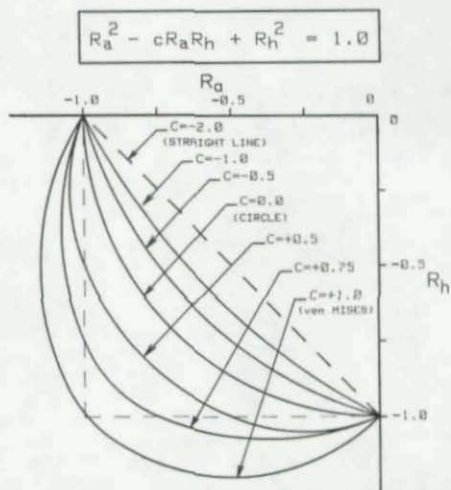


FIG. 1
SHAPE OF INTERACTION CURVE

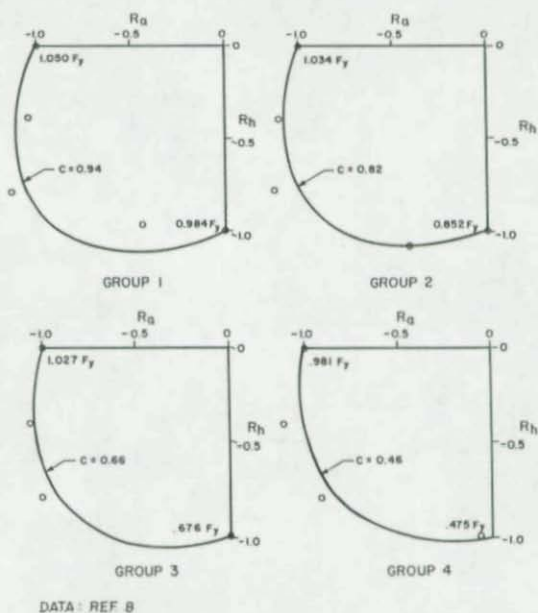


FIG. 2
COMPARISON OF TEST DATA WITH INTERACTION
EQUATION FOR UNSTIFFENED CYLINDERS

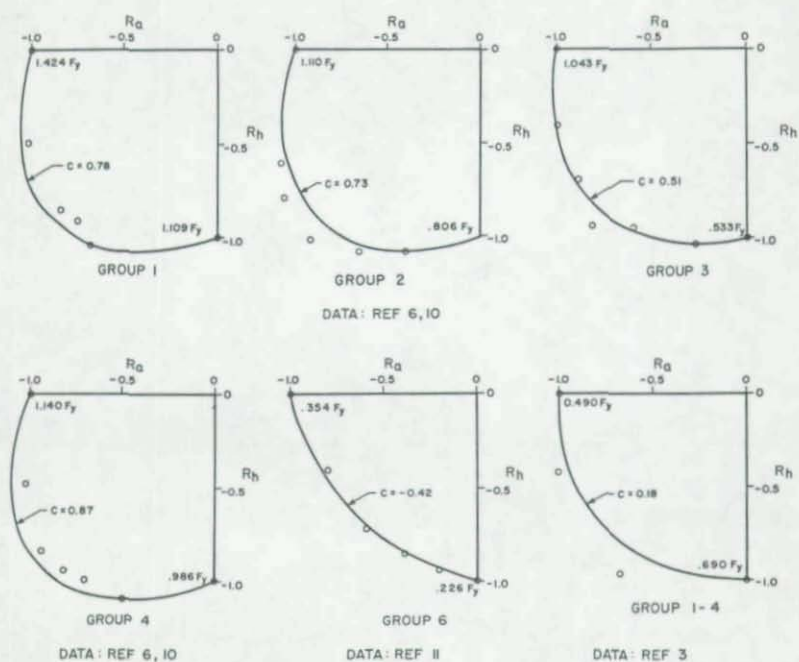


FIG. 3
COMPARISON OF TEST DATA WITH INTERACTION
EQUATION FOR RING STIFFENED CYLINDERS

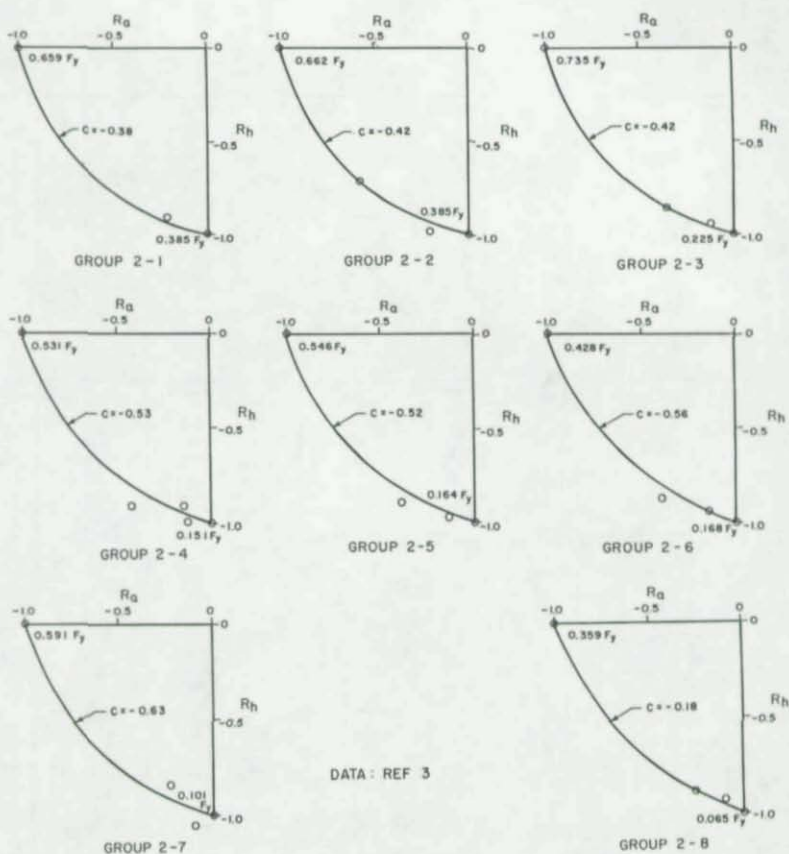


FIG. 4
 COMPARISON OF TEST DATA WITH INTERACTION EQUATION
 FOR LOCAL BUCKLING OF
 RING & STRINGER STIFFENED CYLINDERS

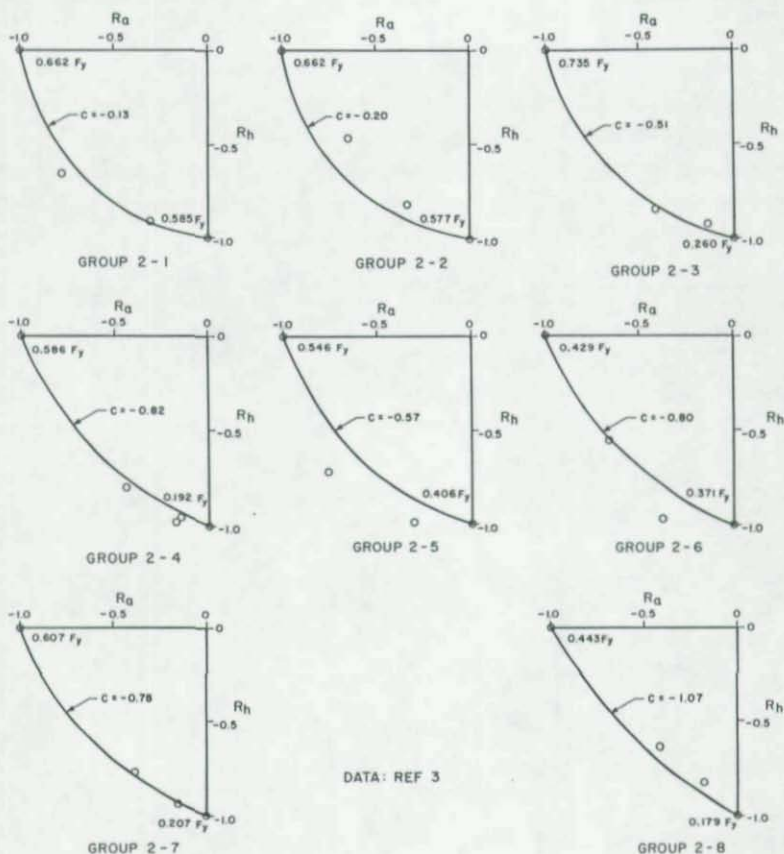


FIG. 5
 COMPARISON OF TEST DATA WITH INTERACTION EQUATION
 FOR BAY INSTABILITY OF
 RING & STRINGER STIFFENED CYLINDERS

GENERAL BUCKLING OF RING AND STRINGER STIFFENED CYLINDERS

by

Tore H. S reide*, Sverre Valsg rd**, Benedicte Brodtkorb***

ABSTRACT

The paper presents recent advances in the general buckling of cylindrical shells. The presentation is based on work carried out at Det norske Veritas /1/ and at the Norwegian Institute of Technology /2/. Special attention is given to the energy formulation for the cylinder wall where the expressions for extensional and inextensional theory are discussed.

Axial compression, external pressure and shear loading are included in the formulation together with the stiffening effect of an elastic medium.

Comparison is made with test results on ring stiffened cylinders. Based on the energy formulations design formulas for elastic buckling of ring and stringer stiffened shells are presented together with analysis examples on real structures. Comparison is made between the formulations.

1. INTRODUCTION

The buckling modes of an orthogonally stiffened cylindrical shell may conveniently be categorized as follows /1/.

- a. Shell buckling: Buckling of shell between stiffeners.
- b. Local stiffener buckling: The shell remains undeformed.
- c. Panel buckling: Buckling of stiffened panels between rings, see Figure 1.
- d. General buckling: Buckling of shell including stiffeners (rings and stringers), Figure 1.
- e. Overall buckling: Column buckling of the cylinder.

* Norwegian Institute of Technology, Trondheim

** Det Norske Veritas, Oslo

*** The Foundation of Scientific and Industrial Research, SINTEF, Trondheim

The present work deals with mode d. on general buckling. One objective of the study has been to develop simplified formulas for necessary stiffener dimensions so as to exclude general buckling as the most critical failure mode. The second aim of the work is to come up with simple computer programs for use in design, based on series expansion and energy methods.

Advanced numerical techniques for handling shell buckling problems have recently been developed /3,4/ based on finite element formulation with nonlinear geometric and material effects included. However, for a designer simpler formulations should be available in the form of either design formulas or small program packages for use on PC-type of computers. An example on this type of program is given in the paper.

The need for a simple computer program as an alternative to formulas is more strengthened in the case of cylinders surrounded by elastic and elastoplastic media, where also a layered distribution of soil stiffness is input. The new concepts of gravity platforms for soft soils include such problems as penetration skirts are being used to ensure soil/structure interaction, see Figure 2. It should also be mentioned that based on the program system FENRIS /3/ a project is going on in Norway /5/ to come up with a nonlinear program system for integrated analysis of gravity platforms including cyclic degradation of the soil.

In the present study special emphasis has been given to the buckling behaviour of the cylindrical shell and to consider the difference between extensional and inextensional energy expressions.

2. BASIC THEORY

The present chapter gives two versions of energy formulation in the sense that potential functions as well as virtual work expressions are being used. The latter could be "anti-varied" into a potential but from the programming point of view this is not necessary and represents extra work.

2.1 ENERGY EXPRESSIONS

In the subsequent derivations U is being used as the symbol for strain energy and the associated variational term is δU . Further, H is the potential of external loads and the total potential function reads

$$\pi = U + H \quad (2.1)$$

The DnV /1/ version of the study is based on the following assumptions:

- Linear membrane theory for the prebuckling state. Includes only membrane stresses uncoupled to the bending mode of deformation.
- Energy contributions from torsion deflection in ring direction and warping are neglected for rings and stringers.
- Effective cross sections are used for ring and stringer stiffnesses.

The energy contribution for the shell from prebuckling state into the buckled configuration comes out to be, see definitions in Figure 3:

$$\begin{aligned}
 U_{sh} = & \frac{D}{2} \int_0^L \int_0^{2\pi r} \{ (w_{,xx} + w_{,yy})^2 - 2(1-\nu) [w_{,xx}w_{,yy} - (w_{,xy})^2] \} dx dy \\
 & + \frac{t}{2E} \int_0^L \int_0^{2\pi r} \{ (F_{,xx} + F_{,yy})^2 - 2(1+\nu) [F_{,xx}F_{,yy} - (F_{,xy})^2] \} dx dy
 \end{aligned} \quad (2.2)$$

For the stringers the simple expression used is

$$U_{st} = \frac{1}{2} EI \sum_{i=1}^N \int_0^L (w_{,xx})^2_{y=y_i} dx \quad (2.3)$$

and for the ring stiffeners

$$U_r = \frac{1}{2} EI \sum_{i=1}^M \int_0^{2\pi r} (w_{,yy} + \frac{w}{r^2})^2_{x=x_i} dy \quad (2.4)$$

The external loads are σ_x in axial compression, p in external pressure and σ_{xy} in torsion with the potential contribution:

$$\begin{aligned} H = & -\frac{t}{2} (1+a_s) \sigma_x \int_0^L \int_0^{2\pi r} (w_{,x})^2 dx dy \\ & - p \int_0^L \int_0^{2\pi r} [1+r (w_{,yy} + \frac{w}{r^2})] w dx dy \\ & - t_s \sigma_{xy} \int_0^L \int_0^{2\pi r} w_{,x} w_{,y} dx dy \end{aligned} \quad (2.5)$$

The relation between Airy's stress function F and lateral deflection according to linear theory reads

$$\nabla^4 F = \frac{E}{r} w_{,xx} \quad (2.6)$$

The interpolation of lateral deflection w is taken as

$$w = C_1 \cdot \sin(\frac{m\pi}{L} x - \frac{n}{r} y) \quad (2.7)$$

where m is the number of half waves in longitudinal direction and n is the number of full waves in the circumferential direction.

The expression (2.7) does not satisfy simply supported boundary conditions at the ends, but may be used for medium length and long cylinders where the end conditions have minor influence on the critical load.

2.2 REFINED SHELL THEORY

Based upon the notation in Figure 4 the six equilibrium equations on component form read /2/.

$$IK_x = 0 : N_{xx,x} + N_{yx,y} + P_x = 0 \quad (2.8)$$

$$IK_y = 0 : N_{yy,y} + N_{xy,x} - \frac{Q_y}{r} + P_y = 0 \quad (2.9)$$

$$IK_z = 0 : Q_{y,y} + Q_{x,x} + \frac{N_{yy}}{r} - P_z = 0 \quad (2.10)$$

$$IM_x = 0 : M_{yy,y} + M_{xy,x} - N_{xy} \cdot w_{,x} - N_{yy} \cdot w_{,y} - Q_y = 0 \quad (2.11)$$

$$IM_y = 0 : M_{xx,x} + M_{yx,y} - N_{yx} \cdot w_{,y} - N_{xx} \cdot w_{,x} - Q_x = 0 \quad (2.12)$$

$$IM_z = 0 : N_{xy} - N_{yx} + \frac{M_{yx}}{r} = 0 \quad (2.13)$$

including geometric effects.

Denoting by an upper bar the virtual displacement the virtualized form of Eqs. (2.8 - 2.13) becomes

$$\begin{aligned} & \iint_A [M_{xx} \cdot \bar{w}_{,xx} + M_{yx} \bar{w}_{,xy} + M_{xy} \cdot \bar{w}_{,yx} + M_{yy} \bar{w}_{,yy}] dA \\ & + \iint_A [N_{xx} \bar{u}_{,x} + N_{xy} (\bar{u}_{,y} + \bar{v}_{,x}) + \frac{M_{yx}}{r} \bar{u}_{,y} + N_{yy} \bar{v}_{,y}] dA \\ & + \iint_A \frac{N_{yy}}{r} \bar{w} dA \\ & - \frac{1}{r} \iint_A [M_{yy} \bar{v}_{,y} + M_{xy} \bar{v}_{,x} + N_{xy} w_{,x} \bar{v} + N_{yy} \cdot w_{,y} \cdot \bar{v}] dA \end{aligned}$$

$$\begin{aligned}
&= \iint_A [p_x \bar{u} + p_y \bar{v} + p_z \bar{w}] dA \\
&- \iint_A [N_{xx} \cdot w_{,x} \cdot \bar{w}_{,x} + N_{xy} (w_{,y} \cdot \bar{w}_{,x} + w_{,x} \cdot \bar{w}_{,y}) + \frac{M_{yx}}{a} w_{,y} \cdot \bar{w}_{,x} \\
&\quad + N_{yy} \cdot w_{,y} \cdot \bar{w}_{,y}] dA \\
&+ \int_c [M_y \cdot \bar{\theta}_y + M_x \bar{\theta}_x] ds - \int_c Q_n \cdot \bar{w} ds + \int_c [N_x \cdot \bar{u} + N_y \cdot \bar{v}] ds \\
&+ \int_c \frac{1}{r} M_x \bar{v} ds \tag{2.14}
\end{aligned}$$

where the left-hand side represents internal virtual work and the right hand side is external work.

Introducing now the Flügge /6/ stress-strain relations the following equation emerges for the first variation of internal shell energy:

$$\begin{aligned}
\delta U_{sh} &= D \iint_A \left\{ [w_{,xx} - \frac{1}{r} u_{,x} + v(w_{,yy} - \frac{1}{r} v_{,y})] \delta w_{,xx} \right. \\
&\quad + (1-\nu) (2w_{,yx} + \frac{1}{2r} u_{,y} - \frac{3}{2r} v_{,x}) \delta w_{,yx} \\
&\quad \left. + (\frac{1}{2} w + w_{,yy} + \nu w_{,xx}) \delta w_{,yy} \right\} dA \\
&\quad \dots \dots \dots \\
&+ \frac{D}{r} \iint_A (-w_{,xx} \cdot \delta u_{,x} \\
&+ \frac{1-\nu}{2} (w_{,yx} + \frac{1}{r} u_{,y}) \cdot \delta u_{,y} \\
&+ \frac{1-\nu}{2} (\frac{3}{r} v_{,x} - 3w_{,yx}) \cdot \delta v_{,x} \\
&- \nu \cdot w_{,xx} \cdot \delta v_{,x} \\
&+ (\frac{1}{r} w_{,yy} + \frac{1}{3} w) \delta w) dA \\
&\quad \dots \dots \dots \tag{2.15}
\end{aligned}$$

$$\begin{aligned}
& + \frac{Et}{1-\nu^2} \iint_A \left([u_{,x} + \nu(v_{,y} + \frac{1}{r} w)] \delta u_{,x} \right. \\
& + \frac{1-\nu}{2} (u_{,y} + v_{,x}) \cdot (\delta u_{,y} + \delta v_{,x}) \\
& \left. + (v_{,y} + \frac{1}{r} w + \nu \cdot u_{,x}) \delta v_{,y} \right) dA
\end{aligned}$$

$$+ \frac{Et}{r(1-\nu^2)} \iint_A \left(\frac{1}{r} w + v_{,y} + \nu \cdot u_{,x} \right) \cdot \delta w \, dA$$

The last integral is of higher order and is neglected in the subsequent considerations.

It should be emphasized that the above expressions have been obtained from equilibrium equations in deformed configuration through virtualization. The alternative way of obtaining a shell energy is to use the assumption behind Eq. (2.2) namely that bending and membrane energy may be separated in the way

$$\begin{aligned}
U_{sh} = & \frac{D}{2} \iint_A \{ (\kappa_x + \kappa_y)^2 - 2(1-\nu)(\kappa_x \cdot \kappa_y - \kappa_{xy}^2) \} dA \\
& + \frac{Et}{2(1-\nu^2)} \iint_A \{ (\epsilon_y + \epsilon_x)^2 - 2(1-\nu)(\epsilon_x \cdot \epsilon_y - \frac{1}{4} \gamma_{xy}^2) \} dA
\end{aligned} \quad (2.16)$$

as described in /7/ with the curvature expressions

$$\begin{aligned}
\kappa_x &= w_{,xx} \\
\kappa_y &= \frac{1}{r^2} w + w_{,yy} \\
\kappa_{xy} &= \frac{1}{r} v_{,x} + w_{,yx}
\end{aligned} \quad (2.17)$$

The curvatures introduced in Eq.(2.15) differ by

$$\kappa_{xy} = \frac{1}{2} r(u_{,y} - v_{,x}) + w_{,yx} \quad (2.18)$$

Combining Eqs.(2.16, 2.17) gives the following first variation of strain energy:

$$\begin{aligned}
 \delta U_{sh} = & D \iint_A \left\{ [w_{,xx} + v \left(\frac{1}{r^2} w + w_{,yy} \right)] \delta w_{,xx} \right. \\
 & + (1-v) \left(-\frac{2}{r} v_{,x} + 2 w_{,yx} \right) \delta w_{,yx} \\
 & \left. + \left(\frac{1}{r^2} w + w_{,yy} + v w_{,xx} \right) \delta w_{,yy} \right\} dA \\
 \hline
 & + \frac{D}{r} \iint_A \left\{ 2(1-v) \cdot \left(\frac{1}{r} \cdot v_{,x} - w_{,yx} \right) \delta v_{,x} \right. \\
 & \left. + \left(\frac{1}{r^3} w + \frac{v}{r} w_{,xx} + \frac{1}{r} w_{,yy} \right) \delta w \right\} dA \qquad (2.19) \\
 \hline
 & + \frac{Et}{1-\nu^2} \iint_A \left\{ [u_{,x} + v(v_{,y} + \frac{1}{r} w)] \delta u_{,x} \right. \\
 & + \frac{1-\nu}{2} (u_{,y} + v_{,x}) \cdot (\delta u_{,y} + \delta v_{,x}) \\
 & \left. + (v_{,y} + \frac{1}{r} w + v \cdot u_{,x}) \delta v_{,y} \right\} dA \\
 \hline
 & + \frac{Et}{r(1-\nu^2)} \iint_A \left(\frac{1}{r} w + v_{,y} + v \cdot u_{,x} \right) \delta w \, dA
 \end{aligned}$$

Comparing now Eqs.(2.15, 2.19) shows that the two alternative formulations give mostly identical energy terms. The discrepancy is partly due to the fact that thick shell effects are incorporated in Eq.(2.15) and partly caused by differences in geometrical considerations on the deformed shell.

The present study will investigate how this difference also effect the buckling load as well as the buckling mode.

Specialization of Eqs.(2.15, 2.19) may be performed for so-called inextensional theory implying

$$\begin{aligned}\epsilon_x &= \delta\epsilon_x = 0 \\ \epsilon_y &= \delta\epsilon_y = 0 \\ \gamma_{xy} &= \delta\gamma_{xy} = 0\end{aligned}\tag{2.20}$$

or with strain-displacement relations incorporated

$$\begin{aligned}u_{,x} &= \delta u_{,x} = 0 \\ v_{,y} + \frac{1}{r} w &= \delta v_{,y} + \frac{1}{r} \delta w = 0 \\ u_{,y} + v_{,x} &= \delta u_{,y} + \delta v_{,x} = 0\end{aligned}\tag{2.21}$$

and the two formulations give identical results.

For the subsequent derivations Eq.(2.15) is taken as the basic variational principle. In the development of a computer program the interpolation functions assumed are simply

$$\begin{aligned}u &= A \cdot \cos \frac{m\pi}{L} x \cdot \sin \frac{n}{r} y \\ \delta u &= \delta A \cdot \cos \frac{m\pi}{L} x \cdot \sin \frac{n}{r} y \\ v &= B \cdot \sin \frac{m\pi}{L} x \cdot \cos \frac{n}{r} y \\ \delta v &= \delta B \cdot \sin \frac{m\pi}{L} x \cdot \cos \frac{n}{r} y \\ w &= C \cdot \sin \frac{m\pi}{L} x \cdot \sin \frac{n}{r} y \\ \delta w &= \delta C \cdot \sin \frac{m\pi}{L} x \cdot \sin \frac{n}{r} y\end{aligned}\tag{2.22}$$

satisfying hinged supports with no tangent displacements at the ends

$$w = w',_{xx} = v = 0 \text{ for } x = 0, L \quad (2.23)$$

2.3 IMPLEMENTATION OF SURROUNDING ELASTIC MEDIUM

The problem of a cylindrical skirt penetrating into the soil is illustrated in Figure 5. The buckling of the shell has to be checked taking into account the interaction with surrounding soil which also may be layered. The below derivations are based upon the assumption that the soil behaves linearly elastic.

Specifying an elastic soil resistance constant $E_{\text{soil}} [\text{MN/m}^3]$ for the lateral deflection of the shell the contribution to strain energy variation becomes

$$\delta U_{\text{soil}} = \iint_A E_{\text{soil}} \cdot w \cdot \delta w \, dA \quad (2.24)$$

where integration is taken over the shell surface and possibly over soil layers with different stiffnesses. The last modification is easily incorporated in the program by predefining the thickness of each layer.

3. DESIGN FORMULAS

The two energy formulations presented in Section 2.1 and 2.2, respectively, have been used in the development of design formulas for ring and stringer stiffened shells /1/. A summary of this work is given below. For a broader discussion of design formulas and code application reference is made to /9,10/.

3.1 INTERACTION FORMULA

Based on Eqs. (2.2 -2.4) the combination of axial compression, lateral pressure and torsion may be checked by the formula

$$\begin{aligned} & \left(\frac{t}{r}\right)^2 [\bar{m}^2 + n^2]^2 + 12(1-\nu^2) \frac{\bar{m}^4}{[\bar{m}^2 + n^2]^2} + \gamma_S \left(\frac{t}{r}\right)^2 \bar{m}^4 + \gamma_R \left(\frac{t}{r}\right)^2 (n^2-1)^2 \\ & = 12(1+a_S) \bar{m}^2 \phi_x + 12(1+a_R) (n^2-1) \phi_\theta + 24 \bar{n} \bar{m} \phi_{xy} \end{aligned} \quad (3.1)$$

where

$$\begin{aligned} \bar{m} &= \frac{m \cdot x}{L} \\ \bar{n} &= \frac{nL}{\pi r} \end{aligned} \quad (3.2)$$

In Eq.(3.1) ϕ_x , ϕ_y and ϕ_{xy} are nondimensional loading parameters for axial stress, circumferential stress and shear stress, respectively

$$\phi = \sigma(1-\nu^2)/E \quad (3.3)$$

Further, γ_S and γ_R are geometric parameters related to stringers and rings, respectively

$$\begin{aligned} \gamma_S &= 12(1-\nu^2) \frac{I_S}{st^3} \\ \gamma_R &= 12(1-\nu^2) \frac{I_R}{Lt^3} \end{aligned} \quad (3.4)$$

and a_s and a_R are the area coefficients

$$a_s = A_s/st \quad (3.5)$$

$$a_R = A_R/Lt$$

From the general expression (3.1) specialized capacity formulas may be derived for the three basic load cases. These formulas are given below on the form usually applied for plate buckling

$$f_i = C_0 \frac{w^2 E}{12(1-\nu^2)} \left(\frac{t}{L}\right)^2 \quad (3.6)$$

where the buckling coefficient C_0 depends on the loading. In the expression (3.6) imperfections are not included so that a knock-down factor ϱ should be applied

$$C = \varrho C_0 \quad (3.7)$$

The imperfection sensitivity for a stiffened shell is different from that of an unstiffened shell. Thus, the stiffener geometry and spacing has to be accounted for when defining ϱ .

3.2 AXIAL COMPRESSION

The solution for axial compression is illustrated in Figure 6 where the buckling coefficient

$$C_x = C_{OX} (1+a_s) \quad (3.8)$$

is plotted against the Batdorf's parameter Z .

The general solution for C_{OX} from Eqs.(2.2 - 2.5) comes out to be

$$(1+a_s) C_{OX} = \gamma_S m^2 + \gamma_R \frac{n^4}{m^2} + \frac{[m^2 + n^2]^2}{m^2} + \frac{12}{w^4} Z^2 \frac{m^2}{[m^2 + n^2]^2} \quad (3.9)$$

The buckling coefficient for short cylinders is obtained for $m = 1$, $n = 0$, that is the axisymmetric mode. The result is (neglected the last term in Eq.(3.9))

$$C_{Ox} = \frac{1+\gamma_s}{1+a_s} \quad (3.10)$$

Eq.(3.10) indicates that the buckling coefficient is independent of Batdorf's parameter only effected by the stringer properties. The buckling stress is like the formula for a wide plate.

For moderately long cylinders $m = 1$ is also assumed. Minimization with respect to n gives

$$n = 2.42 \frac{z^{\frac{1}{4}}}{(1+\gamma_R)^{\frac{1}{8}}} \frac{R}{L} \quad (3.11)$$

and

$$C_{Ox} = \frac{4\sqrt{3}}{w^2} \cdot \frac{(1+\gamma_R)^{\frac{1}{2}}}{1+a_s} \cdot z \quad (3.12)$$

In Figure 6 Eq.(3.12) is shown by

$$C_x^{(2)} = (1+a_s) C_{Ox} \quad (3.13)$$

The curve for $C_x^{(1)}$ represents the exact minimum of the general formula (3.9) for $m = 1$.

For application of Eq.(3.11 - 3.12) the Batdorf's parameter is limited by

$$8.55 \frac{(1-\nu^2)^{\frac{1}{2}}}{(1+\gamma_R)^{\frac{1}{2}}} \left(\frac{R}{L}\right)^2 > z > 1.42 \frac{(1+\gamma_s)^{\frac{1}{2}}}{(1+\gamma_R)^{\frac{1}{2}}} \quad (3.14)$$

3.3 EXTERNAL PRESSURE

The results for external pressure are presented in Figure 7. The lowest value of $C_{O\theta}$ always is associated with one half wave in the longitudinal direction, $m = 1$.

After some manipulation the general form becomes

$$C_{O\theta} = \frac{\gamma_S}{n^2} + \gamma_R n^{-2} + \frac{[1+n^{-2}]^2}{n^2} + \frac{12}{4w^4} z^2 \frac{1}{n^2 [1+n^{-2}]^2} \quad (3.15)$$

and the minimum of this formula is denoted $C_{\theta}^{(1)}$ in Figure 7.

$$C_{\theta} = (1+a_R)C_{O\theta} \quad (3.16)$$

The most interesting case is the one for moderately long cylinders, simplified into

$$C_{O\theta} = \frac{4 \sqrt{6} (1+\gamma_R)^{\frac{3}{4}}}{3w (1+a_R)} \cdot z^{\frac{1}{2}} \quad (3.17)$$

with the buckling mode

$$n = \frac{(6w^2 z)^{\frac{1}{4}}}{(1+\gamma_R)^{\frac{1}{8}}} \frac{r}{L} \quad (3.18)$$

Eq. (3.17) is illustrated by $C_{\theta}^{(2)}$ in Figure 7.

The limitation of Batdorf's parameter for applying Eq.(3.17) is

$$11.7 \frac{(1-\nu^2)^{\frac{1}{2}}}{(1+\gamma_R)^{\frac{1}{2}}} \left(\frac{r}{t}\right)^2 > z > 3.7 \frac{[1+(1+\gamma_R)^{\frac{1}{2}}(1+\gamma_S)]^{\frac{1}{2}}}{(1+\gamma_R)^{\frac{1}{16}}} \quad (3.19)$$

$C_{\theta}^{(1)}$ in Figure 7 gives the exact minimum of the general formula (3.15).

3.4 SHEAR AND TORSION

It is assumed that the cylinder under shear loading may satisfactorily be treated by the expressions for loading in torsion. The illustrations are given in Figure 8 where the solutions for $C_{Ox\theta}$ are plotted directly as function

of the Batdorf's parameter. For moderately long cylinders the following solution appears as represented by $C_{x\theta}^{(2)}$ in Figure 8:

$$C_{ox\theta} = 0.442 \psi_t (1+\gamma_R)^{\frac{5}{8}} Z^{\frac{3}{4}} \quad (3.20)$$

where $\psi_t = 1.937$; is a correlation factor for errors in boundary conditions arising from the assumed deformation mode in Eq.(2.7)

The associated buckling mode reads

$$n = 2.6 \frac{Z^{\frac{1}{4}}}{(1+\gamma_R)^{\frac{1}{8}}} \frac{r}{L} \quad (3.21)$$

$$m = 1$$

For large values of Z Eq.(3.20) has to be checked against the formula for a long cylinder

$$C_{ox\theta} = \frac{0.331 \psi_d}{(1-\nu^2)^{\frac{1}{4}}} (1+0.563 \gamma_R)^{\frac{3}{4}} \left(\frac{t}{r}\right)^{\frac{1}{2}} Z \quad (3.22)$$

with $\psi_d = 0.868$, see Figure 8 curve $C_{x\theta}^{(3)}$. The curve for $C_{x\theta}^{(1)}$ in Figure 8 is the exact minimum for short and moderately long cylinders for $m = 1$.

4. NUMERICAL STUDIES

In this chapter two examples on analysis of unstiffened shells are given by the energy formulations described in Chapter 2. The first case is a sensitivity study on the buckling of axially loaded cylinders while the second example illustrates the application on a real design problem.

4.1 BUCKLING UNDER AXIAL LOADING

The following data are given:

<u>Geometry:</u>	Length	$L = 1000 \text{ mm}$
	Radius	$r = 200 \text{ mm}$
	Thickness	$t = 0.5 - 6.67 \text{ mm}$
	Batdorf's parameter	$z = 0.95 \cdot 10^4 - 0.72 \cdot 10^3$
<u>Material:</u>	Young's modulus	$E = 2.10 \cdot 10^5 \text{ MPa}$
	Poisson's ratio	$\nu = 0.3$

Comparison is made between three alternative procedures. These are the energy expressions in Section 2.1 and the refined theory in Section 2.2 together with empirical formula /8/.

The value of the Batdorf's parameter indicates that the cylinders examined all are classified as long cylinders, see Section 3.2 for the unstiffened case with $\gamma_R = \gamma_S = 0$.

The buckling coefficient as function of the Batdorf's parameter is shown in Figure 9 for the three alternative procedures. It is seen that the two formulations in section 2.1 and 2.2 only differ by 5 percent and that a knock down factor in the range 0.35 -- 0.75 has to be implemented so as to reach the empirical design curve.

Figure 10 shows the number of half waves in longitudinal direction for the refined energy formulations together with the number of half waves according to

the axisymmetric mode for short cylinders.

The dependency of the solution for critical load on the number of longitudinal and circumferential waves is more clearly depicted by the graphical plots in Figure 11, where values of Batdorf's parameter equal to $0.715 \cdot 10^3$ and $0.477 \cdot 10^4$ are considered. It is seen that the solution is highly sensitive with regard to the number of circumferential waves n as opposed to the number of longitudinal half waves m . As a conclusion from this figure the mode in circumferential direction is the most important to represent correctly.

4.2 ANALYSIS OF CONCRETE PENETRATION SKIRT

The present example concerns the buckling analysis of the soil penetration skirt of a Condeep type of gravity platform where the effect of the surrounding elastic medium is included. The effect from soil stiffness E_{soil} on buckling mode and corresponding buckling stress is studied.

The real problem is illustrated in Figure 2 while Figure 12 shows the modelling. The shell data are:

<u>Geometry:</u> Length	$L = 22 \text{ m}$
Average radius	$r = 13.8 \text{ m}$
Wall thickness	$t = 0.4 \text{ m}$
Batdorf's parameter	$Z = 84$

<u>Material:</u> Young's modulus concrete	$= 2.0 \cdot 10^4 \text{ MPa}$
Poisson's ratio concrete	$= 0.2$
Lateral stiffness soil	$= 0.0 - 100 \text{ MN/m}^3$

The loading consists of axial compression together with external radial pressure. The external pressure is applied as an axisymmetric pressure plus a varying contribution according to the deformation mode.

Figure 13 shows the dependency of axial buckling coefficient on lateral soil stiffness ratio. The stiffness ratio is taken as E_{soil} relative to membrane ring stiffness of the shell. A clear indication is given on the stiffening

effect from the soil.

The same figure also shows the variation in buckling mode as function of soil stiffness ratio. It is seen that the number of half waves in longitudinal direction m decreases rapidly from 3 for zero soil stiffness down to 1, while the number of circumferential waves increases from initial 5 up to 7 at the highest soil stiffness.

5. CONCLUSIONS

Alternative energy expressions have been presented for the buckling analysis of stiffened shells. The formulations differ by the strain energy functions for the shell wall.

Design formulas for buckling under axial load, external pressure and shear have been derived. The effect of a surrounding elastic medium has also been included on energy form.

The conclusions from the numerical studies on unstiffened shells are that the simplified energy expressions give results that lies 5 percent on the nonconservative side. Further, the examples demonstrate that an attractive alternative to the use of explicit design formulas is to develop simple computer programs by which sensitivity studies may easily be carried out. Such programs will also be useful for estimating the most critical buckling modes before a detailed finite element model for nonlinear analysis is formed. In many cases the finite element model may be reduced by introducing boundary conditions that satisfy the critical mode of buckling.

The numerical examples also demonstrate that the number of circumferential waves is the most important mode parameter to model correctly.

The work in Norway will continue into the development of computer codes for calculating stresses and amplitudes of deformation. This is necessary for obtaining a full design package.

6. REFERENCES

1. Steen, E. and Valsgaard, S.: "General Buckling of Orthogonally Stiffened Cylindrical Shells under Various Load Conditions". Progress Report No. 10, Det norske Veritas, Oslo, 1981.
2. Brodtkorb, B.: "Energy Formulation for Shell Buckling", Division of Structural Mechanics, Norwegian Institute of Technology, Trondheim, 1985, (in Norwegian)
3. Bergan, P.G. et al.: "FENRIS Manuals Theory - Program Outline - Data Input", NTH-SINTEF-A.S VERITEC; Oslo, 1984.
4. Nygaard, M.K.: "The Free Formulation for Nonlinear Finite Elements with Applications to Shells", Dr.ing. Thesis No. 86-2, Division of Structural Mechanics, Norwegian Institute of Technology, Trondheim, 1986.
5. Sørreide, T.H., Amdahl, J. and Arnesen A.: "Nonlinear Integrated Soil - Structure Analysis of Gravity Platforms", Division of Structural Mechanics, Norwegian Institute of Technology, Trondheim, 1986.
6. Flügge, W.: "Stresses in Shells", 2nd. Ed., Springer, New York, 1973.
7. Timoshenko, S.P. and Gere, J.M.: "Theory of Elastic Stability", McGraw-Hill, Tokyo, 1961.
8. Baker, E.H., Kovalevsky, L and Rish, F.L.: "Structural Analysis of Shells", McGraw-Hill, New York, 1972.
9. Harding, J.E., Dowling, P.J., Valsgaard, S. and Walker, A.C.: "The Buckling Design of Stringer-Stiffened Shells Subjected to Combined Pressure and Axial Compression", Offshore Technology Conference, OTC, 4473, 1983.
10. Ellinas, C.P. and Supple, J.P.: "Buckling Design of Ring-Stiffened Cylinders", Offshore Technology Conference, OTC 4472, 1983.

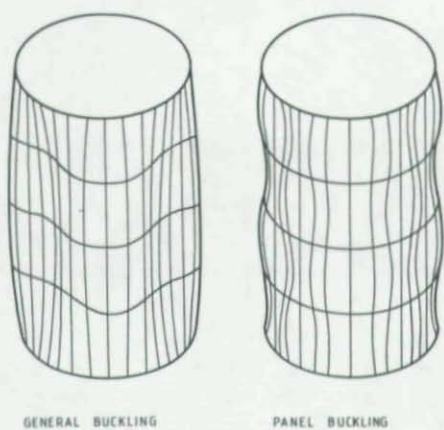


Figure 1 Buckling modes

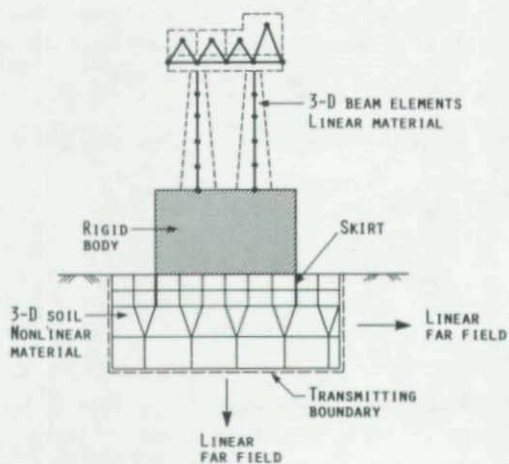


Figure 2 Finite element model for soil-structure interaction analysis of gravity platform

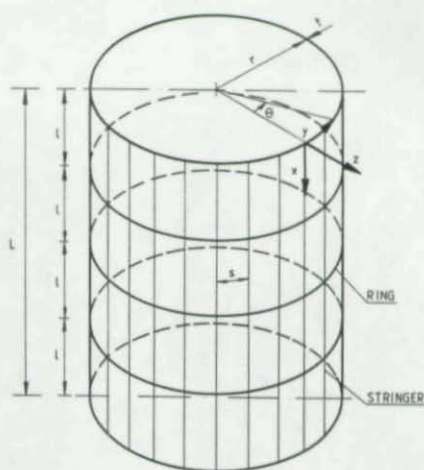


Figure 3 Global geometry with definitions

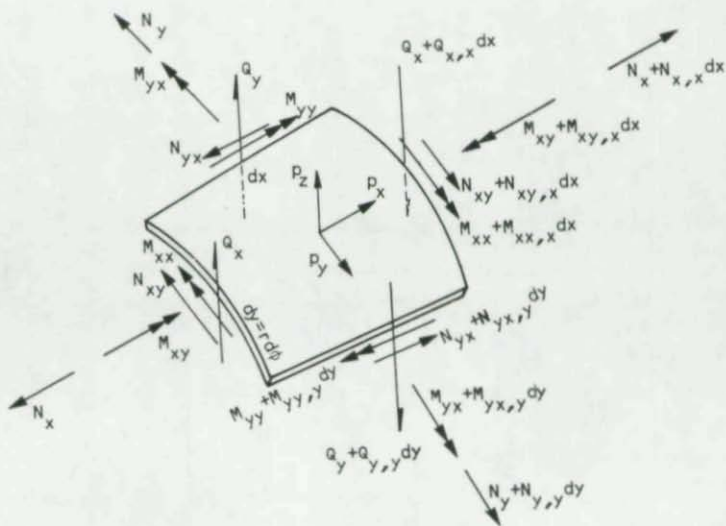


Figure 4 Forces on shell element

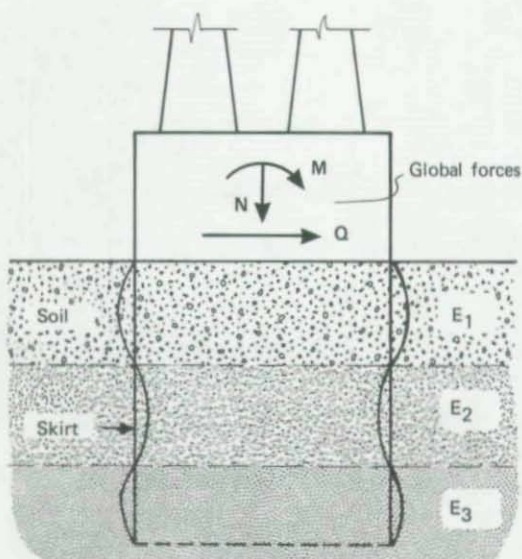


Figure 5 Buckling of penetration skirt

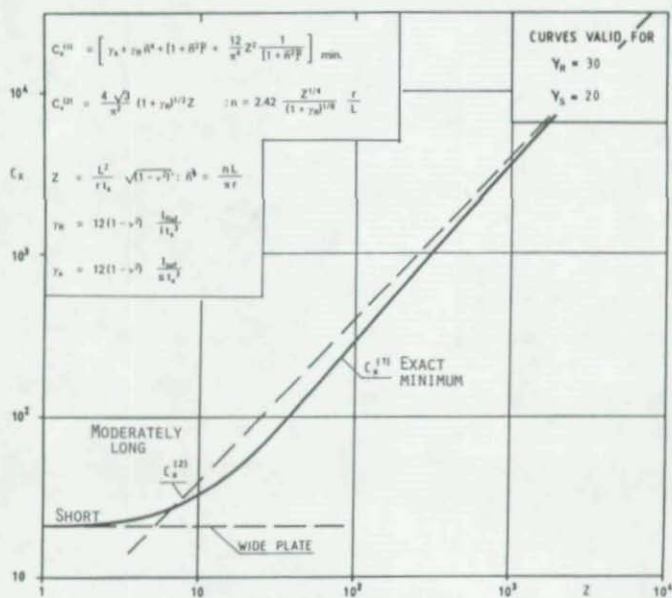


Figure 6 Buckling coefficients for axial compression

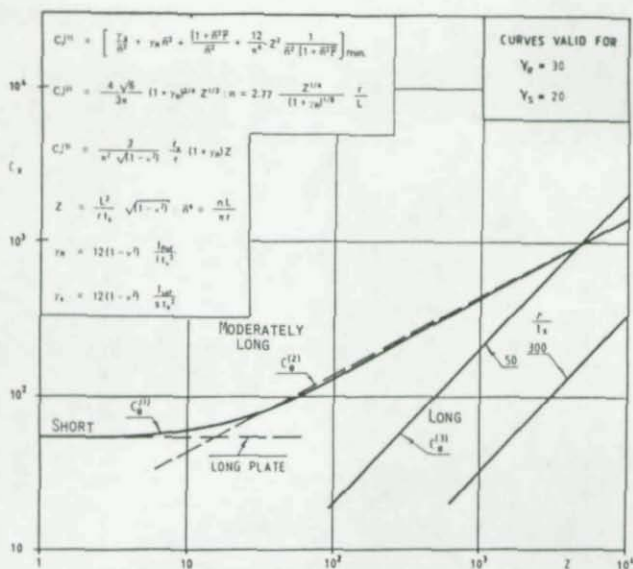


Figure 7 Buckling coefficients for external pressure

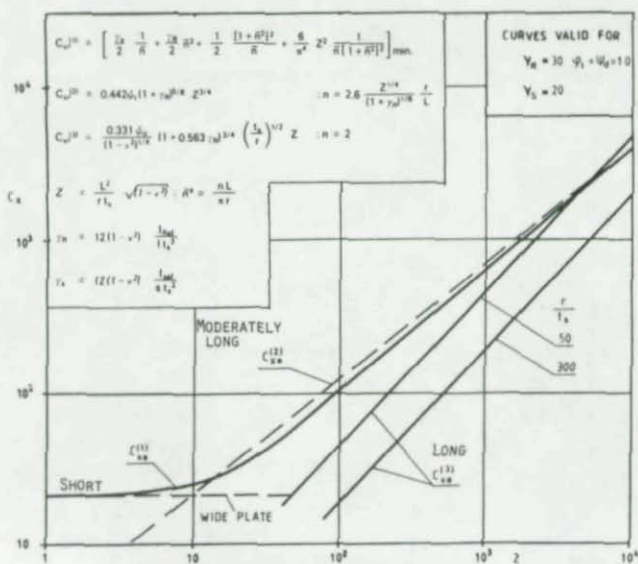


Figure 8 Buckling coefficients for torsion

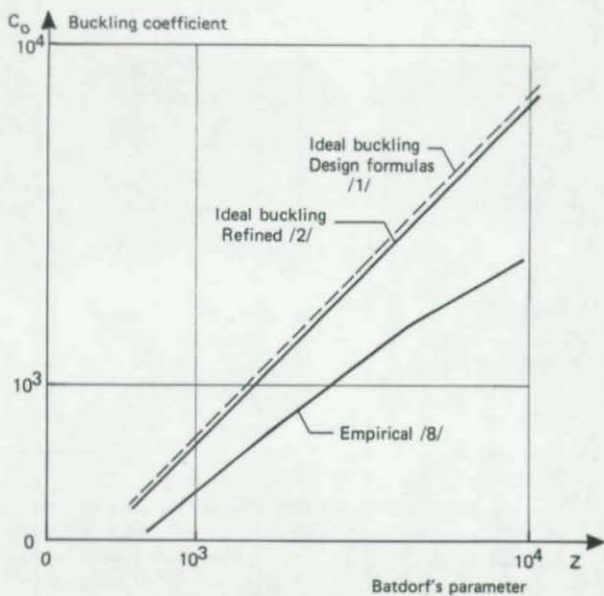


Figure 9 Buckling coefficients for axial compression

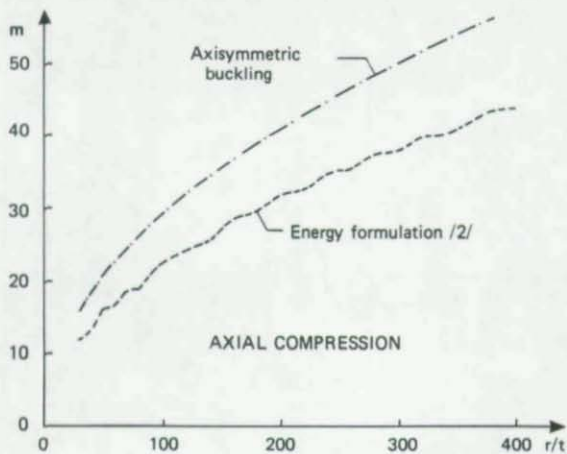


Figure 10 Number of half waves in longitudinal direction

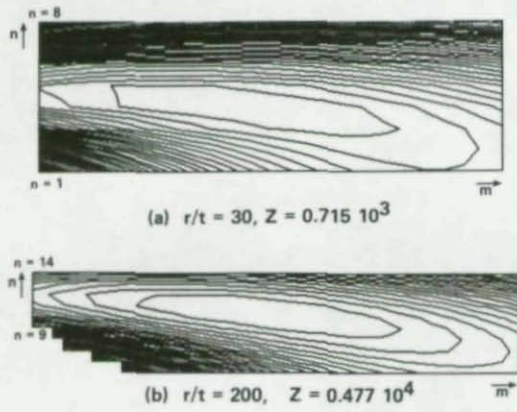


Figure 11 Solution for critical axial stress for different buckling modes

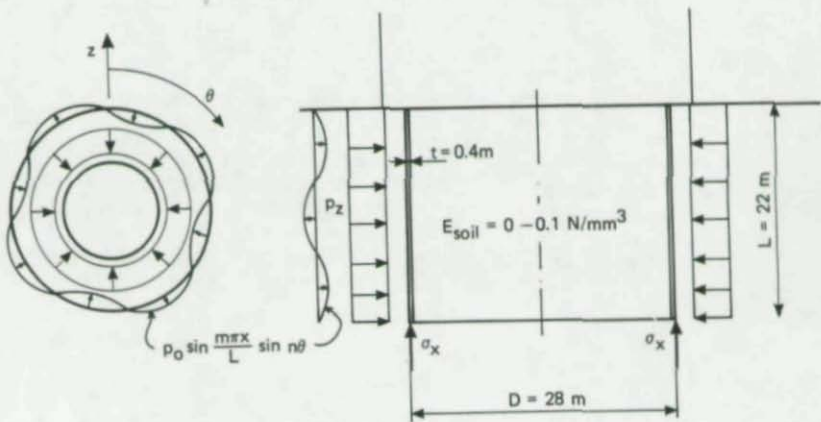


Figure 12 Analysis model for concrete skirt

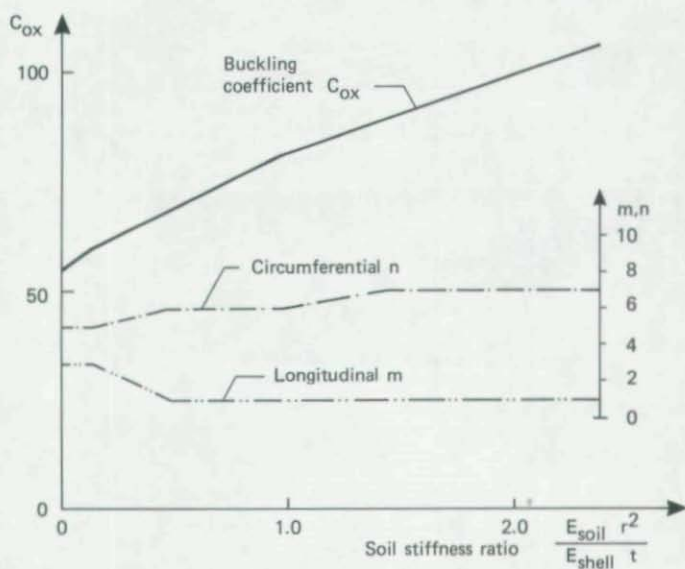


Figure 13 Buckling coefficient and buckling mode as function of soil stiffness

**"STABILITY OF CIRCULAR STIFFENED SHELLS
FROM RESEARCH TO PRACTICE"**

"INCORPORATING RESEARCH INTO CERTIFICATION STANDARDS"

by Joseph E. Herz
American Bureau of Shipping

The theme of this Panel Session "Stability of Circular Stiffened Shells - From Research to Practice" is certainly of interest to ABS both on the research end and the practice side. The majority of our classification and certification work is concerned with new and existing structures that are in service or soon will be. However, new research results must be reviewed and incorporated into our existing standards to prevent them from becoming dated. Probably the best way to bring research results into practice is to incorporate them into accepted standards. The two other speakers on the program spoke of matters having to do with Tension Leg Platforms. I would like to stay with that subject. I wish I could rattle off the names of a several TLPs that ABS has classed or certified and recount our service experience with them. I am unable to do that since there is only one TLP in service - the Conoco Hutton Platform in the UK Sector of the North Sea and ABS was not involved with its certification.

However, Conoco is proceeding with its second TLP which will be installed in Green Canyon Block 184 in the Gulf of Mexico in 1760 ft. of water. The proposed installation date is mid-1989. ABS will be involved with the review and verification of the structural design of this TLP.

I would like to focus on ABS' effort to prepare itself to offer meaningful certification services to the operators of the future TLPs since it involves research and a considerable effort to prepare TLP standards.

I believe it will be helpful to provide a bit of history about ABS and its standard making function.

ABS was formed in 1862 due primarily to the efforts of the insurance industry. (This is our 125th year of operation) ABS' initial function was to certify ship captains and the company was originally called the American Shipmasters Association. The insurance companies evidently reasoned that having a qualified ship captain went a long way towards assuring a safe voyage.

Over the years the work of ABS moved away from evaluating personnel and concentrated on the ships themselves.

Today the major Classification Societies of the world produce standards - called Rules - which contain requirements for the structure, machinery plant, materials, electrical systems, piping systems, fire detection and fire fighting systems, etc., all of which have to do with the safe operation of the vessel.

Most Class Societies initially were concerned exclusively with the ships however, most have extended their certification activities to include offshore installations such as MODUs, fixed and floating production platforms, single point moorings and undersea pipelines. The Societies have produced Rules or Guides applicable to these kinds of installations.

Now back to the TLP. The TLP is a relatively new concept that offers economic advantages over conventional jacket structures for deep water production applications. By deep water I mean over about 1500 feet water depth.

I would like to recount some of ABS' efforts in research and standards preparation applicable to Tension Leg Platforms.

The TLP looks similar to a semi-submersible MODU having corner columns and lower pontoons, however there are significant differences. The TLP is not floating at her natural waterline - she is held deeper in the water by the tension legs or tendons. The tendons are anchored to a foundation template which in turn is attached to the seabed usually by means of piles.

The corner columns of the TLP are circular stiffened shells of large diameter subjected to combined loading i.e. external water pressure, compression due to deck loads and tension or compression from tendon reactions, depending on the location of the tendon attachment points.

The structural designer is faced with difficulties and uncertainties when he starts to design this type of structure. For R/t ratios greater than 150 there is very little test data on the buckling strength of such structures particularly under combined loading, and with an orthogonal stiffening system. The actual structures will be built with residual stresses and fabrication imperfections. All of these factors should be considered in the design to the maximum extent practical.

The Conoco Hutton TLP has corner columns of 58 ft. diameter and these are ring stiffened. At the conclusion of their design effort on the Hutton TLP, Conoco realized that there was potential for more efficient design of this type of stiffened cylindrical structure if applicable test data were available and a reliability based design standard could be developed and used. The belief was that safe structures could be designed with considerable weight savings when compared to what could then be done.

Conoco approached ABS in late 1981 to solicit support for a Joint Industry sponsored Stiffened Cylinder Test Program that would utilize configurations and loadings that would yield test data applicable to TLP structures.

This program began in 1981 with the following participants: Conoco, Mitsubishi Heavy Industries, United Kingdom Department of Energy, Standard Oil Company of California and ABS as Administrator.

- Testing was done at the University of Glasgow under Prof. Doug Faulkner and at CBI under direction of C. Miller.
- Phase I was completed in 1984.
- Phase II testing was done at CBI and is just now complete - Phase II Participants - all Phase I, Shell Development Co. FLUOR, and U.S. Coast Guard.

Under the Phase I Program CBI tested 4 ring stiffened and 44 orthogonally stiffened cylinders. University of Glasgow tested 18 ring stiffened cylinders. This Phase I test program has been reported upon in the following papers:

C.S. Miller, P.A. Frieze, R.A. Zimmer, H.Y. Jan - "Collapse Tests of Fabricated Stiffened Steel Cylinders under Combined Loads" - ASME, 4th National Conference on Pressure Vessels & Piping Technology, Portland, Oregon, June 1983

Y.N. Chen, R.A. Zimmer, J.G. de Oliveira, H.Y. Jan - "Buckling and Ultimate Strength of Stiffened Cylinders: Model Experiments and Strength Formulations" - OTC 4853, 1985

When Conoco first approached ABS to solicit support for the cylinder test program, they also proposed a second related project to develop a reliability based limit state design standard for the main structural components of the TLP. This project got under way in early 1982 and a TLP Rules Case Committee (RCC) was formed to develop this standard. The Committee met 13 times - about once a month - and had its final meeting in March 1983. The results of this RCC work is a Model Code for Structural Design of TLP and is dated 1984.

The RCC had the following members:

Prof. D. Faulkner - University of Glasgow - Chairman
 R. Van Hooft - Conoco
 W. Schott -
 C. Miller - CBI
 P. Wirsching - University of Arizona
 Y.N. Chen - ABS
 H.Y. Jan - ABS - Secretary

Two other visitors who represented organizations who supported the Buckling Test Program should be mentioned since they made important contributions to the work:

Gerry Burns - Standard Oil Company of California
 Vic Davey - U.K. Department of Energy

There is not time for me to go into detail about the Model Code, however, the RCC did include 4 recommendations that say quite a bit about the Code and point out areas where more work is needed. I would like to go over these recommendations:

- 1) The strength formulations for cylindrical structures were derived on the basis of test data available to the Committee, at the time. They may need further development when all the test results (Phase I & II) are compiled and interpreted. The effect of residual stresses should be examined and accounted for in the strength formulations.
- 2) In the Model Code the Target Safety Index β was tentatively selected as 3.72, corresponding to a probability of failure of 10^{-4} . The Committee felt that a β of 3.72 was on the conservative side. If direct design procedures using appropriate level II algorithms could be used in place of code-specified PSF's a lower target safety index is possible.

Model uncertainties and economic considerations should be further studied as to their implications on the β selection process.

- 3) The interim loading model in the Model Code considers that the design levels of wave, wind and current act on the structure in the same directions and their

load components can be directly superimposed to determine extreme load effects.

This direct superposition is done only for convenience. The Model Code could directly account for the situation of different directions if known and if required. For TLP type structures, the maximum extreme environmental effects such as 100 year storm wave may not produce maximum loadings in a structural component. Model Code accounts for this too.

- 4) The main objective of the RCC was to take the development of a reliability-based design standard to the stage where its validity could be demonstrated so that further development could be carried out. The Committee had focused its effort on only one limit state, namely, ultimate strength of cylindrical structures under extreme loading. Further work may be required before the suggested strength formulations can be finalized. Other design limit states relating to serviceability during operation and installation have yet to be considered. Thus the recommended Design Code, while it may serve as the basis for a reliability-based design standard cannot be utilized as a complete design tool at this time.

ABS is currently working on its own Rules for TLP's. Our plan is to produce a standard built around the working stress format but to also include a reliability based alternative which will build upon the framework of the Model Code.

Our work at ABS has been hampered by lack of continuous sustained effort applied to developing this Code. The downturn in the price of oil and cutbacks in deepwater exploration had raised questions in our minds as to when the next TLP will be installed. However, we did make a commitment to complete the TLP Rules and have again taken up the task. We plan to have a version far enough along to submit to our Committee by end of 1987.

The largest effort made to prepare a design standard for TLP's that I know of was that undertaken by the United States offshore oil industry and administered by API. This effort has produced API RP-2T plus two supplementary Bulletins i.e.:

Bulletin 2U - "Stability Design of Cylindrical Shells"
 Bulletin 2V - "Design of Flat Plate Structures"

These three documents are to be published this year and will be available by mid-year.

The buckling formulations in the three standards I mentioned: Model Code, ABS Rules which are in preparation and API-RP-2T and Bulletin 2U, all reflect the work done in the ABS administered Joint Industry sponsored Test Program plus the considerable experience and expertise of some very good people from industry and academia.

We are looking forward to reviewing the structural design of the new Conoco TLP. Conoco provided the impetus to establish the Joint Industry Test program, and the RCC that produced the Model Code. Their people were very active in the API-RP-2T effort. We hope the test program results and the standard making effort has helped with their TLP design.

DEVELOPMENT OF API BULLETIN 2U
FOR STABILITY DESIGN OF CYLINDRICAL SHELLS

by

R.K. Kinra, Staff Civil Engineer
Shell Oil Company, Houston, Texas

and

C.D. Miller, Director of Structural Research
CBI Research Corp., Plainfield, Illinois

Introduction

This paper briefly discusses the background and development of a guide for the stability design of cylindrical shells for offshore structures, API Bulletin 2U (Reference 1). The first edition of the guide will be published in May 1987 by the American Petroleum Institute (API). Work on the guide was started approximately four years ago by the API Task Group on Tension Leg Platform Structural Design. This task group was one of nine task groups formed in 1982 by the newly formed API Subcommittee 2T, which was charged by the API Standardization Committee on Offshore Structures (Committee 2) with the development of a Recommended Practice for the Design of Tension Leg Platforms (TLP's). The diligent efforts of the nine task groups culminated in March 1987 in the publication of the first edition of API RP 2T, Recommended Practice for Planning, Designing and Constructing Tension Leg Platforms (Reference 2). Bulletin 2U was developed by the Task Group on TLP Structural Design in API RP 2T. A companion document, API Bulletin 2V (Reference 3), was also developed to provide guidance for the design of flat plate structures.

The development of Bulletin 2U was undertaken for several major reasons. The columns and pontoons of tension leg platform hull structures, such as depicted in Figure 1, often include very large diameter orthogonally-stiffened shells. Design guidance for such large diameter orthogonally-stiffened shells under combined loading is currently not available in any United States code of practice. The API Recommended Practice for Fixed Offshore Structures, API RP 2A (Reference 4) only covers low D/t unstiffened and ring stiffened cylinders. The broader scope ASME Code Case N-284 (Reference 5) issued in 1980 has not yet been formally adopted and has not been updated to include the results of extensive new fabricated cylinder test data that have become available since 1979. Bulletin 2U is intended to fill this gap in design guidance for large diameter orthogonally-stiffened shells.

Scope of Bulletin 2U

Bulletin 2U covers all the cylinder geometries, buckling modes and loading conditions pertinent for offshore structures. The cylinder geometries and buckling modes included are illustrated in Figure 2. The loads and load combinations covered in the bulletin include:

- Axial compression
- Bending
- Radial or hydrostatic external pressure
- Axial compression, bending and hoop compression
- Axial tension, bending and hoop compression.

Semi-empirical Design Approach

The design approach adopted in Bulletin 2U is semi-empirical. The same basic approach is used for all the different buckling modes. For a given buckling mode, the elastic buckling stress is computed from:

$$F_{eL} = \alpha \sigma_{eL}$$

where σ_{eL} = the theoretical elastic buckling stress, and

α = a reduction factor.

The reduction factor, α , is an empirical factor which accounts for the effect of geometric imperfections, boundary conditions, etc. If the elastic buckling stress, F_{eL} , is above the proportional limit of the material, the effects of inelasticity must be considered. This is done by applying a plasticity reduction factor:

$$F_{cR} = \eta F_{eL}$$

where η = the plasticity reduction factor.

The plasticity reduction factors in Bulletin 2U are empirical factors determined on the basis of available test data. For a given cylinder, the failure mode and corresponding buckling stress are determined by evaluating the lowest buckling stress among all the possible buckling modes for the cylinder.

Key Features of Bulletin 2U

Some key features of Bulletin 2U are discussed below:

1. Working stress design approach - Bulletin 2U is based on a working stress design approach. The available test data are used to develop empirical lower-bound buckling curves. The allowable stresses are obtained by dividing the buckling stresses by safety factors chosen to reflect the lower-bound nature of the buckling stresses.
2. Recommended safety factors - In order to account for the greater sensitivity to geometric imperfections of cylinders which buckle in the elastic range, a variable factor of safety equal to 1.67ψ for normal design conditions is recommended. The partial safety factor ψ depends on the buckling stress. The recommended value of ψ is 1.2 when the buckling stress is elastic and 1.0 when the buckling stress equals the yield stress. A linear variation is recommended between these limits. For extreme loading conditions, where a one-third increase in allowable stresses is appropriate, a factor of safety equal to 1.25ψ is recommended.
3. Mode separation - The buckling stress equations in Bulletin 2U were developed on the basis of no interaction between the buckling modes. The buckling stresses for local shell buckling, however, may be reduced if the predicted buckling stress for either bay instability or general instability is approximately equal to the predicted local buckling stress. Similarly, if the predicted general instability stress is approximately equal to the bay instability stress, the actual buckling stress for either of these modes may be less than predicted.

Mode interaction can be avoided by applying a factor β to the strains corresponding to the buckling stresses. It is desirable to provide a hierarchy for failure with general instability preceded by bay instability and bay instability preceded by local shell buckling, because local shell buckling is generally much less catastrophic than bay or general instability. A minimum factor of 1.2 is recommended for β for both the bay and general instability modes. The designer may elect to choose a higher β value for the general instability mode.

4. Commentary - A detailed commentary is provided in the bulletin, describing the background of the recommended buckling stress equations and showing comparisons of the equations with all the available fabricated cylinder test data.

Summary of Fabricated Cylinder Tests

Table 1 summarizes all the buckling tests carried out in the United States on fabricated steel cylinders that are found in the published literature. Tests on manufactured steel cylinders and cylinders made of other materials such as aluminum and mylar are not included, because it is felt that these may not provide realistic imperfection reduction

factors and plasticity reduction factors for fabricated cylinders such as are used in offshore platforms, due to differences in geometric imperfections and residual stresses. Table 1 lists 176 tests on unstiffened cylinders, 249 tests on ring stiffened cylinders, 28 tests on stringer stiffened cylinders and 51 tests on ring and stringer stiffened cylinders. The geometry of the cylinders, the material yield strength and the loading conditions are described in the table.

Results from the tests listed in Table 1 have been used to develop the empirical reduction factors and plasticity reduction factors recommended in Bulletin 2U. The table shows that a long 40 year hiatus followed the early tests on unstiffened cylinders under axial compression conducted in the 1930's at the University of Illinois. In the mid-seventies, the oil industry realized the importance of fabricated cylinder tests and began a series of tests starting with tests on cylinders under axial compression at Lehigh University. This was followed by many test programs funded by the American Petroleum Institute and joint industry cooperative efforts. Many of the test programs have been conducted at Southwest Research Institute and CBI Research Corporation, which have excellent test facilities for hydrostatic pressure loading.

Figures 3, 4 and 5 from Bulletin 2U have been selected to illustrate the type of calibrations carried out between available test results and the semi-empirical buckling stress equations recommended in Bulletin 2U. Figures 3 and 4 show the results for elastic and inelastic local buckling of unstiffened cylinders under axial compression. Figure 5 shows the calibration for local shell buckling of stringer stiffened cylinders under axial load. The Bulletin 2U Commentary contains many similar figures, which cover the other cylinder geometries and buckling modes included in Bulletin 2U.

Verification of Bulletin 2U

Late in 1985 the Task Group on TLP Structural Design decided that it was necessary to carry out an independent evaluation and verification of Bulletin 2U before it was submitted for approval to the TLP Subcommittee. A joint industry project supported by ten companies was organized and administered by Earl and Wright Consulting Engineers. The verification work, documented in Reference 6, was carried out by Earl and Wright, CBI Research and J.P. Kenny. The intensive verification effort resulted in some important suggestions for changes in Bulletin 2U, which have already been implemented.

A major part of the effort carried out by J.P. Kenny was to compare the Bulletin 2U formulations with the strength formulations recommended by European codes and with the results of fabricated cylinder tests carried out in Europe. In general, the Bulletin 2U formulations were found to compare favorably with test results and formulations from other codes. For example, Figure 6 shows a comparison of test results for local buckling of ring stiffened cylinders under axial compression with the

buckling formulations recommended by Bulletin 2U, ASME Code Case N-284, the DNV-OS Rules (Reference 7) and the ECCS Recommendations (Reference 8). The figure shows that Bulletin 2U compares favorably with the other available codes, providing a reasonable lower bound to the test results and slightly less scatter of the test results than the other code formulations. Reference 6 contains many similar comparisons for other cylinder geometries and loading conditions.

Conclusions and Recommendations

The release of the first edition of API Bulletin 2U represents an important milestone in the development of design guidance for fabricated cylindrical shells. Much work, however, remains to be done in the future. Some recommendations for further research follow:

1. Reliability-based design approach - As discussed, Bulletin 2U is based on a working stress design approach using essentially lower bound formulations. Further work with the existing test data should focus on comprehensive statistical analysis of the test data leading to a reliability-based design approach and more consistent safety factor levels.
2. Additional model tests - In spite of the hundreds of model tests on fabricated cylinders listed in Table 1, it is obvious that the data base is far from complete. For example, the number of tests on stringer stiffened and ring and stringer stiffened cylinders is woefully inadequate. Additional tests are required to fill in gaps in the data base and improve the buckling formulations recommended in Bulletin 2U.
3. Analytical calibration of test results - There is a great need to develop efficient finite element methods which can consider the effect of measured imperfections on buckling loads. Significant progress in this regard is being made in Europe, particularly at Imperial College in London. Earlier efforts were stymied by the prohibitive expense of accurate analyses with available finite element analysis programs. Recent progress in developing improved finite element methods and computer programs offers significant promise for the future. Successful calibration of analytical and model test results will pave the way for future reliance on analytical methods rather than expensive model tests.
4. Review of Bulletin 2U - Periodic review and updating of Bulletin 2U must be undertaken in order to maintain its state-of-the-art status. Problem areas encountered and reported by bulletin users must be investigated and necessary changes implemented expeditiously. Feedback from the user community will play an important role in the future evolution of Bulletin 2U.

References

1. American Petroleum Institute, "Bulletin on Stability Design of Cylindrical Shells," API BUL 2U, First Edition, May 1987.
2. American Petroleum Institute, "Recommended Practice for Planning, Designing and Constructing Tension Leg Platforms," API RP 2T, First Edition, March 1987.
3. American Petroleum Institute, "Bulletin on Design of Flat Plate Structures," API BUL 2V, First Edition, May 1987.
4. American Petroleum Institute, "Recommended Practice for Planning, Designing and Constructing Fixed Offshore Platforms," API RP 2A, Sixteenth Edition, April 1986.
5. American Society of Mechanical Engineers, Boiler and Pressure Vessel Code Case N-284, "Metal Containment Shell Buckling Design Methods," Nuclear Code Case Book, 1980.
6. Earl and Wright Consulting Engineers, "API Bulletin 2U Verification," Volumes I and II, Feb. 1986.
7. Det Norske Veritas, "Rules for the Design, Construction and Inspection of Offshore Structures," Appendix C, 1977 (Rev. 1982).
8. European Convention for Constructional Steelwork, "European Recommendations for Steel Construction," Section 4.6, Buckling of Shells, Publication 29, Second Edition, 1983.

TABLE 1 - SUMMARY OF BUCKLING TESTS ON STEEL CYLINDERS

Date	No. Tests	Geometry		σ_y (ksi)	Loads
		R/t	L/R		
UNSTIFFENED					
1933	21	139-990	1.0-24.7	25-46	Axial Compression
1937	18	35-98	14.8-60	31-40	Axial Compression
1977	10	42-124	2.6-5.8	50,94	Axial Compression
1978	13	23,34	4.3-59	36	Axial Compression
1980	5	38-113	4.0-5.3	35-52	Axial Compression
1981	2	150	0.58	37,47	Axial Compression
1981	13	460	2.0	30	Axial Compression (with and without openings)
1982	7	24	16	36,50	Axial Tension & External Pressure
1983	16	9-48	24-48	36,50	Bending
1983	5	149,222	2.0-2.4	44,55	Axial Compression
1985	66	16-40	6	35-43	Bending Axial Compression Bending, & External Pressure

TABLE 1 - SUMMARY OF BUCKLING TESTS ON STEEL CYLINDERS (continued)

Date	No. Tests	Geometry		σ_y (ksi)	Loads
		R/t	L/R		
RING STIFFENED					
1976	41	250-500	0.05-1.24	29-79	Axial Compression
1978	32	500	0.09-1.08	40	Axial Compression & External Pressure
1981	20	16-64	1-8	36, 50	External Pressure
1981	3	128, 213	0.2, 1.0	42	Axial Compression
1981	8	150, 250	0.33, 1.0	36-47	Axial Compression
1982	8	312	0.8-3.4	50, 80	Axial Compression
1982	6	458	0.18	30	Eccentric Axial Compression
1982	35	17-48	3-6	36, 50	Axial Tension & External Pressure
1983	22	150, 300	0.1-0.4	50	Axial Compression & External Pressure
1983	2	228	0.38	50	External Pressure
1983	33	23-47	1.7-3.5	37-52	Axial Compression & External Pressure
1983	30	23-47	1.7-3.5	36, 50	Axial Compression & External Pressure
1983	5	267	0.15	54	Axial Compression & External Pressure
1986	4	300	0.2	47	Axial Compression & External Pressure
STRINGER STIFFENED					
1981	6	190	0.41, 1.125	50	Axial Compression Eccentric Axial Compression
1981	14	200-360	0.40-1.56	41-49	Axial Compression
1981	2	95, 272	1.33, 1.56	33, 44	Axial Compression
1983	12	190	0.4-1.2	45	Axial Compression & External Pressure
RING AND STRINGER STIFFENED					
1981	1	196	1.11	36	Axial Compression
1983	44	190-500	0.2-1.0	50, 80	Axial Compression & External Pressure
1986	5	300-500	0.8-1.0	54-57	Axial Compression & External Pressure
	1	300	0.1	52	External Pressure

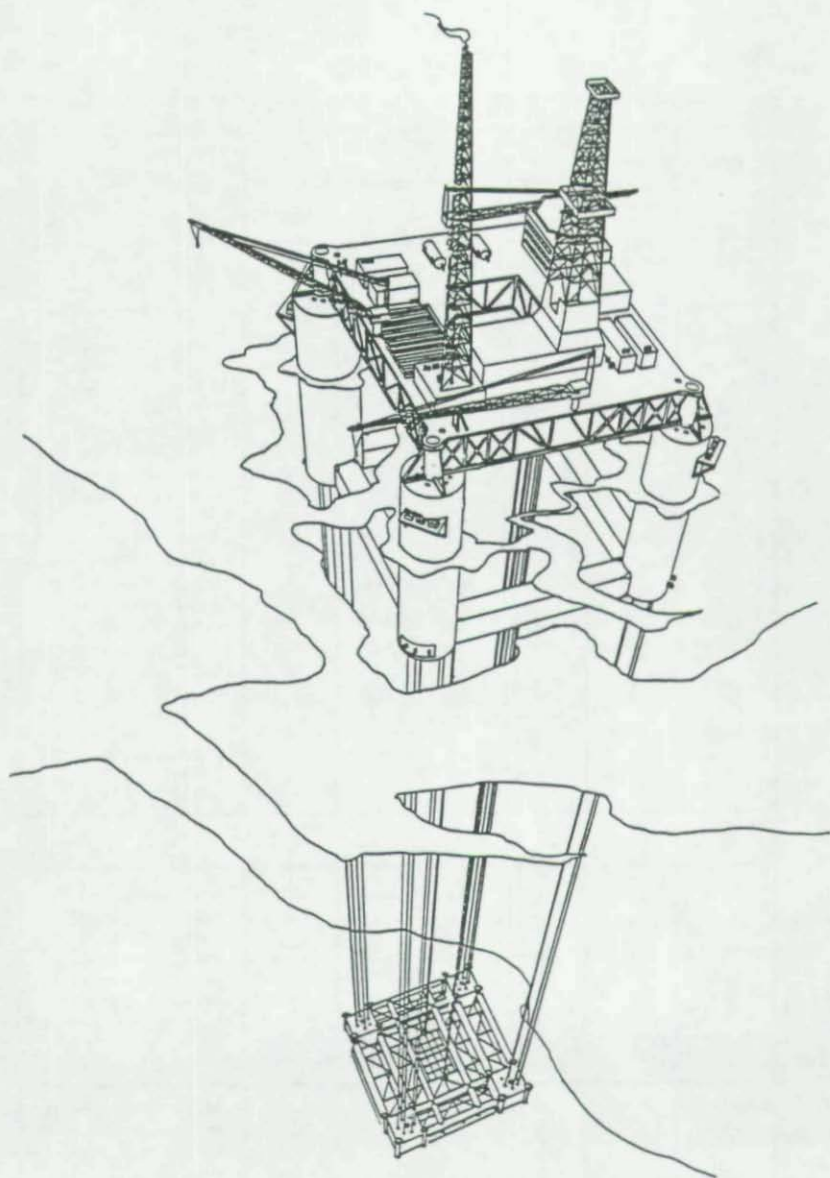


FIGURE 1. EXAMPLE TENSION LEG PLATFORM

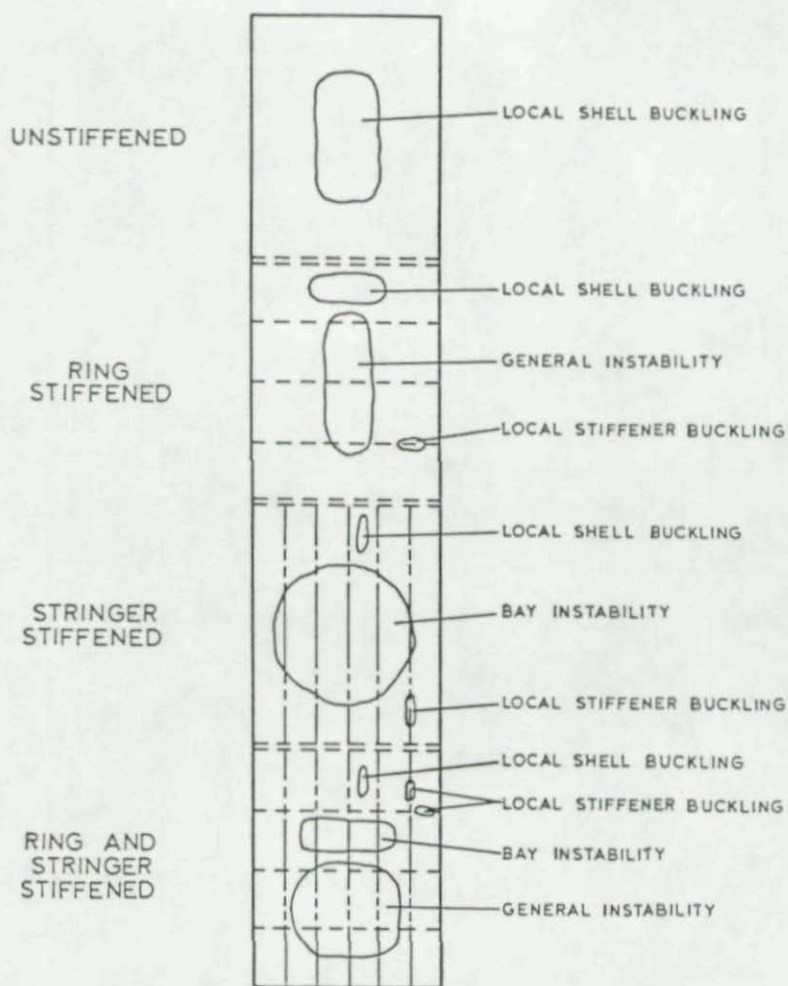


FIGURE 2. CYLINDER GEOMETRIES AND BUCKLING MODES COVERED IN BULLETIN 2U

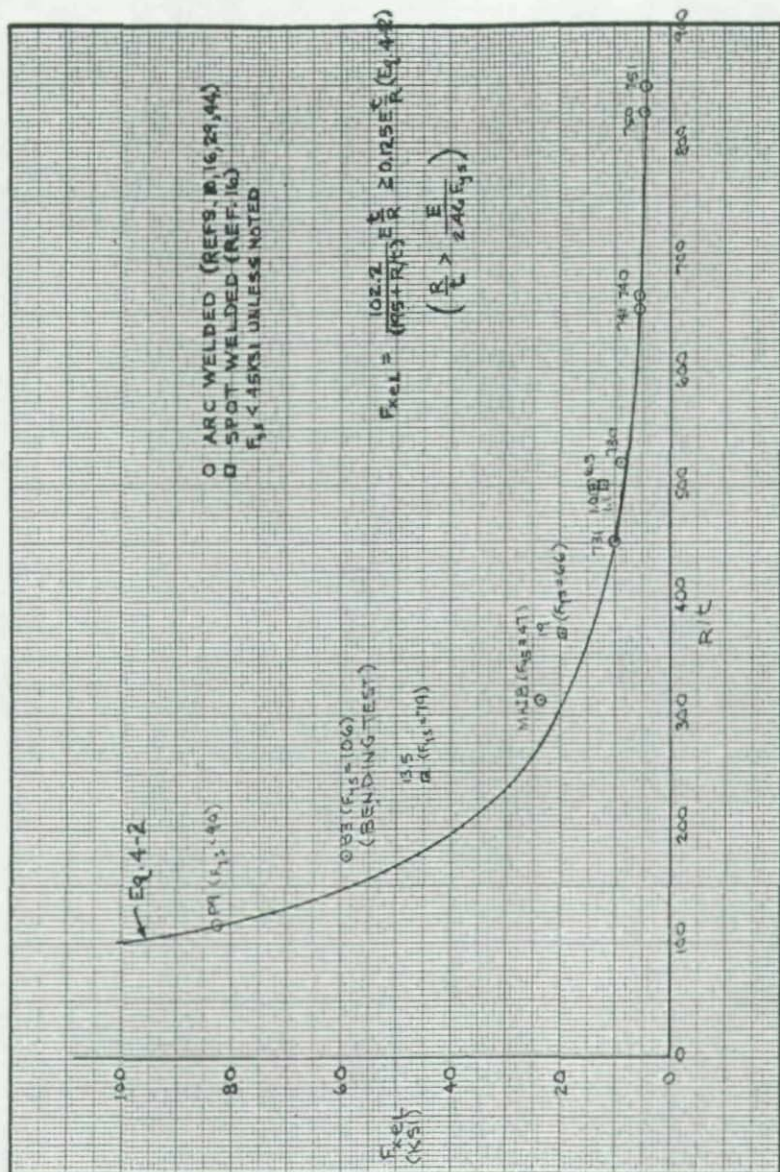
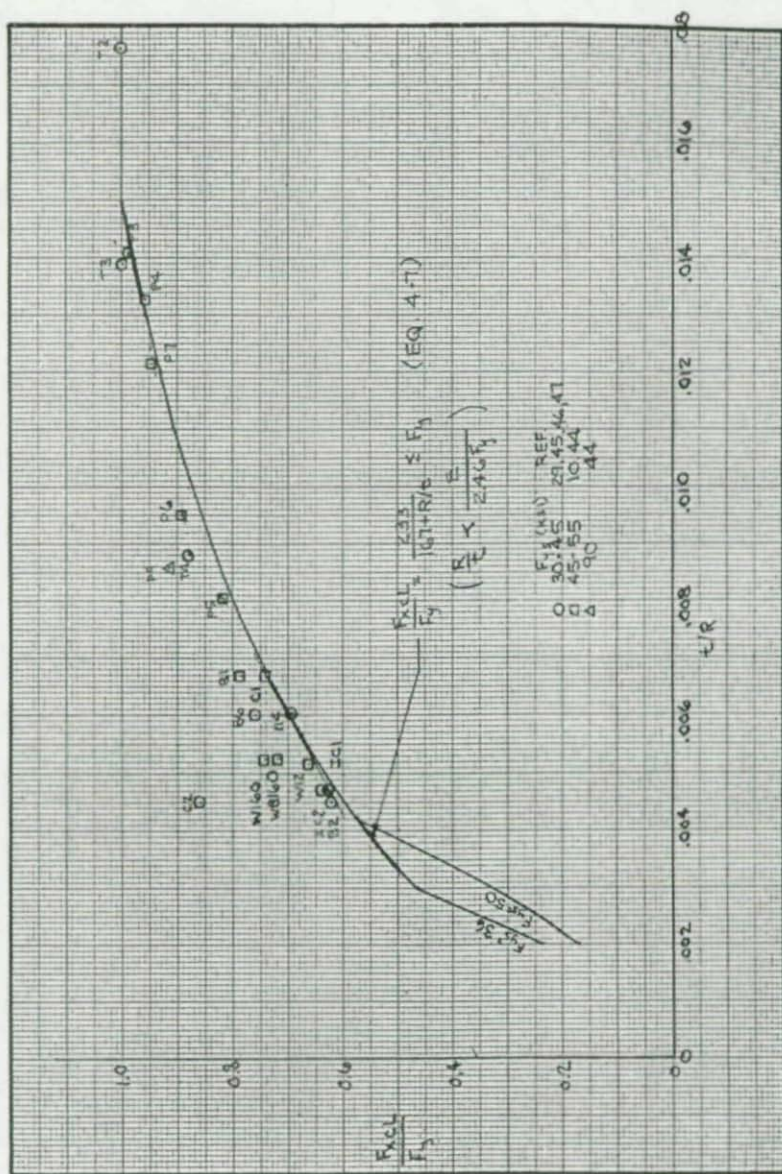


FIGURE 3. AXIAL COMPRESSION OF FABRICATED CYLINDERS — LOCAL BUCKLING IN ELASTIC REGION


 FIGURE 4. AXIAL COMPRESSION OF FABRICATED CYLINDERS —
 LOCAL BUCKLING IN INELASTIC REGION

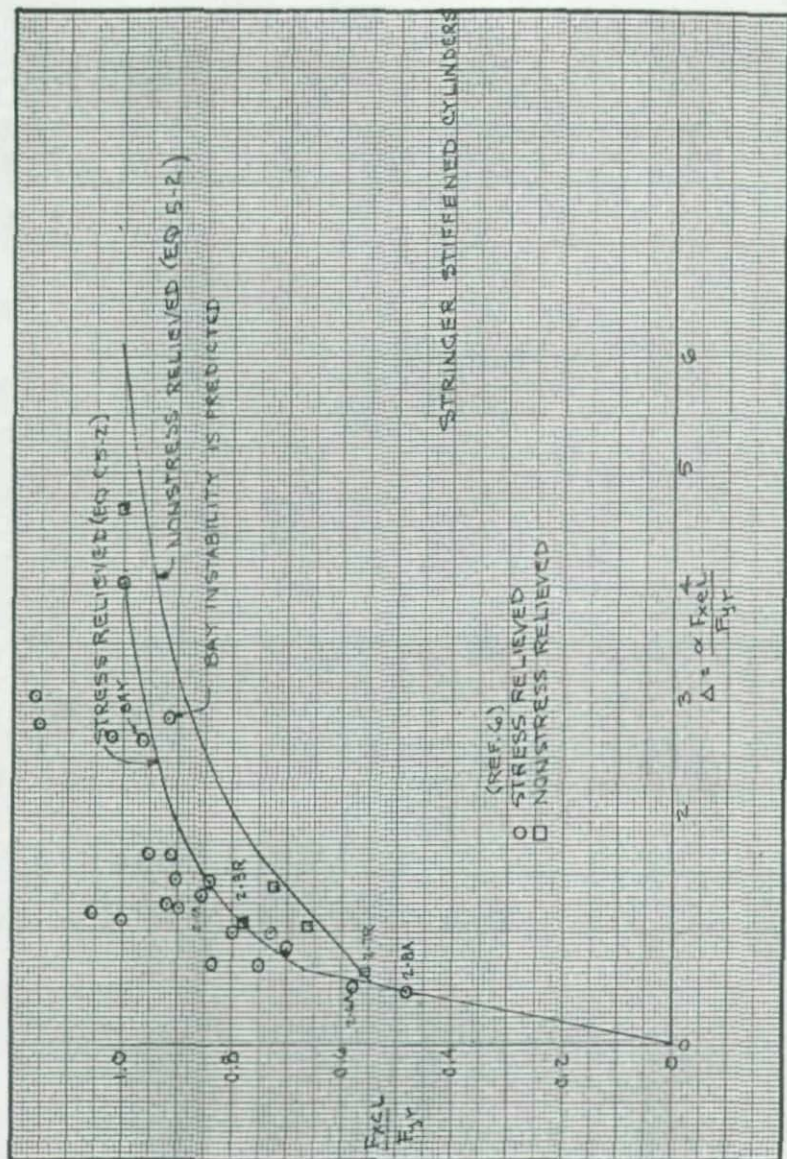


FIGURE 5. COMPARISON OF LOCAL SHELL BUCKLING TESTS WITH PREDICTED STRESSES FOR STRINGER STIFFENED CYLINDERS UNDER AXIAL LOAD

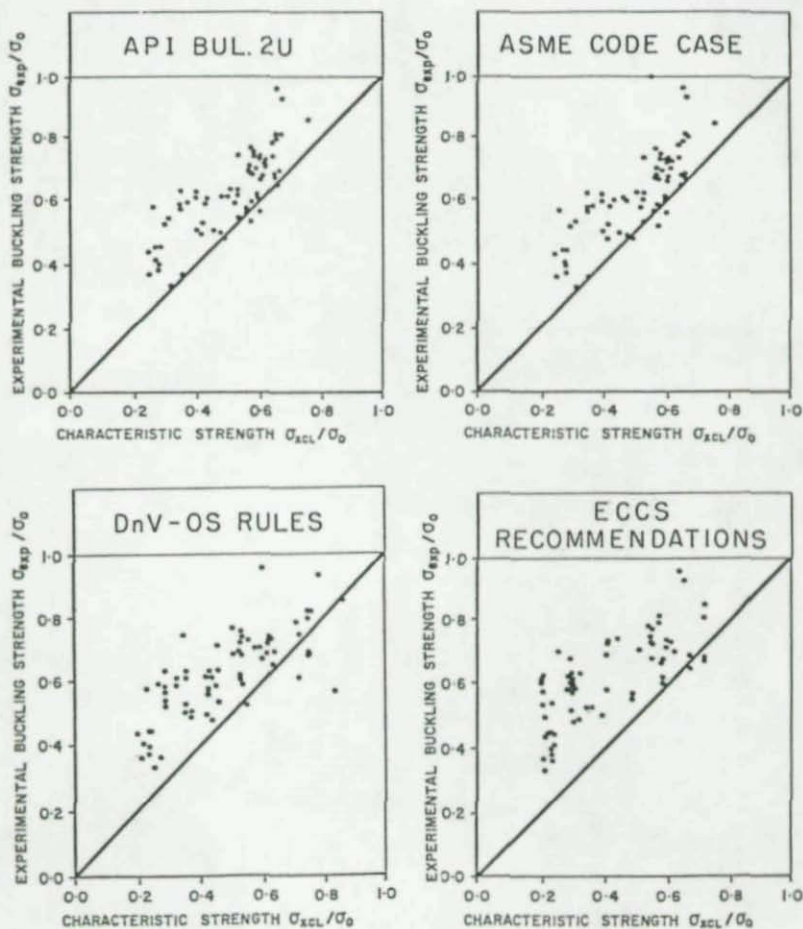
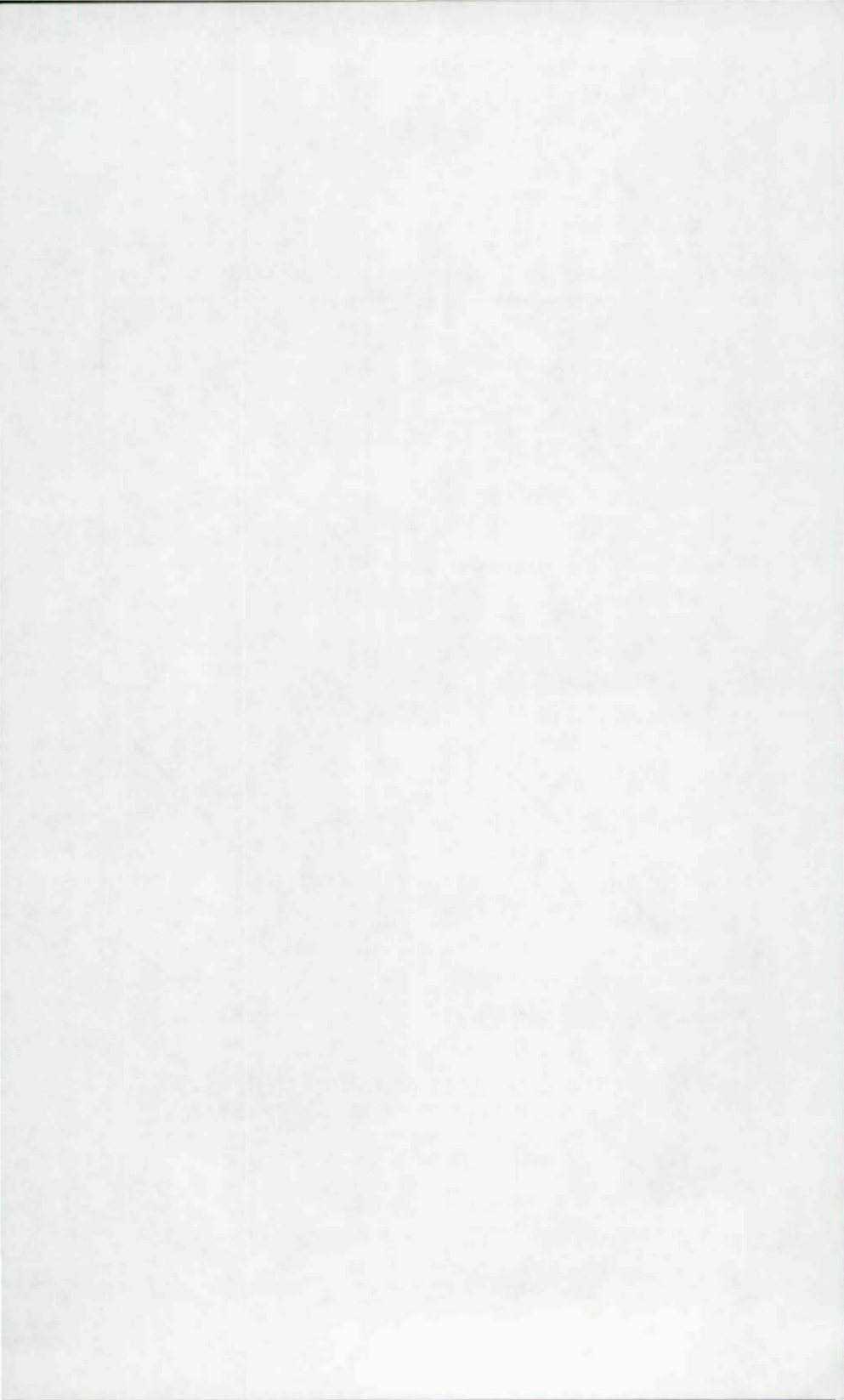


FIGURE 6. LOCAL BUCKLING OF RING STIFFENED CYLINDERS UNDER AXIAL COMPRESSION



STRUCTURAL STABILITY RESEARCH COUNCIL

1987 Annual Technical Session & Meeting

Houston, Texas

March 24-25, 1987

ATTENDEE ADDRESS LISTING

A T T E N D E E S

Mr. M. H. Ackroyd
Techtrol, Ltd.
3870 Cote Vertu Street
St. Laurent, Quebec
Canada H4R 1V4

Dr. N. Agelidis
Ford Motor Company
P. O. Box 2053, Rm-E-3184, SRL
Dearborn, MI 48121-2053

Prof. W. J. Austin
Department of Civil Engrg.
Rice University
P. O. Box 1892
Houston, TX 77251

Dr. L. S. Beedle
Structural Stability Research
Council
Fritz Engineering Lab 13
Lehigh University
Bethlehem, PA 18015

Mr. M. D. Bernstein
Foster Wheeler Energy Corp.
9 Peach Tree Hill Road
Livingston, NJ 07039

Prof. P. C. Birkemoe
Department of Civil Engrg.
Galbraith Building
University of Toronto
Toronto, Ontario
Canada M5S 1A4

Mr. F. Botros
Conoco, Inc.
600 Dairy Ashford
Houston, TX 77079

Mr. J. H. Brown
The Austin Company
3650 Mayfield Road
Cleveland, OH 44121

Mr. K. P. Buchert
S. Illinois University
at Edwardsville
33 Pat Drive
Collinsville, IL 62234

Mr. H. Burton (Student)
Rice University
Dept. of Civil Engrg.
P. O. Box 1892
Houston, TX 77001

Dr. S. S. Chang
Hudson Engineering Corp.
P. O. Box 218218
Houston, TX 77218

Dr. A. C. T. Chen
Exxon Production Research Co.
P. O. Box 2189
Houston, TX 77001

Prof. W. F. Chen
Purdue University
School of Civil Engrg.
West Lafayette, IN 47907

Prof. F. Y. Cheng
Department of Civil Engrg.
University of Missouri-Rolla
Rolla, MO 65401

Prof. J. J. Cheng
Civil Engineering Department
University of Alberta
Edmonton, Alberta
Canada T6G 2G7

Mr. C. R. Clauer
Midgley-Clauer Associates, Inc.
3624 Chestnut Court
Cibolo, TX 78018

A T T E N D E E S

Mr. M. Corazao (Student)
Rice University
Dept. of Civil Engineering
P. O. Box 1892
Houston, TX 77001

Mr. M. Donley (Student)
Dept. of Civil Engineering
Rice University
P. O. Box 1892
Houston, TX 77001

Prof. P. J. Dowling
Civil Engineering Dept.
Imperial College
London SW7 2BU
United Kingdom

Mr. J. L. Durkee
Consulting Structural Engineer
217 Pine Top Trail
Bethlehem, PA 18017

Dr. M. Elgaaly
Department of Civil Engineering
103 Boardman Hall
University of Maine
Orono, ME 04469

Dr. S. J. Errera
Product Applications Group
365 Steel Group Office
Bethlehem Steel Corp.
Bethlehem, PA 18016

Mrs. L. G. Federinic
Structural Stability Research
Council
Fritz Engineering Lab 13
Lehigh University
Bethlehem, PA 18015

Mr. G. F. Fox
Howard Needles Tammen &
Bergendoff
333 Seventh Avenue
New York, NY 10001

Prof. T. V. Galambos
Dept. of Civil & Mineral
Engineering
University of Minnesota
112 Mines & Metallurgy
221 Church Street, S.E.
Minneapolis, MN 55455

Mr. S. L. Gelpi
Chevron, USA-Eastern
935 Gravier Street
New Orleans, LA 70112

Mr. R. Ghanem (Student)
Rice University
Dept. of Civil Engineering
P. O. Box 1892
Houston, TX 77001

Mr. J. A. Gilligan
Consulting Engineer
1289 Firwood Drive
Pittsburgh, PA 15243

Prof. S. C. Goel
Dept. of Civil Engineering
The University of Michigan
Ann Arbor, MI 48109

Dr. J. E. Goldberg
Purdue University
1805 Western Drive
West Lafayette, IN 47906

Mr. S. X. Gunzelman
Design Engineer
Brown & Root Int'l., Inc.
P. O. Box 3
Houston, TX 77001

Mr. D. H. Hall
Bridge Software Development
International, Ltd.
P. O. Box 287
Coopersburg, PA 18036

A T T E N D E E S

Mr. J. E. Herz
American Bureau of Shipping
P. O. Box 910
45 Eisenhower Drive
Paramus, NJ 07653-0910

Mr. D. G. Hitt
Bethlehem Steel Corp.
P. O. Box 3031
Beaumont, TX 77704

Mr. J. S. B. Iffland
Iffland Kavanagh Waterbury, PC
1501 Broadway
New York, NY 10036

Mr. N. R. Iwankiw
American Institute of Steel
Construction
400 N. Michigan Avenue
Chicago, IL 60611-4185

Dr. B. G. Johnston
5025 E. Calle Barril
Tucson, AZ 85715

Mr. T. M. Jones
Exxon Production Research Co.
P. O. Box 2189
Houston, TX 77001

Mr. R. K. Kinra
Shell Oil Company
P. O. Box 2099
Houston, TX 77252-2099

Mr. K. H. Klippstein
Civil Engineering Dept.
University of Pittsburgh
936 Benedum Hall
Pittsburgh, PA 15261

Dr. M. Kubo
Department of Civil Engrg.
Meijo University
501, Shiogamagushi 1-Chome
Tenpaku-Ku, Nagoya 468
Japan

Prof. S. Kyriakides
Dept. of Aerospace Engrg. &
Engrg. Mechanics - WRW 110
The Univ. of Texas at Austin
Austin, TX 78712-1085

Dr. R. A. LaBoube
Butler Manufacturing Co.
Research Center
135th St. & Botts Road
Grandview, MO 64030

Mr. D. C. Lai
Amoco Production Company
P. O. Box 3385
Tulsa, OK 74102

Mr. C. Langewis
Conoco, Inc.
P. O. Box 2197
Houston, TX 77252

Mr. T. T. Laurendine
Chevron Oil Field Research Co.
P. O. Box 446
LaHabra, CA 90631

Mr. F. Lavelle (Student)
Rice University
Dept. of Civil Engineering
P. O. Box 1892
Houston, TX 77001

Mr. T. G. Longlais
Sargent & Lundy Engineers
55 E. Monroe Street
Chicago, IL 60603

A T T E N D E E S

347

Prof. I. Lotsberg
Dept. of Civil Engineering
McMaster University
1280 Main Street West
Hamilton, Ontario
Canada L8S 4L7

Mr. L. A. Lutz
Computerized Structural
Design, Inc.
5678 W. Brown Deer Road
Milwaukee, WI 53223

Dr. M. K. S. Madugula
Dept. of Civil Engineering
University of Windsor
Windsor, Ontario
Canada N9B 3P4

Mr. J. R. Maison
Adaptive Computer Tech., Inc.
1850 Lockhill Selma, Suite 104
San Antonio, TX 78213

Mr. P. W. Marshall
Shell Oil Company
P. O. Box 2099
Houston, TX 77252-2099

Dr. R. E. McConnel
Engineering Department
University of Cambridge
Trumpington Street
Cambridge CB2 1PZ
England

Mr. R. M. Meith
Consultant
3720 Aurora Drive
New Orleans, LA 70114

Mr. C. D. Miller
CBI Industries, Inc.
1501 N. Division Street
Plainfield, IL 60544

Mr. D. L. Miller
American Petroleum Institute
211 N. Ervay, Suite 1700
Dallas, TX 75201

Prof. T. Moan
College of Engineering
Naval Arch. & Offshore Engrg.
Univ. of California-Berkeley
Berkeley, CA 94720

Mr. E. D. Moore
Bethlehem Steel Corporation
P. O. Box 3031
Beaumont, TX 77704

Dr. N. F. Morris
Civil Engineering Department
Manhattan College
Riverdale, NY 10471

Dr. A. Ostapenko
Dept. of Civil Engineering
Lehigh University
Fritz Engineering Lab 13
Bethlehem, PA 18015

Mr. S. Paulson
Chevron Corp.
P. O. Box 5045
San Ramon, CA 94583

Prof. D. Polyzois
Dept. of Civil Engineering
University of Texas at Austin
Austin, TX 78758

Mr. H. G. L. Prion
Dept. of Civil Engineering
University of Toronto
Toronto, Ontario
Canada M5S 1A4

A T T E N D E E S

Dr. Z. Razzag
Dept. of Civil Engineering
Old Dominion University
Norfolk, VA 23508

Mr. I. Robertson (Student)
Civil Engineering Department
Rice University
P. O. Box 1892
Houston, TX

Mr. S. M. Sanzgiri
McDermott, Inc.
1010 Common Street, #1951
New Orleans, LA 70112

Prof. U. Schulz
Universitat Karlsruhe
7500 Karlsruhe 41
ERNST-BALACH-Str. 8
Federal Republic of Germany

Mr. M. L. Sharp
Technical Consultant
Alcoa Technical Center
Aluminum Company of America
Alcoa Center, PA 15069

Prof. D. R. Sherman
Dept. of Civil Engineering
Univ. of Wisconsin-Milwaukee
P. O. Box 784
Milwaukee, WI 53201

Mr. R. F. Siemens, Jr.
Texaco, Inc.
P. O. Box 60252
New Orleans, LA 70160

Prof. T. H. Soreide
Div. of Structural Mechanics
The Norwegian Institute of
Technology
7034 Trondheim - NTH, Norway

Mr. J. Springfield
Carruthers & Wallace Ltd
250 Merton Street
Toronto, Ontario
Canada M4S 1B1

Prof. S. Sridharan
Department of Civil Engrg.
Washington University
Campus Box 1130
St. Louis, MO 63130

Mr. S. B. Stanley
rHBethlehem Steel Corp.
Beaumont Yard
P. O. Box 3031
Beaumont, TX 77704

Mr. G. S. Stewart
Structural Stability Research
Council
Fritz Engineering Lab 13
Lehigh University
Bethlehem, PA 18015

Mr. D. C. Stringer
AMCA International Ltd.
P. O. Box 13160
Kanata, Ontario
Canada K2K 1X4

Mr. Y. H. Sun (Student)
Dept. of Civil Engineering
Rice University
P. O. Box 1892
Houston, TX 77001

Ms. S. Severdon (Student)
Dept. of Civil Engineering
Rice University
P. O. Box 1892
Houston, TX 77001

A T T E N D E E S

349

Mr. J. Taby
Div. of Marine Structures
The Univ. of Trondheim
Norwegian Inst. of Technology
Trondheim, Norway

Prof. A. C. Walker
University of Surrey
Dept. of Mechanical Engrg.
Guildford, Surrey GU2 5XH
England

Dr. L. Tall
School of Engineering
Florida International Univ.
Miami, FL 33119

Dr. C. K. Wang
Dept. of Civil & Environ-
mental Engineering
University of Wisconsin
Madison, WI 53076

Mr. W. Y. Tein (Student)
Dept. of Civil Engineering
Rice University
P. O. Box 1892
Houston, TX 77001

Mr. F. S. Wang
JL Computer Service
2600 S. Gessner, Suite 504
Houston, TX 77063

Dr. M. C. Temple
Dept. of Civil Engineering
University of Windsor
Windsor, Ontario
Canada N9B 3P4

Mr. T. Wierzbicki
Massachusetts Inst. of Tech.
Room 5-218
Cambridge, MA 02139

Mr. P. E. Versowsky
Chevron USA, Inc.
935 Gravier St.
New Orleans, LA 70112

Mr. T. Yamada
Civil & Construction Dept.
Nippon Kokan K.K.
2-1 Chome, Suehiro-cho
Tsurumi-ku, Yokohama
Japan 230

Prof. R. S. Vinnakota
Civil Engineering Dept.
Marquette University
1515 W. Wisconsin Avenue
Milwaukee, WI 53233

Prof. C. H. Yoo
Civil Engineering Dept.
Auburn University
Auburn, AL 36849

Mr. J. F. Vojta
CBI Industries, Inc.
1501 N. Division St.
Plainfield, IL 60544

Prof. W. W. Yu
Dept. of Civil Engineering
University of Missouri-Rolla
Rolla, MO 65401

Ms. M. Wagner
Arizona Public Service Co.
MS-5109, P. O. Box 53999
Phoenix, AZ 85072-3999

Mr. H. Yun (Student)
Dept. of Aerospace Engrg. &
Engrg. Mechanics - WRW 110
University of Texas at Austin
Austin, TX 78712-1085

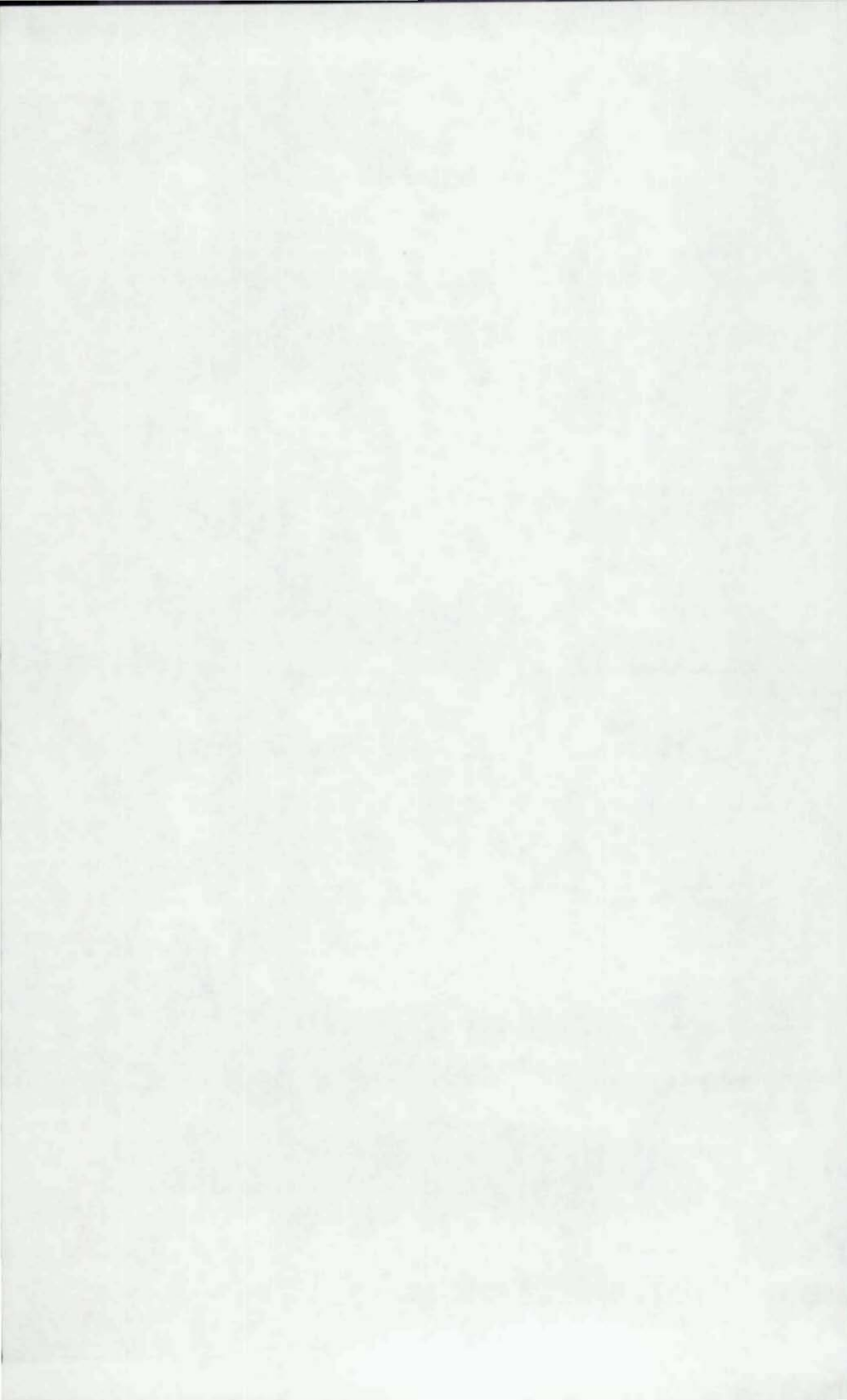
A T T E N D E E S

Dr. J. A. Yura
Dept. of Civil Engineering
University of Texas
Austin, TX 78712

Mr. H. Zerbe (Student)
Dept. of Civil Engineering
Rice University
P. O. Box 1892
Houston, TX 77001

Contributor Index

- Apte, S. C.; 135
 Ashraf Ali, M. A.; 13
- Brodtkorb, B.; 299
 Birkemoe, P. C.; 65,105
 Buchert, K. P.; 39
- Cheng, F. Y.; 149
 Cheng, J. J.; 191
- Darbhamulla, S. P.; 1
 Dowling, P. J.; 265
- Goel, S. C.; 175
 Goldberg, J. E.; 125
- Herz, J. E.; 325
 Hu, S. Z.; 191
- Kinra, R. K.; 329
 Kwok, M. K.; 275
- Li, S. F.; 113
 Lotsberg, I.; 105
- Madugula, M. K. S.; 205
 Manko, Z.; 233,245
 McCall, S.; 275
 McConnell, R. E.; 49
 Miller, C. D.; 287
 Moan, T.; 79
 Mohan, S.; 205
 Morris, N. F.; 55
- Ostapenko, A.; 135
- Pantelides, C. P.; 149
 Pathak, D. V.; 125
 Prion, H. G. L.; 65
- Razzaq, Z.; 1
 Ronalds, B. F.; 265
- Sherman, D. R.; 259
 Soreide, T. H.; 299
 Sridharan, S.; 13
- Taby, J.; 7
 Tagawa, K.; 163
 Takanashi, K.; 163
 Tan, J. C.; 221
 Tang, X.; 175
 Temple, M. C.; 221
- Valsgard, S.; 299
 Vojta, J. F.; 287
- Walker, A. C.; 275
 Wang, S.; 27
 Wang, G. Z.; 113
 Yamada, T.; 163
 Yang, X. M.; 113
- Zhou, Z.; 27

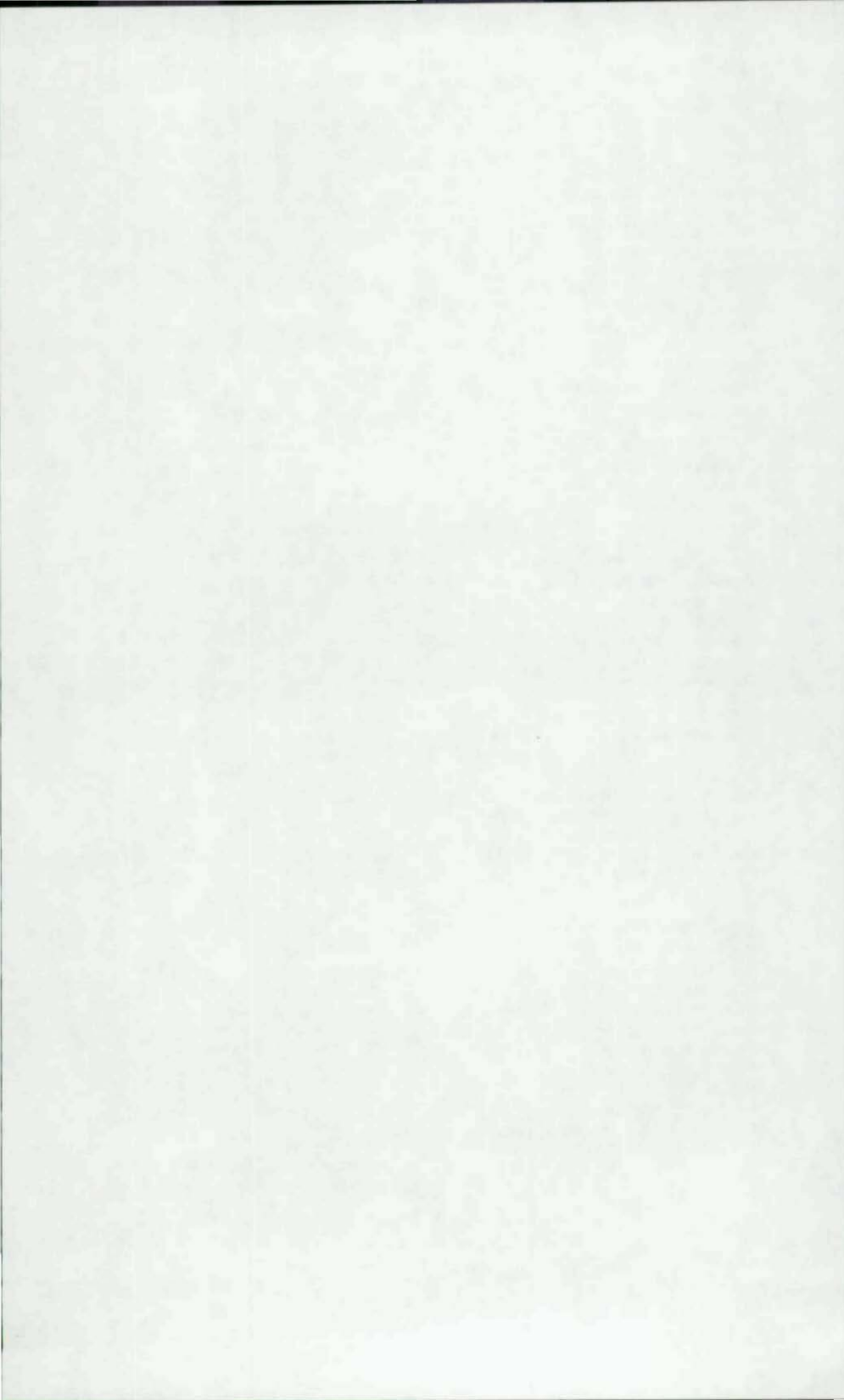


Name Index

- Aalami, B.; 155
 Abbas, B. A. H.; 155
 Akay, H. U.; 196,198
 Akesson, B.; 156
 Alspangh, D. W.; 130
 Amdahl, J.; 317
 Anderson, J. G.; 168
 Anderson, R. A.; 155
 Apte, S. C.; 135
 Ashraf Ali, M.; 13,21
 Archer, J. S.; 149,155
 Arnesen, A.; 317
 Ashraf Ali, M.; 13,21
 Astaneh, A.; 178
 Atsuta, T.; 4
 Atzori, B.; 155
- Baker, E. H.; 317
 Bathe, K. J.; 142
 Benito, R.; 21
 Bergan, P. G.; 317
 Birkemoe, P. C.; 65,105,106
 Birnstiel, C.; 4
 Bjorhovde, R.; 192,198
 Bleich, F.; 35
 Bogdanoff, J. L.; 125,130
 Brodtkorb, B.; 299,317
 Buchert, K. P.; 39,47
 Burns, G.; 327
- Calabrese, J. M.; 228
 Chakrabarti, S. K.; 198
 Chen, W. F.; 4,63,78,121
 Chen, W. Y.; 121
 Chen, Y. N.; 327
 Cheng, F. Y.; 14,156
 Cheng, R.; 191
 Cheung, Y. K.; 246,256
 Chrysos, L.; 63
 Croll, J. G. A.; 256
- Darbhamulla, S. P.; 1,4
 Davey, V.; 327
 Deprez, G.; 243
 Desmond, T. P.; 28,35
 Djodjo, B. A.; 149,156
 Dowling, P. J.; 265,273,274,317
- Eder, M. F.; 294
 Elinas, C. P.; 80,90,120,279,317
 Elnashai, A. S.; 273
 Erzurumlu, H.; 121,210,212
- Fathelbab, F. A.; 52
 Faulkner, D.; 326,327
 Flugge, W.; 304,317
 Fonder, G.; 243
- Gaylord, C. N.; 198
 Gaylord, E. H.; 1,4,192,198
 Gere, J. M.; 257,317
 Goel, S. C.; 175,178
 Goldberg, J. E.; 125,130
 Golub, G. H.; 63
 Graves Smith, T. R.; 246,249,256
 Grimm, D. F.; 78,142
 Grove, R. B.; 294
 Gunzelman, S. X.; 78
- Hanai, M.; 168
 Hanaor, A.; 63
 Hanson, R. D.; 63
 Hardash, S. G.; 192,198
 Harding, J. E.; 273
 Harvey, J. M.; 28,35
 Hatzis, D.; 52
 Herz, J. E.; 325
 Hormby, D. E.; 198
 Howson, W. P.; 149,156
 Howson, W. P.; 149,156
 Hu, J.; 121
 Hu, S. Z.; 191
 Huang, T. C.; 156
- Ishihara, K.; 168
- Jain, A. K.; 178
 Jan, H. Y.; 327
 Johnson, C. P.; 198
 Johnston, B. G.; 4,47,121
- Kahn, L. F.; 63

- Kanaan, A. E.; 179
 Kani, I. M.; 49,52
 Kennedy, D. J. L.; 228
 Kennedy, J. B.; 210,211,212
 Kinra, R. K.; 329
 Kirkwood, W.; 90,111
 Kitipornchai, S.; 211,212
 Kiziltug, A. Y.; 294
 Kloppel, K.; 243
 Kmita, J.; 243,257
 Koiter, W. T.; 21,22
 Kovalevsky, L.; 317
 Kulak, G.; 294
 Kurabe, K.; 168
 Kurzio, K. S.; 142
 Kowk, M. K.; 275,279
- Larson, J. W.; 142
 Lee, H. W.; 211,212
 Lemanczyk, M.; 257
 Li, S. F.; 113,121
 Liu, Z.; 179
 Lotsberg, I.; 105,106
 Love, A. E. H.; 125,130
 Lunden, R.; 156
- Madugula, K. K. S.; 205,210,212
 Manko, B.; 243
 Manko, Z.; 233,245,246,256,257
 Maquoi, R.; 243
 Marsh, C.; 209,212
 Marzulla, M. A.; 78
 Massonnet, C.; 243,257
 Matsui, C.; 78
 McCall, S.; 275,279
 McCloskey, D. C.; 228
 McConnel, R. E.; 49,51,52
 Miller, C.; 326,327
 Miller, C. D.; 287,293,294
 Miller, C. S.; 327
 Moan, T.; 79,90,91,111
 Mohan, S.; 205
 Montgomery, C. J.; 294
 Morris, N. F.; 55,63
 Mroz, Z.; 168
 Mueller, W. H.; 121,210,212
 Muler, R.; 243
 Murty, M. K. S.; 205,210,211,212
- Newmark, N. M.; 78
 Nonaka, T.; 213
 Novozhilov, V. V.; 125,130
 Nygaard, M. K.; 317
- Odland, J.; 91,294
 Oliveira, J. G.; 327
 Olszak, W.; 168
 Onoufriou, A.; 273,274
 Ostapenko, A.; 78,81,91,135,142
- Pantelides, C. P.; 149
 Pathak, D. V.; 125
 Papadrakakis, M.; 63
 Pekoz, T.; 35
 Perzyna, P. 168
 Peters, S. W.; 294
 Pignataro, M.; 22
 Plan, R. J.; 246,257
 Plantema, F. J.; 78
 Powell, G. H.; 179
 Prabhu, T. S.; 210,212
 Prince, J.; 168
 Prion, H. G. L.; 65
 Przemieniecki, J. S.; 257
- Qian, D.; 120
- Rabern, D. A.; 198
 Rashed, S. M. H.; 81,90,111
 Razzaq, Z.; 1,4
 Rhodes, J.; 28,35
 Richard, R. M.; 198
 Rish, F. L.; 317
 Ronalds, B. F.; 265,274
 Ross, D. A.; 78,121
- Sato, J. A.; 78
 Schepers, J. A.; 228
 Schmidt, L. C.; 63,126
 Schmied, R.; 243
 Schott, W.; 327
 Schubert, J.; 243
 See, T.; 49,51
 Setlur, A. V.; 130
 Sharma, S. S.; 1,4
 Sherman, D. R.; 78,259
- Nakamura, Y.; 163
 Narayanan, R.; 120

- Short, J.; 210,212
 Skaloud, M.; 21
 Smith, C. S.; 80,90,121
 Smith, E. A.; 63
 Smith, G.; 246,249
 Somerville, W. C.; 90,111,121
 Soreide, T. H.; 299,317
 Sridharan, S.; 13,21,256
 Steen, E.; 317
 Stephens, J. E.; 156
 Stephens, M. J.; 294
 Supple, J. P.; 317
 Swan, J. W.; 90,111,121
- Taby, J.; 79,81,90,91,111
 Tagawa, K.; 163,168
 Takanashi, K.; 163,168
 Tan, J. C.; 221
 Tanaka, H.; 168
 Tang, X.; 175,179
 Temple, M. C.; 210,212,221,228
 Tomoshenko, S. P.; 149,156,257
 Toma, S.; 63,121
 Tseng, W. H.; 156
 Tsuda, K.; 78
 Tuma, J. J.; 156
 Tvergaard, V.; 21
- Ueda, Y.; 91
- Veda, Y.; 86,91,165,168
 Valsgaard, S.; 279,299,317
 Van Hooft, R.; 327
 Van Loan, C. F.; 63
 Vojta, J. F.; 287,293
- Wagner, A. L.; 121
 Walker, A. C.; 279
 Wang, G. Z.; 113,211
 Wang, S.; 27
 Wang, T. M.; 156
 Wang, Z. M.; 121
 Wagner, D. C.; 142
 Wakabayashi, M.; 213
 Walker, A. C.; 256,275,279,317
 Weaver, Jr., W.; 156
 Whitmore, R. E.; 196,199
 Wilhoite, G. M.; 213
- Will, K. M.; 198
 Williams, F. W.; 149,156
 Williams, G. C.; 198
 Wilson, W. M.; 78
 Winter, G.; 35,210
 Wirsching, P.; 327
 Wittrick, W. H.; 246,257
- Yamada, T.; 163,168
 Yang, X. M.; 113
 Yao, T.; 91,111
 Yokoo, Y.; 213
 Young, D. H.; 156
- Zhao, W. W.; 121
 Zhou, X.; 27
 Zienkiewicz, O. C.; 257
 Zimmer, R. A.; 327



Subject Index

- AASHTO: 192,196
- ABS: 325
- acceleration: 164
Villita; 164
- AISC: 135,175,176,205,222,223,227
LRFD; 206
- AISI; 205
- American Bureau of Shipping; 325
- American Petroleum Institution: 119,287
- analysis:
buckling; 60
dynamic; 58
elastic-plastic; 113
finite element; 138,269,333
frame; 163
linear; 57
nonlinear; 57
non-linear dynamic response; 166
regression; 84
stability; 125
static; 58
vibration; 125
- anchor bolt: 163,165
- angle: 206
back-to-back; 221
boxed; 221
built-up; 206,209
bulb; 206
cold-formed; 205,206,207
column; 205
compound; 206
double; 205,211,221,223
hot-rolled; 205
lipped; 27,206
plain; 206
single; 205,206
starred; 221
widely spaced; 222
- API: 115,119,287
- AS (Standards Association of Australia):
205,209
- ASCE: 197,205,207
- ASME: 333
Boiler & Pressure Vessel Code; 263,288
- aspect ratio: 27
- axisymmetric collapse; 259
Batdorf's parameter; 314
- batten; 223
- beam: 139,164
continuous; 149
rigid; 16,139
Timoshenko; 149
vibration of; 149
- beam-column: 79,113,115,153,155,164
behavior; 65
elastic; 116
elastic-plastic; 116
formulus; 197
imperfect; 3
I-section; 1
tubular; 77,105,106
uniaxially loaded; 1
- behavior:
buckling, 69,113
collapse; 89
column; 65
elastic; 82
elastic-plastic; 82
non-ductile; 175
nonlinear; 118
plastic post-collapse; 82
post-buckling; 27,28,57
post-collapse; 86
- block-shear concept: 192
- boundary condition: 27,87,125,139,
191,192,288
clamped end; 87
end eccentricity; 115

- end restraint; 115
 - pinned-end; 115,224
 - pinned-pinned; 225
 - rigid point support; 264
 - simply supported; 82,153,302
 - terminal; 127
 - two-point; 127
- box:
- bridge; 233
 - span; 233
- brace: 175
- bracing:
- diagonal; 191
 - member; 163
 - system; 165
- bracket; 135
- bridge; 135
- buckling: 39,49,55,79,113,114,119, 154,164,176,192,226,240,245,246, 251,277,288,289,310
- asymmetric; 259
 - behavior; 69,113
 - column; 69,106,175,259,263
 - direction; 120
 - elastic; 69,193,259,299
 - elastic-plastic; 85
 - elastic stress; 206,288,330
 - general; 39,266,299
 - global member; 106
 - inelastic; 259,265
 - interactive; 14
 - inter-ring; 265,277
 - length; 88
 - load; 47,192
 - lobar; 135,259
 - local; 14,65,80,83,175,192, 266,277,292,293
 - local stiffener; 299
 - mode; 154,155,287,288,330
 - non-linear inelastic; 273
 - of cylinder; 261
 - overall; 14,194,197,299
 - panel; 299
 - plate; 191
 - post; 27,28,65
 - postbuckling strength; 14
 - premature local; 83
 - shape; 195
 - shell; 299
 - shell mode; 288
 - stage; 125
 - strength; 81,191,287,326
 - web; 239
- built-up member: 222
- bulkhead: 261,262
- can: 113
- Canadian Steel Construction Council: 192
- channel:
- lipped; 27
- chord: 224
- closed form equation: 40
- column: 113,135,164,329
- angle; 205
 - behavior; 64
 - buckling; 69,106,175,259,263
 - dented tubular; 141
 - Euler; 18
 - locally buckled; 141
 - short; 67
 - slender; 224
 - stocky; 291
 - strength; 120
 - stub; 67,114
 - thinwalled; 13,14
 - tubular; 113,114,119,135,141,291
- complex trajectory: 245
- computer program:
- nonlinear; 49
- concept:
- effective width; 196,197

- connection:
 beam-to-column; 192
 gusset plate; 191,193
- converge: 51,125
- coordinate:
 cylindrical; 139
 orthogonal curvilinear; 125
- cracking; 175,239
- crippling: 192
- critical:
 buckling pressure; 262
 length; 261
 pressure; 264
 ring spacing; 261
- crookedness; 115
 initial; 115
- curve:
 load-shortening; 57
- CSA: 205,208,222
- cylinder: 113,125,266,287,289,330,331
 buckling of; 261
 conoidal; 125
 flat; 125
 moderately long; 313
 paraboloidal; 125
 ring and stringer stiffened; 287,299,332
 ring-stiffened; 125,259,261,275,287,
 329,332
 short; 310
 spheroidal; 125
 stiffened; 40,259,264,266,287
 stiffened steel; 327
 stringer stiffened; 287,332
 unstiffened; 259,261,287,332
 vertical; 109
- cylindrical:
 skirt; 308
 structure; 327
- database: 275
- deformation:
 global; 106
 shear; 149,154
- dent:
- dented region; 105,109
- denting: 109,265
 bending damages; 80
 rig; 109
 test; 277
- diaphragm: 233
- differential equation: 126
 first-order; 126
- dimple: 259
- DIN: 222
- distortion: 71
- dome:
 one-off; 51
 single layer; 49
 shallow; 49
- dynamic:
 instability; 13,20
 non-linear response; 167
 response; 17
- earthquake: 19,163
 Mexico; 163
 Mexico city; 176
 1978 Miyagi-ken Oki; 176
 motion; 175
 U.S.-Japan Cooperative Research
 Program; 175
- ECCS: 115,119,292,33
- eigenvalue: 27,49,125,166
- eigenvectors; 49

- eight-node isoparametric shell element; 265
- elastic:
 - media; 155
 - support; 149
- elephant foot buckle: 71
- end restraint: 1
- energy contribution: 301
- equation:
 - closed form; 40
 - critical stress; 261
 - differential; 150,151
 - first-order differential; 126
 - interaction; 77,287,289
 - non-conjugate; 246
 - static; 151
- equilibrium:
 - bifurcation; 50
 - secondary path; 250
 - trajectory; 248
- fabricated member: 65
- finite difference:
 - approach; 265
 - principle; 113,116
- finite element: 80,107,138,149,192, 197,245,333
 - formulation; 300
 - model; 142,316
 - non-linear shell analysis; 80
 - rigid-plastic; 266
 - two-dimensional; 196
- first order moment: 75
- floating offshore structure: 275
- force-ductility ratio: 167
- forced vibration: 19
- foundation movement: 149
- Fourier:
 - index number; 126
 - series; 125,246
- fracture: 175,177
- frame:
 - bending; 106
 - braced steel; 191
 - moment; 175
 - single story; 13,16
- framework:
 - steel; 163
- free vibration: 19
- frequency: 152,153,155
- full plastification: 75
- function:
 - Airy stress; 28,302
 - displacement; 246
 - polynomial linear; 246
 - strain energy; 316
- gable: 163
- Gaussian curvature: 42,143
- general collapse; 261
- girder:
 - box; 233
 - steel box; 245
 - three-cell box; 253
- global:
 - axis; 139
 - degrees of freedom; 269
- grid system; 149
- ground acceleration; 19
- gusset plate:
 - connection; 191,193

- Hartford Coliseum roof: 58
- Hencky-von Mises curve: 291
- hull structure: 329
- IABSE (International Association of Bridge and Structural Engineering): 233,245
Congress; 233,245
- imperfection: 50,65,75,84,106,113, 263,273,276,288,291,326,333
initial; 17,79,195
local; 79
- instability; 292
bay; 293
general; 293
- interaction:
equation; 77
formula; 75
stability; 75
- interactive effect: 259
- interconnector; 222,227
- IS: 208
- ISI: 205
- iteration: 125
- jacket structure: 106
- jump: 58
- kinematic work-hardening rule: 165
- knockdown factor: 84
- lacing: 223
- lip: 27
- load-axial shortening curve: 55
- load:
buckling; 47,192,195
carrying capacity; 233
collapse; 57
critical buckling; 75
deformation; 75,137,140
denting; 288
Euler buckling; 225
path; 1,2,3
scheme; 233
ultimate; 85,135
- loading:
concentric; 194,197
critical; 13,154
eccentric; 145
lateral; 107
step; 13
system; 225
torsional; 261
- lower boundary formulation: 333
- manufacturing process: 113
- material orthotropy: 254
- matrix:
decomposed stiffness; 49
narrow strip; 256
secant stiffness; 83
tangent stiffness; 49
transfer technique; 149
- membrane:
effect; 301
resistance; 39
stiffness; 262
- method:
Adam's; 127
allowable stress; 140
elastic-plastic frame analysis; 164
finite strip; 233,237,245
Goldberg-Bogdanoff; 125
numerical; 50
numerical analysis; 165
numerical integration; 125
plastic hinge; 165

- predictor-corrector; 127
 - rational design; 192
 - Ritz; 281
 - Runge-Kutta process; 127
 - semi-empirical; 81
 - semi-energy; 27
- Mexico City:
- earthquake; 163,176
- mises yield criterion: 139
- Miyagi-ken Oki earthquake; 176
- mode:
- bifurcation; 49
 - buckling; 154,155,287,288
 - failure; 263
 - local; 17
 - primary local; 15
 - shell buckling; 288
- model: 14,138,233,265
- buckling; 14
 - finite element; 142,316
 - lumped mass; 166
 - plastic; 47
 - small-scale; 265
- modelling: 13
- moment-curvature: 117
- moment-thrust-curvature: 118
- mooring: 325
- motion instrument: 163
- Newton-Raphson iteration: 113,119
- non compact: 206
- nonlinearity: 288
- numerical technique: 300
- offshore:
- installation; 325
 - structure; 105,329
- oil rig: 265
- out-of-straightness: 1,109,113,115,224
- overload capacity: 55
- panel:
- buckle; 263
 - curved; 263
 - inter-stringer; 266
- period:
- natural; 166
 - predominant; 166
- pipeline:
- plastic:
- buckle; 69
 - bulge; 69
 - flow rule; 165
 - hinge; 165,166,175
 - rotation; 177
- plate:
- buckling; 197
 - deck; 233
 - edge-stiffened; 27
 - flat structure; 329
 - orthotropic; 238
 - spliced; 191,193,197
 - stiffened; 264
- platform: 106,325
- deep water drilling; 287
 - offshore production; 65
 - tension leg; 287,326,329
- polynomial: 15
- pontoon: 326,329
- post-buckling: 27,28,65,206,113
- cyclic; 175
- post-collapse: 79

- potential energy: 248,249
stationary; 249
- prebuckling stage: 126,301
- profiling rig: 67
- program:
ADINA; 137,138
BASP; 191,193,196
BCAP; 119
DENTA; 81,88
DENTA-2; 88
DRAIN-2D; 176
FINAS; 265,273
MCTAP; 118
- quadratic:
failure envelope; 289
form; 287,288
- ratio:
ductility; 167
force-ductility; 167
slenderness; 55,77
width-to-thickness; 206
- redundant: 55
- reliability: 333
- repairing: 135
- residual:
damage: 276
dent depth: 277,278
- response:
maximum; 167
non-linear; 167
- rule:
isotropic hardening; 165
kinematic hardening; 165
SAA; 205
- safety factor: 331
- seismic:
- force; 167
response; 19
- shear:
coefficient; 163
- shell: 39
buckling; 139
buckling mode; 288
circular; 325
composite; 39
concrete; 39
cylindrical; 84,259,265,129,329
equivalent orthotropic; 263
framed; 39
latticed; 39
longitudinally-stiffened; 265,266
of revolution; 125
orthogonally-stiffened; 265,266,329
orthotropic; 39
reticulated; 39
ring and stringer stiffened; 309
rigid-stiffened; 265,269
ring-stiffened; 266
sandwich; 39
slender; 292
stiffened; 39,42,263
stiffened cylindrical; 287
stringer-stiffened; 265,299
thin-walled; 275
unstiffened; 316
wooden; 39
- shell-like structure: 39
spherical; 40
- sinusoidal bending: 83
- slenderness ratio: 77,153,154,222,225
modified; 205
non-dimensional; 65
- solution:
closed form; 39
homogeneous; 127
lower bound; 80
nonhomogeneous; 127,129
trivial; 251

specifications and codes:

- American Association of State Highway and Transportation Officials (AASHTO); 192,196
- American Bureau of Shipping (ABS); 325
- American Institute of Steel Construction (AISC); 135,175, 176,205,222,223,227
- American Iron and Steel Institute (AISI); 115,119,287
- American Petroleum Institute (API); 115,119,287
- American Society of Civil Engineering (ASCE); 197,205,207
- American Society of Mechanical Engineering (ASME); 333
- Canadian Standards Association (CSA); 205,208,222
- European Convention for Constructional Steelwork (ECCS); 115,19,292,333
- German Buckling Specification (DIN); 222
- Indian Standard (IS); 208
- Indian Standard Institution (ISI); 205
- Standards Association of Australia (AS); 205,209

spherical bearing; 69

SSRC: 49

- guide; 259
- multiple curve; 115,119

stability: 325

- analysis; 125
- criteria; 259
- design; 329
- interaction; 75
- loss; 243

stationary potential energy; 27

stiffener: 125,197,243

- bridging; 135
- circumferential; 259
- longitudinal; 259

plain ring; 278,279

- ring; 130
- stringer; 263

stiffening:

- effect; 299
- ring; 125,278

stiffness: 55

- membrane; 262

straightness: 65

strain: 246

- energy; 32,301
- residual; 67,71,117

strength:

- buckling; 81,191,326
- column; 120
- formulation; 327
- interaction; 71
- post-buckling; 34
- residual; 88,105,106,265,273
- residual structural; 80
- ultimate; 113,235
- ultimate tensile; 192

stress:

- circumferential residual; 114
- elastic buckling; 206,288,330
- generalized; 165
- hoop; 263
- initial buckling; 254
- instability; 331
- longitudinal residual; 114,120
- plane; 139
- plastic; 164
- residual; 1,65,113,114,117,288,326

stress-strain curve: 114,117

tangent modulus: 55

- curve; 2

tank:

- elevated storage; 135

Target Safety Index: 327

- theorem:
 Stowell-Ilyushin; 34
- theory:
 Bernoulli-Euler; 149
 finite difference principle; 113,116
 inextensional; 307
 plastic potential flow; 164
 tangent modulus; 1
 Timoshenko's beam; 149
 yield-hinge; 86
- thin-walled construction: 233
- threshold: 13
- TLP Standard: 325
- transmission tower: 135
- T-ring: 276
 stiffeners: 278
- truss: 278
 space; 55,57
- tube:
 clamped; 87
 dented; 80
 eccentrically loaded; 89
 manufactured steel; 65
 normal-thick-walled; 87
 simply supported; 87
 steel; 105
 thick-walled; 87
 thin-walled; 87
- tubular: 89
 beam column; 77,105,106
 bracing member; 177
 circular; 79
 column; 113,114,119,120,135,291
 dented; 135
 dented tubular column; 141
 member; 79,106
 section; 67
 unstiffened; 80
- ultimate failure path: 60
- Uniform Building Code: 175
- vessel: 275,287,325
- vibration:
 analysis; 125
 forced; 19
 free; 19
 period of; 19
- virtual work: 301,304
- warping: 192
- wave: 302
 length; 40,254
 number; 128
- weld:
 girth; 69
 pattern; 227
- whitmore's effective width concept: 192
- working stress design: 331
- work-harden: 164
- yielding:
 local; 69,264
- yield moment: 2

